

EXPERIMENTAL INVESTIGATIONS ON
ASSESSMENT AND PREDICTION OF
SPECIFIC ENERGY IN
ROCK INDENTATION TESTS

Thesis

Submitted in partial fulfillment of the requirements for the degree of

DOCTOR OF PHILOSOPHY

by

BALLA KALYAN



DEPARTMENT OF MINING ENGINEERING
NATIONAL INSTITUTE OF TECHNOLOGY KARNATAKA
SURATHKAL, MANGALORE - 575025
APRIL, 2017

Dedicated to

My Sons

DECLARATION

by the Ph.D. Research Scholar

I hereby declare that the Research Thesis entitled “**Experimental Investigations on Assessment and Prediction of Specific Energy in Rock Indentation Tests**” which is being submitted to the **National Institute of Technology Karnataka, Surathkal** in partial fulfillment of the requirements for the award of the Degree of **Doctor of Philosophy in Mining Engineering** is a bonafide report of the research work carried out by me. The material contained in this Research Thesis has not been submitted to any University or Institution for the award of any degree.

123025MN12F01, Balla Kalyan

(Register Number, Name & Signature of the Research Scholar)

Place: NITK, Surathkal

Date:

CERTIFICATE

This is to certify that the Research Thesis entitled “**Experimental Investigations on Assessment and Prediction of Specific Energy in Rock Indentation Tests**” submitted by **Balla Kalyan** (Register Number **123025MN12F01**) as a record of the research work carried out by him, is accepted as the Research Thesis submission in partial fulfillment of the requirements for the award of Degree of **Doctor of Philosophy**.

Dr. Ch. S. N. Murthy
Professor & Research Guide
Department of Mining Engineering

Dr. R. P. Choudhary
Asst. Professor & Research Guide
Department of Mining Engineering

Dr. M. Govinda Raj
Professor & Chairman, DRPC
Department of Mining Engineering
(Signature with date)

ACKNOWLEDGEMENT

I am indebted to my supervisor **Dr. Ch. S. N. Murthy**, Professor, Department of Mining Engineering, National Institute of Technology Karnataka (N.I.T.K), Surathkal, for his excellent guidance and support throughout the research work. His constant encouragement, help and review of the entire work during the course of the investigation are invaluable.

Further I am thankful to my co-guide **Dr. R. P. Choudhary**, Assistant Professor, Department of Mining Engineering, National Institute of Technology Karnataka (N.I.T.K), Surathkal, for his excellent guidance and moral support throughout the research work.

I would like to thank the Government of Andhra Pradesh, Department of Mining Engineering, National Institute of Technology Karnataka (N.I.T.K), Surathkal and All India Council for Technical Education (AICTE), for providing me an opportunity to pursue Ph.D. programme under Q.I.P (Poly) scheme,

I wish to thank all the members of the Research Program Assessment Committee including **Dr. M Govinda Raj**, Professor, Department of Mining Engineering and **Dr. D. Venkata Reddy**, Professor, Department of Civil Engineering for their unbiased appreciation and criticism all through this research work.

I wish to express my sincere thanks to **Dr. M. Govinda Raj**, Professor and Head of the Department, Department of Mining Engineering for extending the departmental facilities, which ensured the satisfactory progress of my research work.

Further I am thankful to my **Dr. P. Navin Karanth**, Assistant Professor, Department of Mechanical Engineering, National Institute of Technology Karnataka (N.I.T.K), Surathkal, for his excellent guidance in numerical modelling (ANSYS).

I would like to thank all the Teaching and Non-teaching staff members of the Department of Mining Engineering, of N.I.T.K Surathkal for their continuous help and support throughout the research work.

I owe my deepest gratitude to Sri Chandrahas Rai, Assistant Executive Engineer and technicians Sri Mahabala Poojari for their help during conducting experiments in Rock Mechanics laboratory.

I am very much thankful to **Mr. M. Nanda Kishore, Mr. G. Uday Kumar, and Mr. P. Sai Naredra**, B.Tech students of GIET, Rajahmundry, A.P for their help during conducting experiments in Rock Mechanics laboratory. I am very much thankful to **Mr. Ajmeer Shareef A N**, M.Tech (By Research) student in Department of Civil Engineering, NITK, Surathkal for his help preparation of Auto-Cad drawings.

I owe my deepest gratitude to Smt Indira Ravidran, S.O (ore Dressing), Indian Bureau of Mines, Bangalore and Sri. **Purna Chandrarao M. and Sri. Prakash N.** for their help while carrying out thin section analysis at their laboratory.

Finally, I would like to share this moment of happiness with my parents, **Sri Balla Veerabhadra Rao, Smt Balla. Bramaramba**; my wife **Smt. Balla Durga Srilakshmi** for their constant encouragement.

The list goes on and there are many others I should mention. There are people who have helped me all the way and provided me support when I didn't even realize I needed it, or needed it now, or needed it constantly. Listing all of them would fill a book itself, so I merely will have to limit myself to a few words: I THANK YOU ALL.....!

(Balla Kalyan)

ABSTRACT

Indentation is a fundamental process in drilling and cutting/sawing of rocks. Assessment of specific energy (SE), which is energy required to excavate (drilling or cutting) a unit volume of rock is important because it is one of the parameters to determine drillability and cuttability of rocks. Drillability of rocks is an important parameter to decide the progress and drilling costs of the excavation. Similarly index angle, which is amount of rotation of bit between successive blows, play an important role in percussive drilling. Static indentation tests were carried out in six types of rocks viz. marble, limestone, basalt, steel gray granite, moon white granite and black galaxy granite by using commercial drill bits of Chisel, Cross and Spherical button of 35mm, 38mm, 45 mm and 48mm diameters as indenters on Micro controller compressive testing machine. The loading was done on rock specimen considered for 60 seconds, and then unloading was done. During loading and unloading, at every 5 seconds forces and penetrations were recorded. Then, F-P curves were drawn for all bit-rock combinations considered. The volume of rock excavated was determined using the density of the rocks. Then, SE (ratio of area under F-P curve (energy expended) to the volume of rock excavated)) was calculated for all bit-rock combinations considered. These experimental investigations were carried out in the laboratory with an objective to determine the SE during indentation and to study the influence of index angle on specific energy. The graphs were drawn between index angle and SE. The results showed that the SE is minimum at 30° index angle for the rocks like marble, limestone whereas; the SE is minimum at 20° index angle for the rocks like basalt, steel gray granite, moon white granite and black galaxy granite. Experimental investigations were also carried out to determine physico-mechanical properties like density, uniaxial compressive strength (UCS), Brazilian Tensile strength (BTS), Hardness (Schmidt Rebound Number (SRN)), Young's Modulus, Poisson's ratio. Regression analysis was carried between SE and above properties to study the influence of the physico-mechanical properties on SE. It was observed that, with the increase in density, UCS, BTS, Hardness (SRN), Young's Modulus, Poisson's ratio of the rock, SE increases. This is because of the fact that, with the increase in the

strength, the resistance to indentation increases. But with increase in percentage abrasion resistance, SE decreases. Similarly the thin section analysis, petrographic studies and X-Ray Fluorescence tests were carried to find the mineralogical composition of rocks considered and regression analysis between minerals present in all rocks considered and SE to find the influence of mineralogical composition on SE. The results showed that except in the case of feldspar, an increase in SE, as the percentages of quartz, hornblende, pyrites, magnetite and biotite mica increases. Similarly predictive models (Regression analysis and Artificial Neural Network (ANN)) were developed to predict the specific energy from operating variables like diameter of bit and index angle and selected properties of rocks like density, UCS, BTS, abrasion resistance, Hardness (SRN), Young's Modulus, Poisson's ratio. The results showed that operating variables and above properties of rocks are significant parameters to predict the specific energy. Further, results (for spherical button bit -prediction performance indices (VAF: 90.18(regression), 99.05135(ANN), RMSE: 6.58(regression), 2.16(ANN), and MAPE 0.19(regression), 0.055 (ANN))) showed that the predictive performance of ANN model are higher than those of multiple regression equations. So, ANN is a good approach for minimizing the uncertainties in the rock and soil engineering projects. The Numerical Modelling (Finite Element Method analysis) was carried out to determine the depth of penetration for all bit-rock combinations considered by using the force values from static indentation test (up to loading cycle only). Then the penetration obtained in FEM analysis of all bit-rock combinations considered were compared with experimental results. The numerical value indicates that experimental values are higher than FEM analysis and ranges from 10 to 19.5% (except few). Further the results indicated that in all the directions, displacement is decreasing from the loading axes towards the boundary. The stress analysis also was carried in all the bit-rocks combinations considered along X- Y and Z- axes. The results showed that maximum compressive stress is generated near the tip of the bit and the magnitude of compressive stresses developed at any point away from vertical axis depends on the geometry of the indenter.

TABLE OF CONTENTS

	CONTENTS	PAGE NO
	Declaration	i
	Certificate	ii
	Acknowledgement	iii
	Abstract	v
	Table of Contents	vii
	List of figures	xiii
	List of tables	xxiv
	Nomenclature	xxix
1	Introduction	1
1.1	General	1
1.2	Principle of indentation in rock drilling/cutting	4
1.3	Indentation test and its operating parameters	4
1.4	Specific energy in indentation	5
1.5	Influence of specific energy on drillability	6
1.6	Influence of indexing on specific energy	7
1.7	Influence of rock properties on specific energy	7
1.8	Thesis outline	9
2	Literature review	11
2.1	Studies on indentation	11
2.1.1	Introduction	11
2.1.2	Studies on indentation concerned to mechanism of rock fracture/ failure	12
2.1.3	Studies on indentation to correlate the indentation indices with mechanical properties of rocks	15
2.2	Studies on Force-Penetration curves	19

2.3	Studies on factors affecting indentation process	22
2.3.1	Influence of static, quasi - static load and dynamic load	22
2.3.2	Influence of rate of loading or strain rate of penetration	22
2.3.3	Influence of indenter geometry	23
2.3.4	Influence of index angle	24
2.4	Studies on specific energy	27
2.4.1	Introduction	27
2.4.2	Studies on specific drilling energy	29
2.4.3	Studies on specific cutting energy	31
2.5	Studies on application of ANN to estimate rock properties and studies on application of artificial neural network for predicting the indentation depth/specific energy in rock indentation	36
2.6	Studies on numerical simulation and analysis of stress distribution and rock fragmentation/fracture in rock indentation	38
2.6.1	Numerical modeling	38
2.6.2	FEM to simulate the rock indentation or rock cutting:	40
2.7	Reasons to carry out Present research work	44
2.8	Origin of present research work	47
2.9	Definition of the problem	47
2.10	Research objectives	48
3	Experimental and Theoretical Investigations	49
I	Experimental Investigations	49
3.0	Introduction	49
3.1	Methodology	49
3.2	Collection of rock samples	51
3.3	Preparation of samples	51
3.4	Static indentation tests	58

3.4.1	Fabrication work	58
3.4.2	Experimental procedure of static indentation test	62
3.4.3	Force-Penetration curves and calculation of specific energy	63
3.5	Tests to determine the properties of rocks	81
3.5.1	Determination of abrasion resistance of rocks	81
3.5.2	Determination of uniaxial compressive strength	82
3.5.3	Determination of Brazilian tensile strength	83
3.5.4	Determination of dry density of rocks	84
3.5.5	Determination of hardness (SRN) of rocks	85
3.5.6	Determination of Young's Modulus of the rock	87
3.5.7	Determination of Poisson's Ratio	87
3.6	Determination of mineralogical and textural features (thin section examination)	90
3.6.1	Sample name: marble	91
3.6.2	Sample name: limestone	93
3.6.3	Sample name: basalt	95
3.6.4	Sample name: steel grey granite	97
3.6.5	Sample name: moon white granite	99
3.6.6	Sample name: black galaxy granite	101
3.7	Determination of elemental/minerals in oxide form using X-Ray Fluorescence (XRF) test	103
3.7.1	Introduction	103
3.7.2	XRF instrument	103
3.7.3	Experiment procedure	104
II	Theoretical Investigations	106
3.8	Development of predictive models for estimation of SE (regression models)	106

3.8.1	Mathematical models using multiple regression analysis	108
3.8.2	Multiple regression analysis of chisel bit	109
3.8.3	Multiple regression analysis of cross bit	110
3.8.4	Multiple regression analysis of spherical button bit	113
3.9	Artificial Neural Network modeling	117
3.9.1	Introduction	117
3.9.2	Fundamental concepts in ANN	118
3.9.3	Multi-layer perceptron	120
3.9.4	Back – Propagation (BP) algorithm	121
3.9.5	Development of ANN model in the present study	123
3.10	Numerical modelling (finite element analysis)	129
3.10.1	General	129
3.10.2	FEM analysis of drill bit penetration into rock	131
3.10.3	Description of the numerical model	131
3.10.4	Assumptions in fem analysis of bit penetration into rocks	131
3.10.5	Defining element type	132
3.10.6	Material properties	132
3.10.7	Mesh generation	132
3.10.8	Boundary conditions adopted	133
4	Results and discussion	136
4.1	F-P curves and influence of index angle on specific energy	136
4.1.1	Introduction	136
4.1.2	Experimental results	136
4.1.3	Analysis of results of F-P curves and influence of index angle on specific energy	136
4.2	Influence of rock properties on specific energy	141

4.2.1	Introduction	141
4.2.2	Experiment work	141
4.2.3	Bivariate correction analysis	141
4.2.4	Linear regression analysis	142
4.2.5	Analysis of results	154
4.3	Influence of mineralogical properties on specific energy	157
4.3.1	Introduction	157
4.3.2	Experimental work	158
4.3.3	Bi-variate correlation	158
4.3.4	Simple regression of SE and minerals	159
4.3.4.1	Simple regression of SE (chisel bit) and minerals	159
4.3.4.2	Simple regression of SE (cross bit) and minerals	159
4.3.4.3	Simple regression of SE (spherical button bit) and minerals	160
4.3.5	Analysis of results	160
4.4	Influence of elements/minerals in oxides obtained from XRF test on specific energy	168
4.4.1	Introduction	168
4.4.2	Bi-variate correlation	168
4.4.3	Simple regression of SE (chisel bit) and elements/minerals in oxides form	169
4.4.4	Simple regression of SE (cross bit) and elements/minerals in oxides form	170
4.4.5	Simple regression of SE (spherical button bit) and elements/minerals in oxides form	172
4.4.6	Analysis of results	174
4.5	Analysis of predicative (regression) models	175
4.5.1	Residual plots for specific energy	176

4.5.2	Performance prediction of the derived models	177
4.6	Analysis of artificial neural network results	178
4.7	Analysis of numerical modelling results	180
4.7.1	Results of compressive stress field	180
4.7.2	Comparison of static indentation results obtained from experimental and fem analysis	181
5	Conclusions and Scope for future work	196
5.1	Conclusions	196
5.2	Scope for future work	197
	References	199
	Appendix- I	217
	Appendix- II	265
	List of Publications	294
	Biodata	295

LIST OF FIGURES

Figure No.	Description	Page No.
2.1	Different types of Force-Penetration curves and the Associated macroscopic models of rock failure for single sharp bit Indentation.	19
3.1	Rock cutting machine	52
3.2	Marble rock samples	52
3.3	Limestone rock samples	53
3.4	Basalt rock samples	53
3.5	Steel gray granite rock samples	53
3.6	Moon white granite samples	54
3.7	Black galaxy granite	54
3.8	Flow chart of plan of experimental design and analysis	55
3.9	Indenter (bit) Holder, Digital Dial Gauge, Magnetic Holder and Stop Watch used in test	59
3.10	Specimen box	59
3.1	Experiment Set up	59
3.12	Experiment Set up (Line diagram)	60
3.13	Geometry of different drill bits used in static indentation tests	61
3.14 (a-f)	Force–Penetration (F-P) curves for 35mm diameter chisel bit at 10 ⁰ index angle for various types of rocks	65
3.15(a-f)	Force–Penetration (F-P) curves for 35mm diameter chisel bit at 20 ⁰ index angle for various types of rocks	66
3.16(a-f)	Force–Penetration (F-P) curves for 35mm diameter chisel bit at 30 ⁰ index angle for various types of rocks	67
3.17(a-f)	Force–Penetration (F-P) curves for 35mm diameter chisel bit at 40 ⁰ index angle for various types of rocks	68

3.62	Los Angeles abrasion testing machine	82
3.63	Compressive testing machine	83
3.64	Brazilian tensile strength testing machine	84
3.65 (a)	Photomicrographs of marble: Quartz (Qz) is present within the inter-granular spaces of Calcite (Ca) in thin section. (Transmitted light, 10X).	92
3.65 (b)	Photomicrographs of marble: Martitized magnetite (M.M) is present as inclusion within the inter- Granular spaces of Calcite (Ca). Free clay (Cl) is also seen in minus 65 plus 200 mesh Mount. (Reflected light, 20X).	92
3.66 (a)	Photomicrographs of limestone: Carbonates and quartz (Qz) grains, in 1.560 Refractive Index Liquid Media. (Transmitted light, 10X)	94
3.66 (b)	Photomicrographs of limestone: Carbonates and pyrite (Py) is present are seen in minus 65 plus 200 mesh mount. (Reflected light, 10X).	94
3.67 (a)	Photomicrographs of basalt: Pyroxene (pyro), Feldspar (Fel) and Biotite mica (BM) are seen in thin section. (Transmitted light, P.P. 5x)	96
3.67 (b)	Photomicrographs of basalt: Magnetite (Ma), pyrite (Py) and silicates are seen in minus 65 plus 200 Mesh mount. (Reflected light, 10X).	96
3.68 (a)	Photomicrographs of Steel Gray Granite: Amphibole (Amp), Biotite mica (BM) and feldspar (Fel) grains, in .560 Refractive Index Liquid media. (Transmitted light, 10X).	98
3.68 (b)	Photomicrographs of Steel Gray Granite:Magnetite (Ma) and chalcopyrite (CP) are seen in Minus 65 plus 200 Mesh mount. (Reflected light, 20X).	98

3.69 (a)	Photomicrographs of Moon white Granite: Quartz (Qz), feldspar (Fel) and Biotite mica (BM) are seen in thin section. (Transmitted light, X polar, 5x)	100
3.69 (b)	Photomicrographs of Moon white Granite: Martitized magnetite (M.M) inclusions within the Feldspar / quartz Groundmass in mount. (Reflected light 10x, Air)	100
3.70 (a)	Photomicrographs of black galaxy Granite: Hornblende (Hb), Biotite mica (BM), Quartz (Qz) and feldspar (fel) grains, in 1.560 Refractive Index Liquid media. (Transmitted light, 10X).	102
3.70 (b)	Photomicrographs of black galaxy Granite: Hornblende (Hb), Biotite mica (BM), and feldspar (Fel) grains, are seen in thin section. (Transmitted light, P.P. 10X).	102
3.71	XRF instrument (Model Epsilon 1)	103
3.72 (a)	Predicted SE versus observed SE for the model of chisel bit for training set	112
3.72 (b)	Predicted SE versus observed SE for the model of chisel bit for testing set	112
3.73 (a)	Residual plots against SE of chisel bit for training set	112
3.73 (b)	Residual plots against SE of chisel bit for testing set	112
3.74 (a)	Predicted SE versus observed SE for the model of cross bit for training set	115
3.74 (b)	Predicted SE versus observed SE for the model of cross bit for testing set	115
3.75 (a)	Residual plots against SE of cross bit for training set	115
3.75 (b)	Residual plots against SE of cross bit for testing set	115
3.76 (a)	Predicted SE versus observed SE for the model of spherical button bit for training set	116
3.76 (b)	Predicted SE versus observed SE for the model of spherical button bit for testing set	116

3.77 (a)	Residual plots against SE of spherical button bit for training set	116
3.77 (b)	Residual plots against SE of spherical button bit for testing set	116
3.78	Architecture of Simple neuron	118
3.79	Feed forward ANN network	119
3.80 (a)	Neural network architecture of chisel bit	126
3.80 (b)	Network training tool of chisel bit	126
3.80 (c)	Network training regression of chisel bit	126
3.81 (a)	Neural network architecture of cross bit	127
3.81 (b)	Network training tool of cross bit	127
3.81 (c)	Neural network performance of cross bit	127
3.82 (a)	Neural network architecture of spherical button bit	128
3.82 (b)	Network training tool of spherical button bit	128
3.82 (c)	Network training regression of spherical button bit	128
3.83	Representation of loading at bit-rock interface for three bit geometries	135
3.84	Discretization showing the boundary conditions adopted for FEM analysis	135
4.1	Influence of index angle on specific energy in static indentation tests on 6 different types of rocks for chisel bits of 48, 45, 38, 35 mm diameter	138
4.2	Influence of index angle on specific energy in static indentation tests on 6 different types of rocks for cross bits of 48, 45, 38 and 35 mm diameters.	139
4.3	Influence of index angle on specific energy in static indentation tests on 6 different types of rocks for spherical button bits of 48, 45, 38 and 35 mm diameter.	140
4.4	Relationship between density and Specific energy	151
4.5	Relationship between uniaxial compressive strength and Specific energy	151

4.6	Relationship between tensile strength and Specific energy	152
4.7	Relationship between abrasion resistance and Specific energy	152
4.8	Relationship between hardness and Specific energy	153
4.9	Relationship between Young's Modulus and Specific energy	153
4.10	Relationship between Poisson's ratio and Specific energy	154
4.11	Relationship between specific energy of chisel bit and quartz mineral in various rocks	161
4.12	Relationship between specific energy of chisel bit and feldspar mineral in various rocks	161
4.13	Relationship between specific energy of chisel bit and hornblende mineral in various rocks	161
4.14	Relationship between specific energy of chisel pyrite mineral in various rocks	161
4.15	Relationship between specific energy of chisel bit and magnetite mineral in various rocks	162
4.16	Relationship between specific energy of chisel bit and biotite mica mineral in various rocks	162
4.17	Relationship between specific energy of cross bit and Quartz mineral in various rocks	162
4.18	Relationship between specific energy of cross bit and feldspar mineral in various rocks	162
4.19	Relationship between specific energy of cross bit and hornblende mineral in various rocks	163
4.20	Relationship between specific energy of cross bit and pyrite mineral in various rocks	163
4.21	Relationship between specific energy of cross bit and magnetite mineral in various rocks	163
4.22	Relationship between specific energy of cross bit and biotite mica mineral in various rocks	163

4.23	Relationship between specific energy of spherical button bit and quartz mineral in various rocks	164
4.24	Relationship between specific energy of spherical button and feldspar mineral in various rocks	164
4.25	Relationship between specific energy of spherical button and hornblende mineral in various rocks	164
4.26	Relationship between specific energy of spherical button bit and magnetite mineral in various rocks	164
4.27	Relationship between specific energy of spherical button bit and pyrite mineral in various rocks	165
4.28	Relationship between specific energy of spherical button and biotite mica mineral in various rocks	165
4.29	Relationship between specific energy of chisel bit and Al_2O_3 in various rocks	169
4.30	Relationship between specific energy of chisel bit and SiO_2 in various rocks	170
4.31	Relationship between specific energy of chisel bit and CaO in various rocks	170
4.32	Relationship between specific energy of cross bit and Al_2O_3 in various rocks	171
4.33	Relationship between specific energy of cross bit and SiO_2 in various rocks	171
4.34	Relationship between specific energy of cross bit and CaO in various rocks	172
4.35	Relationship between specific energy of spherical button bit and Al_2O_3 in various rocks	173
4.36	Relationship between specific energy of spherical button bit and SiO_2 in various rocks	173

4.37	Relationship between specific energy of spherical button bit and CaO in various rocks	174
4.38	Compressive stress contours for chisel bit of 48 mm diameter in three rock types	183
4.39	Compressive stress contours for chisel bit of 48 mm diameter in three types of granite rocks	184
4.40	Compressive stress contours for cross bit of 48 mm diameter in three rock types	185
4.41	Compressive stress contours for cross bit of 48 mm diameter in three types of granite rocks	186
4.42	Compressive stress contours for spherical button bit of 48 mm diameter in three rock types	187
4.43	Compressive stress contours for spherical button bit of 48 mm diameter in three types of granite rocks	188
4.44	Relationship between indentation depth and compressive stress in X and Z- axes for chisel, cross and spherical button bits of 48 mm diameter in marble.	189
4.45	Displacement contours for chisel bit of 48 mm diameter in three types of rocks	190
4.46	Displacement contours for chisel bit of 48 mm diameter in three types of granite rocks	191
4.47	Displacement contours for cross bit of 48 mm diameter in three types of rocks	192
4.48	Displacement contours for cross bit of 48 mm diameter in three types of granite rocks	193
4.49	Displacement contours for spherical button bit of 48 mm diameter in three types of rocks	194
4.50	Displacement contours for spherical button bit of 48 mm diameter in three types of granite rocks	195

3.18(a-f)	Force–Penetration (F-P) curves for 38mm diameter chisel bit at 10 ⁰ index angle for various types of rocks	218
3.19(a-f)	Force–Penetration (F-P) curves for 38mm diameter chisel bit at 20 ⁰ index angle for various types of rocks	219
3.20(a-f)	Force–Penetration (F-P) curves for 38mm diameter chisel bit at 30 ⁰ index angle for various types of rocks	220
3.21(a-f)	Force–Penetration (F-P) curves for 38mm diameter chisel bit at 40 ⁰ index angle for various types of rocks	221
3.22(a-f)	Force–Penetration (F-P) curves for 45mm diameter chisel bit at 10 ⁰ index angle for various types of rocks	222
3.23(a-f)	Force–Penetration (F-P) curves for 45mm diameter chisel bit at 20 ⁰ index angle for various types of rocks	223
3.24(a-f)	Force–Penetration (F-P) curves for 45mm diameter chisel bit at 30 ⁰ index angle for various types of rocks	224
3.25(a-f)	Force–Penetration (F-P) curves for 45mm diameter chisel bit at 40 ⁰ index angle for various types of rocks	225
3.26(a-f)	Force–Penetration (F-P) curves for 48mm diameter chisel bit at 10 ⁰ index angle for various types of rocks	226
3.27(a-f)	Force–Penetration (F-P) curves for 48mm diameter chisel bit at 20 ⁰ index angle for various types of rocks	227
3.28(a-f)	Force–Penetration (F-P) curves for 48mm diameter chisel bit at 30 ⁰ index angle for various types of rocks	228
3.29(a-f)	Force–Penetration (F-P) curves for 48mm diameter chisel bit at 40 ⁰ index angle for various types of rocks	229
3.30(a-f)	Force–Penetration (F-P) curves for 35mm diameter cross bit at 10 ⁰ index angle for various types of rocks	230
3.31(a-f)	Force–Penetration (F-P) curves for 35mm diameter cross bit at 20 ⁰ index angle for various types of rocks	231

3.32(a-f)	Force–Penetration (F-P) curves for 35mm diameter cross bit at 30 ⁰ index angle for various types of rocks	232
3.33(a-f)	Force–Penetration (F-P) curves for 35mm diameter cross bit at 40 ⁰ index angle for various types of rocks	233
3.34(a-f)	Force–Penetration (F-P) curves for 38mm diameter cross bit at 10 ⁰ index angle for various types of rocks	234
3.35(a-f)	Force–Penetration (F-P) curves for 38mm diameter cross bit at 20 ⁰ index angle for various types of rocks	235
3.36(a-f)	Force–Penetration (F-P) curves for 38mm diameter cross bit at 30 ⁰ index angle for various types of rocks	236
3.37(a-f)	Force–Penetration (F-P) curves for 38mm diameter cross bit at 40 ⁰ index angle for various types of rocks	237
3.38(a-f)	Force–Penetration (F-P) curves for 45mm diameter cross bit at 10 ⁰ index angle for various types of rocks	238
3.39(a-f)	Force–Penetration (F-P) curves for 45mm diameter cross bit at 20 ⁰ index angle for various types of rocks	239
3.40(a-f)	Force–Penetration (F-P) curves for 45mm diameter cross bit at 30 ⁰ index angle for various types of rocks	240
3.41(a-f)	Force–Penetration (F-P) curves for 45mm diameter cross bit at 40 ⁰ index angle for various types of rocks	241
3.42(a-f)	Force–Penetration (F-P) curves for 48mm diameter cross bit at 10 ⁰ index angle for various types of rocks	242
3.43(a-f)	Force–Penetration (F-P) curves for 48mm diameter cross bit at 20 ⁰ index angle for various types of rocks	243
3.44(a-f)	Force–Penetration (F-P) curves for 48mm diameter cross bit at 30 ⁰ index angle for various types of rocks	244
3.45(a-f)	Force–Penetration (F-P) curves for 48mm diameter cross bit at 40 ⁰ index angle for various types of rocks	245

3.46(a-f)	Force–Penetration (F-P) curves for 35mm diameter spherical button bit at 10 ⁰ index angle for various types of rocks	246
3.47(a-f)	Force–Penetration (F-P) curves for 35mm diameter spherical button bit at 20 ⁰ index angle for various types of rocks	247
3.48(a-f)	Force–Penetration (F-P) curves for 35mm diameter spherical button bit at 30 ⁰ index angle for various types of rocks	248
3.49(a-f)	Force–Penetration (F-P) curves for 35mm diameter spherical button bit at 40 ⁰ index angle for various types of rocks	249
3.50(a-f)	Force–Penetration (F-P) curves for 38mm diameter spherical button bit at 10 ⁰ index angle for various types of rocks	250
3.51(a-f)	Force–Penetration (F-P) curves for 38mm diameter spherical button bit at 20 ⁰ index angle for various types of rocks	251
3.52(a-f)	Force–Penetration (F-P) curves for 38mm diameter spherical button bit at 30 ⁰ index angle for various types of rocks	252
3.53(a-f)	Force–Penetration (F-P) curves for 38mm diameter spherical button bit at 40 ⁰ index angle for various types of rocks	253
3.54(a-f)	Force–Penetration (F-P) curves for 45mm diameter spherical button bit at 10 ⁰ index angle for various types of rocks	254
3.55(a-f)	Force–Penetration (F-P) curves for 45mm diameter spherical button bit at 20 ⁰ index angle for various types of rocks	255
3.56(a-f)	Force–Penetration (F-P) curves for 45mm diameter spherical button bit at 30 ⁰ index angle for various types of rocks	256
3.57(a-f)	(a-f) Force–Penetration (F-P) curves for 45mm diameter spherical button bit at 40 ⁰ index angle for various types of rocks	257
3.58(a-f)	Force–Penetration (F-P) curves for 48mm diameter spherical button bit at 10 ⁰ index angle for various types of rocks	258
3.59(a-f)	Force–Penetration (F-P) curves for 48mm diameter spherical button bit at 20 ⁰ index angle for various types of rocks	259

3.60(a-f)	Force–Penetration (F-P) curves for 48mm diameter spherical button bit at 30 ⁰ index angle for various types of rocks	260
3.61(a-f)	Force–Penetration (F-P) curves for 48mm diameter spherical button bit at 40 ⁰ index angle for various types of rocks	261
4.51(a)	Relationship between Force-displacement of chisel, cross and spherical button bits of 48 mm diameter in two types of rocks	275
4.51(b)	Relationship between Force-displacement of chisel, cross and spherical button bits of 48 mm diameter in two types of rocks	276
4.51(c)	Relationship between Force-displacement of chisel, cross and spherical button bits of 48 mm diameter in two types of rocks	277
4.52(a)	Relation between density of rocks and displacement obtained in static indentation tests and FEM analysis for three bit geometries	278
4.52(b)	Relation between UCS of rocks and displacement obtained in static indentation tests and FEM analysis for three bit geometries	278
4.52(c)	Relation between abrasion resistance of rocks and displacement obtained in static indentation tests and FEM analysis for three bit geometries	279
4.52(d)	Relation between BTS of rocks and displacement obtained in static indentation tests and FEM analysis for three bit geometries	279
4.52(e)	Relation between Young’s Modulus of rocks and displacement obtained in static indentation tests and FEM analysis for three bit geometries	280
4.52(f)	Relation between Poisson’s ratio of rocks and displacement obtained in static indentation tests and FEM analysis for three bit geometries	280
4.52(g)	Relation between hardness (SRN) of rocks and displacement obtained in static indentation tests and FEM analysis for three bit geometries	281

LIST OF TABLES

Table No.	Description	Page No.
3.1	Details of parametric variations investigated	56
3.2	Values of force, penetration, crater volume and specific energy in static indentation tests for marble rock	69
3.3	Values of force, penetration, crater volume and specific energy in static indentation tests for limestone rock	71
3.4	Values of force, penetration, crater volume and specific energy in static indentation tests for basalt rock	73
3.5	Values of force, penetration, crater volume and specific energy in static indentation tests for steel gray granite rock	75
3.6	Values of force, penetration, crater volume and specific energy in static indentation tests for moon white granite rock	77
3.7	Values of force, penetration, crater volume and specific energy in static indentation tests for black galaxy granite rock	79
3.11	Sizes of sample with respect to Sieve size for abrasion test	81
3.12	Values of Schmidt hammer test	86
3.13	Physico-mechanical properties of Rocks	89
3.14	Mineral constituents of the marble sample	91
3.15	Mineral constituents of the limestone sample	93
3.16	Mineral constituents of the basalt sample	95
3.17	Mineral constituents of the steel gray granite sample	97
3.18	Mineral constituents of the moon white granite sample	99
3.19	Mineral constituents of the black galaxy granite sample	101
3.20	Elemental/ minerals in oxide form – X-Ray Fluorescence results	105
3.21	Analysis of Variance (ANOVA) of chisel bit model	109

3.22	Model Summary of chisel bit model	109
3.23	Coefficients of chisel bit model	109
3.24	Analysis of Variance (ANOVA) of cross bit model	110
3.25	Model Summary of cross bit model	110
3.26	Coefficients of cross bit model	111
3.27	Analysis of Variance (ANOVA) of spherical button bit model	113
3.28	Model Summary of spherical button bit model	113
3.29	Coefficients of spherical button bit model	113
4.1	Pearson's correlations between SE and selected rock properties	142
4.2	Regression Models' Summary of Chisel bit	144
4.3	ANOVA Results of Chisel bit	145
4.4	Significance of model components and confidence intervals of Chisel bit	146
4.5	Regression Models Summary of Cross bit	147
4.6	ANOVA Results of Cross bit	147
4.7	Significance of model components and confidence intervals of Cross bit	148
4.8	Regression Models' Summary of Spherical button bit	148
4.9	ANOVA Results of Spherical button bit	149
4.10	Significance of model components and confidence intervals of Spherical button bit	150
4.11	Pearson's correlation coefficients(SE with mineralogical composition)	158
4.12	Relationship between specific energy (chisel bit) and mineralogical properties	159
4.13	Relationship between specific energy (cross bit) and mineralogical properties	159
4.14	Relationship between specific energy (spherical button bit) and mineralogical properties	160

4.15	Pearson's correlation coefficients(SE with minerals/elements)	168
4.16	Relationship between specific energy (chisel bit) and elements/minerals in oxide form	169
45.17	Relationship between specific energy (cross bit) and elements/minerals in oxide form	171
4.18	Relationship between specific energy (spherical button bit) and elements/minerals in oxide form	172
4.19	Values of performance indices of regression models of all bits	178
4.20	Values of performance indices of ANN models of all bits	179
4.21	Comparison of Regression and ANN models of all bits	179
3.8	Specific energy values for chisel type 35, 38, 45, 48 mm diameters	262
3.9	Specific energy values for cross type 35, 38, 45, 48 mm diameters	263
3.10	Specific energy values for spherical button type 35, 38, 45, 48 mm diameters	264
4.22	Comparison of results of FEM analysis (ANSYS) with static indentation tests for all bit-rock combinations at the peak load in marble	266
4.23	Comparison of results of FEM analysis (ANSYS) with static indentation tests for all bit-rock combinations at the peak load in limestone	266
4.24	Comparison of results of FEM analysis (ANSYS) with static indentation tests for all bit-rock combinations at the peak load in basalt	267
4.25	Comparison of results of FEM analysis (ANSYS) with static indentation tests for all bit-rock combinations at the peak load in steel grey granite	267

4.26	Comparison of results of FEM analysis (ANSYS) with static indentation tests for all bit-rock combinations at the peak load in moon white granite	268
4.27	Comparison of results of FEM analysis (ANSYS) with static indentation tests for all bit-rock combinations at the peak load in black galaxy granite	268
4.28	Comparison of results of FEM analysis (ANSYS) with static indentation tests for twelve load steps	269
4.29	Comparison of results of FEM analysis (ANSYS) with static indentation tests for twelve load steps	270
4.30	Comparison of results of FEM analysis (ANSYS) with static indentation tests for twelve load steps	271
4.31	Comparison of results of FEM analysis (ANSYS) with static indentation tests for twelve load steps	272
4.32	Comparison of results of FEM analysis (ANSYS) with static indentation tests for twelve load steps	273
4.33	Comparison of results of FEM analysis (ANSYS) with static indentation tests for twelve load steps	274
4.34	Magnitude of depth of indentation and the distance along X, Y and Z-axes as obtained in FEM analysis for marble	282
4.35	Magnitude of depth of indentation and the distance along X, Y and Z-axes as obtained in FEM analysis for Limestone	283
4.36	Magnitude of depth of indentation and the distance Along X, Y and Z-axes as obtained in FEM analysis for Basalt	284
4.37	Magnitude of depth of indentation and the distance Along X, Y and Z-axes as obtained in FEM analysis for Steel grey granite	285
4.38	Magnitude of depth of indentation and the distance along X, Y and Z-axes as obtained in FEM analysis for moon white granite	286

4.39	Magnitude of depth of indentation and the distance along X, Y and Z-axes as obtained in FEM analysis for black galaxy granite	287
4.40	Magnitude of compressive stresses and the distance along X, Y and Z-axes as obtained in FEM analysis for marble	288
4.41	Magnitude of compressive stresses and the distance along X, Y and Z-axes as obtained in FEM analysis for Limestone	289
4.42	Magnitude of compressive stresses and the distance along X, Y and Z-axes as obtained in FEM analysis for basalt	290
4.43	Magnitude of compressive stresses and the distance along X, Y and Z-axes as obtained in FEM analysis for steel grey granite	291
4.44	Magnitude of compressive stresses and the distance along X, Y and Z-axes as obtained in FEM analysis for moon white granite	292
4.45	Magnitude of compressive stresses and the distance along X, Y and Z-axes as obtained in FEM analysis for black galaxy granite	293

NOMENCLATURE

SE	: Specific Energy
UCS	: Uniaxial Compressive Strength
BTS	: Brazilian Tensile Strength
SRN	: Schmidt Rebound Number
ISRM	: International Society for Rock Mechanics
ANN	: Artificial Neural Network
VAF	: Variation Account For
RMSE	: Root Mean Square Error
MAPE	: Mean Absolute Percentage Error
FEM	: Finite Element Method
XRF	: X-Ray Fluorescence
Al ₂ O ₃	: Aluminium Oxide
SiO ₂	: Silicon Dioxide
SO ₃	: Sulphur Trioxide
Cl	: Chlorine
K ₂ O	: Potassium Oxide
CaO	: Calcium Oxide

CHAPTER 1

INTRODUCTION

1.1 General

Minerals are one of the basic natural resources and are very much essential for economic growth of any country and are to be extracted economically from the bevels of earth by using the effective mining method(s).

Mining involves removal of earth material or waste rock called overburden and subsequent mining of the ore or mineral. The success of mining project depends on the excavation technology that we use to extract the mineral deposits from the earth's crust and the required technology for excavation varies with the properties of rocks to be excavated.

The forces and energy levels required to break the rock often vary with properties of rocks. The ease of excavating (excavatability) earth materials has to be assessed, so that earthwork can be planned and priced accordingly. Basic classification of rocks or rock mass is often not sufficient to justify the reasons for adopting specific excavation method. For hard rocks, in addition to rock mass classification, the properties that influence excavatability must be addressed (Legget and Hatheway, 1988). Different methods of excavation utilise different mechanisms to loosen or excavate a rock body, and various rock types exhibit different strengths against fracturing. (Amin et al., 2009). Therefore the phenomenon of fracturing of rocks with different mechanisms and tools has to be studied theoretically and experimentally to design the tools for mechanical excavation. Designing faster and efficient excavation systems and developing accurate and reliable performance prediction models would improve the success of mechanical mining (Copur et al., 2003).

In Rock excavation technology, the methods used to excavate the earth/rock materials are drill, Blast and mechanical excavation. There are only two essential types of mechanical

rock cutting tools, indenters and drag bits. In the drag bit, main force applied to effect rock breakage is in a direction approximately parallel to the rock surface whereas an indenter breaks the rock by applying a force, that is, in a direction normal to the rock surface. In drilling and mechanical excavation, breaking the rock by the penetration of indenter is the basic mode of action. The great majority of the rock cutting tools used today are indenters. All types of rolling cone bits, roller cutters-disk cutters, etc. break the rock in indentation process. Similarly, all types of percussive tools, including percussive drill bits, down-hole-drill bits, and high energy impact bits, induce rock fracture by indentation. Only rotary drill bits and picks, employed in coal excavation machines, break the rock or coal by applying the main force in a direction parallel to the rock surface (Hood and Roxborough, 1992).

Indentation is the fundamental process for rock excavation and fragmentation by using mechanical excavation methods and is necessary to investigate the basic deformation and failure mechanisms during the process of rock indentation (Kahraman et al., 2012). Knowledge of mechanisms of failures in rocks is an important basis for the study of mechanical excavation systems in rock engineering. Therefore, a better understanding of the rock fragmentation due to indentation by mechanical tools will help to improve the design and efficiency of rock excavation machines. Also, it is very much essential to know the process of indentation to assess the drill/cutting machine performance and also to know the strength of rocks for the suitability of drill/cutting picks for particular type of rocks (Zhang et al., 2012).

In order to study the rock failure mechanisms with indenter tools it is required to carry out indentation test. In this test, a small indenter is forced into the surface of material to be tested, under controlled conditions of load (stress regulated or strain regulated). Indentation tests have less stringent requirements on sample preparation and the testing equipment may be less sophisticated (Szwedzicki, 1998).

Drillability of rocks is one of the important parameters to decide the progress and drilling costs of the excavation. An accurate prediction of penetration rate/drillability of rocks helps

to make efficient planning of the rock excavation operations (Yarali and Soyer, 2011). Similarly, prediction of cuttability (resistance to cutting by mechanical tools) of rocks with different pick cutters and roller cutters helps in selecting and designing mechanical miners and predicting their performance, which is used for feasibility and planning purposes. The drillability and cuttability can be measured by laboratory/field drill tests, full-scale linear cutting tests, and some index tests requiring core samples, such as small-scale cutting tests, indentation tests, uniaxial compressive strength tests, Brazilian tensile strength tests, point load tests, etc.

Based on these tests, the specific energy (SE), a basic and fundamental parameter, which is energy required to excavate (or cut/ drill) a unit volume of rock and forces acting on drill bits/cutters are measured and/or predicted. Knowing these parameters helps in selecting and designing drills or mechanical miners and predicting their performance, which is used for feasibility and planning purposes (Fowell et al., 1976; McFeat-Smith, 1977; Roxborough, 1975; Ozdemir, 1977).

Similarly an understanding of rock properties is essential for proper design of drilling, cutting, crushing, excavation, breaking, grinding, and polishing operations. The processes cannot be defined in an absolute manner by a single index or measured by a single test. SE is a useful parameter in drilling, cutting, crushing, excavation and breaking (Ersoy et al., 2007). The properties that affect drilling are hardness, strength, elasticity, abrasiveness, plasticity, texture and structure of rocks (Jimeno, 1995).

From the above explanation, it is concluded that the indentation is the fundamental process in drilling and cutting operations and specific energy is an important parameter to know the performance of the drilling and cutting tools. Therefore, the present study is to investigate to assess the Specific Energy in indentation on various types of rocks by using commercial drill bits at different index angles aimed to know the influence of index angle

on specific energy and also to establish relationship between the specific energy and the properties of rocks.

1.2 Principle of indentation in rock drilling/cutting

Indentation is a simple and effective method for drilling and cutting of rocks. An indenter (bit) is driven more or less perpendicularly against the surface of the rock. The process involves i) compression of rock under loading ii) brittle fracture with formation of loose fragments and iii) ductile yielding, with displacement of broken material towards the free surface.

When the force is applied on the indenter, a stress field is developed in the rock material and also in indenter itself. The form and magnitude of the stress field in the rock material depends on the geometry of the indenter, stress distribution within that area and stress-strain characteristics. As the load increases on the indenter, the elastic stress increases in the rock material correspondingly but the deformation is small. On further loading, the elastic limit is reached and plastic yielding begins, the indenter starts to penetrate the rock.

The drilling or cutting operations progress by stepping the indenter (bit) to new location during the interval between successive blows (indexing) so that a series of indentations or craters is formed. If these craters are closely spaced then a continuous groove is formed.

1.3 Indentation test and its operating parameters

Rock indentation by a bit is a simple, effective and fundamental mechanism for most of the mechanical excavation methods. The indentation test is used to determine hardness of the rocks. This technique also can be used for assessing other rock properties such as drillability and cuttability. In rock indentation test, the test machine consists of a loading system, load measuring system and penetration measuring systems (Szwedzicki, 1998a).

The indentation test can be done either by depth-controlled or load-controlled methods. Depth-controlled indentation is done by setting the maximum depth of indentation value, whereas the load-controlled indentation is done by setting the maximum load (Ratiquil, 2010). Various types of indenter used for the test are wedge, cone, spherical, cylindrical and pyramid. Indentation tests have less stringent requirements on preparation of sample (Szwedzicki, 1998a). The operating parameters in the test are i) geometry of the indenter ii) diameter of the indenter iii) rate of loading/ strain rate

1.4 Specific energy in indentation

To reduce drilling time and cost, the development and application of a more efficient and lower cost drilling technology is necessary so that it makes drilling more economical in deep, hard rock formations. To achieve the greater rate of penetration (ROP), drilling engineers need to know the amount of energy required to excavate a unit volume of the various rock formation types encountered during the drilling process and a way of monitoring the energy being delivered to the rock by the drill bit (Okuchaba, 2008). Also the amount of energy required to cut a unit volume of the various rock is important to measure the cutting performance (Yurdakul et al., 2012).

Therefore, Specific Energy (SE), defined as the energy required to excavate a unit volume of rock, is a useful parameter in drilling, cutting, crushing, excavation and breaking of rocks. It may also be taken as index of the mechanical efficiency of drilling or cutting operation, to indicate drill bit or cutter conditions and rock characteristics such as strength, hardness, abrasiveness and texture (Ersoy et al., 2006).

The following formula used to calculate the specific energy.

1) S.E in drilling

$$S. E = \frac{T_r P_o}{\pi d^2 PR} \dots\dots\dots(1.1)$$

Where SE= specific energy, kg-cm/cm³

P_o = power output of drilling system, kg-com/min

d = diameter of bit, cm

PR = penetration rate, cm/min

$T_r = (0.7)$ transfer coefficient, i.e., the ratio of energy available for each blow

2) S.E in cutting

$$S. E = \frac{F_t V_p}{dW V_c} \dots\dots\dots(1.2)$$

Where

S.E = Specific energy (Nm/mm³)

F_t = Tangential Force (N)

V_p = Peripheral speed (m/s)

d = Cutting depth (mm)

W = Width of saw blade segments

V_c = Work piece traverse speed (m/s)

From the above two equations it is evident that, assessment of SE is important because it is a one of the parameters to determine drillability and cuttability of rocks.

Even though the initial concept of specific energy evolved in drilling, investigators (e.g. Teale) imagined drilling as an indentation process that crushes the rock and then produces small cuttings at the sides of the indenter after intense crushing. Therefore, specific energy is a useful concept in any indentation process.

1.5 Influence of specific energy on drillability

The concept of specific energy (SE) was proposed by Teale (1965) as a quick means of assessing rock Drillability. Teale defined S as the energy required to remove a unit volume of rock. However, another definition of SE, defined by Paithankar and Misra (1980) in terms of new surface are created. Teale indicated SE is inversely proportional to fragment size of rock excavated and that the minimum value of SE can be taken as a fundamental

rock property. Further, SE corresponds to the uniaxial compressive strength of rock irrespective of drilling process. However, Mellor (1972) has shown that SE is related to the uniaxial compressive strength (C_o) according to the relation:

$$SE \propto C_o \times 10^{-3} \quad \dots\dots\dots(1.3)$$

Paone, Madson and Bruce (1969), Schmidt (1972), Tandanand and Unger (1975) and Unger and Fumanti (1972), determined specific energy of a large number of rock types, assuming specific energy is independent of size and shape of drill bit, drill type, method of cutting, removal and depth of drill hole.

1.6 Influence of indexing on specific energy

Rotation of the bit (indexing) to furnish a new rock surface for each blow is essential for effective drilling, rotation is a consequence of the movement of the piston and causes a succession of fresh rock surfaces to be interacted at the bit-rock interface. The required rotation between blows for complete rock removal depends on the energy per blow, shape of the bit, and the properties of the rock. Too little rotation results in repeated blows near the same position and does not give the proper indexing to yield maximum chip size, and its results in inefficient drilling. . The specific energy of drilling at the bit-rock interface was found to be a function of rock properties and indexing angle (Rao and Misra, 1998).

1.7 Influence of rock properties on specific energy

A rock's specific drilling energy is influenced by a number of parameters, such as i) Rock strength ii) Rock stiffness iii) Presence of structural discontinuities iv) Abrasivity and hardness of the mineral constituents v) Nature of the rock matrix and vi) Nature of the mineral grain.

In mechanical excavation studies, some rock properties affecting the specific energy were investigated by different researchers (Paone *et al.*, 1969; Schmidt, 1972). But, the estimation of the cutting efficiency by using a single rock property is impossible since many rock properties affect the cuttability of rocks (Altindag, 2003).

1.8 Thesis Outline

To address the various issues discussed in the literature survey the thesis consists of five chapters.

Chapter –1

Introduction includes the types of bits mainly used for drilling and cutting, principle of indentation in rock drilling and cutting, indentation test and its operating parameters, specific energy in indentation, influence of specific energy on drillability, influence of index angle on specific energy and influence of rock properties on specific energy.

Chapter –2

Presents a comprehensive survey of literature on indentation of rocks and specific energy. It includes the factors governing the indentation test, F-P curves and index angle. It includes studies on specific energy, rock properties influencing the specific energy, studies on correlation of specific energy with operational parameters and properties of rocks, studies related to application of ANN in rock mechanics and studies related to Numerical modelling (Finite element method analysis) used in indentation process.

Chapter –3

Experimental investigations like static indentation test to determine specific energy, tests to determine the physico-mechanical properties of rocks, tests to determine the mineralogical composition (thin section studies), and XRF tests to determine minerals in oxides form. Investigations to develop regression models and Artificial Neural Network (ANN) models to predict the specific energy from properties of rocks and operational parameters of indentation test, Numerical modelling (FEM analysis to determine the depth of penetration by indenters during indentation and analysis and analysis of stresses developed in rocks during indentation.

Chapter –4

Results and discussion: Investigation on the influence of index angle on specific energy, influence of rock properties on specific energy, influence of mineralogical composition on specific energy, influence of minerals in oxide form on specific energy, Comparative studies and analysis of regression and ANN models to predict specific energy from operational and rock properties. Numerical modelling (FEM analysis to find the depth of indentation in various rocks and stress distribution in all the axes (X, Y and Z- directions).

Chapter –5

Presents the summary of conclusions on the investigations carried out in this research work and also included further recommendations addressing various issues for the future work.

CHAPTER 2

LITERATURE REVIEW

The literature presented in this section is divided into six main parts.

2.1 Studies on Indentation

2.1.1 Introduction

Rock indentation by a bit is a simple, effective and fundamental mechanism for most of the mechanical excavation methods. The indentation test is used to determine hardness of the rocks. This technique also can be used for assessing other rock properties such as drillability and cuttability. In rock indentation test, the test machine consists of a loading system, load measuring system and penetration measuring systems (Szwedzicki, 1998).

In rock indentation, the indenter is forced into the rock in a direction more or less perpendicular to the surface of the rock. The rock portion near the indenter is initially crushed into small fragments leaving subsurface cracks in the remaining rock. The mechanics of rock failure under and around an indenter is a complicated function and depends on physico-mechanical properties mainly elastic properties of rocks. The zone which is disturbed around the indenter is important, since the penetration of the indenter is directly related to the efficiency of the indenter and the distribution of cracks under the indenter influences the stability of the remaining rock (Kou et al., 1998).

Therefore it has been a subject that has attracted much attention since 1960 when Gnirk and Cheatham (1965) made an experimental study on single-tooth penetration into dry rock at confining pressure (Kou et al., 1998). However, the main research works which we found started from the 1970s. Among them are those carried out by Maurer(1967), Simon(1967),Wagner and Schumann (1971), Nishimatsu (1972), Sikarskie and Altiero (1973), Lindqvist (1982), Kumano and Goldsmith (1982), Cook et al. (1984), Pang and

Goldsmith (1990), Hood (1993), Lindqvist et al. (1994), Kou et al. (1995), Mishnaevsky (1995); Alehossein and Hood (1996) and Tan (1996).

Some of the researchers explained a qualitative description of the indentation process; others propose physical mechanisms and behaviour under the indenter based on mathematical models relying on some hypotheses about material. Such relationships are then compared to experimental results obtained for different types of indenter (wedge, cone, sphere, and pyramid) or disc cutters and for different rock types (Paul and Siskarskie, 1965; Miller and Siskarskie, 1968; Lundberg, 1974; Gill et al., 1980; Kou et al., 1995). Finally, some researchers try to establish a correlation between some kinds of index obtained from indentation tests to mechanical properties (uniaxial compressive strength, in general) obtained from conventional tests (Leite et al., 2001).

2.1.2 Studies on indentation concerned to mechanism of rock fracture/ failure

A number of theoretical studies of bit penetration into brittle materials have been published which have their origin in the wedge penetration model developed by Paul and Sikarski (1965). Some of the explanations are based on tensile fracturing, shearing, elasticity theory and on the plasticity theory (Copur et al., 2003).

The studies of crater formation under an indenter were studied by Maurer (1967) who identified the following distinct phases:

1. Crushing of surface irregularities and elastic deformation.
2. Extension of crushing zone beneath an indenter.
3. Formation of chips.

The main stages of rock fragmentation during indentation process under the indenter are crushing and chipping. The physical mechanism of crushing zone formation has been investigated by researchers (e.g. Kutter and Sanio, 1982; Sanio, 1985; Nelson et al., 1985; Fowell, 1993; Kou et al., 1995; Tan et al., 1996; Alehossein et al., 1996). The efficiency of the mechanical breakage depends on the ability to initiate and propagate fractures in the

rock during indentation. The lateral confining pressure influences the development of the damages rock under the tool and on the condition of initiation of tensile fractures. The mechanism of chipping induced by indentation has been the subject of many investigations in the last two decades. In the absence of confinement, models that contain the essential elements observed in the indentation of brittle materials appear to have been first developed in the 1970's by Lawn and his colleagues, who were motivated by the problem of indentation of ceramics (Lawn and Fuller, 1975; Lawn and Swain, 1975; Lawn and Marshall, 1979; Lawn and Wilshaw, 1975; Lawn and Evans, 1977). These studies considered the development of a plastic zone under the indenter and the propagation of a vertical crack, which initiates at the elasto-plastic interface (Huang, 1998).

Experimental studies of rock indentation (e.g., Kou et al., 1995; Chen and Labuz, 1998) have been carried out using a technique, acoustic emission (AE). These indentation studies have confirmed that the rock, initially, undergoes crushing due to compression, later rock follows initiation and propagation of tensile fractures. The AE events recorded during indentation tests in rocks (such as charcoal granite, norite and quartzite) indicated that, in the absence of confinement, formation of the inelastic zone is followed by the initiation and propagation of a deep-seated vertical crack (Chen and Labuz, 1998). The AE events also showed that development of the damaged zone is constrained by lateral confinement. Further AE events showed that lateral (sub-horizontal) cracks are initiated instead of vertical cracks. Observations from many experiments with various types of indenters led to the conclusion that two major types of cracks initiated in the vicinity of the crushed zone during loading are: (i) deep-seated vertical cracks and (ii) lateral or sub-horizontal cracks. Experimental observations also showed that rock chipping was caused by lateral or sub-horizontal cracks, and not by vertical cracks (Huang, 1998).

The rock fracturing phenomenon given by Kou et al., 1998 that when a force was applied on indenter during rock indentation process, a stress field was developed in rock material and in the indenter itself. The form of the stress field in the rock depends on the geometry

of the contact area, distribution of pressure within that area and stress-strain characteristics of the rock. The increasing load caused the closing of the pre-existing flaws in the rock at the beginning, followed by elastic deformation of the rock surface. Thereafter crushed and cracked zones were formed. In this stage, dilatation and movement of the rock fragments in the crushed zone are restrained by the surrounding intact rock. In order to break the rock, the force was further increased. This caused intense comminution of the rock fragments and the comminuted rock in the crushed zone was then partly re-compacted under the combined action of the lateral confinement and the normal stress caused by the indenter. The moving and dilating tendency of rock fragments in the crushed and cracked zones have pushed the surrounding rock outwards. During the process of rock fracturing the indenter was gradually penetrated into the rock. When the side cracks reach the rock surface, the surrounding rock was quickly moved away forming the so-called chips. At that moment the strain energy stored in the rock will convert into the kinetic energy of the rock chips, so that they move away rather at a high speed. The force acting on the indenter at this moment was reduced suddenly to a lower value within a short time. Again on increasing load the bit penetrated corresponding to the loads applied (Kou et al., 1998).

Closure:

Therefore it can be concluded that there are different theoretical explanations for the mechanism of rock breakage with different types of indenters. In all of the explanations, there are similar mechanisms: a crushed zone is formed in the rock due to the high compressive stress concentrations generated by the indenter, tensile hoop stresses occur in the perimeter of the crushed zone. If the rock is brittle, hoop stress creates tensile cracks or fractures propagating outwards or towards the adjacent cutting lines. If the two cracks from adjacent indentations meet, the ridge so formed between the cut lines is removed. In the case of ductile failure, shear fractures play a major role. In reality, the mechanical rock breakage process includes, to varying degrees, tensile and shear types of failure modes, depending on rock properties, indenter and cutting geometry.

2.1.3 Studies on indentation to correlate the indentation indices with mechanical properties of rocks

The indentation test, is used to measure rock's surface hardness (Hamilton and Handewith 1970; Dollinger et al. 1998; Szwedzicki 1998 a; Yagiz and Ozdemir 2001; Yagiz 2002). It can be also used to estimate some properties of rock such as brittleness, toughness, cuttability and drillability of rocks (Cook et al. 1984; Dollinger et al. 1998; Yagiz 2002, 2006, 2008a, b; Copur et al. 2003).

The first indentation test apparatus was designed by Hamilton and Handewith (1970) and built by the Lawrence Manufacturing Company in Seattle, Washington, USA (Dollinger et al. 1998; Yagiz 2002). A description of this test apparatus with the test procedure is included in a paper presented by Handewith in (1970). The test was intended to provide a direct method to estimate the normal loads on disc cutters in mechanical excavation of rock. Szwedzicki (1998 a, b) stated that the indentation hardness index (IHI) can be computed by using the first elastic-linear phase of the force penetration profile as follows.

$$\text{IHI (kN/mm)}=L/P \quad \dots\dots\dots(2.1)$$

In his approach, at the first deviation from linear behaviour, the peak load (L) and corresponding penetration (P) are taken to calculate the hardness index. He also developed the relationship between uniaxial compressive strength (UCS) and IHI as given in equation 2.2.

$$\text{UCS(MPa)}= 3.1 \times \text{IHI}^{1.09} \quad \dots\dots\dots(2.2)$$

Yagiz (2002, 2006, 2008a, b) stated that the test can be used for investigating the brittleness and toughness behaviour of rock under the indenter or cutters as the test has three distinct phases in the force-penetration curves which represent various rock properties (i.e.

drillability, brittleness, toughness, hardness). As result, the brittleness index (BI) was computed by Yagiz (2002) using the slope of the entire phase of the force-penetration profile, obtained by drawing a line from the origin to the maximum applied force at the end of the test, given as;

$$BI(kN/mm) = F_{max}/P \quad \dots\dots\dots(2.3)$$

In this method, F_{max} is the maximum applied force on the rock sample in kN, and P is the corresponding penetration at maximum force in mm. Yagiz (2008) also gave a rock brittleness classification based on the force-penetration profile and the index introduced. Further, the equation for predicting the rock brittleness was developed as a function of UCS, Brazilian tensile strength (BTS) and rock density (Yagiz, 2008b).

$$BI(kN/mm) = 0.198 UCS - 2.174 BTS + 0.913 p - 3.8 \quad \dots\dots\dots(2.4)$$

Likewise, Copur et al. (2003) determined a set of brittleness indices (BI) computed from the count of increment and decrement data points on the force-penetration force-penetration profile. He stated that the indentation test could be used for investigating brittleness, which is one of the most crucial rock properties for predicting borability (Yagiz, 2009).

$$BI = k(m+k) \quad \dots\dots\dots(2.5)$$

In his equation, k is the total number of force increment points and m is the total number of force decrement points on the force-penetration graph. The testing procedures described in the literature were often developed for specific purposes but do not specify certain rock conditions or properties (Hamilton and Handewith 1970; Deketh et al. 1998; Dollinger et al. 1998; Szwedzicki 1998a, b; Yagiz 2002; Copur et al. 2003; Yagiz 2006, 2008a, b, Yagiz, 2009).

The hourly production in diamond sawing is estimated by carrying out indentation test on the rocks and the indentation hardness index values have been correlated with the hourly production in diamond sawing (Kahraman et al., 2008). A linear inverse relationship was found between hourly production and IHI value. The equation of the line is

$$P_h = -0.067 \text{ IHI} + 18.93 \quad r^2 = 0.77 \quad \dots\dots\dots (2.6)$$

Where P_h is the hourly production (m^2/h), IHI is the indentation hardness index (kN/mm) The prediction of UCS and BTS of rocks from indentation test is possible by correlating with IHI. The prediction of rock properties like UCS and BTS from indentation test is economical particularly for preliminary investigations (Kahraman et al., 2012). A good linear correlation between the IHI and UCS and BTS was found. The equation of the line is

$$\text{UCS} = 0.07 \text{ IHI} + 28.28 \quad R^2 = 0.76 \quad \dots\dots\dots (2.7)$$

Where UCS = Uniaxial Compressive Strength (MPa), IHI is the indentation hardness index (kN/mm)

$$\text{BTS} = 0.07 \text{ IHI} + 3.79 \quad R^2 = 0.58 \quad \dots\dots\dots (2.8)$$

where BTS= Brazilian Tensile Strength (MPa).

A brittleness index obtained by indentation test as a multiplication of uniaxial compressive strength and Brazilian tensile strength, indicated a correlation between the index and performance of percussive and rotary blast hole drilling (Altindag, 2002, 2003); he also stated a correlation between the coarseness index of rock cuttings and performance of percussive drilling.

The correlations between indentation modulus (IM, which is a ratio of change in load to the change centre in proportionality zone of load vs penetration curve of indentation test) and mechanical properties of sand stones are developed by Jefferson et.al, 2007 as follows.

$$\text{UCS} = 17.38 \times \text{IM} \quad R^2 = 0.82 \quad \dots\dots\dots(2.9)$$

Similarly, the correlations between critical transition force (CTF, load level wherein the rock loses its linear behaviour in load vs penetration curve of indentation test) and mechanical properties of sand stones are developed by them as follows.

$$\text{UCS} = 91.97 \times \text{CTF} \quad R^2 = 0.70 \quad \dots\dots\dots(2.10)$$

In the same manner, Haftani et al., (2014), developed correlation equations by linear regression and exponential regressions between indentation modulus (IM) and mechanical properties of Lime stone rocks as follows

$$\text{UCS} = 0.20(\text{IM}) - 226.21 \quad R = 0.91 \quad (\text{Linear Regression}) \quad \dots\dots\dots(2.11)$$

$$\text{UCS} = 3.32 e^{0.0019(\text{IM})} \quad R = 0.97 \quad (\text{Exponential Regression}) \quad \dots\dots\dots(2.12)$$

Similarly, they developed correlation equations by linear regression and exponential regressions between critical transition force (CTF) and mechanical properties of Lime stone rocks as follows

$$\text{UCS} = 0.48(\text{CTF}) - 19.36 \quad R = 0.74 \quad (\text{Linear Regression}) \quad \dots\dots\dots(2.13)$$

$$\text{UCS} = 20 e^{0.0049(\text{CTF})} \quad R = 0.85 \quad (\text{Exponential Regression}) \quad \dots\dots\dots(2.14)$$

The ductile rocks showed relatively flatter (smoother) force-penetration curves in macro-scale indentation tests (Dollinger, 1977). The correlation analysis of indentation test indices with rock properties is helpful for in-situ calibration of the geological models since the indentation test can be performed in real time, thus reducing costs and time associated with delayed conventional characterization (Mateus et al., 2007).

Closure: It can be concluded that by correlating the indentation indices with properties of rocks, indirect estimation or prediction of certain properties without conducting the direct tests can be determined.

2.2 Studies on Force-Penetration curves

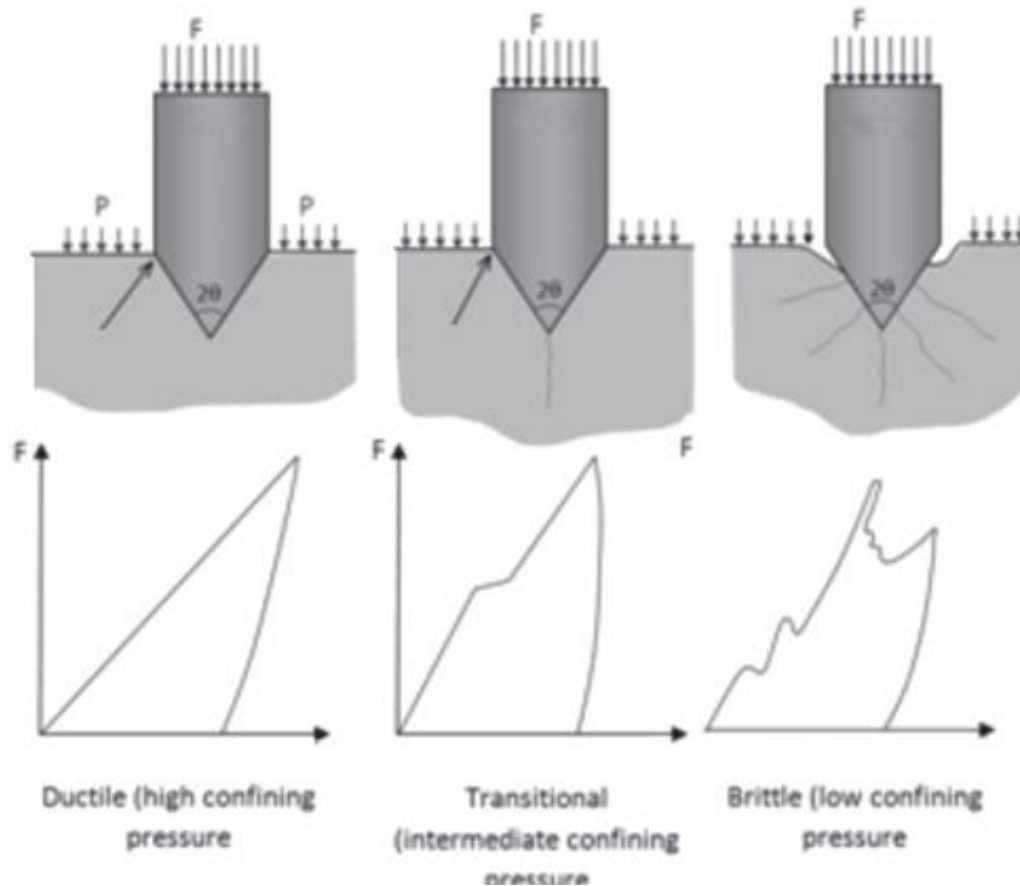


Figure 2.1 Different types of Force-Penetration curves and the associated macroscopic models of rock failure for single sharp bit indentation (Gnirk and Cheatham, 1967)

In indentation test, when load is applied on the indenter at external confining pressures, the material under an indenter will usually exhibit brittle response to some extent, if it is a non-metallic substance. As the force further increases and the indenter penetrates, there is likely to be a series of fractures that produce chips and develop a crater by a discontinuous process. If the brittle rock is being loaded, it yields relatively more fluctuated force-

penetration due to chipping, and less fluctuation for more ductile rocks. The general pattern of the force-penetration graph depends partly on the micro (texture, grain geometry, matrix material) and macro (strength, elasticity) properties of rocks, partly on the compliance of the loading system and also on geometry of indenter (sharpness, shape, dimension), and some environmental parameters (type of loading, temperature, confinement amount and material, data sampling rate).

In addition to the authors cited above, Paul and Sikarski (1945) and Miller and Sikarski (1969) mentioned the importance of force increase (increment) rates based on their experimental and theoretical studies.

With real loading systems, the indenter might be pushed into rock by a hydraulic arrangement, while the applied force is measured by a load cell. However, in some experiments some odd features may be produced in test records due improper control on the rate of penetration or the rate of loading. For example, some records show reversal of penetration after each yield, probably because the indenter is backed off each time, or because displacements are not being measured directly between the indenter and the target material.

The force-penetration curve drawn through the peaks of indentation of brittle materials record perhaps ought to show similar trends to the force-penetration curves for ductile material. Linear force-penetration curves have been accepted as good approximations for a number of materials subjected to both ductile and brittle penetration by wedges and spheres. These materials include Indiana limestone (Pariseau and Fairhurst, 1967; Benjumea and Sikarskie, 1969; Hustrulid F and Fairhurst, 1971), Berea sandstone and Carthage marble (Gnirk, 1966; Cheatham and Gnirk, 1967), Solenhofen limestone (Paone and Tandanand, 1966), Tennessee marble (Pariseau and Fairhurst, 1967) and wide variety of other rocks (Dollinger, 1977).

Nonlinear force-penetration curves have been recorded for penetration of cones into granite and limestone by Miller and Silkarskie (1968), and into granite by Lundberg (1974) which led to the expectation that force would be proportional to the square of penetration depth, and results were in reasonable agreement with the expectation. The slope of a linear force-penetration curve is sometimes called a "penetration index"; it is usually designated by the symbol K , and has dimensions force/length.

A hypothetical F-P curve was generated by Copur et. al (2003) to express their ideas about quantification of the force-penetration response. They have stated that force increments take certain periods and a force increment period is followed by a force drop (or force decrement period) due to chipping. If a rock is more prone to breakage that shows brittle characteristics, it might break frequently and violently after taking mostly elastic and some plastic deformation. The increment periods (or the number of incrementing points for a certain indentation penetration) of a brittle material might be shorter than a ductile material. If a rock possess ductile characteristics, it would not break frequently and it would take mostly plastic and some elastic deformation, and its increment periods might be longer. The increment and decrement periods (or the number of incrementing and decrementing points) might vary depending on the size of the chips, cracks and crushed zone and the violence of the breakage. The larger chips and disturbance of the crushed zone due to violence of the chipping might increase the decrement periods. Based on these, it can be concluded that the percentage of the incrementing (or decrementing) data points on the total data points in the indentation test might be a measure of the breakage characteristic of the rocks (Copur et. al 2003).

Closure: It can be concluded, based on all these studies, that the shape of force-penetration response might be considered as an indicator of rock breakage characteristics.

2.3 Studies on factors affecting indentation process

2.3.1 Influence of static, quasi - static load and dynamic load

A static load is a force applied slowly to an assembly or object whereas dynamic load is a force that is applied rapidly. A static load is time independent. A dynamic load is time dependent and inertial effects should be considered. A quasi-static load is time dependent but is "slow" enough such that inertial effects can be ignored. Note that a load quasi-static for a given structure (made of some material) may not be quasi-static for another structure (made of a different material). Tests of static load are useful in determining the maximum allowable loads on engineering structures, and they can also be useful in determining the mechanical properties of materials (Yavari and Arash, 2011).

In static indentation the word "static" or "quasi-static" implies that the time of response of rock indentation is not considered. In this case, the strain rate effects of the strength and the density of the rock, ρ , namely the inertia, have no influence on the results. In case of dynamic or impact indentation the time response of rock indentation is to be considered (Kou, 1998).

The advantage of a static loading is that the details of the formation of the crater can be observed and recorded (Miller, et al., 1968).

2.3.2 Influence of rate of loading or strain rate of penetration

Indentation experiments are conducted under static and dynamic loading conditions. The static results can be a good approximation to the practical cases. This was confirmed by Evan and Wilshaw (1977). The advantage of static loading is that the details of the penetration of the crater can be observed and recorded easily (Miller et al., 1968). In case of dynamic loading conditions, indenter completes their penetration very rapidly. The rate of loading (kN/sec) or strain rate (mm/sec) influences, the force-penetration relationship.

Many researchers used strain rate in rock indentation ranging from 0.0025 to 0.01 mm/sec. Szwedzicki (1998) has stated in draft ISRM suggested method for determining the indentation hardness index of rock materials that the rate of loading is 0.05 to 0.15 kN/sec.

2.3.3 Influence of indenter geometry

The geometry of the indenter in indentation is an important factor that influences the distribution of stress in the rock and leads to different rock responses and failure mechanisms (Thiercelin and Cook 1988). There are two broad varieties of indenters namely sharp and blunt indenters. Cone, wedge, pyramidal indenters are sharp indenters whereas spherical and cylindrical indenters are blunt indenters. Researchers used different indenters to study the rock breakage mechanism under the indenters and also to find the indentation index used to correlate indentation index with properties of rock. Miller and Sikarskie (1968) used conical, spherical and pyramidal indenters in indentation test with an objective to study the specific energy and crushing, chipping characteristics of indenters. They compared and concluded that sharper cone is the best following the order of success pyramid and sphere. Further, they concluded that compared to sharper indenters, a spherical indenter button bit might perform better in hard rock than in soft rocks and in agreement with results of Hartman (Miller et al., 1968).

Alehossein and Hood (1996) carried out experiments on Hart court granite by a spherical indenter. Alehossein et al.(2000) developed analytical model and compared it with experimental data. A good agreement was shown between the theoretical indentation pressures and experimental values, and he concluded that the behaviour of the indentation pressure is highly nonlinear as a function of the scaled penetration depth.

Similarly, Kahraman et al.,(2000) carried out indentation tests using conical and spherical bit tooth indenters. They concluded that when the rock properties are constant, the drillability (force/penetration) of the spherical bit-tooth is greater than conical bit.

Zhlobinsky (1970) concluded that the rock fragmentation proceeds most intensively when hard brittle rock is loaded by spherical indenter, the hard plastic rock does by conical and weak rock does by wedge-shaped indenters.

Blokhin V.S. (1982) has shown the difference between the rock fragmentation under the indentation of spherical and cylindrical bits. The indentation of spherical bit showed that the cracks are initiated in the centre of contact surface (not on the contour of contact surface). The spherical button is effective for hard rocks, the prismatic bits are more effective for hard, viscous, non-cracked rocks, the cylindrical does for cracked, brittle and weak rocks.

Cook et al., (1984) and Magnenet et al. (2009) used flat-end indenters, Santarelli et al., (1996) and Ringstad et al., (1998) used flat-end indenters. Zausa and Satarelli (1995) used a spherical indenter, Brooks et al. (2010) employed a diamond indenters in indentation. All these experiments were carried by these researchers to correlate the indentation index with uniaxial compressive strength of rock. These investigations resulted in different correlation equations which were affected by the different procedures (Haftani, 2014).

2.3.4 Influence of Index angle

In percussion drilling reciprocating motion is imparted to the drill rod attached with a drill bit. The raising and dropping of drill bits on the rock results in chipping and the broken materials are removed by flushing with compressed air to form the hole. Between successive strokes the drill rod is rotated, which is called Indexing, and is essential to create proper shape and favourable down hole environment (Hartman, 1966).

The interaction of a bit tooth at a new surface with a previously formed crater is referred to as indexing. When an insert is loaded adjacent to a previously performed crater, the tensile fracture generally progresses towards its direction and chip breaks into the crater.

Indexing is more efficient because of the reduced proportion of crushed material formed per unit volume of broken rock. The optimum indexing distance may be as great as five times the penetration depth. Gnirk and Cheatam (1965) found that the optimum indexing distance was related to the insert and the penetration depth. This is (of important) in determining the optimum spacing of individual insert on a roller bit and for the selection of the tooth angle for various rock types (Lebel, 1984).

The objective of drilling is to achieve a larger average volume of crater per impact blow of the drilling tool (Hartman, 1966). The indexing provides new surface at the bottom of the hole at each blow. This action helps in achieving a larger volume of crater per impact. Hartman and Gnirk (1966) and other researchers studied the influence of indexing and the influence of adjacent craters on each other in rock drilling.

Hartman, 1966, focused investigation on the mechanics of indexing and its relation to the drilling operation. He has concluded that (i) in rock drilling with impact (percussion and roller-bit) tools, indexing does not play a major role in affecting the drilling process or in influencing drill performance, e.g. rate of penetration. (ii) Single-crater volume measurements by drop tester are proposed as a reasonable guide to rock drillability.

Gnirk, (1966) carried out an experimental study of indexed single bit-tooth penetration into dry rock at confining pressures of 0 to 7500 psi. He stated that the optimum distance between successive bit-tooth penetrations required for maximum rock damage and chip formation decreases substantially with increasing confining pressure above the brittle-to-ductile transition pressure of a particular rock, however, the distance remains approximately constant for a variation in confining pressure below the transition pressure. He further stated that at a given confining pressure, the bit-tooth force required for chip formation is constant for indexing distances greater than optimum, but generally decreases linearly with decreasing indexing distance for distances less than optimum. Specifically, the optimum or minimum distance between successive penetrations required for maximum

interaction or chip generation tends to decrease with decreasing bit-tooth angle and increasing differential pressure.

For efficient drilling with single or multiple type cutting wedges, the bit must rotate as each blow is applied to the drill rod. If the bit is not rotated, a groove is broken in the rock and chipping and penetration cease after a few blows. Rotating of the bit presents a new surface to the bit for each blow, causing chipping, crushing and consequent penetration. For the angular indexing that occurs in percussive and rotary-percussive drilling in a borehole, it has been found that the angle of indexing between each blow of a percussive hammer is not critical. In an operating drill it is probable that, although the rotating mechanism provides for a relatively constant revolution of the steel for each blow, there are many factors that could cause the indexing angle to vary, such as resistance to rotation, effects of reflected stress waves in the rod, inertia of rotating parts, and rock defects (Rao and Misra, 1998).

When these and related factors are considered it is logical that there should be a range of indexing angles at which the cutting edges of the bit will impact on ridges or new surfaces in the bottom of the drill hole. The grooves are usually shallow enough that a second impact on a groove will chip out additional rock. At a given energy to establish the relation between depth per blow and indexing angle many investigations have been carried out. From these tests, the inference drawn is that the optimum indexing angle is a function of: (1) impact energy and bit diameter or, more precisely, a function of energy per unit length of bit cutting edge, and (2) the rock properties (Rao and Misra, 1998).

Paithankar and Misra (1976) found that percussive drillability of rock from small-scale laboratory tests does not correlate well with the measured 'standard' physical properties. They performed full-scale drillability tests in five different rocks - basalt, granite, soda granite, limestone and dolomite-and compared these rates with those from laboratory tests with a microbit. The apparatus consisted of a W_c (tungsten carbide) micro-

bit of 110° wedge angle, 10 mm diameter, impacted by a drop weight, giving 0.14 kg-m energy. In the study, it was assumed that all of the impact energy was transmitted to the rock. The cuttings were removed after each blow to avoid regrinding, and the volume of cuttings was measured to determine the specific energy. The specific energy of drilling at the bit-rock interface was found to be a function of rock properties and indexing angle (Rao and Misra, 1998).

Closure: The study of factors like static load, rate of loading, influence of loading, indenter geometry etc. affecting indentation process is important to design the static indentation tests. Similarly the index angle important parameter which influence the rate of drilling in percussive drilling. It can be concluded that the indentation tests can be easily measurable and recordable if we use static loading since the rate of loading or rate penetration is small. Further it is concluded that designing certain index angle to percussive drills for the properties of rocks is critical.

2.4 Studies on Specific Energy

2.4.1 Introduction

Drilling is a prime operation in the mining without which exploration, development, and exploitation of ore bodies or mineral deposits could not succeed (Tatia, 2004). The drillability of the rocks mainly depends on operational parameters and characteristics of rocks. Operational parameters are controllable parameters like rotational speed, thrust, blow frequency and flushing and properties of rock influence the drillability of rocks. An accurate estimation of rate of drilling (drillability) helps to make more efficient planning of the rock excavation projects (Kahraman et al., 2003). The cost of drilling and time are important factors for the success of drilling operation. The choice of cutting and drilling methods and their implementation economically depend to a large extent on the quality and quantity of the rock (Becker et al., 1984). To reduce drilling time and cost, the development and application of a more efficient and lower cost drilling technology is necessary so that

it makes drilling more economical in deep, hard rock formations. To achieve the greater rate of penetration (ROP), drilling engineers need to know the amount of energy required to excavate a unit volume of the various rock formation types encountered during the drilling process and a way of monitoring the energy being delivered to the rock by the drill bit (Okuchaba, 2008).

The prediction of the cuttability/sawability of natural stones is very important in cost analysis and production planning. Determining the proper cutting parameters, physico-mechanical and mineralogical–petrographical characteristics of the rock to be cut plays an important role in cost analysis, product quality, production planning, and the selection of an appropriate machine-equipment for the stone to be cut and also the amount of energy required to cut a unit volume of the various rock is important to measure the cutting performance (Yurdakul et al., 2012).

Therefore, Specific Energy (SE), defined as the energy required to excavate a unit volume of rock, is a useful parameter in drilling, cutting, crushing, excavation and breaking of rocks. It may also be taken as index of the mechanical efficiency of drilling or cutting operation, to indicate drill bit or cutter conditions and rock characteristics such as strength, hardness, abrasiveness and texture (Ersoy et al., 2007).

The drilling specific energy (SE_{drill}) and the cutting specific energy (SE_{cut}) are very significant measures of the drilling and cutting performance since they indicate the amount of energy required to cut the rock and are directly compatible cost per meter. These can also be used to quantify the efficiency of rock working (cutting, drilling, excavation, breaking, etc.) operations (Atici et al., 2009). In practice, specific energy is a useful parameter to estimate the energy requirements for a particular cutting operation (Atici, et al., 2007, Falcao, et al., 2012).

To determine the economics of a mechanized mining and/or tunnelling operation, the main concern is prediction of the excavation performance of any mechanical excavator such as

continuous miners, roadheaders and shearers for any geological formation. The specific energy is used to predict the performance of mechanical miners (Balci et al., 2004; Acaroglu et al., 2008).

Ripping is a method used to excavate rocks that are relatively weak to be blasted but, too strong to be removed by excavator. The degree of difficulty to rip a rock which can be evaluated in laboratory by specific energy, represents power required to rip a given volume of the rock sample. Specific Energy can be used as indicator for degree of difficulty to rip a rock mass in the field (Amin et al., 2009).

SE is highly dependent upon the mode of rock breakage, and the size and nature of the equipment for breaking used. There are many ways of determining specific energy but results are only comparable if the drill or apparatus is the same. A number of factors influence specific drilling energy in relation to the rock type and the drilling apparatus (Reddish, 1996).

2.4.2. Studies on specific drilling energy

Teale, initially proposed the concept of specific energy (SE) in rock drilling in 1965. He derived the equation for specific energy by determining the torsional and axial work done by the bit and dividing it by the volume of rock drilled. Teale concluded that the energy per volume of rock drilled to be relatively constant, regardless of changes in rate of penetration (ROP), weight on bit (WOB) or revolutions per minute (RPM). Teale noticed that laboratory drilling data showed the SE value to be equal to rock compressive strength, the SE cannot be represented by a single and accurate number due to the heterogeneity of the rock formations and the fluctuations of the drilling variables. He concluded that concept specific energy is useful because it provides a reference point for efficiency. The value of SE changes as the lithology changes. Teale's specific energy concept of 'Mechanical

Specific Energy' (MSE), has been used for determining the efficiency of drilling for drill bit designs and in specialized drilling field applications.

Pessier and Fear (1992) gave an improved solution for MSE and derived an equation for ROP based on the specific energy equation derived by Teale. They modified Teale's specific energy model by substituting an equation they derived, that expresses torque as a function of WOB, bit diameter and a bit-specific coefficient of sliding friction. They showed that under atmospheric drilling conditions the MSE is approximately equal to the UCS of the formation drilled and that when drilling under hydrostatic pressure the mechanical efficiency which is the inverse of specific energy, dropped significantly. Their analysis of field data revealed a good correlation between their field results and simulator model.

Waughman *et al.*(2002), developed an approach that real-time monitoring of specific energy data in combination with drilling data and sonic data, so that the decision process of when to pull the bit out of hole. They outlined a guide on application of specific energy monitoring technique to the field. The concept has been proven to work in synthetic based mud systems and water based mud treated with anti-balling chemicals.

Apart from the above research numerous publications related to application of specific energy concepts as a basis for bit selection and performance; however Curry *et al.*(2005), apply specific energy as an index to facilitate drilling performance evaluation. Curry *et al.* introduced a method to represent the difficulty of drilling a particular formation in its down-hole pressure environment using the concept of mechanical specific energy. They developed an algorithm to assess the technical limit of specific energy, from wire-line sonic, lithology and pressure data. They concluded that, the technical limit of specific energy represents the lowest specific energy that can be reasonably expected for a particular combination of rock properties and air pressures.

Dupriest and Koederitz (2005) adopted Teal's specific energy equation in present drilling units and arrived at a new model for mechanical specific energy. It was used in a drilling information system for mud drilling and has been implemented successfully on different rigs. They demonstrated the usefulness of MSE through practical field application. They also showed that bit hydraulics, though not incorporated in the MSE equation, had a noticeable influence on MSE and ROP.

Chiang and Izquierdo (2004) adopted the down-the-hole pneumatic hammer dynamic model developed by Chiang and Stamm (1998) in their research work. They developed a methodology to assess the instantaneous specific rock energy using corrected down-the-hole (DTH) drill monitoring data. Consequently, they were able to generate a specific rock energy profile for every hole drilled and thus mapping an entire drilling site for this index. They stated the development procedure for a special data acquisition system used to measure and register operational variables that are inputs for two simulation models that estimate the power absorbed by the rock through impact and then the specific rock energy index. Correlations were found between the specific rock energy and impact frequency, as well as between the rate of penetration and applied torque and between the rate of penetration and impact frequency.

2.4.3 Studies on specific cutting energy

The prediction of performance of any mechanical excavator such as continuous miners, roadheaders and shearers for any rock formation is one of the main concerns in determining the economics of a mechanized mining and tunnelling operation. There are many methods of performance prediction and are generally classified as full-scale linear cutting test, small-scale cutting test (core cutting), semi-theoretical approach, empirical approach, and field trial of a real mechanical machine. The full-scale linear cutting test is widely accepted and a precise approach, since a large block of rock is cut in the laboratory with an industrial cutter. The specific energy values can be obtained for different cut spacing and depth

values. The specific energy is used to predict the performance of mechanical miners (Balci et al., 2004).

Many researchers used these linear cutting tests to find the specific energy in cutting (Balci et al., 2004; Ersoy et al. 2005; Aydin et al., 2012; Aydin et al., 2013).

Prediction of the optimum specific energy, at a given geological formation at an optimum cutting geometry in the most energy efficient manner, from mechanical rock properties is the main concern in many research studies to predict the performance/efficiency of any mechanical excavator. For this purpose many researchers (Copur (2001); Altindag(2003); Balci et al., 2004; Tiryaki et al., 2006; Ersoy et al. 2006; Aydin et al.,2012; Yurdakul et al., 2012; Aydin et al.,2013; Engin et al., 2013) correlated the properties of rock with specific energy and developed many predictive models to find the performance of mechanical miners.

Evans (1962, 1984) developed a theoretical relationships between the cutting force for wedge and conical-type cutters, which were directly related to specific energy, and the uniaxial compressive and tensile strength of coals and soft rocks.

Nishimatsu (1984) developed a theoretical relationship between cutting and normal force for wedge-type cutters, and shear strength of soft rocks.

Fowell and McFeat-Smith (1976, 1977) carried out experimental studies to correlate specific energy obtained by small scale cutting tests to some rock properties such as cone indenter index, cementation coefficient, Schmidt hammer rebound value and compressive strength. Singh (1986) performed experimental studies to find out relationships between in-seam coal cutting performance and brittleness index related to compressive strength and tensile strength.

Goktan (1991) established the relationship between specific energy obtained from small-scale rock cutting tests and the brittleness index related to compressive and tensile strength.

Copur et al. (2001) conducted full-scale laboratory cutting tests with a conical cutter on 11 types of rocks/ores and determined optimum specific energy values. They also determined UCS and BTS for the rocks under study. The test results were used to develop predictive equations by establishing relationships between SE and UCS and BTS.

Altindag (2003) used previous experimental data and found relationships between SE and brittleness. He used three brittleness indices B1 (σ_c / σ_r), B2 ($\sigma_c - \sigma_r / \sigma_c + \sigma_r$), B3 ($\sigma_c \sigma_r / 2$) and developed models between these with SE ($\sigma_c = \text{UCS}$, $\sigma_r = \text{BTS}$). He concluded that there was no correlation between B1 and B2 with SE, however, the SE is strongly correlated with brittleness B3. To develop models he has used test data of Roxborough and Sen (1986) and the model equation is

$$SE = 0.5816 + 0.0946(B3) \quad (r = 0.982) \quad \dots\dots\dots(2.15)$$

He has developed another equation and test data of Bilgin and Shahrias (1988) used for the development of model and the equation is

$$SE = 2.4147(B3)^{0.486} \quad (r = 0.802) \quad \dots\dots\dots(2.16)$$

Balci et al. (2004) carried out full scale linear cutting tests on 23 different rock, mineral and ore samples and determined the specific cutting energy values. They also determined UCS, BTS, SRN, static and dynamic elastic moduli. They carried out regression analysis and established relationships between optimum specific energy and above properties of rocks. They found good correlations between SE and UCS (0.89), SE and BTS (0.85), SE and static elastic modulus (0.72), SE and dynamic elastic modulus (0.72), SE and SRN (0.79).

According to Tiryaki et al. (2006) specific cutting energy (SE) has been widely used to assess the rock cuttability for mechanical excavation purposes. He has developed some prediction models for SE through correlating properties of rocks with SE values. He investigated the effects of some rock parameters along with engineering rock properties on SE. Mineralogical and petrographic analyses and linear rock cutting tests were performed on sandstone samples. He evaluated relationships between SE and rock properties using bivariate correlation and linear regression analyses. The test results and analyses revealed that the texture coefficient and feldspar content of sandstones affected rock cuttability, evidenced by significant correlations between these parameters and SE at a 90% confidence level. He found that cementation coefficient, effective porosity, and pore volume had good correlations against SE. He further found that that Poisson's ratio, Brazilian tensile strength, Shore scleroscope hardness, Schmidt hammer hardness, dry density, and point load strength index showed very strong linear correlations against SE at confidence levels of 95% and above, all of which were also found suitable to be used in predicting SE individually.

Ersoy et al. (2007) have computed specific cutting energy (SE_{cut}) at different feed rates and depths of cut at a constant peripheral speed on 11 varieties of rocks. They measured velocities of P (V_p) and S (V_s) waves for above rocks as per ISRM(1981) standards. They found relationships between P, S waves and dominant rock properties like hardness, abrasiveness, density, porosity and silica contents. They also found relationships between P & S waves and SE_{cut} . An excellent linear relation exists between V_p and SE_{cut} (0.94) and a good linear relationship between V_s and SE_{cut} (0.80). The clear trend was that an increase in the SE_{cut} increases the velocities of P and S waves.

Atici et al. (2009) carried rock cutting tests and fully instrumented laboratory drilling tests on 5 types of rocks. They determined SE_{cut} and SE_{drill} . They carried out regression analysis to find relationship between SE_{cut} and SE_{drill} with rock brittleness B1 (σ_c / σ_r), B2 ($\sigma_c - \sigma_r / \sigma_c + \sigma_r$), B3 ($\sigma_c \sigma_r / 2$). The results of regression analyses indicated that, there are strong

linear, exponential and logarithmic relationships between SE_{cut} of circular diamond saw blades and the brittleness of $B1$, $B2$ and $B3$ with high correlation coefficients of 0.98, 0.93 and 0.85, respectively. There is no good correlation between SE_{drill} of PDC (Poly diamond crystalline) and impregnated diamond both core bits and non-core bits, brittleness of $B1$ and $B3$.

Murat Yurdakul et al. (2012) have developed models to predict the specific energy based on the operational parameters of block cutters and properties of rock for large circular saws during natural stone cutting. They have used uniaxial compressive strength, bending strength, Brazilian tensile strength, point load strength, Shore hardness test, Schmidt hammer hardness test, seismic velocity, water absorption at atmospheric pressure, apparent density, open porosity, sawblade diameter, and depth of cut values as input parameters in the statistical analysis for the prediction of SE_{cut} . The SE_{cut} values for carbonate rocks in the stone cutting process can be predicted successfully for large diameter circular saws in natural stone processing by using the model developed.

Aydin et al. (2013) developed predictive model for specific cutting energy of circular diamond sawblades in the sawing of granite rocks. They have investigated the influence of operating variables and rock properties on the specific energy (SE_{cut}). They employed statistical analyses to determine the most significant operating parameters and rock properties influencing the specific cutting energy. They developed models to predict the SE_{cut} from operating variables and also to predict the SE_{cut} from rock properties.

Irfan Celal Engin et al. (2013) carried out rock cutting experiments on 12 different types of rock samples using a circular sawing machine (CS) and an abrasive water jet cutting (AWJC). In their study, the specific energy values were determined and compared to evaluate the efficiency of rock cutting method. The experimental results showed that the specific energy values in AWJC were generally higher than that in circular sawing (CS). They found relationship between specific energy values and rock properties. Multiple

regression equations for specific energy for AWJC system ($R^2 = 0.95$) and CS system ($R^2 = 0.98$) were generated. The developed equations were statistically significant.

Closure:

The specific energy is important performance indicator in drilling, cutting and other excavation process. It can be concluded that the specific drilling energy is an important parameter for an assessment of rate of drilling in drilling operation. Similarly specific cutting energy is an importance performance indicator for cuttability of rocks in cutting operation and can be useful design of cutting picks.

2.5 Studies on application of ANN to estimate rock properties and studies on application of Artificial Neural Network for predicting the Indentation depth/specific energy in rock indentation

Artificial Neural Networks(ANN) can be effectively used to develop the models to predict the rock properties accurately as well as precisely (Haykin, 1999).Neural networks may be used as a direct substitute for statistical methods such as correlation, multivariable regression, linear regression and other statistical analysis and techniques (Singh et al., 2003). Neural networks, with their remarkable capability to derive useful output from complicated or imprecise data, can be used to find the extract patterns and detect trends that are too complex to be noticed by either humans or other computer techniques. Rumelhart and McClelland (1986) reported that a trained neural network can be thought of as an “expert” in the category of information it has been given to analyze to provide information for a given new situations of interest (Simpson, 1990).

Other advantages of ANN include:

Adaptive learning, Self-organization, Real time operation and Fault tolerance via redundant information coding. However, some network capabilities may be retained even with major network damage (Yılmaz and Yuksek, 2008).

ANN technology, because of its ability to learn and generalize interactions among many variables, has been reported to be very useful in modeling the behaviour rock material by many researchers (Ghabousi et al., 1991; Ellis et al., 1992).

Meulenkamp and Alvarez Grima (1999) investigated the possibility of predicting UCS by ANN from hardness of rocks using Equotip hardness tester and other rock properties like hardness, porosity, density, grain size. Singh et al. (2001) developed predictive models for UTS, UCS, and axial point load strength from the intrinsic rock properties. Similarly, many researchers have developed the ANN models to predict the UCS and shear strength from physical properties (Sarkar et al., 2010). The ANN methods could be applied as a new acceptable method for the prediction of uniaxial compressive strength and modulus of elasticity of intact rock properties (Dehghan, 2010). Zorlu et al., 2008 developed ANN models to predict the UCS from petrographic properties.

ANN models were developed by Sonmez et al. (2006) and Ibrahim et al.(2012) to predict the Elastic modulus of intact rock from UCS and unit weight. Similarly ANN models were developed for predicting UCS and E of intact rocks from their other properties such as NCB cone indenter hardness, dry density and Shore scleroscope hardness (Tiryaki, 2008). ANN models were developed by Yilmaz et al., 2008 to predict rock properties like elasticity modulus, unconfined compressive strength from slake durability index, Schmidt hammer rebound number, effective porosity and point load index. ANN models of RBF and MLP exhibit were developed by Yilmaz et al. (2011) for predicting swell percent of soils.

And ANN modeling concepts are used to find the drillability, optimum bit selection (Yilmaz, 2002) and cuttability of rocks. Neural network system has also been used in predicting the advance rates of tunnel boring machines (Benardos and Kaliampakos, 2004), and sawability prediction of carbonate rocks (Kahraman et al., 2006).

The similarity methods offer a profound understanding of the physical problem like to find indentation depth in rocks caused by a hemispherical indenter and help to identify the most important governing parameters or factors that reflect the essence of the rock indentation events, thus simplifying the target problem and the artificial neural network provides an advanced computing model, which allows more factors to be involved and the predictions obtained using this combined approach (similarity methods and artificial neural network) is in better agreement with the experimental results than predictions using other methods(Kou et al.,1998).

Furthermore, in the last few years, the fuzzy logic and ANN have been used for building predictive models in mining and tunnelling applications. However, ANN has not yet been used to predict the specific energy (SE), a rock indentation index, from intact rock properties in rock drillability applications where tungsten carbide drill bits are employed. In the present study, ANN models are developed to predict SE from selected rock properties.

Closure: The conclusion from all the above ANN modeling methods is that the prediction performances of neural network model are higher than those of multiple regression equations. The use of neural network may provide new approaches and methodologies, and minimize the potential inconsistency of correlations.

2.6 Studies on Numerical Simulation and analysis of Stress distribution and rock fragmentation/fracture in Rock Indentation

2.6.1 Numerical Modeling

Various procedures, processes and phenomenon treated in science and engineering are often described in terms of differential equations formulated by using their continuum mechanics models. Solving differential equations under various conditions such as

boundary or initial conditions leads to the understanding of the phenomena and can predict the future of the phenomena. But, exact solutions for differential equations are generally difficult to obtain. So, numerical methods are adopted to obtain approximate solutions for differential equations. Among these numerical methods, those which approximate continua with infinite degree of freedom by a discrete body with finite degree of freedom are called “discrete analysis.” (Stolarski et al., 2006).

Modeling has been a useful tool for engineering design and analysis. The definition of modeling may vary depending on the application, but the basic concept remains the same: the process of solving physical problems by appropriate simplification of reality. In engineering, modeling is divided into two major parts: physical/empirical modeling and theoretical/analytical modeling. Laboratory and in situ model tests are examples of physical modeling, from which engineers and scientists obtain useful information to develop empirical or semi-empirical algorithms for tangible application. With the increase in computational technology, many numerical models and software programs have been developed for various engineering practices.

The most commonly applied numerical methods for rock mechanics problems are:

Continuum methods

Finite Difference Method (FDM),
Finite Element Method (FEM), and
Boundary Element Method (BEM).

Discontinuum methods

Discrete Element Method (DEM),
Discrete Fracture Network (DFN) methods.
Hybrid continuum/discontinuum models
Hybrid FEM/BEM,
Hybrid DEM/DEM,
Hybrid FEM/DEM, and

Other hybrid models

The FEM requires the division of the problem domain into a collection of elements of smaller sizes and standard shapes (triangle, quadrilateral, tetrahedral, etc) with fixed number of nodes at the vertices and/or on the sides. The trial functions, usually polynomial, are used to approximate the behaviour of Partial differential equations at the element level and generate the local algebraic equations representing the behaviour of the elements. The local elemental equations are then assembled, according to the topologic relations between the nodes and elements, into a global system of algebraic equations whose solution then produces the required information in the solution domain, after imposing the properly defined initial and boundary conditions. The FEM is perhaps the most widely applied numerical method in engineering today because its flexibility in handling material heterogeneity, non-linearity and boundary conditions, with many well developed and verified commercial codes with large capacities in terms of computing power, material complexity and user friendliness. Due to the interior discretization, the FDM and FEM cannot simulate infinitely large domains (as sometimes presented in rock engineering problems, such as half-plane or half-space problems) and the efficiency of the FDM and FEM will decrease with too high a number of degrees of freedom, which are in general proportional to the numbers of nodes(Jing, 2003).

2.6.2 FEM to simulate the Rock Indentation or Rock Cutting:

FEM method has been used by Wang (1976), Tang (1997), Kou et al. (1999) and Liu (2002) to simulate fracture propagation during rock indentation or rock cutting. Generally these models used a stress based criterion to form cracks normal to the maximum principal stress (tensile stresses taken as positive) at the element integration points. Failure occurs if the maximum tensile stress exceeds the specified fracture strength. In compression, the models utilized a Mohr- Coulomb failure criterion to form shear cracks at the element integration

points. After the cracks have formed, the strains normal to both the tensile and shear cracks are monitored in subsequent time/load steps to determine if the cracks are open or closed. If a crack is open, the normal and shear stresses on the crack face are set equal to zero for a tensile crack.

Wang (1975) developed a general mathematical rock failure model and applying the available finite element technique to established computer code, which allows simulation of the sequence of penetration mechanisms and provide better description of the failure phases such as initial cracking, crushing and chipping. Wang (1975) also used the ‘stress transfer’ method suggested by Zienkiewicz (1968) to convert excessive stresses that an element cannot bear to nodal loads and reapplies these nodal loads to the element nodes and thereby to the system. If a crack is closed, a compressive normal stress can be carried, but the shear stress is limited to a value described by the Coulomb friction model. The analytical results presented in the studies conducted by Wang (1975) show reasonable agreement with experimental observations.

Numerical analysis of the wedge indentation problem was conducted by Huang, Damjanac and Detournay (1997) using the code FLAC software and the numerical analysis indicates that the location of maximum tensile stress (interpreted as the point of crack initiation) moves away from the indentation axis as the lateral confinement increases. They found that a small increase in the confining stress from zero induces a large increase in the inclination of this point on the indentation axis. However, the confinement does not reduce significantly the maximum tensile stress and it hardly influences the indentation pressure.

Carpinteri, Chiaia and Invernizzi(2004) conducted tests of indentation of brittle and quasi-brittle materials and Fracture patterns in homogeneous brittle solids are obtained by the finite element method in the framework of linear elastic fracture mechanics. Microstructural heterogeneities are taken into account by the lattice model simulation. Although the reality is often much more complex than the theoretical models applied, the

study provides interesting indications for improving performance of cutting tools. The FRANC2D software, developed at Cornell University, has been used to simulate fracture in the homogeneous case. This software is able to simulate plane-stress, plain-strain as well as axisymmetric crack propagation in the framework of linear elastic fracture mechanics (LEFM). They concluded that the cutting performances could be significantly improved by reducing the crushing component and enhancing the chipping ability of the indenters (e.g. by increasing their sizes or depth of penetration).

Liu, Kou, Lindqvist and Tang (2002) have simulated the rock fragmentation processes induced by single and double truncated indenters by the rock and tools interaction code, R-T2D, based on the Rock Failure Process Analysis (RFPFA) model. The simulated crack patterns are in good agreement with indentation experiments and a better understanding is gained. According to the simulated results, a simple description and qualitative model of the rock fragmentation process induced by truncated indenters has been developed. The simulated results for the rock fragmentation process induced by double indenters reproduced the propagation, interaction and coalescence process of side cracks induced by the two indenters, and the formation of large rock chips. They have pointed out that the simultaneous loading of the rock surface by multiple indenters seems to provide a possibility of forming larger rock chips, controlling the direction of subsurface cracks and consuming a minimum total specific energy.

Wang, Sloan, Liu and Tang (2011) have examined the rock fragmentation processes induced by double drill bits subjected to static and dynamic loading by a numerical method. Micro-heterogeneities of the rock are taken into account in this numerical model. For the static case, the simulated results reproduce the progressive process of brittle rock fragmentation during indentation. For the dynamic case, numerical simulations represent radial cracks, incipient chips, pulverized zones, and shell cracks. Comparing the static and dynamic cases, the dynamic loading can lead to rock fragmentation more efficiently. In addition, numerical results indicate that the dynamic pressure (P_{\max}) plays an important

role in the failure process of specimens with two indenters. Furthermore, the heterogeneity of the rock can also affect the failure modes of the rock when two indenters are used. Finally, the numerical results demonstrate the effect of the spacing between the indenters on the rock. The numerical code RFPA2D (Rock Failure Process Analysis, 2D) (Zhu and Tang 2006) is used to consider the heterogeneity of rock and simulate the evolution of dynamic fracture initiation and propagation due to impact loading from double indenters.

Saksala, Gomon, Hokka and Kuokkala (2013) simulated with a numerical method for dynamic indentation. The method was validated via dynamic indentation experiments with single and triple indenters on Kuru granite. The simulation method includes a constitutive model for rock and a model, implemented in FEM, to simulate the dynamic bit-rock interaction. The constitutive model, being a combined viscoplastic-damage model, accommodates the strong strain-rate dependency of rock via viscoplastic hardening/softening laws both in tension and compression. They have carried out indentation experiments with single and triple-button indenters using a setup similar to percussive drilling. Despite the present continuum approach, the model can capture the salient features of the dynamic bit-rock interaction involved in dynamic indentation and applications alike. They concluded that a fairly good agreement between the simulated and experimental results on dynamic indentation on Kuru granite and the model can be a useful tool in, e.g. percussive drill design.

Sulem and Cerrolaza (2002) carried out numerical analysis of the indentation test. They modelled rock as an elasto-plastic medium with Cosserat microstructure and consequently possess an internal length. The response of the indentation curve is studied by them for various values of the size of the indenter as compared to the internal length of the rock in order to assess the scale effect. Using finite element numerical simulations, they concluded that for a material with cosserat microstructure, the apparent strength and rigidity increase as the size of the indenter decreases. This scale effect for the strength can reach 15% for a statistical model and 50% for a kinematical Cosserat model when the size of the indenter

tool is comparable to the grain size of the rock. They concluded that this scale effect is not significantly affected by the interface condition at the rock tool interface and such a scale effect has been observed experimentally for metals. They expressed that in the lack of relevant quantitative experimental data for the scale effect in the case of rocks, further they expressed that the analysis suggests that this effect may be of importance and has to be investigated further. The indentation tests appear as an experimental tool for the testing and validation of continuum theories with microstructure and calibration of internal lengths parameters.

Closure:

Numerical modelling in rock indentation is an important tool to demonstrate the effect of the spacing between the indenters on the rock which a parameter for percussive drill design.

2.7 Reasons to carry out Present Research work:

- Mechanical excavation, such as drilling and TBM tunneling and other excavators play an important role in mining industry. Rock indentation is the fundamental process for rock excavation using such mechanical excavation methods. Therefore, it is necessary to investigate the basic deformation and failure mechanisms during the process of rock indentation. Also, it is very much essential to know the process of indentation to assess the drill/cutting machine performance and also to know the strength of rocks for the suitability of drill/cutting picks for particular type of rocks.
- The shaping of the brittle materials including rocks by cutting, abrasion, grinding and drilling which cause damage and subsequent erosion and wear of surfaces; the creation of particular matter by comminution, fragmentation and milling etc; all are intimately tied up with the manner in which small scale fractures initiate and propagate with in highly stress fields. Central to such scientific phenomenon is the indentation test.

- A standard indentation test is proposed as a measure of hardness and its use as a predictor of the UCS is evaluated. The indentation technique can also be used for an independent assessment of other rock properties such as rock drillability and cuttability. The simplicity of the indentation test means that rock properties can be determined in any direction, for example, in the direction of advance of mining, cutting or drilling equipment (Szwedzicki, 1998).
- The indentation tests appear as an experimental tool for the testing and validation of continuum theories with microstructure and calibration of internal lengths parameters. It explains the rock breaking characteristics and failure mechanism. The indentation indices can be used for assessment of certain rock properties like drillability and cuttability which are important in rock drilling and rock cutting operations.
- Rock indentation has been the subject of a great number of studies for more than three decades for two main reasons: first, during the last few decades, the need for underground space (tunnels, storage, and mining) has constantly increased and mechanized excavation of rock has shown a remarkable development. The performance of full-face rock boring machines depends mainly on its penetration rate, which can be predicted by many methods. Some of these methods are based on the results of indentation tests on rock specimens. The second reason for taking a closer look at indentation tests is that they can, in principle, be used to characterize the mechanical behavior of rocks. One of the major challenges of rock engineers is the determination of significant mechanical properties for a rock mass due to the intrinsic spatial variability of rock properties. Since indentation tests are relatively simple to perform, they can be used to characterize the mechanical behavior of rocks by obtaining a greater amount of information than would be possible with the same budget using conventional tests. (Leite et al. 2000).

- The specific energy is one of the most important performance indicators in drilling and cutting processes and is derived from the amount of energy required to remove a given volume of rock and has been successfully used for the performance evaluation of drill bits and circular diamond saw blades. Therefore this performance indicator is considered in the present research.
- Many researchers have used different indentation indices like Indentation Hardness Index, Indentation Modulus and Critical Transition Force to correlate with properties of rock for the development of models for prediction. But none of the researchers so far used specific energy in rock indentation to correlate with properties of rock for the development of models for prediction which is a research component in the present research.
- Also it is necessary to investigate at what index angle the specific energy is minimum during percussive drilling for different bit rock combinations to assess the number of blows totally required for making a hole for different varieties of rocks.
- So far many researchers used small diameter indenter less than 5mm in indentation test. None of the researcher used commercial drill bits of chisel, cross and spherical button bits with different diameters. These bits were used in rock indentation tests in the present research to obtain more realistic values of depth of penetration and specific energy
- The prediction models for laboratory SE were developed for proper selection and optimization of mechanical excavators for particular rock conditions which involved rock properties as predictors
- Designing faster and better excavation systems and developing accurate and reliable performance prediction models would improve the success of mechanical mining. For this reason the predictive models were development to assess the specific energy in rock indentation to improve the success of percussive drilling.

2.8 Origin of Present Research work

Earlier many researchers used small diameter indenters (wedge, cone, spherical and pyramidal) in rock indentation test. None of the researchers used commercial drill bits (Chisel, cross and button) with different diameters. However, Murthy, Ch. S. N (1998) used commercial bits of 48 mm with only one diameter (Chisel, cross and spherical button) and carried out experimental work in rock indentation to find at what index angle the specific energy is minimum in static rock indentation test.

But the Specific Energy in static indentation test with different bit geometries [using commercial drill bits (Chisel, cross and button)] of different diameters at different index angles with a view to find out the at what indexing angle the specific energy is minimum for various bit-rock combinations in static indentation test, and correlating specific energy with the properties of rocks to predict the specific energy in indentation test has not been reported anywhere in the literature. Keeping this point in mind, the present research proposal was formulated.

2.9 Definition of the Problem

The Specific energy (amount of energy required to remove unit volume of rock) is an important performance indicator in drilling operation. Mechanical properties (Strength properties) of rocks are essential and important parameter for designing suitable equipment and rock working process (e.g. drilling, cutting, crushing, excavation, breaking, grinding, polishing etc.) for various rock excavations and engineering projects.

In the field it is difficult to measure specific energy. Hence, the experimental investigations are planned in the laboratory for measurement of specific energy in rock indentation (static) test for various types of bit-rock combinations with different indexing angles. The aim is to find the indexing angle at which specific energy is minimum in rock indentation test.

Also, to correlate specific energy with mechanical properties of rocks with a view to develop predictive models for specific energy in rock indentation.

2.10 Research Objectives

- 1) To make necessary fabrication for the existing Microcontroller Compressive testing machine to hold different types of bits (indenters namely chisel cross and spherical button bits) of different diameters to carry out rock static rock indentation test.
- 2) To carry out laboratory investigations to determine depth of penetration (P) and relationship between force (F) and penetration (P) for all bit-rock combinations at different indexing angles, keeping loading time constant for all bit-rock combinations considered.
- 3) To determine the Specific energy from F-P curves for all bit-rock combinations considered.
- 4) To determine the properties of rocks viz. uniaxial compressive strength (UCS), Brazilian tensile strength (BTS), abrasion resistance, hardness (Schmidt Rebound Number (SRN)) , Young's Modulus, Poisson's ratio, density, mineralogical properties in the laboratory according to the standards given by ISRM.
- 5) To study the influence of index angle (10^0 , 20^0 , 30^0 , and 40^0) on specific energy for all bit-rock combinations considered.
- 6) To study the influence of above rock properties on specific energy for all bit-rock combinations considered.
- 7) To develop the multiple regression models to predict the specific energy from properties of various rocks for different geometries and diameters of indenters.
- 8) To develop Artificial Neural Network model to predict specific energy in static indentation test from properties of rocks.
- 9) To carry out Finite Element Modelling (FEM) analysis to determine the depth of penetration for all bit-rock combinations considered taking the force values from static indentation test (up to loading cycle), And to compare penetrations obtained in FEM analysis of all bit-rock combinations considered with experimental results.

CHAPTER 3

EXPERIMENTAL AND THEORITICAL INVESTIGATIONS

I EXPERIMENTAL INVESTIGATION:

3.0 INTRODUCTION

This chapter elucidate on experimental design, procedure of conducting experiments in the laboratories, statistical analysis, development of Artificial Neural Network models and numerical modelling (Finite Element analysis). It illustrates the setup used in the laboratory to determine the specific energy in static indentation tests. It explicates the procedure to determine the specific energy in static indentation tests and procedures to find the physico-mechanical properties of various rocks considered for the study, thin section examination to find the mineralogical composition and textural properties of rocks used for study and the procedure to find the elements/minerals in oxides form of the rocks under study using X-Ray Fluorescence test. It explicates the mathematical modelling i.e development of predictive models using multiple regression analysis and also development of Artificial Neural Network models to estimate the specific energy from the operational parameters and some selected properties of rocks. Finally it explicates the numerical modelling (Finite Element analysis) analysis to determine the depth of penetration and comparison of these results with experiment results.

3.1 RESEARCH METHODOLOGY

The following methodology is adopted in present research work.

- 1) Fabrication work carried out to the existing Micro-controller compression testing machine available in the rock mechanics laboratory, to hold different bits/indenters for static indentation test.

- 2) Collection of igneous, sedimentary and metamorphic rocks from various mines and cutting and polishing those to suitable sizes (0.2032 m length \times 0.1524 m width \times 0.127 m height) to carry out experiments.
- 3) Determination of mineralogical composition of rocks using thin section analysis and X-Ray Fluorescence Test.
- 4) Determination of physico-mechanical properties of rocks like UCS, BTS, abrasion resistance, SRN, Young's Modulus, Poisson's ratio and density in the laboratory according to the suggestive methods given by ISRM.
- 5) Determination of depth of penetration in rock static indentation tests, plotting of F-P curves and determination of specific energy at various index angles for different bit-rock combinations. Plotting of curves between index angle and specific energy to study the influence of index angle on SE.
- 6) Development linear regression models between properties of rocks individually with SE with an aim to find the influence of each property on SE. Development of mathematical and regression models to correlate of properties of rock and specific energy for different bit-rock combinations.
- 7) Development of Artificial Neural Network models to estimate the specific energy in static indentation for different bit-rock combinations. And also determination the performance indicators like VAF, RMSE and MAPE.
- 8) Finite Element Modelling for stress distribution in rock indentation process and determination of depth of penetration for different bit-rock combinations and their comparison with experimental data.

Justification

The results in this thesis regarding the influence of the index angle on specific energy is used for design of percussive drills. The developed models presented in this thesis can be used to assess the specific energy in rock indentation from the physic-mechanical properties of rocks Hence, the proposed investigation has the potential to serve the mining,

civil and geotechnical industries during drilling. Similarly the numerical models presented in the thesis can be used to design the drill bits and its suitability various rock structures.

3.2 COLLECTION OF ROCK SAMPLES

Different igneous, sedimentary and metamorphic rocks were collected for research study from various mines/places in India from Figure 3.2 to 3.7.

Marble: It is a metamorphic rock collected from Babarmal mine near Kewada village, 28 km away from Udaipur, Rajasthan.

Basalt: Basalt is an igneous rock collected from quarry at Gauripatnam, near Kovvur, 38 km from Rajahmundry, West Godavari district, Andhra Pradesh.

Limestone: Limestone is a sedimentary rock collected at Tummala Limestone mine (Ultratech Cements Ltd) Tummalapenta Village, Kolimigundla Mandal, Kurnool dist, Andhra Pradesh.

Steel gray granite: It is an igneous rock collected at Balli Kurava Quarry, 10 km away from Martoor (60 km away from Ongole), Andhra Pradesh.

Moon white granite: It is an igneous rock collected at Goura Minerals, 8 km away from Chodavaram, Visakhapatnam district, Andhra Pradesh.

Black galaxy granite: It is an igneous rock collected at Krishan Sai Granites quarry, Chimakurthy, 25km away from Ongole, Andhra Pradesh.

3.3 PREPARATION OF SAMPLES

All the rock samples are reduced to sizes (0.2032 m length \times 0.1524 m width \times 0.127 m height) and neatly polished at various rock cutting factories at Chimakurthy factory, Andhra Pradesh, Sunshine Enterprises, Mangalore and at Rock Mechanics Laboratory, NITK, Surathkal (Figure 3.1).



Figure 3.1 Rock cutting machine



Figure 3.2 Marble rock samples



Figure 3.3 Limestone rock samples



Figure 3.4 Basalt rock samples



Figure 3.5 Steel gray granite rock samples



Figure 3.6 Moon white granite rock samples



Figure 3.7 Black galaxy granite rock samples

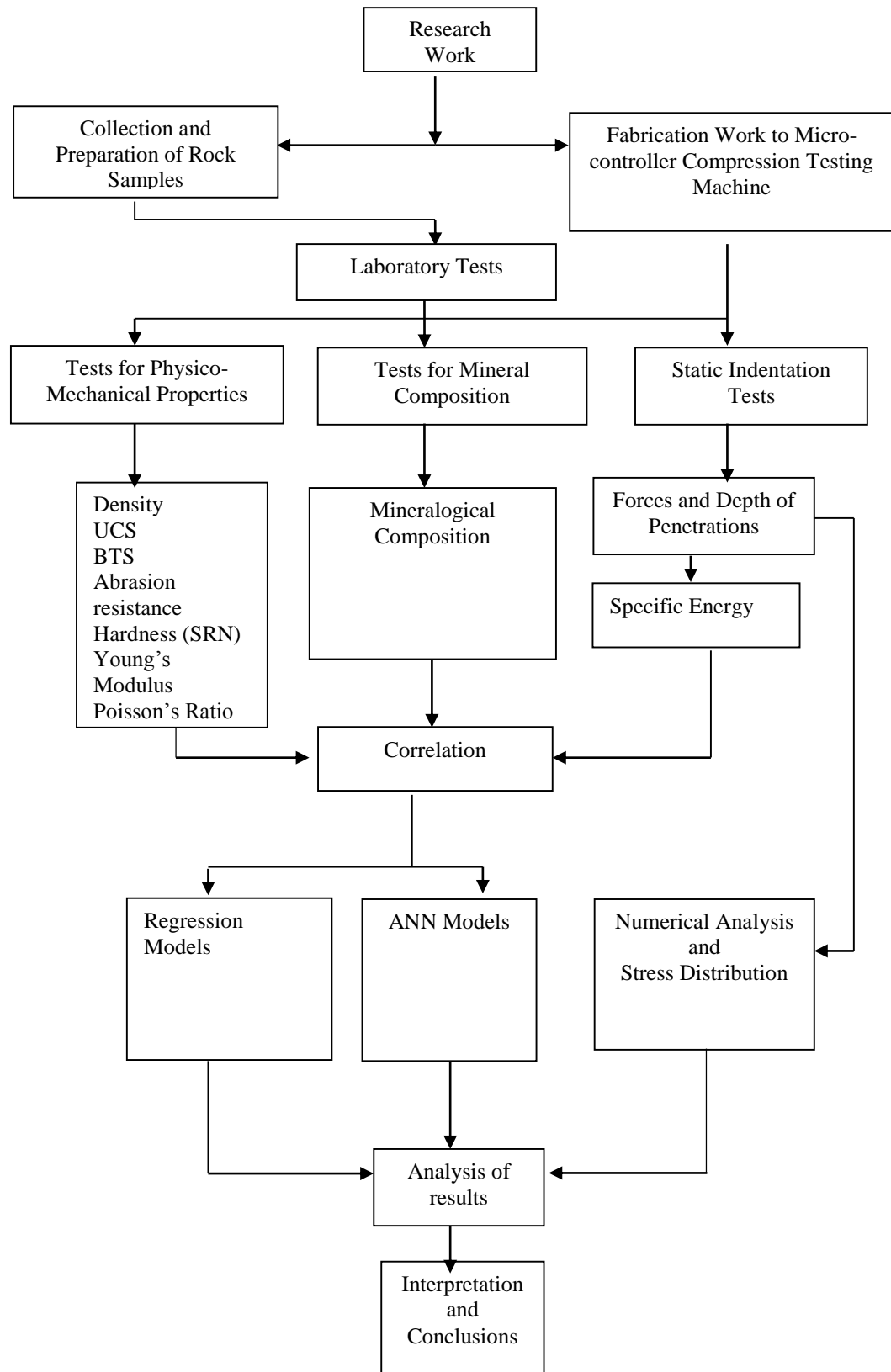


Figure 3.8 Flow chart of plan of experimental design and analysis

Table 3.1 Details of parametric variations investigated

PARAMETERS	VARIABLES
LABORATORY INVESTIGATIONS	
1. STATIC INDENTATION TESTS	
a) Bits used	
i. Bit type	Integral(Chisel only) Threaded (R22) type
ii. Bit geometry	Chisel, Cross, and Spherical button
iii. Bit diameter	35mm, 38mm, 45 mm and 48mm
iv. Indexing angle	10°, 20°, 30° and 40°
b) Rock Parameters	
i. Type of rocks	Marble, Limestone, Basalt, Steel gray granite, Moon white granite, Black galaxy granite
c) Rock Properties	Elastic Properties : (Static young's modulus and Poisson's ratio)
d) Measured Parameters	Displacement, Volume and Specific Energy
2. DETERMINATION OF PHYSICO-MECHANICAL PROPERTIES	Density, Hardness (Schmidt Rebound Number), Uniaxial compressive strength, Brazilian tensile strength, Young's Modulus, Poisson's ratio
3. DETERMINATION OF MINERAL COMPOSITION OF ROCKS	Minerals like quartz, feldspar, hornblende, pyrite, magnetite, biotite mica

PARAMETERS	VARIABLES
THEORITICAL INVESTIGATIONS	
a. Bits used	
i. Bit type	Integral(Chisel only) Threaded (R22) type
ii. Bit geometry	Chisel, Cross, and Spherical button
iii. Bit diameter	35mm, 38mm, 45 mm and 48mm
iv. Indexing angle	10°, 20°, 30° and 40°
b. Rock Parameters	
i. Type of rocks	Marble, Limestone, Basalt, Steel gray granite, Moon white granite, Black galaxy granite
c. Rock Properties	Elastic Properties : (Static young's modulus and Poisson's ratio)
d. Measured parameters	Displacement and compressive stress developed under chisel, cross and spherical button bits

3.4 STATIC INDENTATION TESTS

The entire plan of experimental design and analysis is shown in Figure 3.8. The Static indentation tests were conducted on a Microcontroller compression testing machine (2000kN) capacity. The Microcontroller Compressive testing machine is a micro controlled based intelligent pace rate controller used in conjunction with a compression testing machine. It performs the data logging and control functions. It has features, among others, of automatic pace rate control, data-logging, data printing and load hold. It has 64 kilobytes of memory for storing runs. This means that for a 2000 kN machine runs at a pace rate of 5 kN/sec and can store upto 150 runs. Any of these runs can be assessed and printed.

An indenter (bit) holder was fabricated to compression testing machine as shown in the Figure 3.9 to attach indenter (drill bit) to the machine. At one end of the indenter (bit) holder, the different types of bits namely chisel, cross and spherical button bits shown in Figure 3.13 were attached by clamp and screw arrangement. The rock blocks were confined inside a specimen box which was fabricated specially for this purpose as shown in the Figure 3.10 and rigidly held on four sides with the help of nut and bolt arrangement. This specimen box was placed on the top of the bottom platen of the compression testing machine during the test. Similarly a digital dial gauge was attached to the magnetic holder and the assembly was mounted to the side plate of the testing machine. The total set up is shown in Figure 3.11 and 3.12.

3.4.1 Fabrication Work

The following fabricating works were carried out for the testing machine, without disturbing the original function of the machine.

- 1) Fabrication of indenter holder.
- 2) An arrangement was made in the machine for indenter holder at the upper platen.
- 3) Fabrication of rock specimen box.

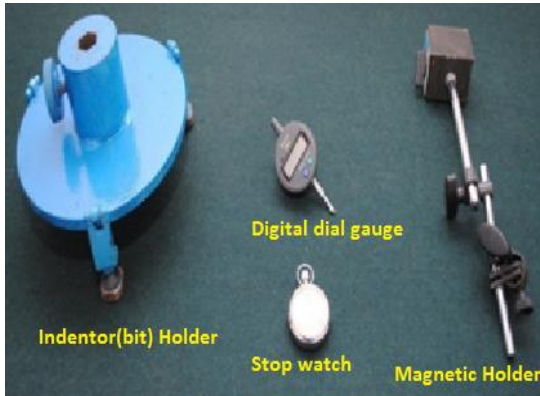


Figure 3.9 Indenter (bit) Holder, Digital Dial Gauge, Magnetic Holder and Stop Watch used in test



Figure 3.10 Specimen box

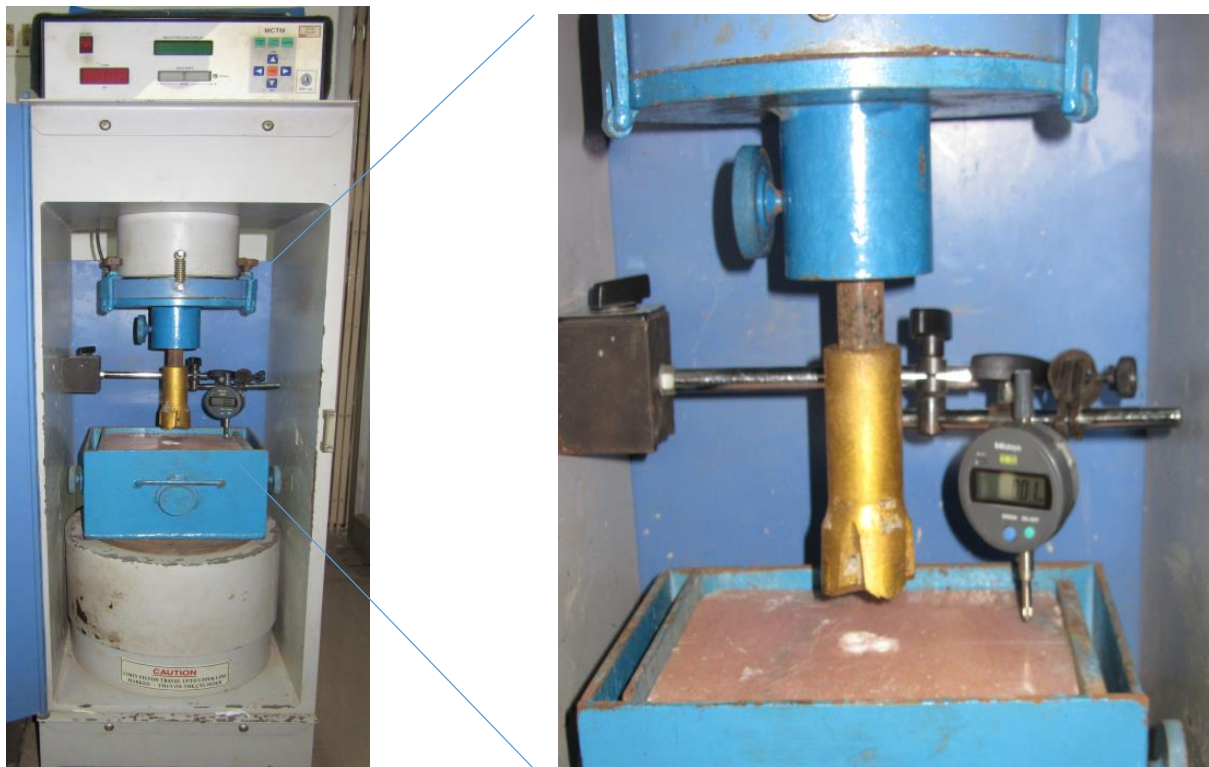


Figure 3.11. Experimental Set up

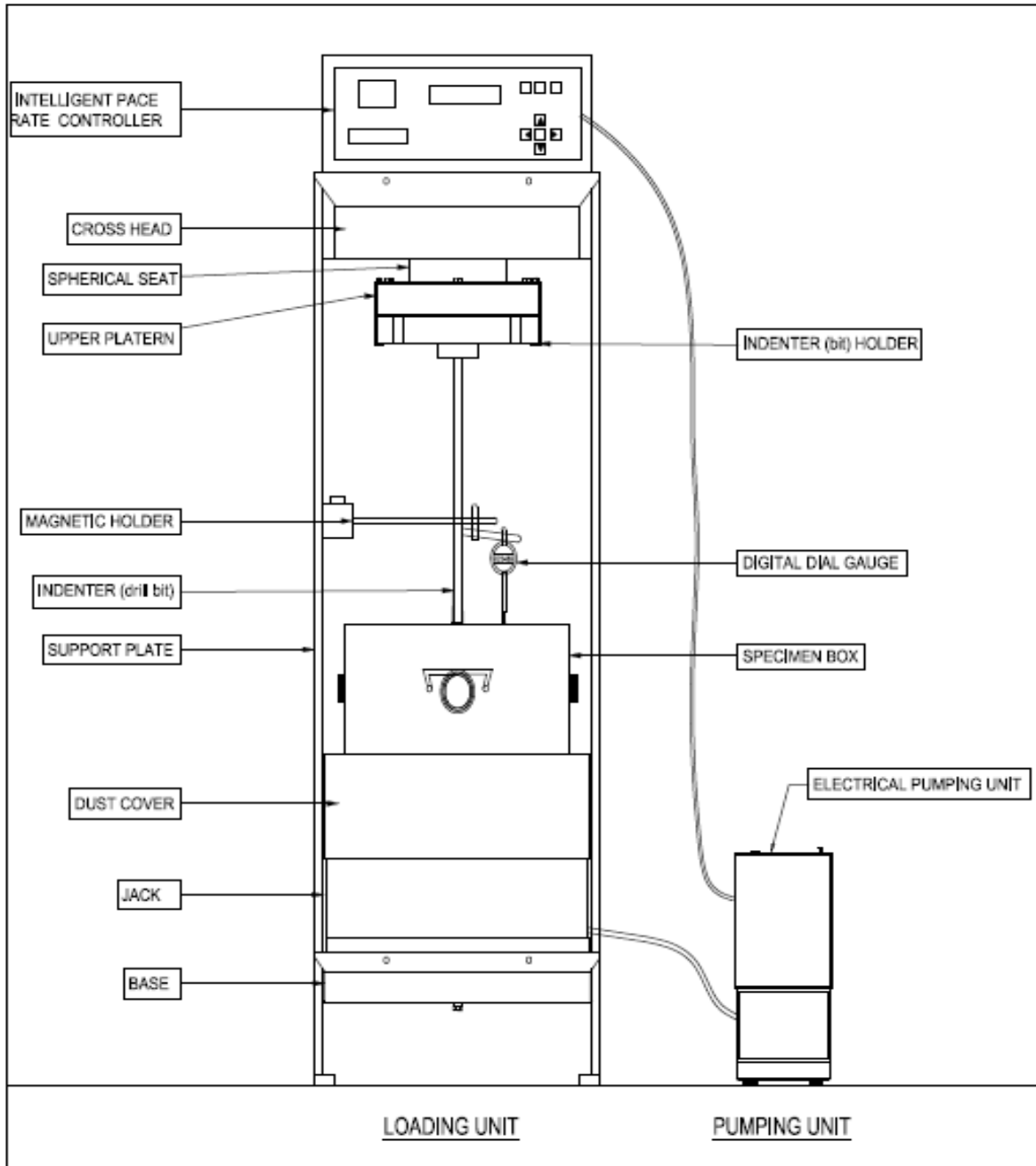
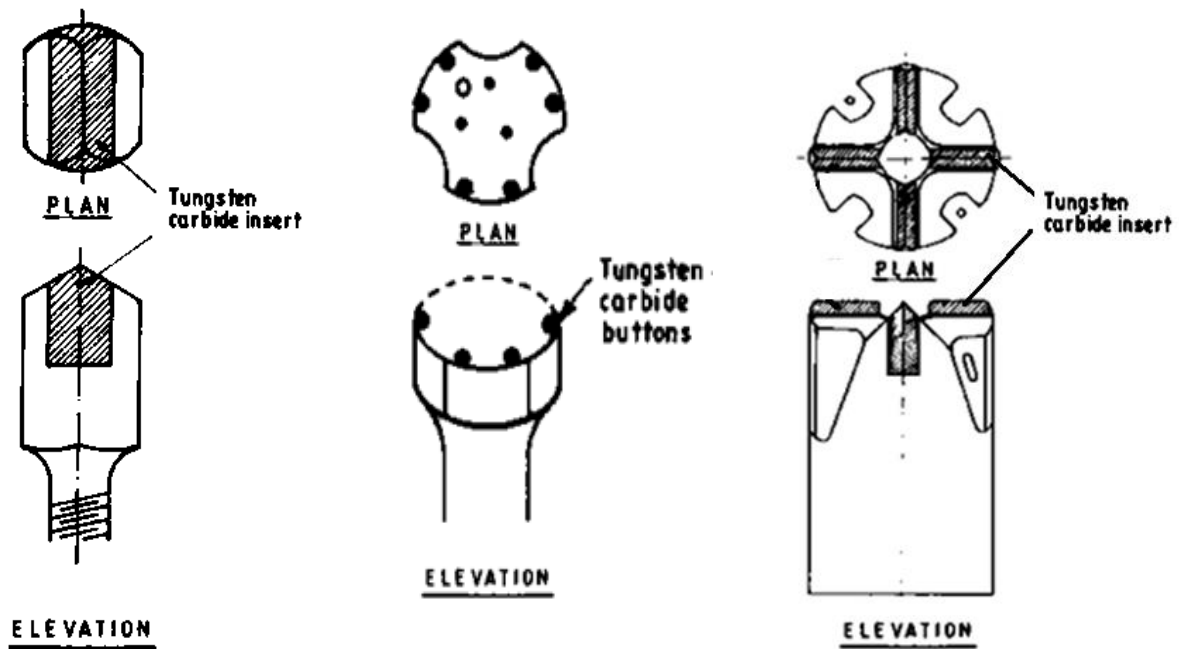


Figure 3.12. Experimental set up (Line diagram)



a) Chisel bit

b) Cross bit

b) Spherical button bit



Figure 3.13 Geometry of different drill bits used in static indentation tests

3.4.2 EXPERIMENTAL PROCEDURE OF STATIC INDENTATION TEST

Indentation tests were conducted on the rock types rocks namely marble, limestone, basalt, steel gray granite, moon white granite and black galaxy granite. These tests were carried out at four indexing angles viz 10^0 , 20^0 , 30^0 and 40^0 for 35 mm, 38 mm, 45 mm, 48 mm diameter of chisel, cross bit and spherical button bits. The details of parametric variations investigated are shown in Table 3.1.

To carry out static tests, cubical blocks (0.2032 m length \times 0.1524 m width \times 0.127 height) were prepared with the help of a rock cutting machine (Figure 3.1) from the rock blocks collected from various mines/quarries in India. They were polished to produce perfectly parallel and mutually perpendicular faces.

All rock samples were marked with lines of desired index angles. Then rock sample with above markings was placed in the specimen box and thoroughly clamped by packing materials and with the help of nuts and bolts of the specimen box simulating the in-situ rock in the field. The complete assembly of specimen box along with the rock sample was placed on the top of the bottom platen of the testing machine. The indenter (bit) holder assembly fabricated for this purpose was attached at the bottom of the upper platen, and the length adjusted for the indenter (bit) to rest on the surface of the rock sample. Then rate of loading was set to 0.1 kN/sec in the control unit of the machine. The static indentation tests were conducted at the above rate of loading which was kept constant for all the experiments. This rate was chosen as per ISRM guide lines. A digital dial gauge with a least count of 0.01 mm, was fixed, with help of a magnetic holder attached to the side frame of the compression testing machine and it was adjusted such that the tip of its needle touched the top surface of the rock sample, so as to measure the depth of penetration of the indenter (bit) into the rock during each cycle of loading and unloading.

During testing, a start button was pressed for applying the axial compressive load. The bottom platen was moved up by the pump unit mechanism of the machine, so that the

indenter (bit) was pressed onto the rock simulating a situation as prevailing in actual drilling. The sample was loaded continuously for 60 seconds for all the bit-rock combinations. After 60 seconds the loading is stopped. Afterwards unloading is done. During loading and unloading, at every 5 seconds, force (from control unit) and penetration (from digital dial gauge) readings were noted down. However, the unloading time varied depending upon the bit-rock combinations. The time during loading and unloading was carefully recorded with the help of a stop watch.

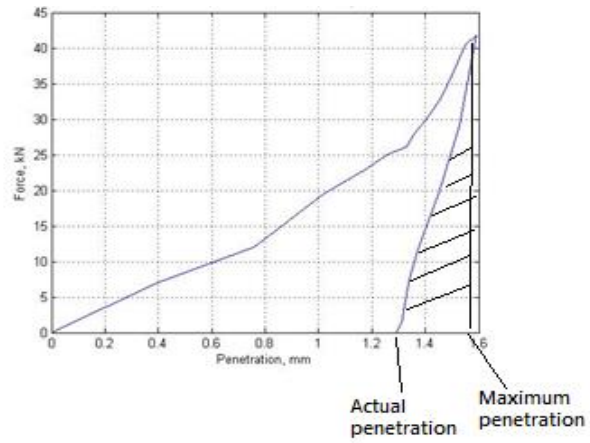
The sequence followed for every indentation involved loading and unloading, and then clearing so formed crater during indentation by collecting the rock chips. Then the bit was rotated through the desired indexing angle before new indentation was made. For each indexing angle, three indentations, each time on new rock sample, were made and the average of these three results were considered for calculating the energy under Force-penetration (F-P) curve and specific energy.

The volume of the crater was calculated by dividing the weight of the rock chips and its powder collected from the crater by the density of the rock. The volumes of very few craters were also measured using dental wax by pressing into the crater and the volume of the wax filled in the crater was determined using water displacement method. The volume calculated from the weight of the rock chips and its powder was found to be approximately 2 % higher than the one obtained by the dental wax method. Therefore, the crater volumes were calculated using the weight of the rock chips and powder was generated during the static indentation tests for all the bit- rock combinations.

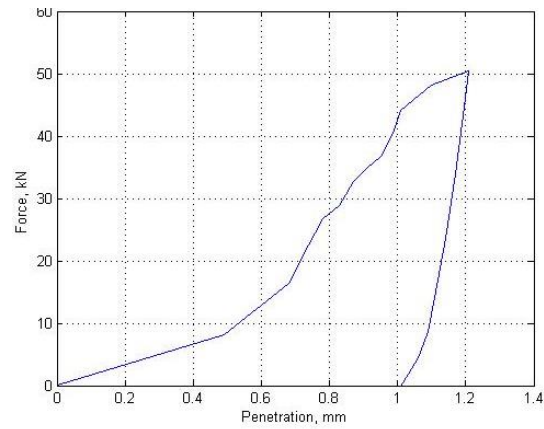
3.4.3 Force-Penetration Curves and Calculation of Specific Energy

Force-Penetration curves were plotted for all the bit-rock combinations. The energy expended in each test was the area under the force-penetration curve. This area was measured using a digital planimeter.

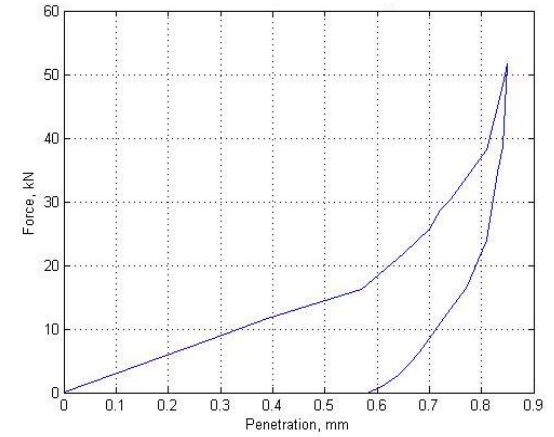
The penetration at the end of loading cycle (60 seconds) was the maximum penetration, whereas the penetration obtained at the end of unloading cycle was the actual penetration as shown Figure 3.14 (a). After unloading, the rock was relaxed and this relaxation depends on elastic properties such as Young's modulus and Poisson's ratio of rocks. The hatched portion in graph shown in Figure 3.14 (a) is relaxation of rock after unloading cycle. Energy used, i.e., the difference of energy given (area of the F-P curve up to the maximum penetration) and the energy due to the elastic rebound (area of F-P curve within the maximum penetration and the actual penetration) were calculated from the area of F-P curve as shown in Figure 3.14 (a). The ratio of the expended energy to the crater volume is the specific energy, (which is the energy required to break a unit volume of rock), was determined for all the bit-rock combinations at all the index angles. Force-Penetration (F-P) curves of static indentation test for all index angles for all 6 types of rocks for 35, 38, 45 and 48 mm are shown in Figures 3.14 to 3.61. The F-P curves for all index angles for all 6 types of rocks for 35 are shown from Figure 3.14 (a-f) to 3.17 (a-f) are shown in this section. Remaining F-P curves from Figure 3.18 (a-f) to Figure 3.61 (a-f) are shown in Appendix-I. The values of maximum penetration, actual penetration, energy used in each indentation and corresponding values of specific energy are shown from Tables 3.2 to 3.7. The actual specific energy is obtained by adding the value of specific energy determined at 0^0 index angle to the value of specific energy determined at corresponding index angle (10^0 or 20^0 or 30^0 or 40^0). The average of three values of specific energy were determined for chisel, cross and spherical button bits of 35, 38, 45 and 48 mm diameter are shown in Tables 3.8 to 3.10 (Appendix-I).



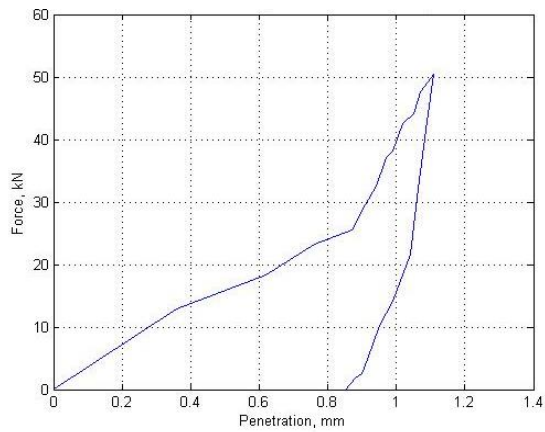
a) Marble



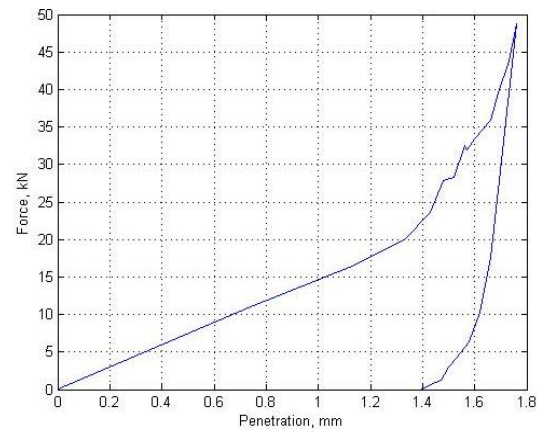
b) Limestone



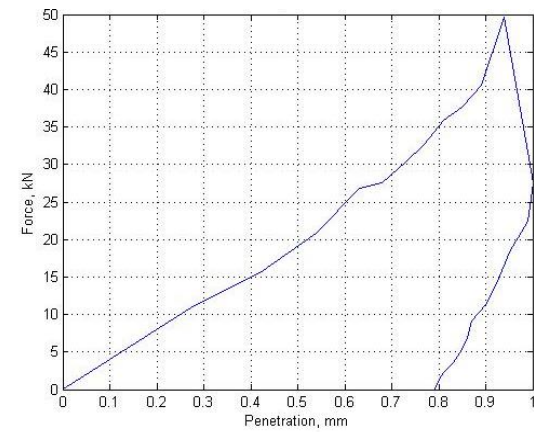
c) Basalt



d) Steel gray granite

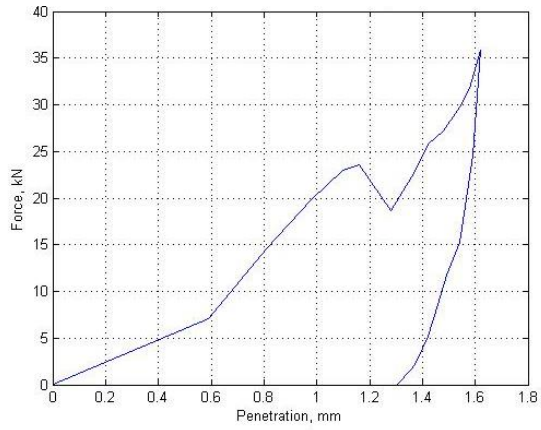


e) Moon white granite

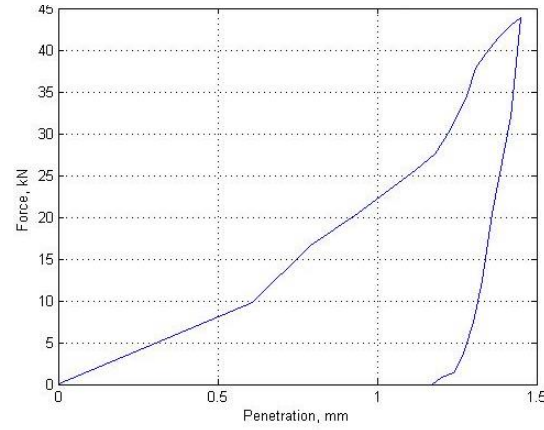


f) Black galaxy granite

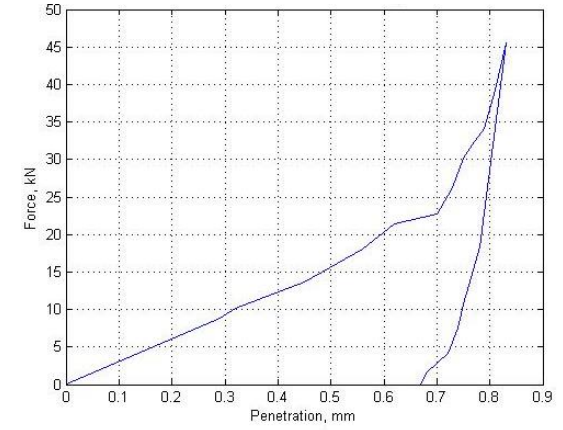
Figure 3.14 (a-f) Force–Penetration (F-P) curves for 35mm diameter chisel bit at 10^0 index angle for various types of rocks



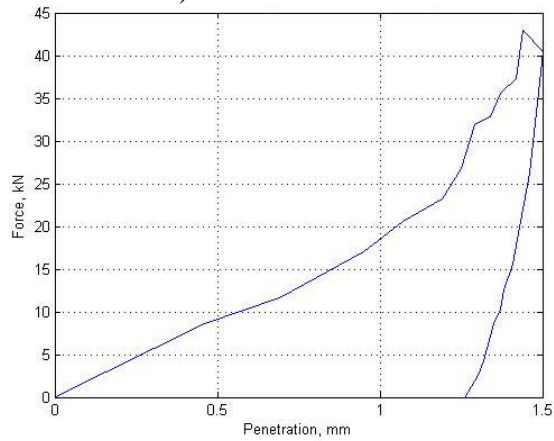
a) Marble



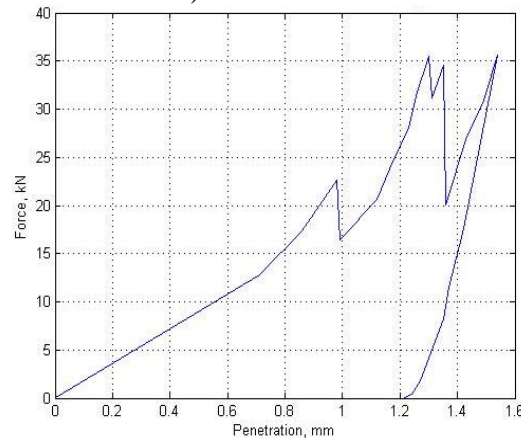
b) Limestone



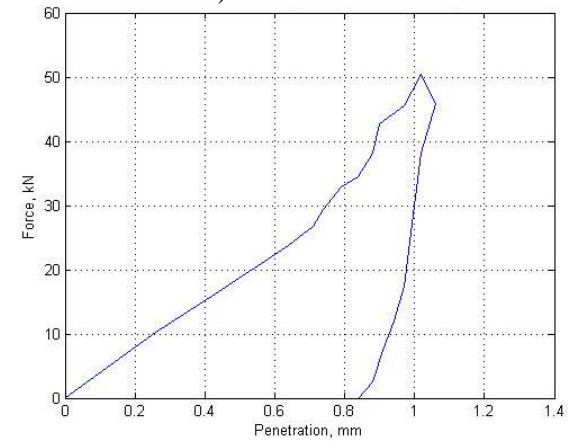
c) Basalt



d) Steel gray granite

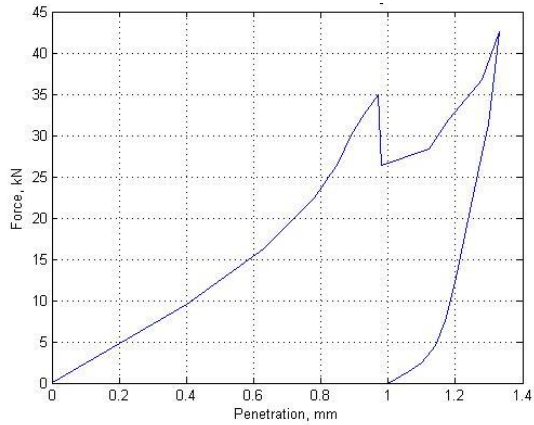


e) Moon white granite

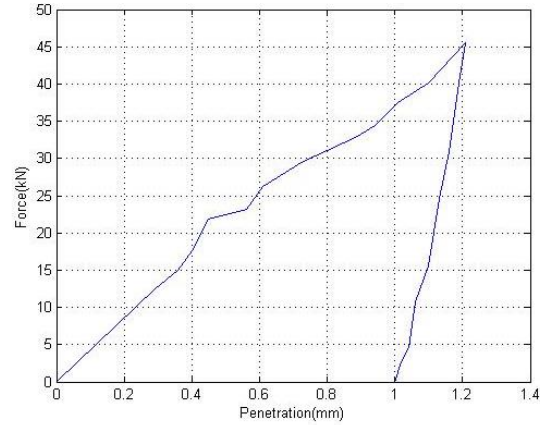


f) Black galaxy granite

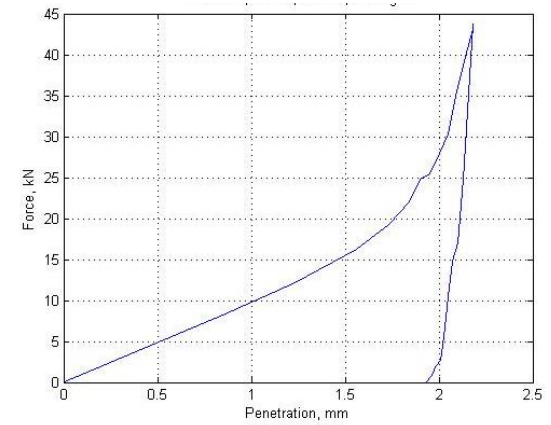
Figure 3.15 (a-f) Force–Penetration (F-P) curves for 35mm diameter chisel bit at 20° index angle for various types of rocks



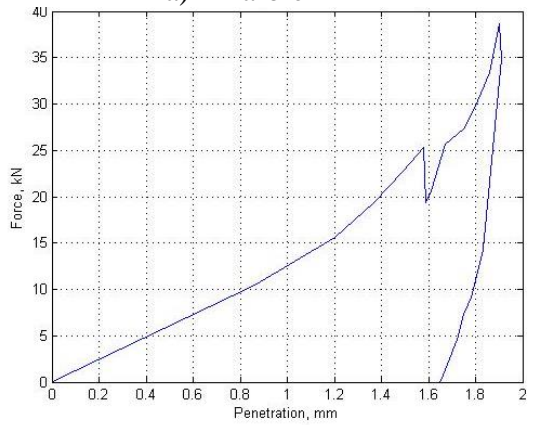
a) Marble



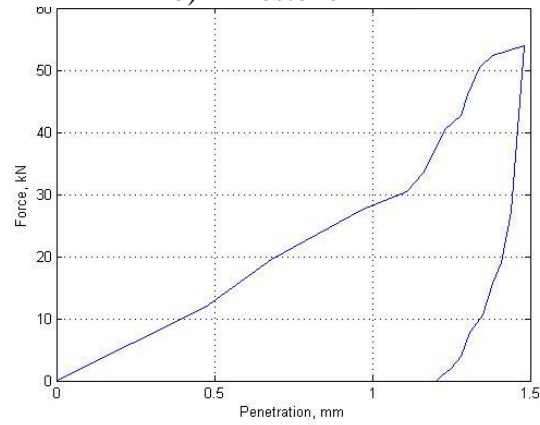
b) Limestone



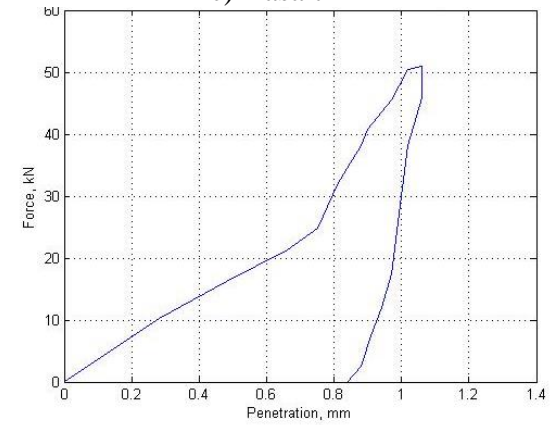
c) Basalt



d) Steel gray granite

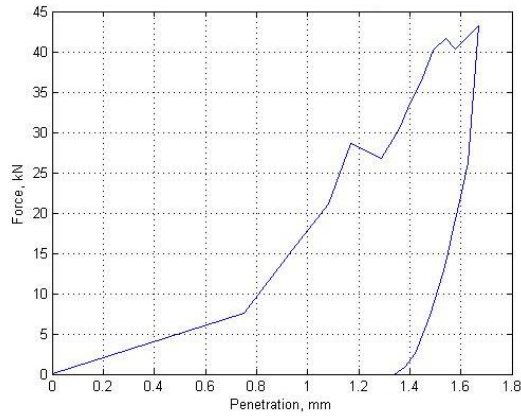


e) Moon white granite

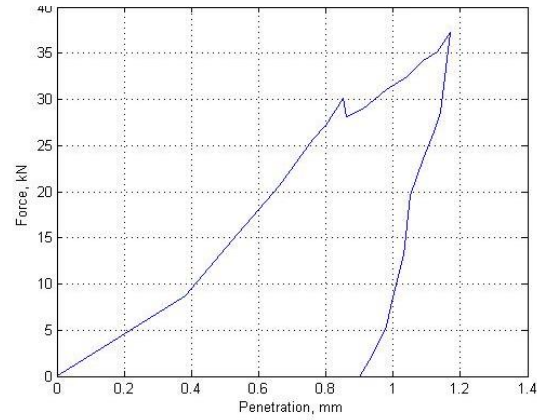


f) Black galaxy granite

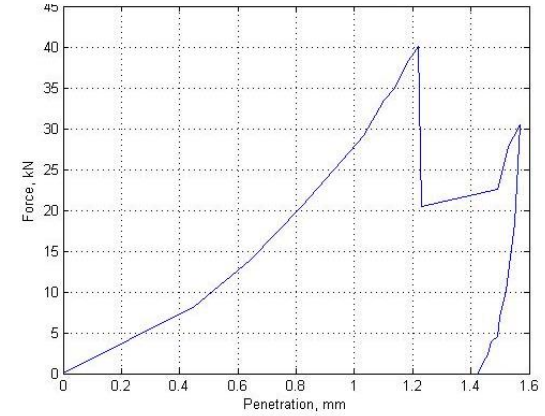
Figure 3.16 (a-f) Force–Penetration (F-P) curves for 35mm diameter chisel bit at 30° index angle for various types of rocks



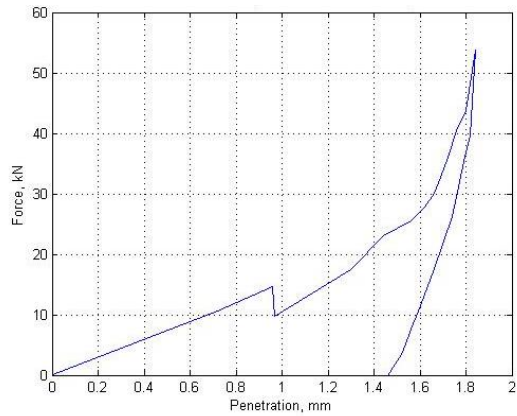
a) Marble



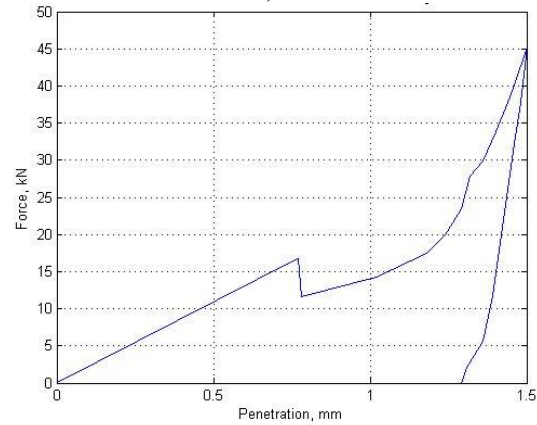
b) Limestone



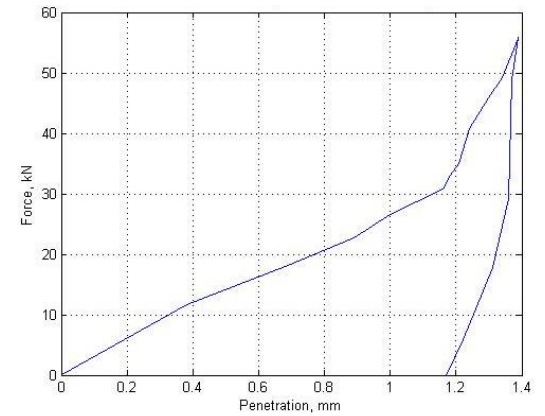
c) Basalt



d) Steel gray granite



e) Moon white granite



f) Black galaxy granite

Figure 3.17 (a-f) Force–Penetration (F-P) curves for 35mm diameter chisel bit at 40° index angle for various types of rocks

Table 3.2: Values of force, penetration, crater volume and specific energy in static indentation tests for marble rock

Dia- meter of bit (mm)	Bit geometry	Index angle (degrees)	Force (kN)	Maximum penetration (mm)	Actual penetration (mm)	Volume (m ³) x 10 ⁻⁷	Energy used (Nm)	Specific energy (Nm/m ³) x 10 ⁷ (8/7)
1	2	3	4	5	6	7	8	9
35	Chisel	10	41.8	1.55	1.29	0.627	17.86	28.46
		20	35.9	1.62	1.3	0.477	12.63	26.47
		30	42.6	1.33	1	0.590	14.50	24.57
		40	43.2	1.67	1.34	0.587	16.83	28.66
	Cross	10	38.4	1.47	1	0.348	10.76	30.89
		20	39.8	0.97	0.6	0.365	10.52	28.81
		30	46.9	1.13	0.68	0.473	13.04	27.58
		40	49.3	1.1	0.74	0.406	13.65	33.63
	Spherical button	10	42.9	1.41	1.17	1.953	20.57	10.54
		20	42.1	1.47	1.13	1.871	20.71	11.07
		30	38.2	1.61	1.4	2.342	20.60	8.79
		40	32.4	1.37	1.09	1.637	21.77	13.30
38	Chisel	10	49.7	0.81	0.45	0.858	17.90	20.87
		20	44.4	0.88	0.77	0.912	16.89	18.53
		30	50.8	1.38	0.99	0.939	17.63	18.79
		40	50.2	1.34	0.98	0.909	19.25	21.18
	Cross	10	46.8	0.74	0.5	0.658	14.06	21.38
		20	43.2	1.01	0.62	0.580	11.11	19.17
		30	37.9	1.04	0.63	0.580	10.48	18.09
		40	42.6	1.32	0.89	0.712	16.83	23.62
	Spherical button	10	42.7	1.71	1.48	2.708	35.78	13.21
		20	42.6	1.27	1.02	2.775	26.99	9.72
		30	36.1	1.91	1.56	2.704	25.78	9.53
		40	34.7	1.27	1.03	2.326	30.29	13.02

45	Chisel	10	54.7	1.69	1.36	0.850	11.63	13.68
		20	34.3	1.47	1.23	1.160	14.87	12.82
		30	39.5	1.43	1.24	1.666	20.30	12.19
		40	48.2	1.22	0.84	1.152	14.72	12.78
	Cross	10	50.1	0.84	0.41	0.522	11.05	21.15
		20	50.7	0.96	0.48	0.637	10.64	16.69
		30	55.8	0.89	0.41	0.850	13.50	15.88
		40	52.8	0.76	0.42	0.674	13.26	19.68
	Spherical button	10	42.7	1.71	1.41	2.712	18.68	6.89
		20	29.3	1.27	1.07	3.102	17.02	5.49
		30	33.9	1.51	1.25	3.615	19.58	5.42
		40	34.9	1.52	1.26	2.638	18.06	6.85
48	Chisel	10	36.8	1.23	0.88	1.368	15.05	11.00
		20	42.8	1.27	0.96	1.446	15.33	10.60
		30	46.2	1.08	0.7	0.938	9.92	10.58
		40	32.8	1.49	1.15	0.990	10.86	10.97
	Cross	10	51	1.09	0.74	1.179	18.26	15.49
		20	46.1	1.46	1	1.166	13.75	11.79
		30	61.5	1	0.79	1.163	12.24	10.52
		40	55.2	1.07	0.77	0.751	10.63	14.15
	Spherical button	10	37.5	1.11	0.77	3.527	18.46	5.23
		20	31.2	1.34	1.08	4.644	19.84	4.27
		30	43.7	1.13	0.79	4.654	15.42	3.31
		40	34.8	1.91	1.61	3.129	15.46	4.94

Table 3.3: Values of force, penetration, crater volume and specific energy in static indentation tests for limestone rock

Dia- meter of bit (mm)	Bit geometry	Index angle (degrees)	Force (kN)	Maximum penetration (mm)	Actual penetration (mm)	Volume (m ³) x 10 ⁻⁷	Energy used (Nm)	Specific energy (Nm/m ³) x 10 ⁷ (8/7)
1	2	3	4	5	6	7	8	9
35	Chisel	10	50.5	1.06	0.94	0.786	18.00	22.91
		20	43.9	1.38	1.17	0.974	18.47	18.96
		30	40.1	1.02	0.9	0.993	16.35	16.47
		40	37.2	1.34	1.24	0.776	17.45	22.50
	Cross	10	44.8	0.98	0.94	0.578	17.21	29.76
		20	46.5	1.04	1.04	0.658	18.00	27.37
		30	46.8	0.97	0.95	0.658	16.56	25.17
		40	46.5	1.33	1.33	0.656	19.00	28.98
	Spherical button	10	45.1	0.92	0.82	2.078	17.51	8.43
		20	49.4	1.77	1.5	2.018	15.76	7.81
		30	49.3	1.21	0.91	2.298	17.51	7.62
		40	48.4	1.29	1.07	2.024	18.99	9.38
38	Chisel	10	53.2	0.99	0.69	1.069	16.45	15.38
		20	51.2	1.82	1.46	1.153	16.28	14.12
		30	48.2	1.01	0.84	1.195	16.11	13.48
		40	45.1	1.24	0.96	1.242	18.59	14.97
	Cross	10	44.7	0.81	0.66	0.689	12.32	17.90
		20	40.7	1.65	4.21	0.802	12.44	15.50
		30	51.1	1.79	0.63	0.765	12.07	15.78
		40	54.9	0.8	0.58	0.746	13.80	18.51
	Spherical button	10	31.9	1.5	1.25	2.006	19.60	9.77
		20	42.9	1.36	1.06	2.547	20.39	8.01
		30	42.4	1.71	1.3	2.550	19.60	7.68
		40	42.9	1.06	0.93	1.605	17.24	10.74

45	Chisel	10	41.6	0.96	0.66	1.205	10.98	9.12
		20	45.8	1.46	1.07	1.329	11.42	8.59
		30	46.9	1.37	1.1	1.408	12.78	9.08
		40	46.8	1.08	0.96	1.157	15.05	13.00
	Cross	10	53.5	0.69	0.58	0.898	15.13	16.83
		20	54.9	0.61	0.4	0.936	16.04	17.14
		30	45.7	1.2	0.98	0.879	12.96	14.74
		40	45.8	1.21	0.83	0.773	15.77	20.41
	Spherical button	10	45.8	1.72	1.39	3.092	22.97	7.43
		20	43.5	1.66	1.17	3.066	21.11	6.88
		30	46.8	1.68	1.31	3.104	21.25	6.85
		40	41.2	1.02	2.09	2.720	22.54	8.28
48	Chisel	10	50.9	1.04	0.77	1.147	13.47	11.75
		20	49.9	1.06	0.79	1.574	13.16	8.36
		30	46.9	1.87	1.46	1.531	12.50	8.16
		40	43.2	1.3	1.01	1.320	10.00	7.58
	Cross	10	54.5	1.18	0.88	1.318	15.77	11.96
		20	58.7	0.94	0.74	1.352	16.36	12.10
		30	56.2	1.11	0.86	1.677	17.94	10.70
		40	48.6	1.05	0.87	1.356	18.17	13.39
	Spherical button	10	53.8	1.01	0.71	1.956	11.48	5.87
		20	45.9	1.34	1.03	1.547	8.00	5.17
		30	47.8	1.03	0.86	2.070	8.50	4.10
		40	36.7	1.19	0.92	2.770	12.97	4.68

Table 3.4: Values of force, penetration, crater volume and specific energy in static indentation tests for basalt rock

Dia- meter of bit (mm)	Bit geometry	Index angle (degrees)	Force (kN)	Maximum penetration (mm)	Actual penetration (mm)	Volume (m ³) x 10 ⁻⁷	Energy used (Nm)	Specific energy (Nm/m ³) x 10 ⁷ (8/7)
1	2	3	4	5	6	7	8	9
35	Chisel	10	51.7	0.85	0.58	0.258	9.94	38.54
		20	45.6	1.83	0.67	0.390	14.89	38.14
		30	43.7	2.13	1.93	0.502	20.80	41.43
		40	30.4	1.57	1.42	0.276	10.48	38.00
	Cross	10	47.2	0.91	0.52	0.233	11.08	47.67
		20	48.8	1.13	0.83	0.252	12.15	48.25
		30	44.8	0.89	0.66	0.269	12.43	46.28
		40	43.1	1.99	1.77	0.337	16.53	49.07
	Spherical button	10	48.6	1.46	1.24	0.840	20.13	23.98
		20	55.1	0.67	0.48	0.447	10.89	24.36
		30	51.5	0.77	0.62	0.418	10.13	24.22
		40	49.7	1.16	0.95	0.581	15.49	26.64
38	Chisel	10	50.7	1.41	1.23	0.311	9.06	29.11
		20	54.9	0.98	0.83	0.548	15.87	28.96
		30	55.7	1.74	1.59	0.372	11.93	32.07
		40	56.6	1.27	1.02	0.290	10.59	36.55
	Cross	10	54.2	0.64	0.39	0.280	12.94	46.21
		20	49.4	1.41	1.14	0.233	9.45	40.63
		30	51.8	1.35	1.05	0.217	9.08	41.81
		40	40.5	0.59	0.39	0.189	7.94	42.12
	Spherical button	10	40.7	1.47	1.27	0.405	11.05	27.28
		20	44.7	1.43	1.28	0.862	18.37	21.30
		30	35.9	1.71	1.52	0.466	11.05	23.72
		40	34.8	1.37	1.16	0.577	14.64	25.37

45	Chisel	10	38.8	1.41	1.23	0.108	4.01	37.15
		20	50.4	0.99	0.83	0.130	4.55	35.03
		30	50.6	1.77	1.59	0.183	6.86	37.52
		40	22.4	1.2	1.02	0.165	6.34	38.50
	Cross	10	48.1	0.65	0.4	0.198	8.40	42.45
		20	51.8	0.49	0.23	0.247	8.32	33.73
		30	63.7	0.69	0.43	0.231	9.04	39.07
		40	63.1	0.55	0.29	0.224	9.49	42.30
	Spherical button	10	51.9	1.11	0.8	0.412	10.17	24.67
		20	41.3	1.17	0.85	0.330	6.84	20.73
		30	48.9	1	0.71	0.510	13.09	25.69
		40	49.3	0.83	0.62	0.483	13.36	27.69
48	Chisel	10	51.8	0.85	0.69	0.387	10.66	27.53
		20	44.8	1.21	0.96	0.360	9.84	27.33
		30	24.6	1.56	1.35	0.322	9.28	28.81
		40	53.2	0.83	0.63	0.359	11.06	30.84
	Cross	10	48.2	0.79	0.59	0.201	9.27	46.04
		20	57.8	0.57	0.33	0.161	6.63	41.15
		30	52.8	0.72	0.5	0.160	7.37	46.04
		40	56.6	0.94	0.58	0.160	7.25	45.34
	Spherical button	10	53.1	0.84	0.6	0.568	10.09	17.76
		20	51.6	0.81	0.58	0.708	10.99	15.52
		30	51.5	0.99	0.74	0.768	13.36	17.39
		40	56.4	0.84	0.58	0.797	16.98	21.31

Table 3.5: Values of force, penetration, crater volume and specific energy in static indentation tests for steel gray granite rock

Dia- meter of bit (mm)	Bit geometry	Index angle (degrees)	Force (kN)	Maximum penetration (mm)	Actual penetration (mm)	Volume (m ³) x 10 ⁻⁷	Energy used (Nm)	Specific energy (Nm/m ³) x 10 ⁷ (8/7)
1	2	3	4	5	6	7	8	9
35	Chisel	10	50.5	1.11	0.85	0.411	12.74	31.04
		20	40.6	1.46	1.26	0.324	10.86	33.50
		30	34.9	1.91	1.65	0.454	14.95	32.91
		40	53.7	1.84	1.46	0.329	11.66	35.41
	Cross	10	52.6	1.04	0.75	0.302	12.44	41.16
		20	52.4	1.15	0.86	0.226	9.25	40.84
		30	49.8	1.06	0.72	0.311	12.89	41.50
		40	55.6	0.77	0.45	0.378	16.97	44.94
	Spherical button	10	64.5	0.64	0.44	0.744	15.84	21.29
		20	53.6	1.06	0.95	0.450	7.62	16.94
		30	53.4	1.29	1.06	0.798	15.84	19.85
		40	58.9	1.02	0.81	0.753	18.32	24.35
38	Chisel	10	48.1	1.47	1.31	0.335	10.24	30.59
		20	44.8	1.02	0.78	0.590	15.89	26.93
		30	49.1	0.62	0.42	0.363	10.65	29.35
		40	40.6	1.3	1.01	0.363	9.77	26.95
	Cross	10	52.9	0.97	0.66	0.291	10.64	36.54
		20	52.8	0.79	0.53	0.212	7.36	34.74
		30	52.5	0.75	0.45	0.270	9.70	35.89
		40	54.9	0.56	0.34	0.295	11.40	38.64
	Spherical button	10	44.6	1.41	1.17	0.612	13.10	21.43
		20	24.3	1.34	1.18	0.705	13.31	18.87
		30	50.7	1.51	1.32	1.132	24.75	21.86
		40	28.3	1.59	1.42	0.617	15.51	25.16

45	Chisel	10	46.8	0.95	0.81	0.551	15.68	28.43
		20	45.8	1.24	1.01	0.544	16.37	30.08
		30	39.3	0.98	0.83	0.400	12.52	31.29
		40	45.5	1.4	1.18	0.440	14.08	32.02
	Cross	10	60.5	1.13	0.79	0.360	11.95	33.19
		20	56.8	0.84	0.53	0.292	9.45	32.40
		30	57.7	0.81	0.58	0.303	10.67	35.21
		40	57.9	0.51	0.3	0.183	6.43	35.19
	Spherical button	10	46.3	1.2	0.98	0.588	13.79	23.43
		20	42.6	1.73	1.54	1.209	26.67	22.05
		30	37.8	1.42	1.18	0.896	20.24	22.58
		40	42.1	1.24	0.98	0.887	19.18	21.63
48	Chisel	10	58.7	0.75	0.61	0.276	8.08	29.29
		20	59.6	1.05	0.79	0.233	6.05	26.02
		30	57.2	0.76	0.6	0.363	11.11	30.64
		40	58.7	0.94	0.78	0.294	10.14	34.48
	Cross	10	53.6	0.87	0.57	0.262	10.20	38.88
		20	56.1	0.86	0.56	0.328	10.85	33.10
		30	60.1	0.93	0.62	0.299	10.85	36.26
		40	56.3	0.86	0.57	0.291	11.25	38.62
	Spherical button	10	43.3	1.1	0.86	0.780	10.79	13.83
		20	38.9	0.87	0.68	0.697	8.42	12.08
		30	52.8	0.72	0.57	1.107	14.99	13.54
		40	55.9	1.13	0.94	0.921	12.51	13.58

Table 3.6: Values of force, penetration, crater volume and specific energy in static indentation tests for moon white granite rock

Dia- meter of bit (mm)	Bit geometry	Index angle (degrees)	Force (kN)	Maximum penetration (mm)	Actual penetration (mm)	Volume (m ³) x 10 ⁻⁷	Energy used (Nm)	Specific energy (Nm/m ³) x 10 ⁷ (8/7)
1	2	3	4	5	6	7	8	9
35	Chisel	10	48.7	1.76	1.39	0.380	14.02	36.89
		20	35.6	1.54	1.21	0.437	14.93	34.21
		30	53.9	1.48	1.2	0.432	15.10	34.99
		40	45.2	1.5	1.26	0.363	14.46	39.80
	Cross	10	45.7	0.89	0.5	0.128	5.22	40.67
		20	52.9	0.61	0.41	0.168	7.11	42.21
		30	56.1	0.68	0.45	0.209	9.20	44.04
		40	56.5	0.84	0.57	0.202	9.26	45.75
	Spherical button	10	40.4	1.19	1	0.649	12.95	19.94
		20	39.1	1.7	1.67	0.848	12.62	14.89
		30	58.7	0.81	0.67	0.480	8.96	18.66
		40	44.7	1.62	1.43	0.385	10.75	27.91
38	Chisel	10	50.8	0.95	0.73	0.423	13.17	31.10
		20	34.3	1.19	0.92	0.389	12.25	31.51
		30	47.8	0.77	0.64	0.428	14.60	34.08
		40	27.8	1.27	1	0.384	12.91	33.62
	Cross	10	56.1	0.95	0.6	0.253	9.56	37.78
		20	52.8	0.97	0.7	0.240	9.19	38.31
		30	58.3	0.47	0.32	0.282	11.67	41.45
		40	58.1	0.46	0.24	0.280	12.14	43.29
	Spherical button	10	56.9	1.19	0.95	0.500	10.28	20.55
		20	56.1	1.18	0.94	0.602	10.38	17.25
		30	64.4	1.5	1.35	0.470	10.31	21.95
		40	61.2	1.6	1.43	0.655	16.89	25.80

45	Chisel	10	50.1	0.72	0.61	0.393	13.05	33.19
		20	47.9	1.03	0.85	0.530	17.60	33.20
		30	44.3	1.04	0.99	0.400	13.69	34.18
		40	44.5	0.97	0.77	0.403	14.55	36.09
	Cross	10	52.9	1.01	0.65	0.277	11.38	41.02
		20	50.1	0.92	0.61	0.398	14.95	37.58
		30	56.4	0.78	0.46	0.278	9.92	35.72
		40	55.8	0.72	0.4	0.246	9.46	38.47
	Spherical button	10	22.5	1.67	1.44	0.893	21.75	24.36
		20	39.1	1.22	0.96	1.152	24.11	20.93
		30	58.7	1.12	0.88	0.821	17.88	21.78
		40	44.7	1.15	0.89	0.682	18.41	26.98
48	Chisel	10	58.9	0.5	0.4	0.462	13.18	28.51
		20	47.9	0.95	0.81	0.420	12.18	29.00
		30	61.3	0.57	0.43	0.155	4.91	31.73
		40	61.4	0.7	0.56	0.395	12.17	30.79
	Cross	10	55.1	1.04	0.72	0.276	11.07	40.10
		20	52.3	0.96	0.61	0.378	12.79	33.79
		30	53.3	0.89	0.48	0.447	19.41	43.43
		40	54.2	0.76	0.52	0.218	10.15	46.55
	Spherical button	10	58.4	0.55	0.39	0.802	12.39	15.45
		20	25.1	1.04	0.87	0.952	12.83	13.47
		30	64.4	0.61	0.43	0.572	8.15	14.24
		40	61.2	0.66	0.4	0.740	11.33 2	15.31

Table 3.7: Values of force, penetration, crater volume and specific energy in static indentation tests for black galaxy granite rock

Dia- meter of bit (mm)	Bit geometry	Index angle (degrees)	Force (kN)	Maximum penetration (mm)	Actual penetration (mm)	Volume (m ³) x 10 ⁻⁷	Energy used (Nm)	Specific energy (Nm/m ³) x 10 ⁷ (8/7)
1	2	3	4	5	6	7	8	9
35	Chisel	10	27.6	1	0.79	0.420	15.85	37.70
		20	45.9	1.06	0.84	0.494	19.17	38.85
		30	50.9	1.04	0.83	0.398	15.02	37.73
		40	55.7	1.37	1.17	0.283	11.93	42.21
	Cross	10	54.4	0.56	0.33	0.160	7.45	46.56
		20	42.6	0.98	0.71	0.287	12.45	43.34
		30	63.3	0.71	0.43	0.304	14.20	46.67
		40	61.9	0.77	0.52	0.343	14.05	41.00
	Spherical button	10	50.4	1.19	1.01	0.533	12.39	23.26
		20	55.9	1.33	1.21	0.700	14.71	21.02
		30	56.5	0.94	0.75	0.542	12.99	23.97
		40	64.4	0.51	0.4	0.682	18.79	27.55
38	Chisel	10	43.6	1.17	0.9	0.323	8.84	27.34
		20	36.2	1.09	0.88	0.305	8.07	26.45
		30	40.1	0.88	0.72	0.283	8.83	31.24
		40	42.3	0.5	0.42	0.380	12.26	32.24
	Cross	10	46.7	0.54	0.28	0.290	12.29	42.35
		20	59.9	0.73	0.49	0.291	12.19	41.89
		30	63.9	0.58	0.34	0.270	12.03	44.53
		40	64.9	0.6	0.36	0.222	10.23	46.11
	Spherical button	10	51.2	1.91	1.74	0.703	16.73	23.79
		20	50.2	1.88	1.7	0.767	16.87	22.00
		30	40.9	1.81	1.63	0.718	16.73	23.30
		40	36.9	1.8	1.6	0.763	21.21	27.79

45	Chisel	10	57.7	1.07	0.85	0.342	12.38	36.18
		20	55.2	1.06	0.9	0.375	13.69	36.53
		30	56.7	0.92	0.7	0.415	15.26	36.74
		40	48.3	1.23	0.97	0.281	10.06	35.73
	Cross	10	62.1	0.62	0.4	0.192	7.38	38.53
		20	45.5	0.63	0.36	0.192	7.39	38.42
		30	65.1	0.71	0.41	0.145	5.93	41.04
		40	60.1	0.77	0.53	0.165	7.33	44.43
	Spherical button	10	36.6	1.16	0.9	0.501	13.20	26.34
		20	30.9	1.55	1.34	0.500	11.95	23.92
		30	38.9	1.24	1	0.569	15.09	26.50
		40	59.3	0.95	0.71	0.581	15.94	27.42
48	Chisel	10	60.3	0.75	0.55	0.314	9.52	30.32
		20	63.3	0.71	0.59	0.464	12.39	26.73
		30	64.1	0.42	0.28	0.287	8.18	28.50
		40	62.6	0.6	0.37	0.329	9.96	30.26
	Cross	10	55.2	0.89	0.6	0.343	15.43	44.94
		20	61.9	0.78	0.47	0.245	10.06	40.98
		30	65.8	0.9	0.66	0.327	14.20	43.43
		40	60.2	0.86	0.63	0.226	10.18	45.08
	Spherical button	10	47.9	0.86	0.65	0.480	7.23	15.07
		20	48.3	0.93	0.72	0.438	6.05	13.81
		30	49.5	0.89	0.57	0.419	6.79	16.20
		40	48.5	0.88	0.62	0.629	13.01	20.68

3.5 TESTS TO DETERMINE THE PROPERTIES OF ROCKS

This elucidate on the different procedures to determine the physico-mechanical properties of rocks like density, hardness(SRN), UCS, BTS, abrasion resistance, Young's Modulus and Poisson's ratio as per the methods suggested by International Society for Rock Mechanics (ISRM).

3.5.1 Determination of Abrasion resistance of rocks

Abrasivity means the abrasiveness i.e resistance to wear of a rock against other materials e.g. steel. It is an important measure to estimate the wear of rock drilling and boring equipment. Abrasion test measures the resistance of rocks to wear. These tests include wear when subject to an abrasive material, wear in contact with metal and wear produced by contact between the rocks. Abrasiveness tests can also measure the wear on metal components (e.g. tunnelling machine cutters) as a result of contact with the rock. Los Angeles abrasion test was used for determination of abrasivity of all the rocks in the present study. The abrasive charge and the test sample used are dependent on the aggregate size and grading. The coarse aggregate of four sizes for the test are shown in Table 3.11.

Table 3.11 Sizes of sample with respect to Sieve size for abrasion test

Sieve size, mm (Square openings)		Weights of indicated sizes, grams
Passing	Retained on	
38	25.5	1250
25	19	1250
19	13.2	1250
13.2	9.5	1250



Figure 3.62 Los Angeles abrasion testing machine

The recombined aggregate(test sample) of above sizes and the abrasive charge(11 steel balls) were placed in the Los Angles abrasion testing machine (Figure 3.62) and rotated the cylinder at a speed of 30-33 rev/min for 500 revolutions(as per ISRM standards). After the prescribed number of revolutions, discharged the material from the machine and sieved the tested sample on a sieve courser than 1.7 mm. The sieved portion of fines is the loss of the material. The value of the percentage wear is obtained by expressing the difference between the original weight and the final weight of the test sample as a percentage of the original weight of the test sample.

The results of abrasion resistance test are shown in Table 3.13.

3.5.2 Determination of Uniaxial Compressive Strength

The ability of rock to resist compressive load/stress is called compressive strength of rock. The ISRM has suggested the method to determine uniaxial compressive strength of rock samples in the form of specimens of regular geometry. To determine the Uniaxial

Compressive Strength (UCS) of the rock samples, 54 mm diameter NX-size core specimens, having a length-to-diameter ratio of 2.5 to 3: 1. The oven-dried and NX-size core samples were tested by using a microcontroller compression testing machine in the Rock Mechanics Laboratory (Figure 3.63). Load was applied continuously at a stress rate 0.5 MPa/s until the failure occurred. The maximum load (in kN) at failure was recorded.



Figure 3.63 Compressive testing machine

The UCS of the specimen was calculated by dividing the maximum load carried by the specimen during the test, by the original cross-sectional area. Three readings were taken and the average of results of compressive test are shown in Table 3.13.

3.5.3 Determination of Brazilian Tensile Strength

The ability of rock to resist tensile (pulling) load/stress is called Tensile Strength of rock. The ISRM has suggested direct and indirect methods to determine tensile strength of rock samples. But in the laboratory no facilities were there to find tensile strength of rock samples. Therefore, indirect method of determination of tensile strength by Brazil test was used. To determine the Brazilian tensile strength (BTS) of the rock samples, 54mm

diameter NX- size core specimens, having a length (thickness) less than 27mm were prepared as per ISRM suggestions. The cylindrical surfaces were made free from any irregularities across the thickness using polishing machine. End surfaces were made flat to within 0.25 mm and parallel to within 0.25⁰. The specimen was wrapped around its periphery with one layer of the masking tape and loaded into Brazil tensile test machine (Figure 3.64) across its diameter. The test specimen was placed between the two steel loading jaws in the testing machine in such a way that the load transfer system is properly aligned. The tensile load on the specimen was applied continuously at stress rate of 200 N/s until sample failed. The maximum load (in kN) at failure was recorded.



Figure 3.64 Brazilian tensile strength testing machine

The BTS of the specimen was calculated by dividing the maximum load applied to the specimen by the original cross-sectional area. Ten readings were taken and the average of results of test are shown in Table 3.13.

3.5.4 Determination of dry density of rocks

The volume of a sample may be determined by water displacement. The specimen is dropped under water and its volume determined from the displaced water volume. A

graduated measuring container was used for this purpose. Density is a mass per unit volume of rock. Initially the weight of the sample was measured. The initial reading of water level (height of water column) in the graduated container was taken. Then the sample was dropped slowly in the water container. The final reading of height of water column in graduated container was taken. Difference of the two readings was the volume of water displaced. The density data of sample was obtained from measurement of volume and mass and volume of each sample and using the following formula.

Density (gm/cc) = mass of the sample/ volume of sample. Ten readings were taken and the average of results of test are shown in Table 3.13.

3.5.5 Determination of Hardness of rocks:

Hardness is one of the physical properties of rocks. The Schmidt hammer (SH), which was originally developed for determination of hardened concrete hardness (Schmidt, 1951). Later it has been improved to measure the hardness of rocks. The Schmidt hardness test is also quick, cheap and non-destructive. In the field of rock mechanics, it is widely used for its simplicity, portability and the capability of instant data production. Today, even though different types of Schmidt hammers are available for use, the models of L-type and N-type are extensively employed (Guney et al., 2005).

The earlier ISRM method suggested the use of only the L-type SH. But now standard L- and N-type hammers, with respective impact energies of 0.735 and 2.207 Nm, are used. The N-type hammer is less sensitive to surface irregularities, and should be preferred in field applications; while the L-type hammer has greater sensitivity in the lower range and gives better results when testing weak, porous and weathered rocks (Aydin, 2015).

For specimens, diameter of cores should be of at least NX size i.e 54 mm for the L-type hammer and preferably T2 size (84 mm) for the N-type should be used. Block specimens should also be at least 100 mm thick at the point of impact Length of cores and surface area of blocks should be large enough to accommodate these suggestions; for example, if a 2 cm spacing of impact points is chosen, a core length of 43.5 cm (for NX size) or a block surface area of 268 cm² (for 10 cm thickness) is required to gather 20 readings (Adnan

Aydin, 2015). Rock blocks were collected from various locations in India. Six rock types of igneous, sedimentary and metamorphic origins were selected to conduct the Schmidt tests on cubic samples of 0.127 m length \times 0.1524 m width \times 0.2032 m height. All the tests were carried out with the hammer held vertically downwards and at right angles to horizontal faces of large rock blocks. The tests were performed by an N type Schmidt hammer with an impact energy of 2.207 Nm. For data gathering, 20 rebound values, as recommended by the ISRM suggested method, were taken from single impacts separated by a plunger diameter of 15mm. The mean of 20 readings is the hardness of the specimen. The values are shown in the Table 3.12.

Table 3.12: Values of Schmidt hammer test

S.No	Schmidt hammer number (SRN)					
	Marble	Limestone	Basalt	SGG	MWG	BGG
1	40	46	54	54	54	62
2	48	48	54	62	48	54
3	52	50	50	60	50	60
4	48	46	50	58	60	64
5	44	52	51	58	54	58
6	46	48	54	56	56	60
7	52	49	52	54	56	60
8	52	52	53	52	56	60
9	50	52	50	50	52	62
10	48	51	52	62	50	64
11	44	52	50	52	54	62
12	44	50	51	62	54	60
13	48	51	53	58	52	50
14	46	50	55	50	48	58
15	46	47	52	52	43	56
16	46	48	54	52	56	62
17	50	52	55	60	50	60
18	52	48	54	62	48	56
19	48	46	55	54	46	60
20	50	46	53	52	50	58
Mean value (SRN)	47.7	49.2	52.6	56	51.85	59.3
Rounded value of SRN	48	49	53	56	52	59

3.5.6 Determination of Young's Modulus of the rock

Young's modulus is modulus of elasticity measuring the stiffness of a rock. For, small strains, it is defined as the ratio of the rate of change of the stress with strain. The ends of the specimens were made flat and perpendicular to the axis of the specimen. Their sides were smoothed and polished and the specimens were inspected to be free of cracks, fissures, veins and other flaws, which could act as selective plans of weakness and cause any undesirable change in the real properties of the rocks. The rock samples, 54 mm diameter NX-size core specimens, having a length-to-diameter ratio of 2.5 to 3: 1, were used for the test. The oven-dried and NX-size core samples were tested by using a microcontroller compression testing machine in the Rock Mechanics Laboratory. A dial gauge was used for measuring the axial strain. An arrangement to mount the dial gauge was fixed to the sample during testing. Load was applied continuously at a stress rate 0.5 MPa/s until the failure occurred. The load was applied generally up to 70% of the compressive strength. Loads and axial or deformations were recorded at evenly spaced load intervals during the test. Ten readings were taken over the load range to define the axial stress-strain curves. Then, the Young's Modulus of the specimen was calculated by dividing the ratio of the axial stress change to axial strain produced by the stress change.

Ten readings were taken and the average of results of test are shown in Table 3.13.

3.5.7 Determination of Poisson's ratio

To determine Poisson's ratio, ends of the specimens were made flat and perpendicular to the axis of the specimen. Their sides were smoothed and polished and the specimens were inspected to be free of cracks, fissures, veins and other flaws, which could act as selective plans of weakness and cause any undesirable change in the real properties of the rocks. The rock samples, 54 mm diameter NX-size core specimens, having a length-to-diameter ratio of 2.5 to 3: 1, were used for the test. Two dial gauges were used for axial and

circumferential strains. The oven-dried and NX-size core samples were tested by using a microcontroller compression testing machine in the Rock Mechanics Laboratory. Load was applied continuously at a stress rate 0.5 MPa/s until the failure occurred. The load was applied generally up to 70% of the compressive strength. The applied loads and axial (ϵ_a) and circumferential/diametrical strains (ϵ_d) or deformations were recorded at evenly spaced load intervals during the test.. At least ten readings should be taken over the load range to define the axial and diametric stress-strain curves.

Poisson's ratio was calculated from the equation

$$\nu = - \frac{\text{Slope of Axial Stress–Strain curve}}{\text{Slope of the diametrical Stress–strain curve}}$$

Ten readings were taken and the average of results of test are shown in Table 3.13.

Table 3.13:Physico-mechanical properties of Rocks

S.No	Properties of Rocks	Marble	Limestone	Basalt	Steel gray granite	Moon white granite	Black galaxy granite
1	Density (gm/cc)	2.59	2.62	2.8	2.76	2.6	2.635
2	Uniaxial Compressive strength (MPa)	24.52	29.55	54.13	30.59	28.83	56.97
3	Brazilian Tensile strength (MPa)	2.58	2.66	5.58	3.09	2.98	5.83
4	Abrasion resistance (%)	35.8	29.6	16.2	24.2	31.6	17.2
5	Hardness(SRN)	46	48	53	56	52	59
6	Young's Modulus (GPa)	21.31	24.94	29.09	28.24	24.675	30.63
7	Poisson's Ratio	0.22	0.235	0.3	0.26	0.24	0.29

3.6 DETERMINATION OF MINERALOGICAL AND TEXTURAL FEATURES (THIN SECTION EXAMINATION)

Rock is aggregate of minerals. Depending upon the minerals present in rock, the properties of rock varies. Gokhan Aydin(2012) has carried out mineralogical characterisation tests and multiple regression analysis was carried out between the percentage of minerals present in the rocks and SE. He concluded that the mineralogical properties could primarily be responsible for the specific energy rather than the physico-mechanical properties of the rock.

Similarly B. Tiryaki et al.(2005) carried out mineralogical characterisation tests and texture coefficient. He then carried out and multiple regression analysis was carried out between the percentage of minerals present in the rocks, texture coefficient and SE. He concluded that certain minerals like minerals like Feldspar and quartz content in sandstone were found to influence SE. Based on these findings the objective of influence of mineralogical composition on SE was taken up. It can be concluded that apart from the physic-mechanical properties of rocks, mineralogical composition of rocks also influence the SE.

Based on the above, it is planned to find out mineralogical composition of rocks with an aim to find the influence of mineralogical composition of rocks on SE.

For this purpose, few lumps were selected from samples and thin sections were prepared to study the mineralogical composition and textural features. The remaining sample was crushed and ground to minus 65 mesh size. Subsequently minus 65 plus 200 mesh size fraction was studied under the microscope. The result of the samples are given below:

3.6.1. Sample Name: Marble

a) Megascopic Studies

The rock sample is pink coloured, hard and compact lump of about 10 cm size.

b) Microscopic Studies

Carbonates (calcite) are the predominant minerals present in the sample with sub-ordinate amount of quartz. Biotite mica, martitized magnetite, clay and pyrite are found in trace amounts. Carbonates (calcite) are medium to coarse grained (200 to 900 microns) present as granular aggregates and also form to other minerals. Inter-granular spaces of carbonates are filled with quartz and biotite mica.

Quartz is fine to medium grained (120 to 400 microns) present as patches within the inter-granular spaces of carbonates.

Biotite mica is fine to medium grained medium (30 to 300 microns) present as discrete grains within the inter-granular spaces of carbonates.

The approximate relative abundance of different mineral constituents are given in Table 3.14 and photomicrographs of marble are shown in Figure 3.65 (a) and (b).

Table 3.14: Mineral constituents of the marble sample

Mineral	Percentage
Carbonates (calcite)	86
Quartz	15
Biotite mica	1
Martitized magnetite	0.8
Pyrite	0.1
Clay	0.6
Hornblende	0.2

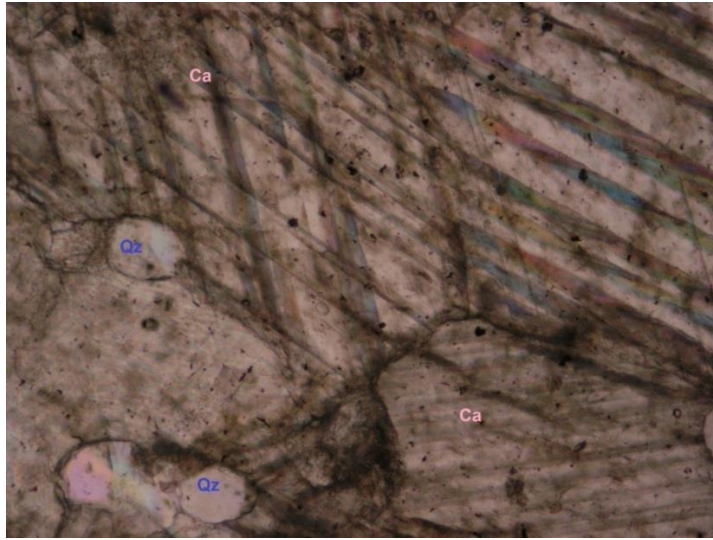


Figure 3.65 (a) Photomicrographs of marble: Quartz (Qz) is present within the inter-granular spaces of Calcite (Ca) in thin section. (Transmitted light, 10X).

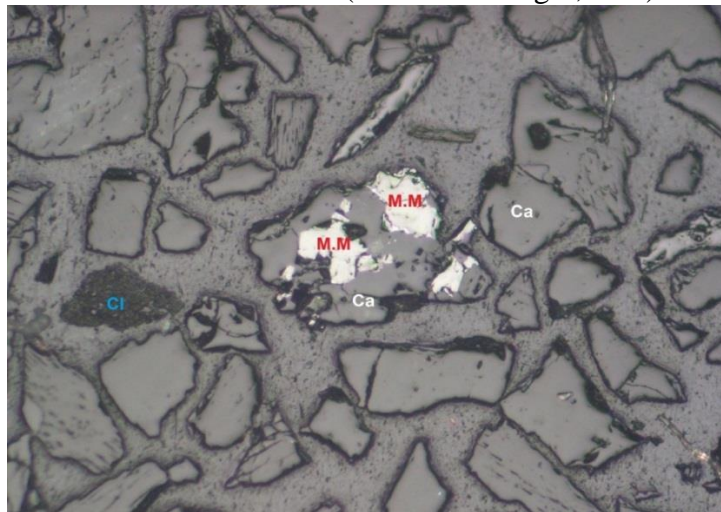


Figure 3.65 (b) Photomicrographs of marble: Martitized magnetite (M.M) is present as inclusion within the inter-Granular spaces of Calcite (Ca). Free clay (Cl) is also seen in minus 65 plus 200 mesh Mount. (Reflected light, 20X).

3.6.2. Sample Name: Limestone

a) Megascopic Studies

The rock sample is grey coloured, hard and compact lump of about 10 cm size.

b) Microscopic Studies

Fine grained Carbonates are the predominant mineral present in the sample. Biotite mica, clay and pyrite are found in very minor to trace amounts.

Carbonates are very fine grained present as granular aggregates.

Pyrite is fine grained (less than 30 micron) present as inclusion within the carbonate groundmass.

The approximate relative abundance of different mineral constituents are given in Table 3.15 and photomicrographs of limestone are shown in Figure 3.66 (a) and (b).

Table 3.15: Mineral constituents of the limestone sample

Mineral	Percentage
Carbonates	88
Clay	4
Biotite mica	3
Pyrite	0.9

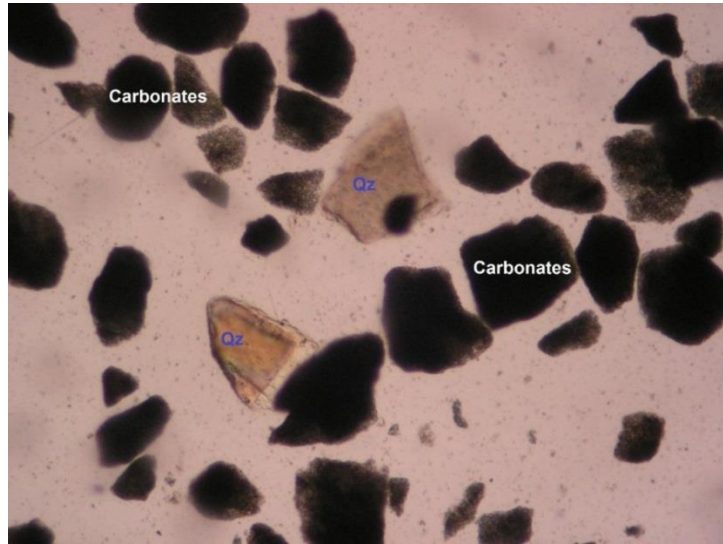


Figure 3.66 (a) Photomicrographs of limestone: Carbonates and quartz (Qz) grains, in 1.560 Refractive Index Liquid media. (Transmitted light, 10X)

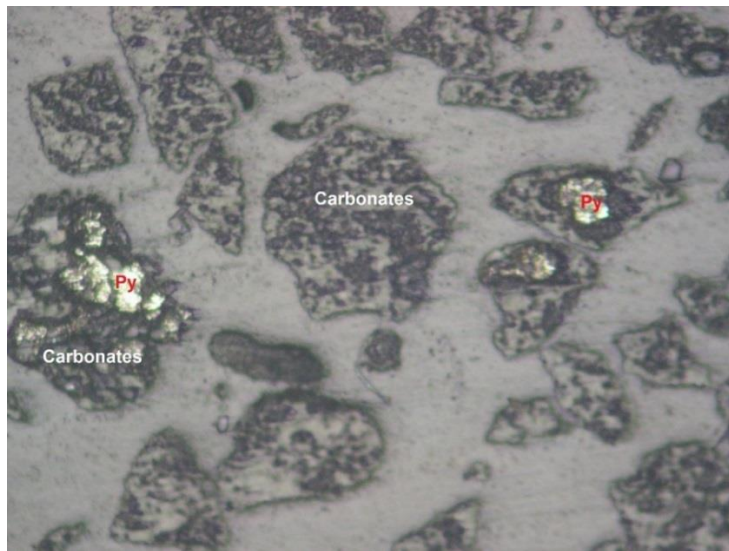


Figure 3.66 (b) Photomicrographs of limestone: Carbonates and pyrite (Py) is present are seen in minus 65 plus 200 mesh mount. (Reflected light, 10X).

3.6.3. Sample Name: Basalt

a) Megascopic Studies

The sample is dark brown coloured, hard and compact lump of about 10 cm size.

b) Microscopic Studies

Pyroxene + amphibole and feldspar are the major minerals present in the sample with subordinate amount of magnetite. Biotite mica, olivine, pyrite and hematite are found in very minor to trace amounts.

Pyroxenes are fine to medium grained (40 to 250 microns), present as patches within the inter-granular spaces of feldspar and amphibole.

Feldspar is fine grained (20 to 80 microns), present as patches and discrete grains within the inter-granular spaces of pyroxene and amphiboles.

Magnetite is fine to medium grained (20 to 120 microns), present as discrete grains within the groundmass of silicates are seen in minus 65 plus 200 mount.

Biotite mica is fine to medium grained (20 to 80 microns), present as patches and discrete grains within the inter-granular spaces of pyroxene, amphibole and feldspar.

The approximate relative abundance of different mineral constituents are given in Table 3.16 and photomicrographs of basalt are shown in Figure 3.67 (a) and (b).

Table 3.16: Mineral constituents of the basalt sample

Mineral	Percentage
Pyroxene + Amphibole	58
Feldspar	56
Magnetite	15
Biotite mica	3
Olivine	5
Pyrite	0.9
Hematite	0.8

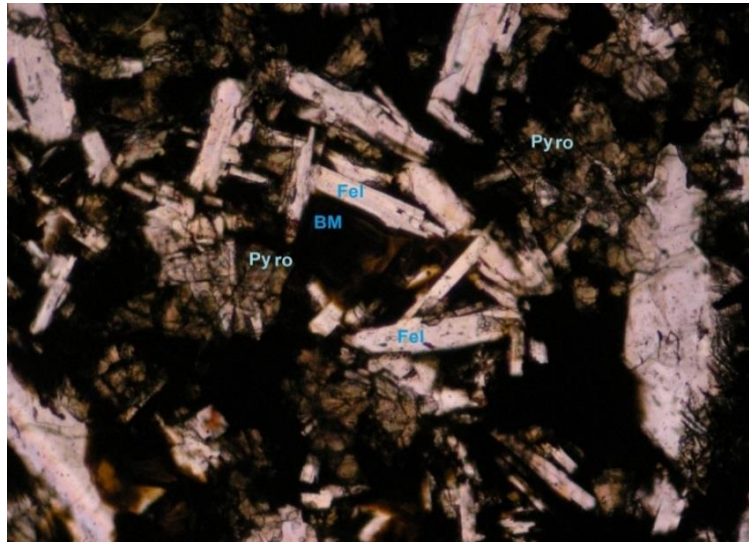


Figure 3.67 (a) Photomicrographs of basalt: Pyroxene (pyro), Feldspar (Fel) and Biotite mica (BM) are seen in thin section. (Transmitted light, P.P. 5x)

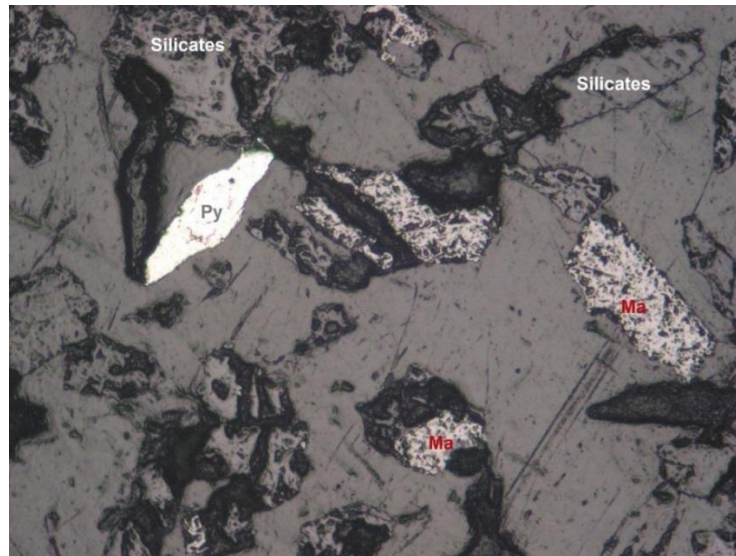


Figure 3.67 (b) Photomicrographs of basalt: Magnetite (Ma), pyrite (Py) and silicates are seen in minus 65 plus 200 Mesh mount. (Reflected light, 10X).

3.6.4. Sample Name: Steel grey granite

a) Megascopic Studies

The sample is grey coloured, hard and compact lump of about 12 cm size.

b) Microscopic Studies

Feldspar and amphibole are the major minerals present in the sample with sub-ordinate amount of biotite mica. Quartz, magnetite, pyroxene, chalcopyrite, pyrite and arsenopyrite are found very minor to trace amounts.

Feldspar is fine to coarse grained (80 to 400 microns), present as granular aggregates and form groundmass to other minerals.

Amphiboles are fine to medium grained (50 to 240 microns), present as patches within the inter-granular spaces of quartz and feldspar.

Biotite mica is fine to medium grained (70 to 350 microns), present as patches and discrete grains within the inter-granular spaces of feldspar and amphibole.

Quartz is fine to medium grained (20 to 180 microns), present as patches and discrete grains within the inter-granular spaces of feldspar and amphibole.

The approximate relative abundance of different mineral constituents are given in Table 3.17 and photomicrographs of steel gray granite are shown in Figure 3.68 (a) and (b).

Table 3.17: Mineral constituents of the steel gray granite sample

Mineral	Percentage
Feldspar	59
Amphibole	55
Biotite mica	15
Quartz	45
Magnetite	5
Pyroxene	4
Chalcopyrite	0.8
Pyrite	0.9
Arsenopyrite	0.8

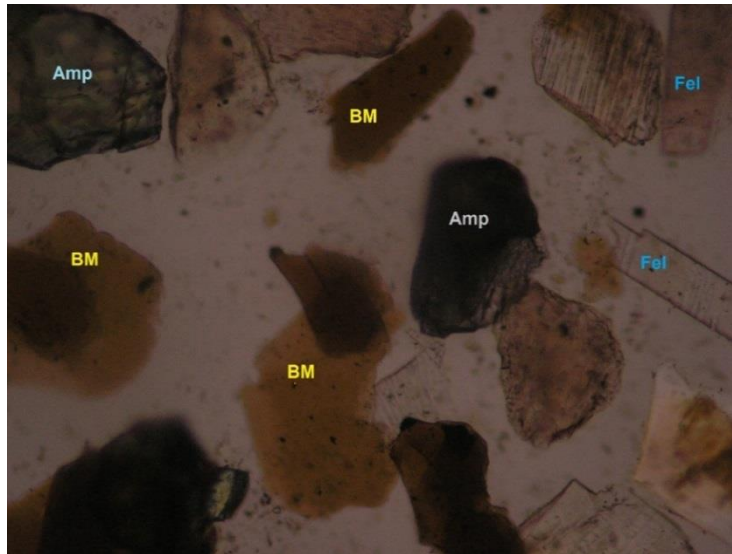


Figure 3.68 (a) Photomicrographs of Steel Gray Granite: Amphibole (Amp), Biotite mica (BM) and feldspar (Fel) grains, in .560 Refractive Index Liquid media. (Transmitted light, 10X).

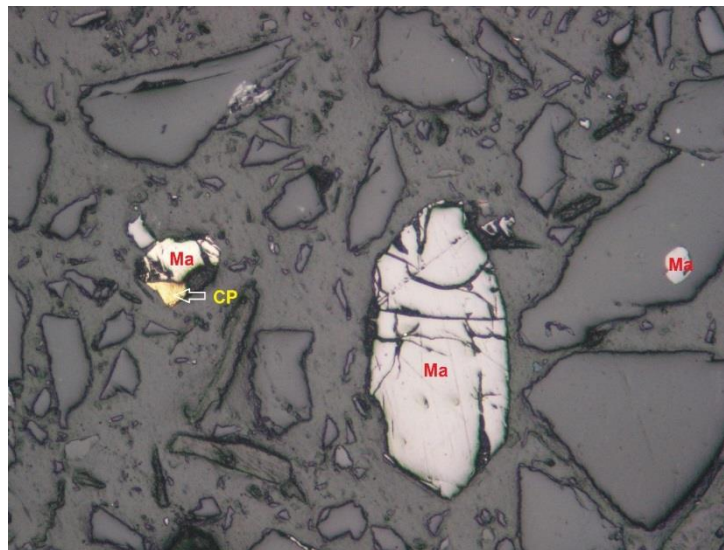


Figure 3.68 (b) Photomicrographs of steel gray granite: Magnetite (Ma) and chalcopyrite (CP) are seen in Minus 65 plus 200 Mesh mount. (Reflected light, 20X).

3.6.5. Sample Name: Moon white granite

a) Megascopic Studies

The sample is white coloured, hard and compact lump of about 8 cm size.

a) Microscopic Studies

Quartz and feldspar are the major minerals present in the sample. Biotite mica, amphibole, garnet, magnetite / martitized magnetite, pyrite and ilmenite found in very minor to trace amounts.

Quartz is fine to medium grained (30 to 200 microns), present as granular aggregates and forms the groundmass to other minerals. Inter-granular spaces of quartz are filled with feldspar and amphibole.

Feldspar is fine to medium grained (60 to 300 microns), present as granular aggregates within the inter-granular spaces of quartz and amphibole.

Biotite mica is fine to medium grained, present as discrete grains within the inter-granular spaces of quartz and feldspar.

Amphiboles are fine to medium grained (40 to 250 microns), present as patches within the inter-granular spaces of quartz and feldspar.

The approximate relative abundance of different mineral constituents are given in Table 3.18 and photomicrographs of steel gray granite are shown in Figure 3.69 (a) and (b). Table 3.18: Mineral constituents of the moon white granite sample

Mineral	Percentage
Quartz	60
Feldspar	58
Biotite mica	5
Amphibole	5
Garnet	4
Magnetite / martitized magnetite	1
Pyrite	1
Ilmenite	0.8

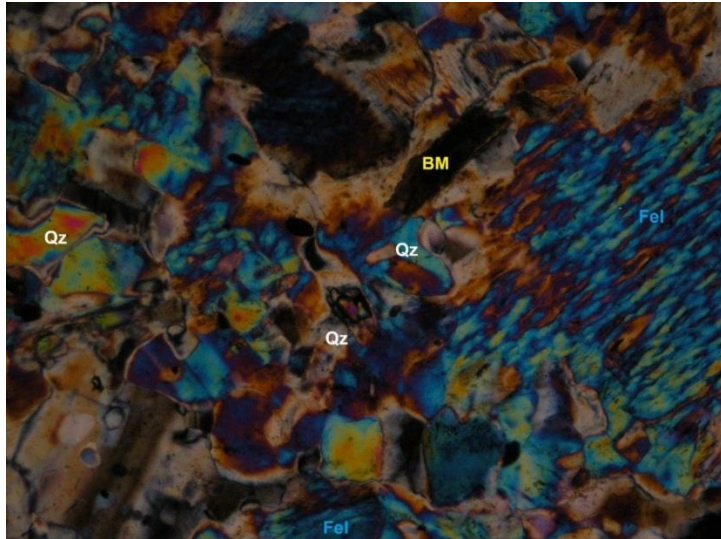


Figure 3.69 (a) Photomicrographs of Moon white Granite: Quartz (Qz), feldspar (Fel) and Biotite mica (BM) are seen in thin section (Transmitted light, X polar, 5x)

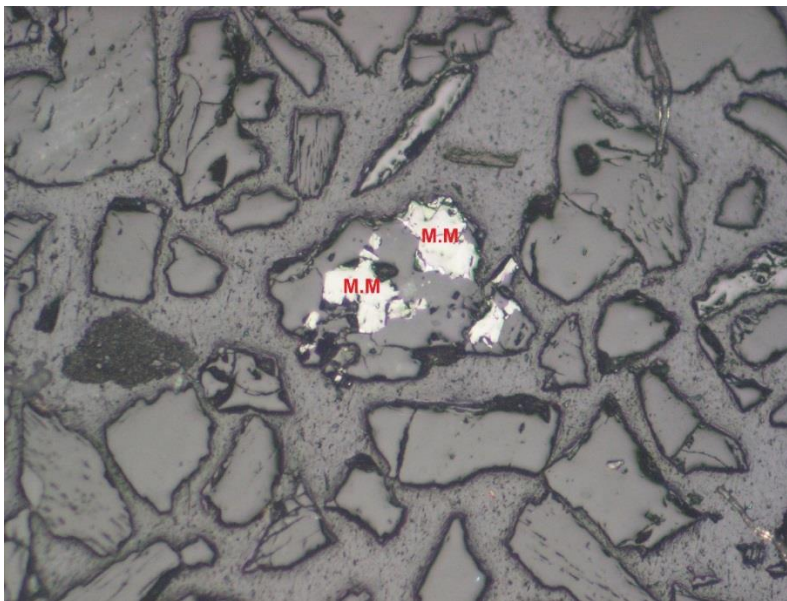


Figure 3.69(b) Photomicrographs of Moon white Granite: Martitized magnetite (M.M) inclusions within the Feldspar / quartz Groundmass in mount. (Reflected light 10x, Air)

3.6.6. Sample Name: Black galaxy granite

a) Megascopic Studies

The sample is black coloured, hard and compact lump of about 10 cm in size.

b) Microscopic Studies

Feldspar and amphibole (hornblende) are the major minerals present in the sample with sub-ordinate amount of quartz. Biotite mica, pyrite, magnetite and hematite are found in minor to trace amounts.

Feldspar is medium to coarse grained (150 to 500 microns) present as granular aggregates. Amphibole (hornblende) is fine to coarse grained (40 to 600 microns) present as patches and discrete grains within the inter-granular spaces of feldspar, quartz and biotite groundmass.

Quartz is fine to medium grained (40 to 200 microns) present as granular aggregates.

Biotite mica is fine to medium grained (60 to 250 microns) present as patches within the inter-granular spaces of amphibole, quartz and feldspar. It is also present as discrete grain within the other silicates.

Pyrite is fine grained mineral present as inclusions within the silicates.

The approximate relative abundance of different mineral constituents are given in Table 3.19 and photomicrographs of steel gray granite are shown in Figure 3.70 (a) and (b).

Table 3.19: Mineral constituents of the black galaxy granite sample

Mineral	Percentage
Feldspar	57
Amphibole (hornblende)	60
Quartz	42.7
Biotite mica	5
Pyrite	5
Magnetite	1
Hematite	0.8

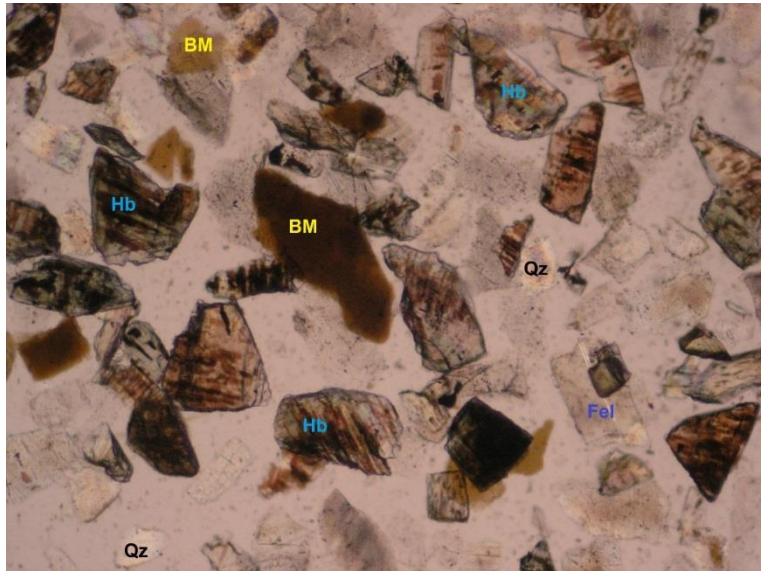


Figure 3.70 (a) Photomicrographs of black galaxy Granite: Hornblende (Hb), Biotite mica (BM), Quartz (Qz) and feldspar(fel)grains, in 1.560 Refractive Index Liquid media. (Transmitted light, 10X).

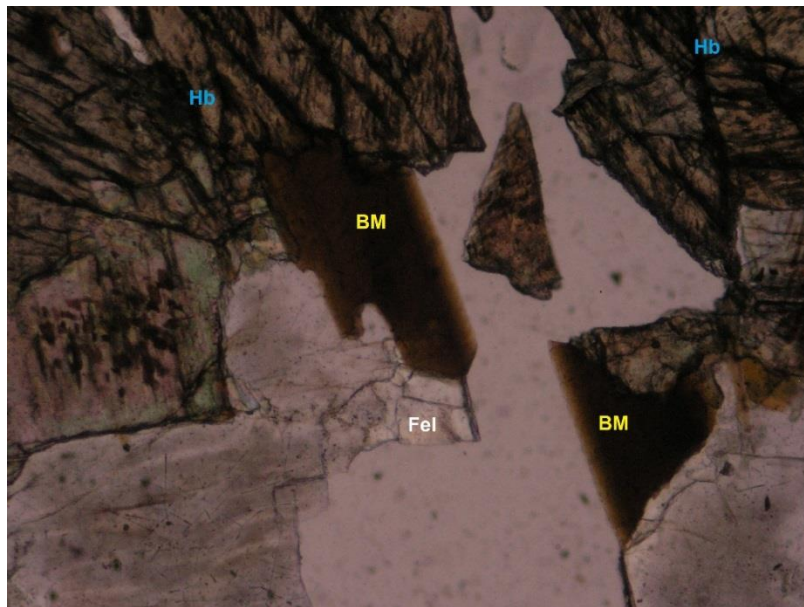


Figure 3.70 (b) Photomicrographs of black galaxy granite: Hornblende (Hb), Biotite mica (BM) and feldspar (Fel) grains, are seen in thin section. (Transmitted light, P.P. 10X).

3.7 DETERMINATION OF ELEMENTAL/MINERALS IN OXIDE FORM USING X-RAY FLUORESCENCE (XRF) TEST

3.7.1 INTRODUCTION

An X-ray fluorescence (XRF) spectrometer is an X-ray instrument used in non-destructive chemical analyses of rocks, minerals, sediments and fluids. It works on principles of wavelength-dispersive spectroscopic that are similar to an electron microprobe (EPMA). XRF is a robust technique with high precision with straightforward, fast sample preparation. It can be used in high-throughput industrial environments.

The atoms of the test sample absorb energy from the X-rays, become excited and then emit secondary X-rays. Each chemical element emits X-rays at a unique energy. By measuring the intensity and energy of the emitted X-rays, an X-ray Fluorescence Analyser can provide qualitative and quantitative analysis regarding the thickness and composition of the test sample.

The technology used for the dispersion, identification and intensity measurement of a test sample's X-ray fluorescence spectrum gives rise to two main types of spectrometer: wavelength dispersive (WDXRF) and energy dispersive (EDXRF) systems.

3.7.2 XRF INSTRUMENT



Figure 3.71. XRF instrument (Model Epsilon 1)

The XRF instrument model Epsilon 1 (Figure 3.71) is a fully integrated energy dispersive XRF analyzer consisting of a spectrometer, built-in computer, touch screen and analysis software. Powered by the latest advances in excitation and detection technology the Epsilon 1 is a star performer in the low-cost bench top instrument class.

Epsilon 1 produces fast, cost-effective, precise and accurate data with minimal operator dependence and sample preparation. The total running cost is therefore much lower than other analytical techniques and wet chemical methods that are costly and also require a dedicated skilled operator.

Epsilon 1 is built for the characterization and analysis of any type of sample in many industry segments such as cement, cosmetics, environmental, food, forensics, metals and coatings, mining and minerals, nano-materials, petrochemicals, pharmaceuticals and polymers.

Four software options are available to further enhance the capabilities of the Epsilon 1:

Omnian: Advanced standardless analysis

Stratos: Chemical composition and thickness analysis of layered materials

FingerPrint: Material type confirmation routine with Yes/No answer

Enhanced Data Security: designed for GMP and GLP environments and enables to comply with FDA 21 CFR part 11.

3.7.3 EXPERIMENT PROCEDURE

A few lumps were selected from the samples to study the mineralogical composition. The sample was placed in the tray of the instrument. The step-wise procedure available in the software was followed and the composition of the minerals/elements in oxides form was saved and noted down. The XRF results i.e. composition of the minerals/elements in oxides form is shown in Table 3.20.

Table 3.20: Elemental/ minerals in (%) oxide form in XRF test

Type of the Rock	Al ₂ O ₃	SiO ₂	SO ₃	Cl	K ₂ O	CaO	TiO ₂	V ₂ O ₅	Cr ₂ O ₃	MnO	Fe ₂ O ₃	NiO	CuO	ZnO	SrO	Co ₃
Marble	1.73	8.47	0.74	0.18	0.23	46.39	592.6*	-	-	486.8*	6.43	-	-	-	191.5*	41.15
Lime stone	7.14	19.01	0.23	0.16	1.80	27.98	0.84	365.7*	-	417.1*	0.43	61.6*	91.4*	132.9*	283.7*	-
Basalt	13.36	41.71	0.45	0.33	0.53	10.00	1.93	813.1*	-	0.230	18.14	186.5*	813.8*	144.7*	469.1*	-
Steel Gray Granite	16.99	44.85	0.29	0.45	7.85	10.69	1.63	427.2*	233.9*	0.126	8.45	-	85.5*	136.9*	0.271	-
Moon White Granite	10.59	55.39	0.14	6.58	9.88	8.92	0.77	188.6*	-	0.316	10.23	-	169.3*	515.9*	334.3	-
Black Galaxy Granite	16.61	42.66	0.65	0.34	1.03	13.52	0.79	374.300*	394.3*	0.173	10.47	214.3*	63*	114.6*	0.105	-
Sand stone	23.09	58.54	1.62	0.41	5.65	3.69	2.00	235.8*	151.7*	693.5*	3.8	61.6*	120.9*	414.7*	0.713*	49.6*

* Parts per million (PPM)

II THEORETICAL INVESTIGATIONS

3.8 DEVELOPMENT OF PREDICTIVE MODELS FOR ESTIMATION OF SE (REGRESSION MODELS)

In experimental research, after obtaining the experimental data, the data has to be processed and analysed to carry out scientific study. The processing of data comprises operations like editing, coding, classification and tabulation of collected data so that they are amenable to analysis. The analysis refers to the computation of certain statistical measures along with searching for relationship among data-groups. Analysis involves estimating the values of unknown parameters and testing of hypotheses, if any, for drawing inferences.

There are many types of analysis, but for the experimental research, Multiple regression analysis to establish relationships among the data groups and Multivariate analysis of variance (or multi-ANOVA) to check for appropriateness of the multiple regression model are very important (Kothari, 1985).

A regression analysis is a process of estimating the relationships among variables. It includes many techniques for modeling and analysing several variables, when the focus is on the relationship between a dependent variable and one or more independent variables. More specifically, regression analysis helps one understand how the typical value of the dependent variable (or 'criterion variable') changes when any one of the independent variables is varied, while the other independent variables are held fixed. The regression analysis is a statistical method used for the formulation of mathematical model depicting relationship amongst variables and can be used for the purpose of prediction of the values of dependent variable, given the values of the independent variable. Multiple regression analysis is used when one dependent variable is a function of two or more independent variables. The objective of this analysis is to make a prediction about the dependent variable based on its covariance with all the concerned independent variables (Kothari, 1985).

It generally uses the ordinary least squares method which derives the equation by minimizing the sum of the squared residuals. Its results indicate the direction, size, and statistical significance of the relationship between a predictor and response. The sign of each coefficient indicates the direction of the relationship, coefficients represent the mean change in the response for one unit of change in the predictor while holding other predictors in the model constant and p-value for each coefficient tests the null hypothesis that the coefficient is equal to zero (no effect). Therefore, low p-values suggest the predictor is a meaningful addition to your model.

In practice, the performance of regression analysis methods depends on the form of the data generating process, and how it relates to the regression approach being used. The regression analysis often depends, to some extent, on making assumptions about this process because the true form of the data-generating process is generally not known. These assumptions can be sometimes testable if a sufficient quantity of data is available. Regression models for prediction are useful even when the assumptions are moderately violated, although they may not perform optimally. However, in many instances, especially with small effects or questions of causality based on observational data, regression methods can give misleading results.

The ANOVA is an important technique in the context of all situations to compare more than two groups. The basic principle of ANOVA is to test for differences among the means of the groups by examining the amount of variation within each of these samples, relative to the amount of variation between the samples. In short, we have to make two estimates of group's variance viz., one based on between samples variance and the other based on within samples variance. Then the said two estimates of group variance are compared with *F*-test, which is given by following equation (Kothari, 1985).

$F = \text{Estimate of population variance based on between samples variance} / \text{Estimate of population variance based on within samples variance.}$

A significant F indicates a linear relationship between dependent variable and at least one of the independent variables. Once a multiple regression equation has been constructed, one can check how good it is (in terms of predictive ability) by examining the coefficient of determination (R^2). R^2 always lies between 0 and 1. All software provides it whenever regression procedure is run. The closer R^2 is to 1, the better is the model and its prediction (Kothari C R, 1985).

The R, R^2 and Adjusted R^2 , are important measures of regression analysis, where R is a measure of the correlation between the observed value and the predicted value of the criterion variable. R Square (R^2) is the square of this measure of correlation and indicates the proportion of the variance in the criterion variable, so an Adjusted R^2 value is calculated which takes into account the number of variables in the model and the number of observations the model is based on. This Adjusted R^2 value gives the most useful measure of the success of the model. If, for example, we have an Adjusted R Square value of 0.75, we can say that the model is accounted for 75% of the variance in the criterion (Orlov, 1996).

3.8.1 MATHEMATICAL MODELS USING MULTIPLE REGRESSION ANALYSIS

A computing Minitab 17 program was used for the statistical analysis. Multi-variable linear regression analysis was carried out to predict the specific energy. A number of statistical parameters or terms are associated with multi-variable linear regression analysis were determined. Predictors that were used in multiple linear model of SE are diameter of drill bit, index angle, density, UCS, BTS, Abrasion resistance, SRN, Young's Modulus and Poisson's ratio.

For the development of regression models for all the bits, 70% of the data (66 data sets) have been considered for training and 30% of the data (30 data sets) have been considered for testing.

3.8.2 Multiple Regression Analysis of Chisel bit

Table 3.21 Analysis of Variance (ANOVA) of chisel bit model

Source of variations	Degree of freedom	Sum of squares	Mean squares	F-value	p-value
Regression	9	34543.3	3838.14	158.63	0.000
Diameter of the bit	1	1258.2	1258.2	52.00	0.000
Index angle	1	721.8	721.8	29.83	0.000
Density	1	1951.1	1951.1	80.64	0.000
UCS	1	314.4	314.4	13.00	0.001
Hardness(SRN)	1	153.8	153.8	6.36	0.015
BTS	1	183.5	183.5	7.59	0.008
Abrasion resistance	1	816.6	816.6	33.75	0.000
Young's Modulus	1	795.1	795.1	32.86	0.000
Poisson's ratio	1	1961.9	1961.9	81.09	0.000
Error	56	1354.9			
Total	65	35898.2			

Table 3.22 Model Summary of chisel bit model

R ²	Predicted R ²	Adjusted R ²	Standard error
96.23%	94.26%	95.62%	4.91889

Table 3.23 Coefficients of chisel bit model

Model terms	Parameter estimate (coefficients)	t-value	p-value
Constant	3469	6.16	0.000
Diameter of the bit	-0.898	-7.21	0.000
Index angle	0.3504	5.46	0.000
Density	-1074	-8.98	0.000
UCS	-59.8	-3.61	0.001
Hardness(SRN)	-2.52	-2.52	0.015
BTS	416	2.75	0.008
Abrasion resistance	-27.32	-5.81	0.000
Young's Modulus	-27.22	-5.73	0.000
Poisson's ratio	6543	727	0.000

Regression Equation

$$SE = 3469 - 0.898 D_i + 0.3504 IA - 1074 D_e - 59.8 UCS - 2.52 SRN + 416 BTS - 27.32 AR - 27.22 Y + 6543 PR \quad \dots\dots\dots (3.1)$$

Where

- SE = Specific energy
- D_i = Diameter of the bit
- IA = Index angle
- D_e = Density
- UCS = Uniaxial compressive strength
- SRN = Hardness (Schmidt Rebound Number)
- BTS = Brazilian tensile strength
- AR = Abrasion resistance
- Y = Young's Modulus
- PR = Poisson's Ratio

3.8.3 Multiple Regression Analysis of Cross bit

Table 3.24 Analysis of Variance (ANOVA) of cross bit model

Source of variations	Degree of freedom	Sum of squares	Mean squares	F-value	P-value
Regression	9	35466.2	3940.69	148.32	0.000
Diameter of the bit	1	1395.5	1395.5	52.52	0.000
Index angle	1	707.2	707.2	26.62	0.000
Density	1	2737.7	2737.7	103.04	0.000
UCS	1	460.3	460.3	17.32	0.000
Hardness(SRN)	1	220.2	220.2	8.29	0.016
BTS	1	276.9	276.9	10.42	0.003
Abrasion resistance	1	1293.1	1293.1	48.67	0.000
Young's Modulus	1	1079.2	1079.2	40.62	0.000
Poisson's ratio	1	2192.7	2192.7	82.53	0.000
Error	56	1487.9	1487.9		
Total	65	36954.1	36954.1		

Table 3.25 Model Summary of cross bit model

R^2	Predicted R^2	Adjusted R^2	Standard error
95.97%	93.70%	95.33%	5.15456

Table 3.26 Coefficients of cross bit model

Model terms	Parameter estimate (coefficients)	t-value	p-value
Constant	4320	7.35	0.000
Diameter of the bit	-0.939	-7.25	0.000
Index angle	0.3371	5.16	0.000
Density	-1267	-10.15	0.000
UCS	-72.3	-4.16	0.000
Hardness(SRN)	-3.02	-2.88	0.006
BTS	510	3.23	0.002
Abrasion resistance	-34.24	-6.98	0.000
Young's Modulus	-31.67	-6.37	0.000
Poisson's ratio	6920	9.08	0.000

Regression Equation of cross bit

$$S.E = 4320 - 0.939 D_i + 0.3371 IA - 1267 D_e - 72.3 UCS - 3.02 SRN + 510 BTS - 34.24 AR - 31.67 Y + 6920 PR \dots\dots\dots (3.2)$$

Where

- SE = Specific energy
- D_i = Diameter of the bit
- IA = Index angle
- D_e = Density
- UCS = Uniaxial compressive strength
- SRN = Hardness (Schmidt Rebound Number)
- BTS = Brazilian tensile strength
- AR = Abrasion resistance
- Y = Young's Modulus
- PR = Poisson's Ratio

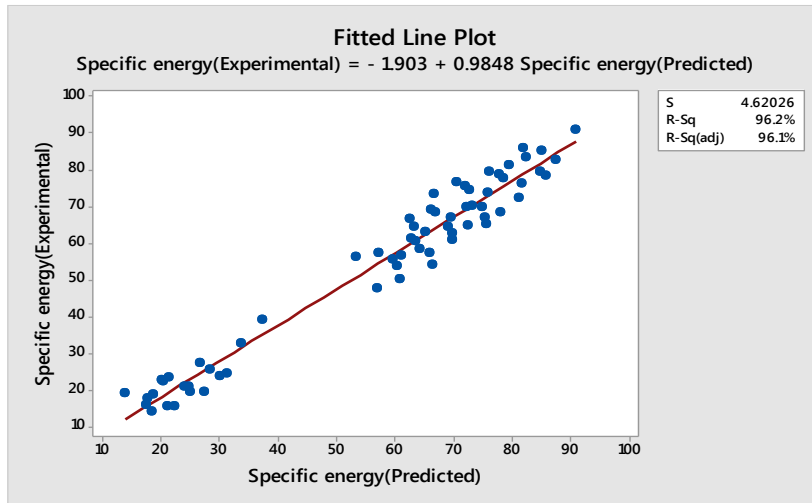


Figure 3.72 (a) Predicted SE versus observed SE for the model of chisel bit for training set

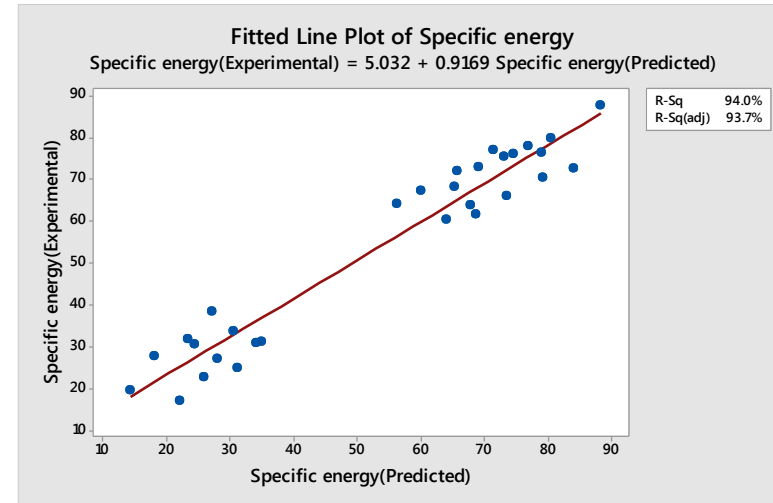


Figure 3.72 (b) Predicted SE versus observed SE for the model of chisel bit for testing set

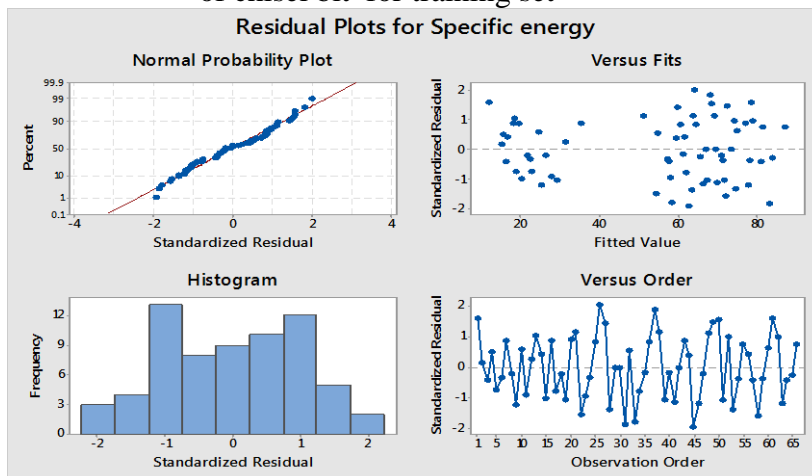


Figure 3.73 (a) Residual plots against SE of chisel bit for training set

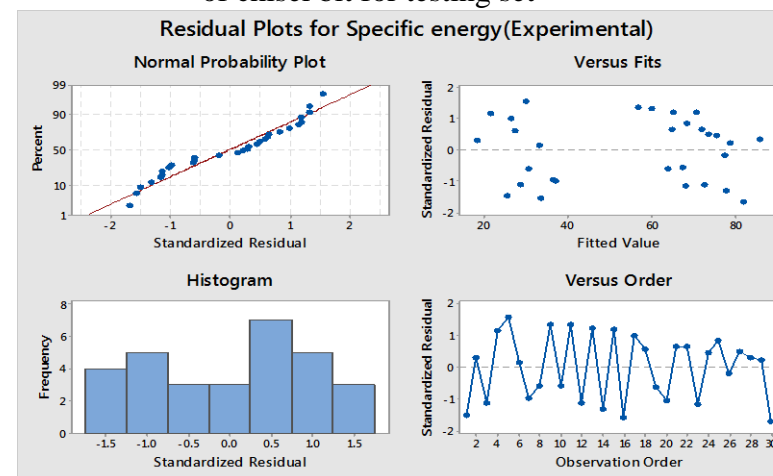


Figure 3.73(b) Residual plots against SE of chisel bit for testing set

3.8.4 Multiple Regression Analysis of Spherical button bit

Table 3.27 Analysis of Variance (ANOVA) of spherical button bit model

Source of variations	Degree of freedom	Sum of squares	Mean squares	F-value	p-value
Regression	9	26633.5	2959.28	119.03	0.000
Diameter of the bit	1	745.7	745.65	29.99	0.000
Index angle	1	756.6	756.63	30.43	0.000
Density	1	1091.4	1091.38	43.9	0.000
UCS	1	227.6	227.56	9.15	0.004
Hardness(SRN)	1	163.7	163.71	6.59	0.013
BTS	1	167.4	167.4	6.73	0.012
Abrasion resistance	1	481.1	481.14	19.35	0.000
Young's Modulus	1	194.6	194.57	7.83	0.007
Poisson's ratio	1	647.1	647.08	26.03	0.000
Error	56	56	1392.2		
Total	65	65	28025.7		

Table 3.28 Model Summary of spherical button bit model

R ²	Predicted R ²	Adjusted R ²	Standard error
94.44%	93.20%	94.23%	4.98605

Table 3.29 Coefficients of spherical button bit model

Model terms	Parameter estimate (coefficients)	t-value	p-value
Constant	3746	4.61	0.000
Diameter of the bit	-0.712	-5.48	0.000
Index angle	0.3662	5.52	0.000
Density	-1058	-6.63	0.000
UCS	-82.0	-3.03	0.004
Hardness(SRN)	-4.32	-2.57	0.013
BTS	638	2.59	0.012
Abrasion resistance	-29.98	6.81	0.000
Young's Modulus	-16.72	5.97	0.007
Poisson's ratio	4684	-4.4	0.000

Regression Equation

$$\begin{aligned} SE = & 3746 - 0.712 D_i + 0.3662 IA - 1058 D_e - 82.0 UCS - 4.32 SRN + 638 BTS \\ & - 29.98 AR - 16.72 Y + 4684 PR \end{aligned} \quad \text{..... (3.3)}$$

Where

- SE = Specific energy
- D_i = Diameter of the bit
- IA = Index angle
- D_e = Density
- UCS = Uniaxial compressive strength
- SRN = Hardness (Schmidt Rebound Number)
- BTS = Brazilian tensile strength
- AR = Abrasion resistance
- Y = Young's Modulus
- PR = Poisson's Ratio

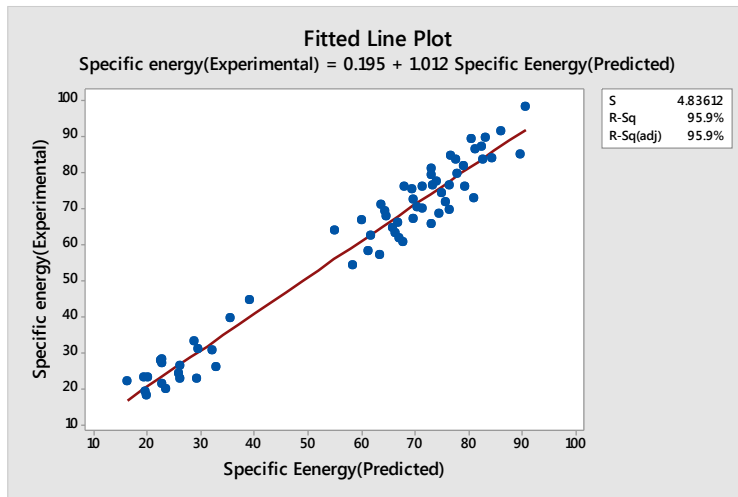


Figure 3.74(a) Predicted SE versus observed SE for the model of cross bit for training set

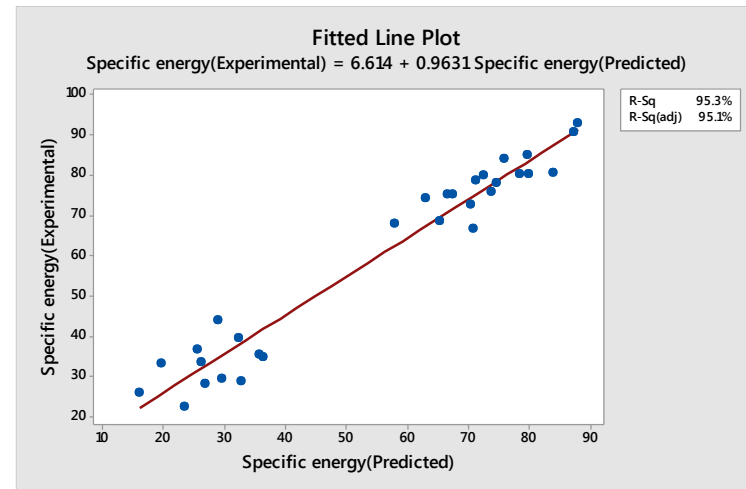


Figure 3.74 (b) Predicted SE versus observed SE for the model of cross bit for testing set

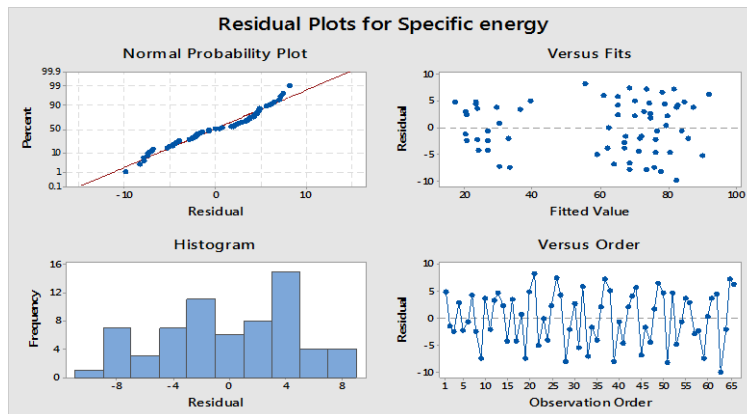


Figure 3.75 (a) Residual plots against SE of cross bit for training set

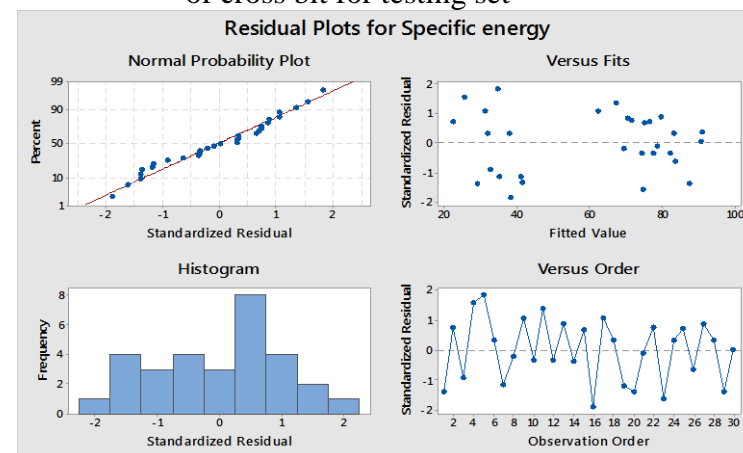


Figure 3.75 (b) Residual plots against SE of cross bit for testing set

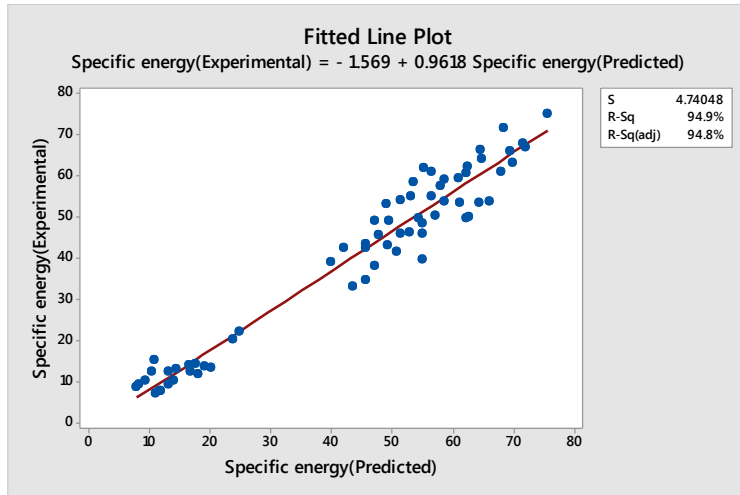


Figure 3.76(a) Predicted SE versus observed SE for the model of spherical button bit for training set

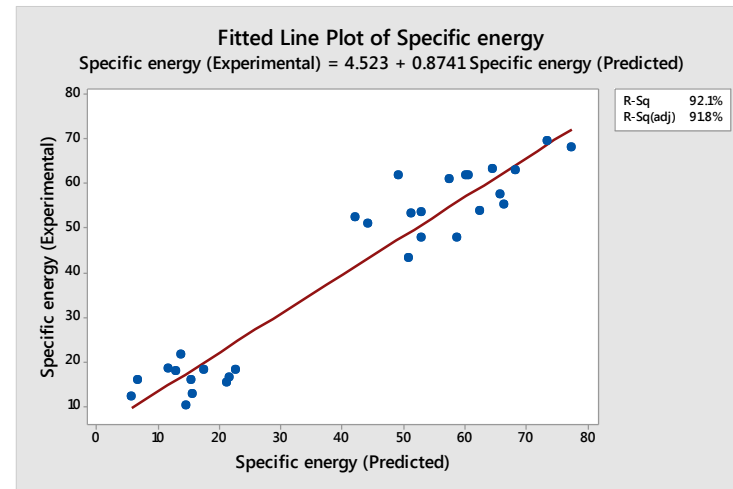


Figure 3.76(b) Predicted SE versus observed SE for the model of spherical button bit for testing set

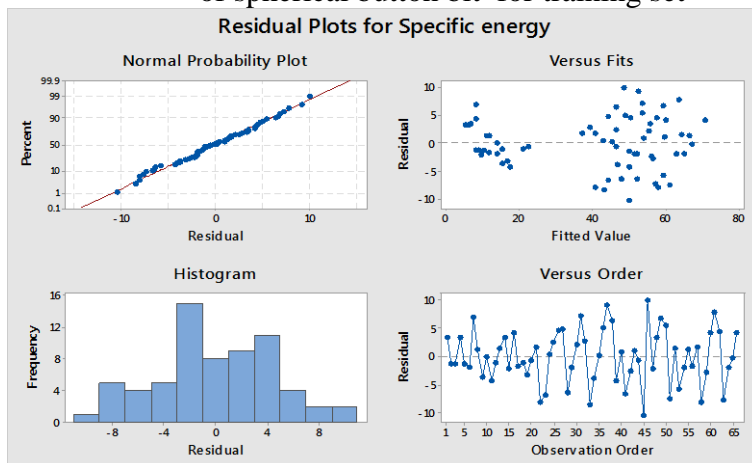


Figure 3.77 (a) Residual plots against SE of spherical button bit for training set

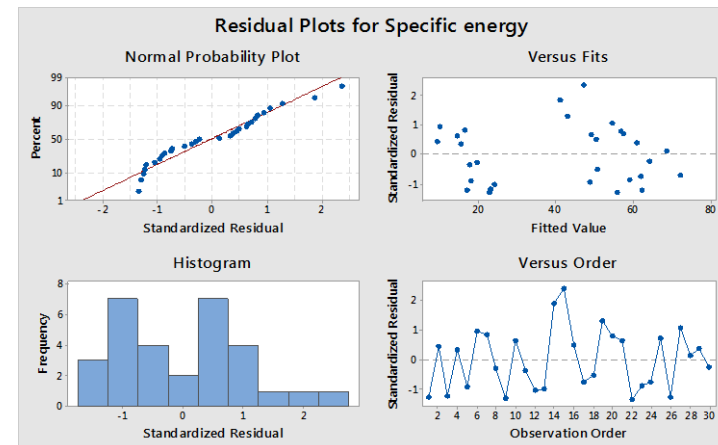


Figure 3.77(b) Residual plots against SE of spherical button bit for testing set

3.9 ARTIFICIAL NEURAL NETWORK MODELING

3.9.1 INTRODUCTION

The approach of statistical methods to predict the properties is better, but they are limited by the degree of non-linearity. The statistical methods primary objective is to develop a methodology under stringent statistical rules than prediction accuracy. Moreover statistical methods constrain the data along a particular geometry which may not always be favourable to capture non-linear relationships existing between various parameters. In general, the problems encountering in real engineering applications are more complex. The algebraic and differential equations are used to describe the behaviour and functionality of properties or processes of real systems and mathematical models are used to represent them. The complexity in the problem itself may introduce uncertainties which make the modeling non-realistic or inaccurate. In mining and geotechnical engineering, the study of rock is important as the excavations and constructing the structures are made in or on the rocks and rock mass. The behaviour of rock under stress conditions and geo-engineering characteristic of rock are complex and not properly defined.

Artificial Neural Networks have been reported to be very efficient to handle these non-linear and complex relationships and accurate prediction of the required parameters is possible. ANNs implement various algorithms to achieve neurological related performances such as learning from experience, making generalization from similar situations and judging states where poor results are achieved in the past. When the data is analysed using a neural network, it is possible to detect important patterns that are not previously apparent to a non-expert (Yilmaz et al., 2008).

Various prediction models have been utilized for the selection and optimization of drilling/ cutting machines since long time (Tiryaki, 2008). Prediction of certain measures like rate of penetration, cutting rate, SE etc of drilling and cutting performance for mining machines helps to reduce the capital cost (Rostami et al., 1994). The assessment and prediction of specific energy during indentation of rock is so complicated that accurate modeling will be difficult because of the complexity of the

indentation process and nonlinear relationship existing between the SE and other dependant parameters like properties of the rocks. So ANN is used in the present study to predict specific energy in rock indentation test.

3.9.2 Fundamental concepts in ANN

ANN is an efficient information processing system which resembles in characteristics with a biological brain. In the biological brain, natural neurons receive signals through *synapses* located on the dendrites or membrane of the neuron. If the signals received are strong (*threshold*), the neuron is *activated* and emits a signal through the *axon*. This signal may be sent to another synapse, and may activate other neurons as well. The axon of each neuron transmits information to a number of neurons. The neuron receives the information at the synapses from a large number of other neurons. Groups of these neurons are organised into subsystems and the integration of these subsystems form the brain.

An ANN is a group of interconnected artificial neurons, interacting with one another in a concerted manner. Figure 3.78 shows how information is processed in a single neuron in ANN. Each node in a layer (except input layer) provides threshold value. Initially, the scalar input ' p ' is multiplied by the scalar weight ' w ' to form the product wp . Later, the weighted input wp is added to the scalar bias ' b ' to form the net input n . (In this case, we can view the bias as shifting the function f to the left by an amount b . The bias is just like a weight, except that it has a constant input of 1.) Finally, the net input is passed through the transfer function f , which produces the scalar output a . The names given to these three processes are: the weight function, the net input function and the transfer function.

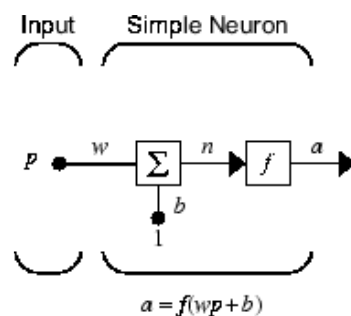


Figure 3.78 Architecture of Simple neuron

The transfer function f that transform the weighted inputs into the output ‘ a ’ is usually a nonlinear function, either sigmoid or logistic, which restricts the nodes output between 0 and 1.

ANN consists of a large number of highly interconnected processing elements called nodes or neurons and a huge number of connection links between them. According to the architecture of the connections, they have been identified as feed forward and recurrent networks. Feed forward networks have one way connections, from input to output layer. They are most commonly used for prediction and nonlinear function fitting. Here the neurons are arranged in the form of layers. Neuron in one layer gets input from previous layer and feed their outputs to the next layer. The last layer is called the output layer. Layers between input and output layers are called hidden layers and architecture of this type is termed as multi-layered networks.

The Figure 3.79 shows the schematic representation of a multi-layered feed forward network. The number of nodes in the input and output layers are dictated by the nature of the problem to be solved and the number of input and output variables needed to define the problem. The number of hidden layers and neurons in the hidden layer is usually defined by trial and error method.

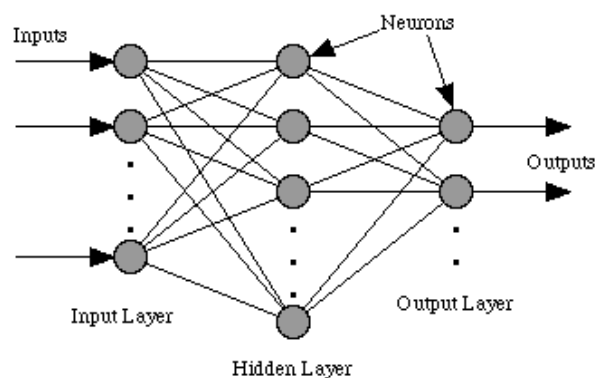


Figure 3.79 Feed forward ANN network

ANN studies the input output relationships by suitably adjusting the synaptic weights in a process known as training. The weights of the given interconnection are adjusted by means of some learning algorithms.

The methods of learning in neural networks are classified into three types. They are

- a) Supervised learning
- b) Unsupervised learning
- c) Reinforcement learning

In the supervised learning, the target values which are obtained from experimental results are given to ANN during training so that ANN can adjust its weights to try to match its output to the target values. All the weights are randomly initialized, before the learning algorithms are applied to update the weights (Haykin 1998). The network then produces its own output. These outputs are compared with the target outputs and the difference between them called the error is used for adjusting the weights.

In the unsupervised learning method (also known as self-organized learning), the inputs of similar type are grouped without the use of training data to specify how a member of each group looks or to which group a number belongs. The training process, the network receives the input patterns and organizes these patterns to form clusters. When a new input signal pattern is applied, the neural network gives an output response indicating the class to which the input belongs (Sivanandhan et al, 2011).

In reinforcement learning method, learning is similar to supervised learning. In case of supervised learning, the correct target values are known for each input pattern. But, in some cases, less information may be available. So in this method the learning is based on with 50% of available information called critic information (Sivanandhan et al, 2011).

3.9.3 Multi-Layer Perceptron

Multi-layer perceptron is one of the widely used network architectures for function approximation, classification and prediction problems (Haykin, 1999). It is an efficient neural network type, capable of modeling complex relationships between variables. The architecture of MLP is a multi-layered feed forward neural network, in which nonlinear elements (neurons) are arranged in successive layers and the information flow is

unidirectional, ie. from the input layer to the output layer through hidden layers. The Figure 3.79 shows a typical MLP architecture with the following characteristics.

1. The perceptron network consists of three units, namely, input, hidden and output layers.
2. The network contains one or more layers of hidden neurons between input and output of the network. These hidden neurons enable the network to learn and solve complex tasks by extracting progressively more meaningful features from the input patterns.
3. The network exhibits a high degree of connectivity.
4. The binary activation function is used in input and hidden layer.
5. The output of perceptron is given by $y = f(y_{in})$
6. The perceptron learning rule is used in the weights between the hidden and output layer.
7. The error calculation is based on the comparison of values of targets and with output values.
8. The weights will be adjusted on the basis of learning rule if error occurs.

MLP is trained by using one of the supervised algorithms of which the best known is back propagation algorithm. The basic idea of back propagation was first described by Werbos (1974), and then it was rediscovered by Rumelhart, Hinton and Williams (1986). The development of this algorithm is considered a landmark in neural networks, in that it provides a computationally efficient method for training MLPs (Anderson 1995).

3.9.4 Back –Propagation (BP) Algorithm

The Back Propagation (BP) algorithm is one of the most popular learning algorithms used in ANN. It is applied to multi-layered feed forward networks. There are basically two passes through the different layers of the network; a feed forward pass and a backward pass. In the forward pass, all the synaptic weights are fixed, and in the backward pass, the synaptic weights are all adjusted depending upon the error between the actual output and target output. The process is continued until all the input patterns

from the training set are learnt with an acceptable overall error. The error is cumulative and computed over the entire training set. This computation is called Training Epoch. During the testing phase, the trained network itself operates in a feed forward manner (Haykin 1999). The BP algorithm is presented below.

1. Initialize the weights and biases to small random values.
2. Choose an input pattern from the training set and present to the input layer
3. Compute the activation of the neurons in the hidden layer.
4. Compute the output of each neuron in the output layer
5. Compute the mean squared error (MSE)
6. If MSE is minimum go to step 8.
7. Update the weights between the outputs and the hidden layer.
Update the weights between the hidden and input layer.
Go to step 2.
8. Save all the weights and exit.

The performance of the BP algorithm depends upon the initialization of weights, learning, output functions of the units, presentation of the training data and the specific pattern recognition tasks like classification, prediction or mapping.

- 1) Initial weights- The network weights are initialized to small random values. The initialization strongly affects the final solution.
- 2) Transfer function of the nodes- For calculating the value of δ in the backward pass, the requirement is that the activation function should be differentiable. One of the most widely used functions, which is continuously differentiable and also nonlinear is the sigmoidal nonlinearity. A particular form defined for the sigmoidal nonlinearity is given by $f(x) = \frac{1}{1+e^{-x}}$ where it has been used for nodes in the hidden layer and output layer.
- 3) Learning rate- The effectiveness and convergence of back propagation algorithm depends significantly on the value of the learning rate η . By trial and error, the value for the learning rate has to be selected, which provides an optimum solution. The value is generally less than 1.

- 4) Momentum coefficient- The momentum term is generally used to accelerate the convergence of the error BP algorithm. This involves the use of momentum coefficient α .

This is a simple method of increasing the rate of learning and yet avoids the danger of instability. The value chosen is generally less than 1.

- 5) Number of hidden neurons: The number of hidden layer and number of neurons in hidden layer are most important considerations, while solving actual problems using MLP neural network. The optimal number of hidden layers and hidden neurons in any network for solving any given problem is determined by trial and error. Hidden units play a critical role in the operation of the multilayer perceptron with BP algorithm learning as they act as feature detectors.

Various prediction models have been utilized for the selection and optimization of drilling/ cutting machines for many years (Tiryaki, 2008). Prediction of certain measures like rate of penetration, cutting rate, SE etc of drilling and cutting performance for mining machines helps to reduce the capital cost (Rostami et al., 1994). The assessment and prediction of specific energy during indentation of rock is so complicated that accurate modeling will be difficult because of the complexity of the indentation process and nonlinear relationship existing between the SE and other dependant parameters like properties of the rocks. So ANN is used in the present study to predict specific energy in rock indentation test.

3.9.5 Development of ANN model in the present study

For the development of models, neural network tool box in MATLAB 2015 software was used. The ANN developed in this study is a back-propagation layered feed-forward network to build the prediction models for SE that consists of three layers: input, hidden, and output layer. The learning algorithm is composed of two sub-sequent steps; feed forward and error back propagation. For feed forward calculations, tangent sigmoid transfer function neurons in the hidden layer and a pure linear transfer function neuron corresponding to SE in the output layer.

Designing a network architecture requires more than selecting a certain number of neurons in input, output and hidden layers followed by training only. Predictors that were used in multiple linear model of SE (Diameter of drill bit, index angle, density, UCS, BTS, Abrasion resistance, SRN, Young's Modulus and Poisson's ratio) were employed in developing SE models with ANN in order to compare both methods in SE prediction accurately.

Therefore, nine neurons were used in input layer corresponding to nine independent variables. One neuron corresponding to SE was used in the output layer. According to Seibi and Al-Alawi (1997), determining the number of hidden layers to use and the proper number of neurons to include in each hidden layer are of crucial importance in designing neural network structures.

Research in this area proved that one or two hidden layers with an adequate number of neurons are sufficient to model any solution surface of practical interest. The number of trials were conducted initially to fix the number of neurons in hidden layer. The number of neurons for which MSE is minimum, was selected as optimum number of neurons in hidden layer, as there is no standard procedure to find the optimum numbers of neurons in the hidden layer. The number of neurons in hidden layer used were 9, 10, and 11 for chisel bit model, cross bit model and spherical button model respectively and only one hidden layer was used in the study.

The supervised learning algorithm `trainlm`, a network training function that updates weight and bias values according to Levenberg-Marquardt optimization, was used for training of data in the study. The `trainlm` is often the fastest back propagation algorithm in the toolbox, and is highly recommended as a first-choice supervised algorithm, although it does require more memory than other algorithms. In the network, the following data sets were used to process the data.

- (i) The training set, used for computation of the gradient and updating the weights and biases of the neural network;

- (ii) The validation set, used for monitoring the error during the training process because it tends to increase when data is overfitted; and
- (iii) The test set, whose error can be used to assess the quality of the division of the data set.

In this study the data is randomly divided so that 70% (66 data sets) of the samples are assigned to the training set, 15% (15 data sets) to the validation set, and 15% (15 data sets) to the test set.

The neural network architecture, network training tool and network training regression of chisel bit are shown in Figure 3.80 (a) to (c), the neural network architecture, network training tool and network training regression of cross bit are shown in Figure 3.81 (a) to (c) and neural network architecture, network training tool and network training regression of spherical button bit are shown in Figure 3.82 (a) to (b).

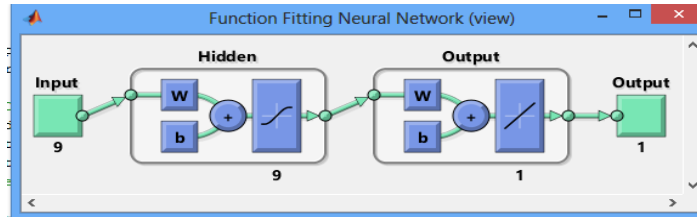


Figure 3.80 (a) Neural network architecture of chisel bit

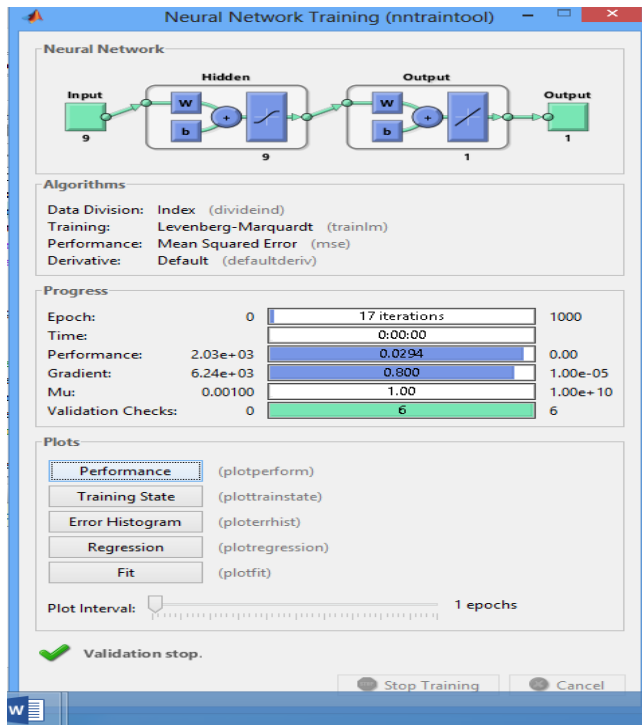


Figure 3.80 (b) Network training tool of chisel bit

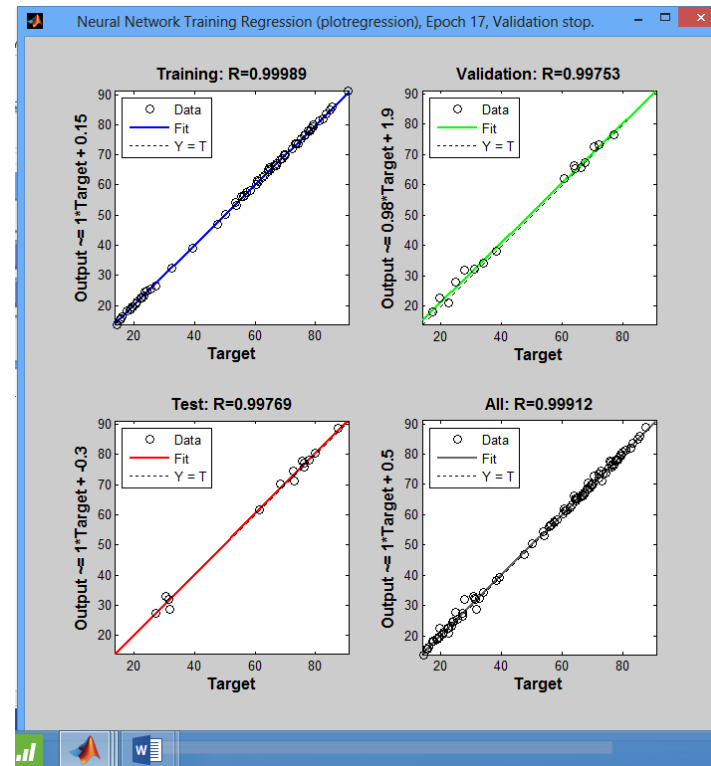


Figure 3.80 (c) Network training regression of chisel bit

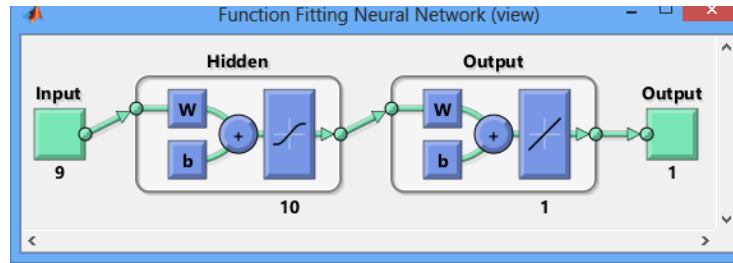


Figure 3.81 (a) Neural network architecture of cross bit

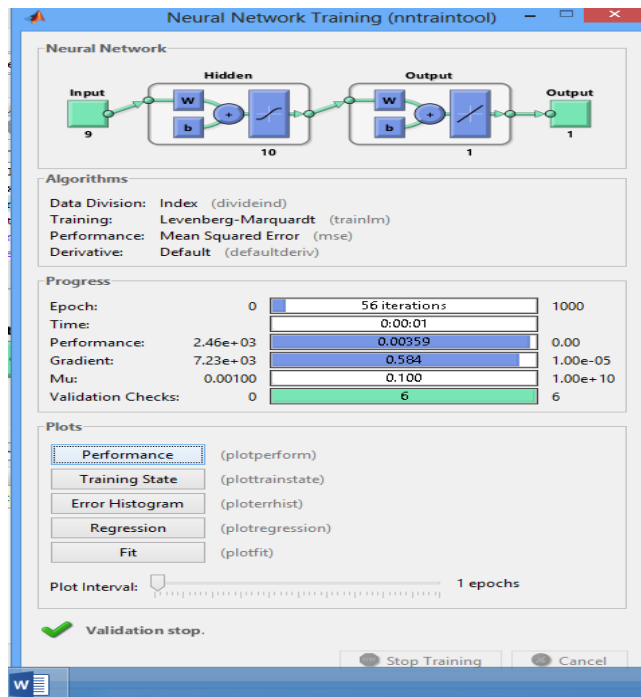


Figure 3.81 (b) Neural network training of cross bit

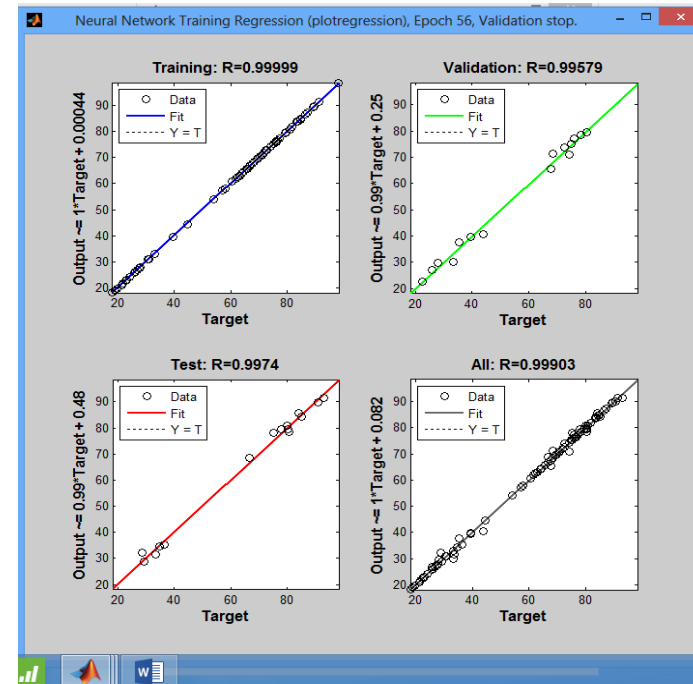


Figure 3.81 (c) Neural network performance of cross bit

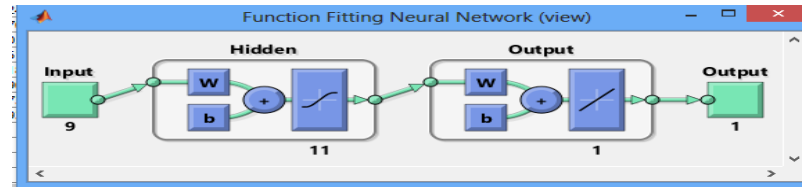


Figure 3.82 (a) Neural network architecture of spherical button bit

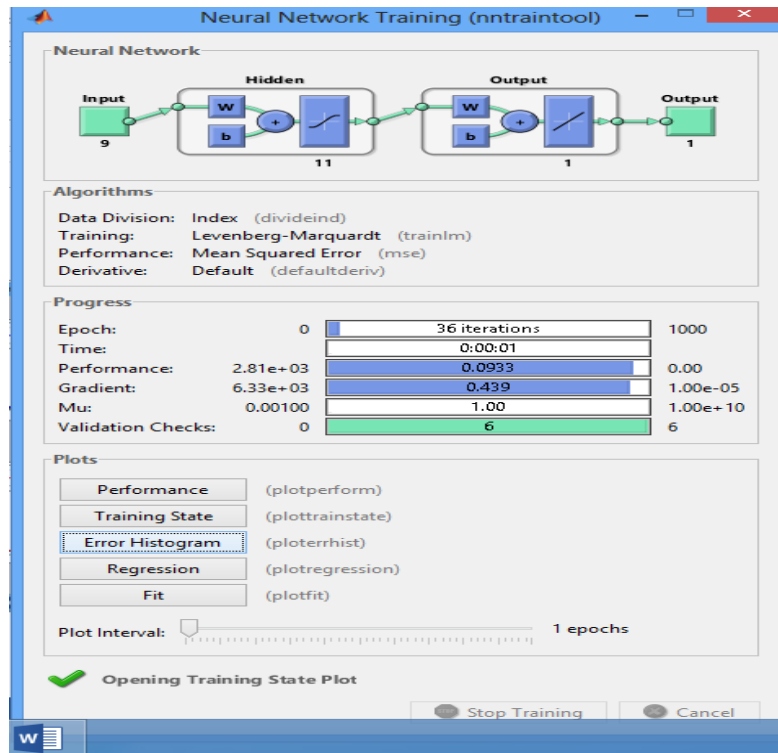


Figure 3.82 (b) Network training tool of spherical button bit

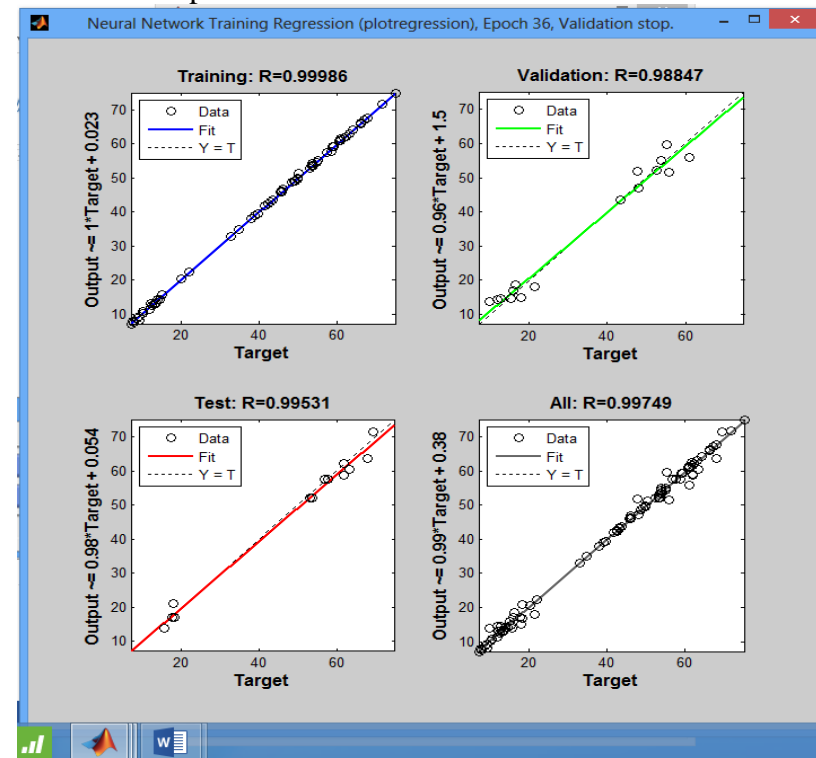


Figure 3.82 (c) Network training regression of spherical button bit

3.10 NUMERICAL MODELLING (FINITE ELEMENT ANALYSIS)

3.10.1 General

In general various phenomena and engineering problems are mathematical models of physical situations. Mathematical models are differential equations with a set of boundary and initial conditions. Solving differential equations under the various conditions such as boundary and initial conditions leads to the understanding of the phenomena and can predict the future of the phenomena. However, exact solution for differential equations are generally difficult to obtain for many engineering problems. This inability to obtain exact solutions may be due to either the complex nature of governing differential equation or difficulty in dealing with the boundary and initial conditions. To deal with such problems, numerical methods are adopted to obtain approximate solutions for differential equations. The advent of high speed computers has revolutionized the scope of analysis by numerical methods, such as finite element method (FEM), for complex problems in all branches of engineering. The FEM has become a powerful tool for solving numerous rock mechanics problems. This is one of the most popular, flexible and useful techniques for analytical computations, available to the engineers. The basic principle of this method is that the behavior of parts defines the behavior of the whole.

The random geometric norms, unusual loading conditions and varying material properties, make rigorous mathematical analysis almost impossible in almost all rock mechanics problems. The need for the FEM analysis has been felt by the mining engineers in solving all such complex problems taking into account non-linearity, non-homogeneity and anisotropy of rock properties. The method has been extensively used for problems related to stress analysis in mining, especially in the location and design of mine structures. However, it has not been extensively used for problems related to bit penetration into rock, except the two dimensional plane strain representation of the problem.

The two basic, approaches of FEM analysis are : (i) force approach, in which, forces at

the nodal points are the unknowns of the problem and (ii) displacement approach, in which, displacement at the nodal points are the unknowns of the problem. The governing equations are established in terms of nodal forces or in terms of nodal displacements, as the case may be, for each node, using appropriate equilibrium condition for the problem investigated. The general procedure for the solution of a problem by FEM involves the following steps:

a) Preprocessing Phase:

- (i) Create and discretize the solution into finite elements- divide the problem into number of nodes and elements.
- (ii) Selection of the approach, either displacement or force.
- (iii) Development of equations for an element and generation of element stiffness matrices
- (iv) Computation of the global stiffness matrix from the element stiffness matrices.
- (v) Applying the boundary conditions like force, displacement or mixed, as applicable for the specific problem.
- (vi) Formulation of the system of governing equations for the specific problem.

b) Solution Phase:

- (vii) Solving a set of linear or nonlinear algebraic equations simultaneously to determine the unknown nodal displacements or forces at nodes.

c) Post processing phase:

- (viii) Computation of the other quantities of interest, such as, nodal stresses and displacements by averaging the values of the adjacent elements.
- (ix) Presentation and analysis of results.

The accuracy and the effectiveness of the FEM depends on discretization that is the type and the number of elements used in the mesh depending upon the geometry. The type of element chosen should be compatible to the problem. The compatibilities at the boundaries of the adjoining elements must be taken into account.

3.10.2 FEM analysis of drill bit penetration into rock

A number of commercial finite element software are available to solve a variety of engineering problems (e.g. NASTRAN, ANSYS, SAPSO, SOSMOS and EMRC).

Some of the programs have been developed in a flexible manner, such that, the same program could be used for the solution of problems relating to different branches of engineering with little or no modification (e.g. NASTRAN, ANSYS). The present investigation was carried out using the finite element program, ANSYS, which was available in CAD-CAM Centre of NITK.

3.10.3 Description of the numerical model

The numerical simulations were developed with the commercial finite element software ANSYS 15 version. To reduce the processing time, only a quarter of both the rock block was considered in the model.

3.10.4 Assumptions in FEM analysis of bit penetration into rock:

(i) Rock was considered as homogenous, isotropic and linear elastic for the simplification of the analysis. In case of rocks, because of the experimental difficulties for establishing the non-linear behaviour in the three mutually perpendicular directions, even though non-linear analysis programme is available in ANSYS, the present work was limited to elastic analysis.

(ii) Loading at the contact plane between the bit and the rock surface was represented as shown in Figure 3.83: (a) a line load, along one axis for the chisel bit (b) two line loads along two mutually perpendicular axis for the cross bit and (c) a circular area load, of diameter that of a single button, placed centrally for the spherical button bit. The loads were all symmetrically placed with respect to the vertical axis.

For the spherical button bit of 48 mm diameter and 45 mm diameter, three buttons, each of 8 mm diameter, are placed in an isosceles triangular geometry (of base 26.6

mm and sides of 23.4 mm) around the center of the bit. In actual theoretical representation, one third of the load applied through the spherical button bit should be assigned to each of the three buttons. In such case, the contact area of each button to start with is also much less than the area of 8 mm diameter. With the progress of indentation, this contact area diameter will gradually increase to 8 mm. Similarly in case of spherical button bit of 38mm diameter, two buttons each of 8 mm diameter, are placed in a line (18mm apart) around the center of the bit. But in case of spherical button bit of 48 mm diameter, only one button is placed around the centre of bit. In the present theoretical investigation, this type of complicated loading has been replaced by assuming that the total load of the spherical button bit is transmitted through a single button over a circular contact area of 8 mm diameter placed at the centre of the bit.

3.10.5 Defining element type:

(iii) Composite brick elements with eight nodes were considered in this investigation for all the three types of bits. A mapped volume mesh which contains only hexahedron elements was used for meshing. In all the cases, only continuity of displacements across interfaces were ensured. All other interface variables were not taken into consideration.

3.10.6 Material properties

In finite element analysis, the geo-mechanical properties namely Young's modulus and Poisson's ratio, of respective rocks, as mentioned in Table 3.13, were considered.

3.10.7 Mesh generation

A mapped volume mesh with hexahedron elements (brick) was used in modelling as the geometry developed as a series of fairly regular volumes and/or areas that can accept a mapped mesh.

The analysis of bit penetration into rock was carried out by adopting 3-D (3-dimensional) analysis with displacement approach. On account of the restriction the size of 2 GB RAM, working on a single user basis, a limitation to the total number of elements for the 3-D model was imposed, forcing the mesh to be relatively coarse.

However, a total of 400 elements for chisel and 142 nodes, 800 elements and 284 nodes for cross bit and 820 elements and 220 nodes for spherical button bit for a cuboidal block size of 203.2 mm long, 152.4 mm wide and 127 mm can be considered as a reasonably fine mesh formation. The aspect ratio (ratio of two adjacent sides of elements) of the elements is maintained 4, since it is structural analysis, so a similar element divisions are maintained in all the sizes of the indenters.

The problem of memory space requirement was overcome even for the above mentioned large number of elements by generating the element stiffness matrices for the one-fourth of the cuboidal block because of the symmetry of the problem. The accuracy of the analysis is, thus, not sacrificed in any way. The detailed theory and formulation of the ANSYS programme are not discussed in this volume, as it is a very well-known FEM software.

3.10.8 Boundary conditions adopted

In the present work, the symmetric boundary condition (one-fourth of the cuboidal block) was adopted for the analysis. Because of the limitation of obtaining sufficient numbers of large size blocks of each rock type for the static indentation test, 152.4 mm width of the rock block for 35, 38, 45, 48 mm loading widths (for both chisel and cross bits) is considered to represent reasonably the semi-infinite condition.

However, for spherical button bit, the actual loading is three individual hemi-spherical buttons, each of 8 mm diameter, in an isosceles triangular pattern (of 26.6 mm base and 23.4 mm sides for 48mm diameter drill bit) around the center point of the drill bit. This ratio of 5.7 (152.4 divided by 26.6) times between the loading length and the rock dimension is a more accurate representation of the semi-infinite condition.

Similarly the actual loading, in case of 45mm diameter drill bit, is three individual hemi-spherical buttons, each of 8 mm diameter, in an isosceles triangular pattern (of 24 mm base and 20 mm sides) around the center point of the drill bit. This ratio of 6.35

(152.4 divided by 24) times between the loading length and the rock dimension is a more accurate representation of the semi-infinite condition. But in case of 38mm diameter drill bit the actual loading is two individual hemi-spherical buttons each of 8 mm diameter and one individual hemi-spherical button in case of 35 mm diameter the actual loading is one hemi-spherical button of 8 mm diameter, for 38mm diameter drill bit and 18 mm base and 16 mm base for 35mm diameter) around the center point of the drill bit. The ratio of 8.47 (152.4 divided by 18) times between the loading length and the rock dimension for 38 mm diameter and the ratio of 9.525 (152.4 divided by 16) times between the loading length and the rock dimension for 38 mm diameter are more accurate representation of the semi-infinite condition.

Hence, the boundary conditions have been chosen to match with semi-infinite case. Accordingly, all the nodes of the five boundary planes, except the top plane, have been restrained in all the three directions to represent zero deformation of infinite distance (Figure 3.84). All the nodes on the vertical axis were restrained along both X and Z directions because of the symmetry.

For the purpose of comparison of the results obtained from the ANSYS programme and static indentation tests, the FEM analysis was carried out on the same dimensions of rock blocks as well as the same magnitude of loading corresponding to the 12 steps of loading as recorded during the static indentation tests. In static indentation tests, the 12 steps of loading recorded (Table 4.28 to 4.33 in Appendix-II) was at intervals of 5 seconds.

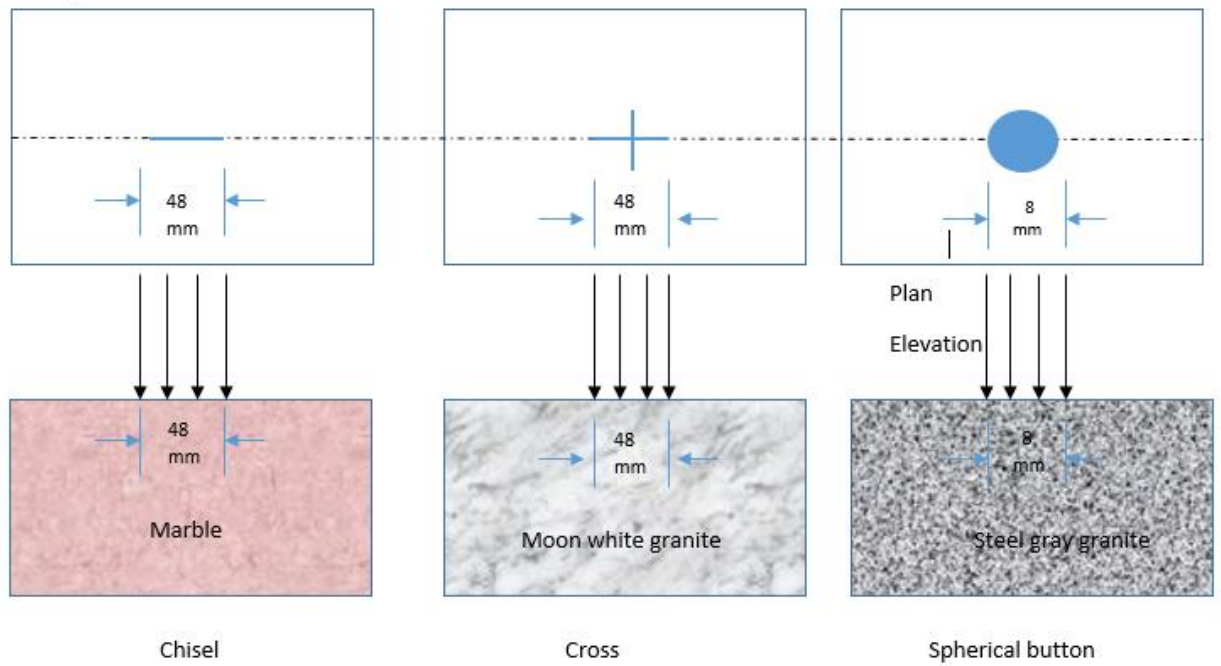


Figure 3.83 Representation of loading at bit-rock interface for three bit geometries

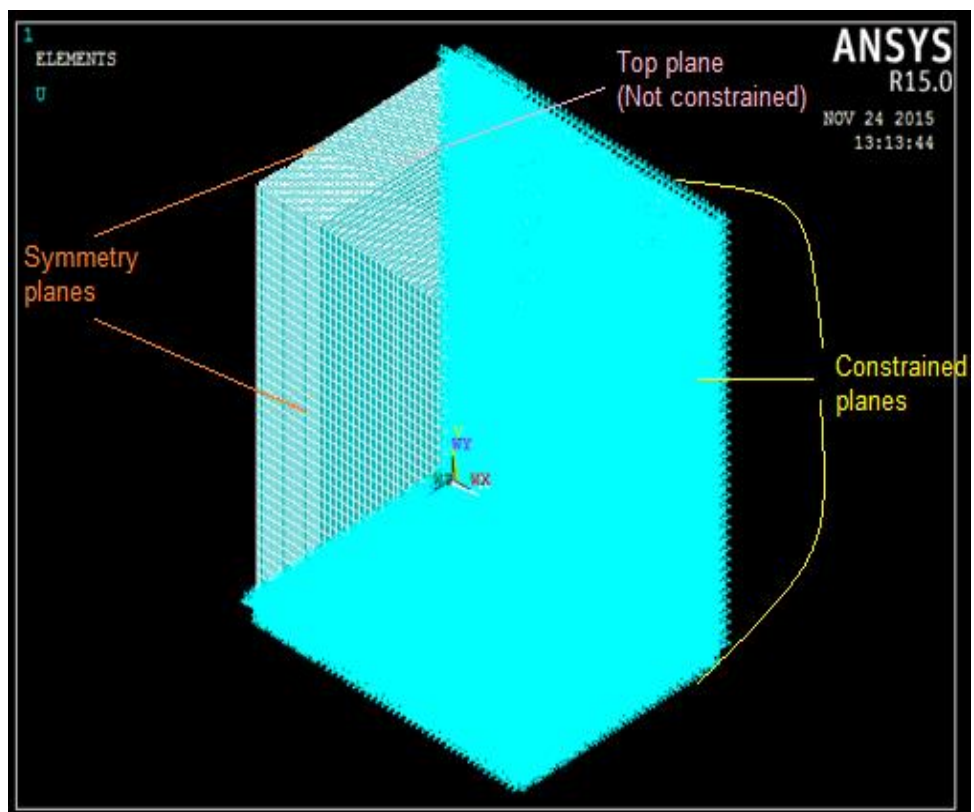


Figure 3.84 Discretization showing the boundary conditions adopted for FEM analysis

CHAPTER 4

RESULTS AND DISCUSSION

4.1 F-P CURVES AND INFLUENCE OF INDEX ANGLE ON SPECIFIC ENERGY

4.1.1 INTRODUCTION

The F-P curves plotted for loading and unloading cycle are shown from Figure 3.14 to 3.61. The influence of index angle on specific energy in static indentation tests on various types of rocks were investigated. The operating parameters, mainly index angles chosen from literature and also the minimum values of specific energy, lie between 10^0 and 40^0 as per the literature survey. The experiments on static indentation tests were conducted at various index angles 10^0 , 20^0 , 30^0 , and 40^0 . The influence of index angle on specific energy was studied.

4.1.2 EXPERIMENTAL RESULTS

The static indentation tests were carried in six types of rocks at 10^0 , 20^0 , 30^0 , and 40^0 index angles and various plots were prepared to study the influence of index angle on specific energy for various bit-rock combination (Figure 4.1 to 4.3). The specific energy values obtained at 10^0 , 20^0 , 30^0 , and 40^0 index angles with chisel, cross and spherical button of 35, 38, 45, 48 mm were determined, and are listed in Table 3.8 to 3.10 (Appendix –I).

4.1.3 ANALYSIS OF RESULTS OF F-P CURVES AND INFLUENCE OF INDEX ANGLE ON SPECIFIC ENERGY

The static indentation tests on rocks such as limestone and marble showed that the F-P curves are represented by initial large penetration at low forces followed steep rising

curve. The steepness indicates that after reaching certain penetration, penetration was less against the rise in forces.

Whereas in rocks like basalt, steel gray granite, moon white granite and black galaxy granite the F-P curves showed an increasing slope followed by a decreasing sloping. This event was repeated until a maximum force was reached. The combination of increasing and decreasing sloping (force drop) was observed which represents crushing and chipping phases. More force drops were recorded in case of three varieties of granite rocks and basalt. The specific energy values at 20° index angle for the group of rocks (like basalt, steel gray granite, moon white granite and black galaxy granite) were found to be less than other indexing angles and specific energy values at 30° index angle for limestone and marble rocks were found to be less than other indexing angles.

In case of marble and limestone rocks, if the indexing is less than 30° , then breaking of rock is not efficient and volume of chips formed is less due to over crushing between successive indentations. Similarly, if the indexing is less than 30° , then breaking of rock is not efficient and volume of chips formed is less since the fracture from adjacent indentations cannot intersect to form a chip. And also soft rock possess less strength properties and offers less resistance to penetration, the chip formation is more between adjacent indentations. With higher index angle in soft rocks, the rock breakage is effective between successive indentations so that with less number of indentations the hole is formed in case of percussive drilling.

The harder group of basalt, steel gray granite, moon white granite and black galaxy granite rocks offer more resistance to penetration. To get more penetration along with chip formation, more number of indentations/blows with indenter (drill bit) per revolution is required. This can be better achieved, if the indexing angle is smaller or, in other words, the successive indentations/blows are required at closer interval (indexing). These results are in line with the previous studies made by Murthy, Ch.S.N, (1998) in this area.

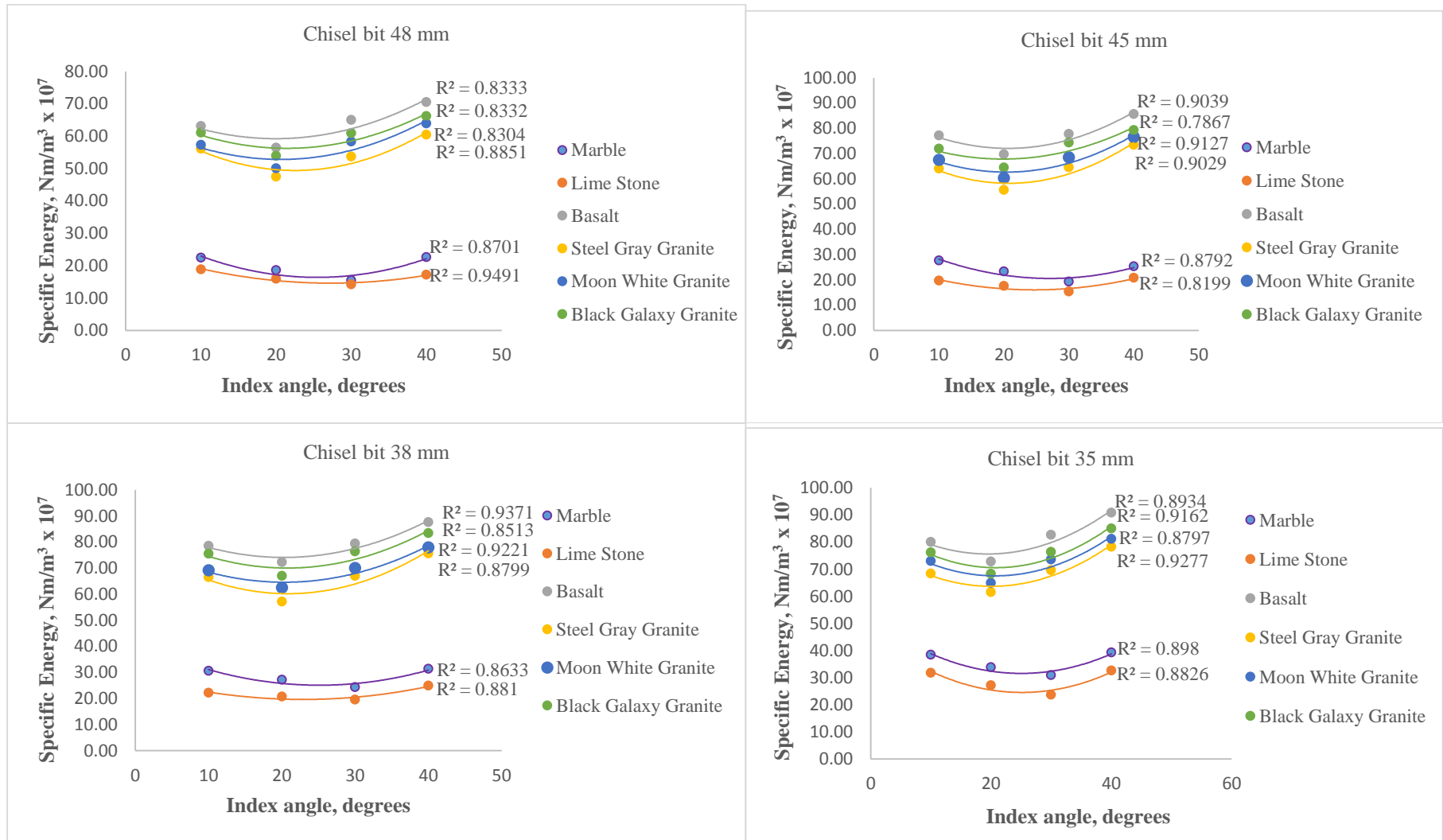


Figure 4.1 Influence of index angle on specific energy in static indentation tests on 6 different types of rocks for chisel bits of 48, 45, 38, 35 mm diameters

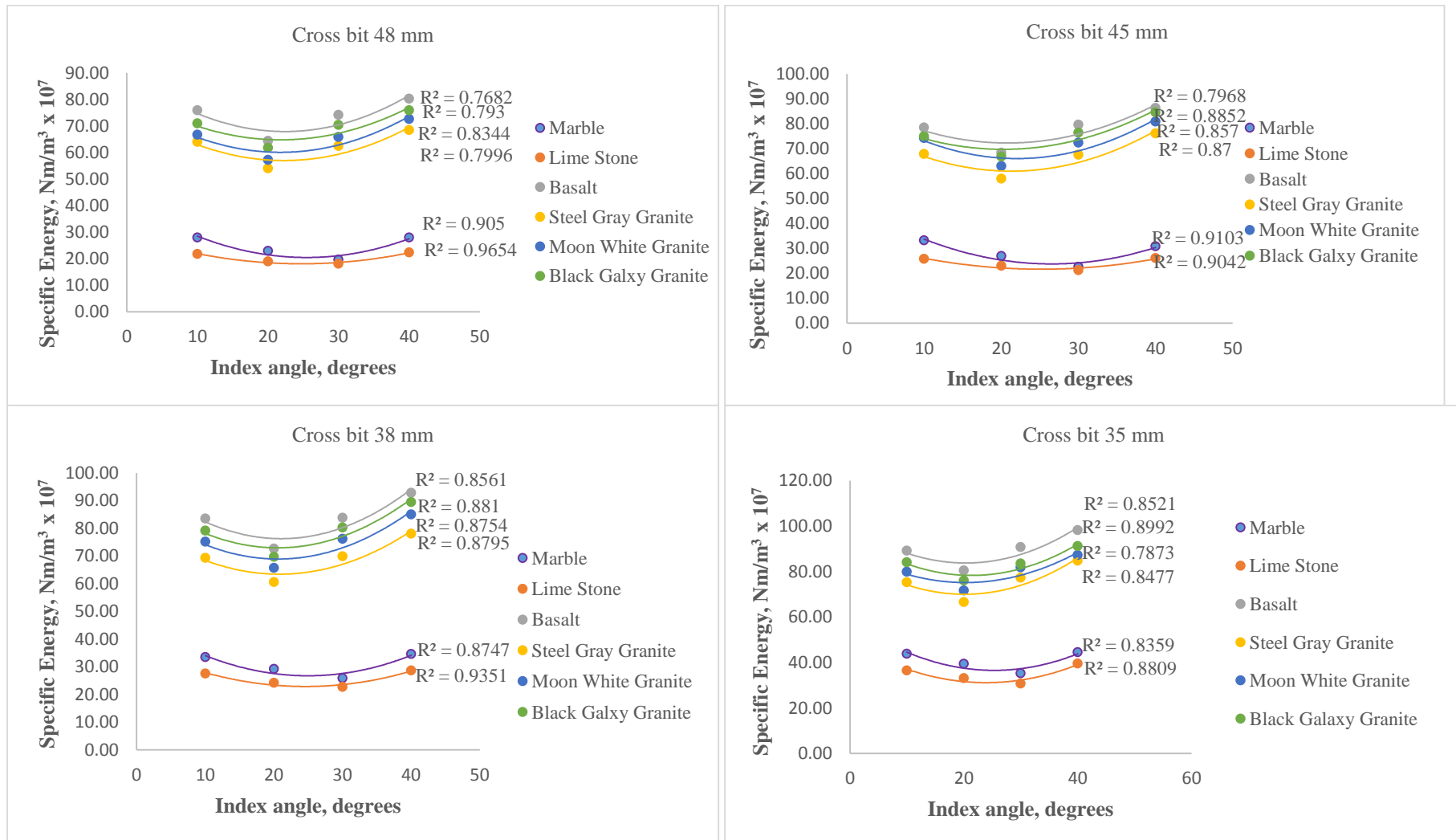


Figure 4.2 Influence of index angle on specific energy in static indentation tests on 6 different types of rocks for cross bits of 48, 45, 38 and 35 mm diameters.

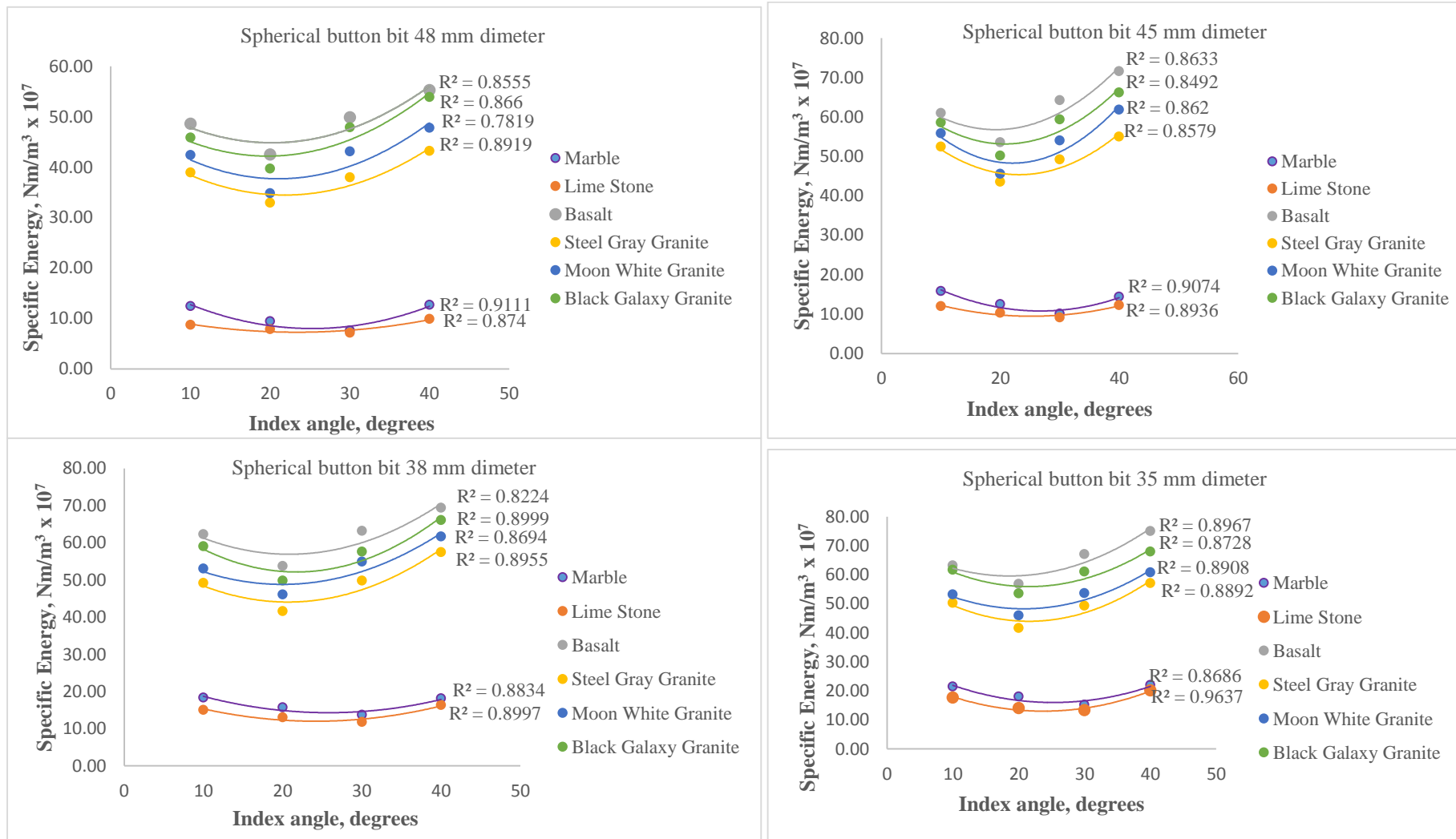


Figure 4.3 Influence of index angle on specific energy in static indentation tests on 6 different types of rocks for spherical button bits of 48, 45, 38 and 35 mm diameter.

4.2 INFLUENCE OF ROCK PROPERTIES ON SPECIFIC ENERGY

4.2.1 INTRODUCTION

Data obtained from the experimental tests (static indentation tests for all bit-rock combinations) and tests to determine the properties of rocks) were subjected to a comprehensive statistical analysis with an objective to find the influence of properties of rocks on specific energy. Bivariate correlations and linear regression analyses were used in determining the relationship between SE and properties of rocks (Tiryaki et al., 2006).

4.2.2 EXPERIMENT WORK

The specific energy values obtained by carrying out static indentation tests on six varieties of rocks with chisel, cross and spherical button bits of 35, 38, 45 and 48 mm were considered for analysis. The physico-mechanical properties of rocks like density, UCS, BTS, abrasion resistance, hardness (SRN), Young' Modulus and Poisson's ratio were determined as per ISRM standards.

4.2.3 BIVARIATE CORRECTION ANALYSIS

Correlation coefficients between independent and dependent variables were determined through bivariate correlation techniques by using Windows version of SPSS 15 software. In this analysis, the correlation coefficients between SE (dependent variable) and selected rock properties (independent variables) were investigated. The correlation coefficients obtained with SE values of spherical bit of 35mm diameter at 40⁰ index angle, SE values obtained by chisel bit of 38 mm diameter at 20⁰ index angle and SE values obtained by cross bit at 48 mm at 10⁰ index angle with physico-mechanical properties found to be higher as compared to others. So, these were considered for entire correlation analysis. Correlation coefficients were obtained after applying bivariate correlation technique to test the data. Pearson's correlation coefficient is a measure of linear relationship. Two variables can be perfectly related, but if the relationship is not

linear, Pearson's correlation coefficient is not an appropriate statistic for measuring their association (Tiryaki et al., 2006). Pearson's correlation coefficients ('r' values) are given in Table 4.1.

Table 4.1: Pearson's correlations between SE and selected rock properties

S.No	Independent variable	Chisel bit	Cross bit	Spherical button bit
		r	r	r
1	Density	0.551	0.569	0.592
2	UCS	0.690	0.663	0.726
3	Hardness(SRN)	0.757	0.775	0.768
4	BTS	0.693	0.665	0.727
5	Abrasion resistance	-0.736	-0.730	-0.783
6	Young's Modulus	0.750	0.758	0.794
7	Poisson's ratio	0.812	0.775	0.850

4.2.4 LINEAR REGRESSION ANALYSIS

Properties of rock that were found to be statistically significant correlations with SE were then subjected to a linear regression analysis in order to establish relationship individually all the properties of rock with SE. Linear regression analysis is a popularly used method to fit straight line to data which belong to two variables. With this analysis, the value of dependent variable can be predicted for any value of independent variable. A linear regression analysis that is based on the least square method was used on the data. Relationship between SE and properties of rocks established through linear regression analysis are given in Figure 4.4 to 4.10 for all the bits.

Regression analyses and along with analysis of variance (ANOVA) or the F-test are important parameters. ANOVA is used to determine the significance of the deviation from linearity for the regression lines and helps to decide whether the regression line is the best fit curve which represents the relationship between the sample data sets of two correlated variables. The null hypothesis which states that there is no linearity between

two variables has been tested through ANOVA. ANOVA produced two values for each model; F value showed how regression equation fitted the data, whereas the other one revealed the significance of F value (p value). When the p value was less than 0.05, then null hypothesis was rejected. This meant that the relationship between SE and the particular independent variable could be expressed as a linear equation at 95% confidence level. Otherwise, it was assumed that there is not a significant statistical relationship represented as a linear regression model (Tiryaki et al., 2006). But, this does not mean that there is no relationship between any of two variables under investigation. Nonlinear regression equation in such cases may be suitable to represent the relationship between such variables. Results of ANOVA for chisel bit are given in Table 4.3. Depending on these results, models including the density, UCS, hardness(SRN), BTS, abrasion resistance, Young's Modulus and Poisson's ratio were the predictors, and were found statistically significant in terms of linearity.

After these regression models were verified through ANOVA to determine whether they could be used to predict SE from the population reliably, Student's t-tests were used.

In other words, significances of the model components (equation constant and the regression coefficient in each regression model) were tested respectively at 95% confidence level. Depending on the probability values (p values) obtained, each of the above-mentioned model components were considered either significant or not. If p value was less than or equal to 0.05, then the relevant model component was taken significant, otherwise not significant. All the regression models for all bits that were verified through ANOVA were understood to have components that were also statistically significant (Table 4.3, 4.6 and 4.9). This reveals the practicability of these models in predicting SE values from the population (Tiryaki et al., 2006)

Upper and lower boundaries of these regression models in estimating the mean values of SE of all the bits from the population were also calculated considering the standard errors of estimations and boundaries for the models that are given in Table 4.4, 4.7 and 4.10.

Further, the coefficients of determination (r^2) were determined which are used to measure the goodness of the fit for the proposed regression models. r^2 is equal to the square of the correlation coefficient between the observed and predicted values of the dependent variable. r^2 equals one (plus or minus) if all the predicted values are exactly over the regression line. The values of these two statistical measure that were calculated for each model are given in Table 4.2, 4.5 and 4.8. According to these values, most of the changes in SE values of chisel are successfully expressed by the density, UCS, hardness(SRN), BTS, abrasion resistance, Young's Modulus and Poisson's ratio, individually, in line with the ANOVA and Student's t-test.

Table 4.2: Regression Models' Summary of SE with Chisel bit

Predictor	r	r^2	Adjusted r^2	Standard Error of Estimate
Density	0.551	0.304	0.261	17.615
UCS	0.690	0.476	0.443	15.282
Hardness (SRN)	0.757	0.573	0.546	13.797
BTS	0.693	0.480	0.448	15.221
Abrasion resistance	0.736	0.542	0.513	14.294
Young's Modulus	0.750	0.563	0.535	13.962
Poisson's ratio	0.812	0.659	0.638	12.327

Table 4.3: ANOVA Results of SE with Chisel bit

Predictor	Sum of squares		df	Mean squares	F	p value
Density	Regression	2109.347	1	2169.347	6.992	0.018
	Residual	4964.367	16	310.273		
	Total	7133.714	17			
UCS	Regression	3397.194	1	3397.194	14.547	0.002
	Residual	3736.521	16	233.533		
	Total	7133.714	17			
Hardness (SRN)	Regression	4088.044	1	4088.044	21.476	0.000
	Residual	3045.671	16	190.354		
	Total	7133.714	17			
BTS	Regression	3426.866	1	3426.866	18.917	0.000
	Residual	3706.848	16	31.678		
	Total	7133.714	17			
Abrasion resistance	Regression	3864.803	1	3864.803	18.917	0.000
	Residual	3268.911	16	204.307		
	Total	7133.911	17			
Young's Modulus	Regression	4014.946	1	4014.946	30.971	0.000
	Residual	3118.768	16	194.874		
	Total	7133.714	17			
Poisson's ratio	Regression	4703.733	1	4703	30.971	0.000
	Residual	2429.981	16	151.874		
	Total	7133.714	17			

Table 4.4: Significance of model components and confidence intervals of SE with Chisel bit

Regression Model	Unstandardized coefficients		Standardized coefficients	t	Sig of t	95% Confidence interval for B	
	B	Std. Error				Beta	Lower bound
(constant)	-307.572	135.72		-	0.038	-595.294	-19.870
Density	134.475	50.857	0.551	2.266 2.644	0.018	26.663	242.287
(constant)	11.414	11.021		1.036	0.316	-11.949	34.778
UCS	1.060	0.278	0.690	3.814	0.002	0.471	1.650
(constant)	-158.156	45.280		-	0.003	-254.14	-62.160
SRN	3.961	0.855	0.757	3.493 4.634	0.000	2.149	5.774
(constant)	11.177	10.993		1.071	0.324	-12.126	34.482
BTS	10.393	2.702	0.693	3.846	0.001	4.664	16.122
(constant)	103.104	12.413		8.306	0.000	76.789	129.419
Abrasion resistance	-2.017	0.464	-0.736	- 4.344	0.000	-3.000	-1.034
(constant)	-74.389	27.854		-	0.017	-133.438	-15.341
Young's Modulus	4.740	1.044	0.750	2.671 4.538	0.000	2.526	6.954
(constant)	-97.369	26.843		-	0.002	-154.273	-40.464
Poisson's ratio	578.606	103.96 9	0.812	3.627 5.565	0.000	358.202	799.010

Table 4.5: Regression Models Summary of SE with Cross bit

Predictor	r	r ²	Adjusted r ²	Standard Error of Estimate
Density	0.569	0.324	0.282	18.65416
UCS	0.663	0.440	0.405	16.98410
Hardness (SRN)	0.775	0.601	0.576	14.33757
BTS	0.665	0.442	0.407	16.94820
Abrasion resistance	0.730	0.553	0.504	15.50687
Young's Modulus	0.758	0.574	0.548	14.80507
Poisson's ratio	0.803	0.644	0.622	13.53332

Table 4.6: ANOVA Results of SE with Cross bit

Predictor	Sum of squares		df	Mean squares	F	p value
Density	Regression	2669.579	1	2669.579	7.672	0.014
	Residual	5567.643	16	347.978		
	Total	8237.223	17			
UCS	Regression	3621.867	1	3621.867	12.558	0.003
	Residual	4615.356	16	288.460		
	Total	8237.223	17			
Hardness (SRN)	Regression	4948.812	1	4948.812	24.069	0.000
	Residual	3289.191	16	205.574		
	Total	8237.223	17			
BTS	Regression	3641.360	1	3641.360	12.677	0.003
	Residual	4595.862	16	287.241		
	Total	8237.223	17			
Abrasion resistance	Regression	4389.813	1	4389.813	18.256	0.001
	Residual	3847.409	16	240.463		
	Total	8237.223	17			
Young's Modulus	Regression	4730.182	1	4730.182	21.580	0.000
	Residual	3507.041	16	219.190		
	Total	8237.223	17			
Poisson's ratio	Regression	5306.812	1	5306.812	28.975	0.000
	Residual	2930.411	16	183.151		
	Total	8237.223	17			

Table 4.7: Significance of model components and confidence intervals of SE with Cross bit

Regression Model	Unstandardized coefficients		Standardized coefficients	t	Sig of t	95% Confidence interval for B	
	B	Std. Error				Lower bound	Upper bound
(constant)	-343.350	143.734		-2.384	0.03	-648.054	-38.647
Density	149.176	53.858	0.569	2.770	0.014	35.001	263.350
(constant)	13.558	12.249		1.107	0.285	-12.408	39.524
UCS	1.095	0.309	0.663	3.543	0.003	0.440	1.750
(constant)	-175.685	47.056		-3.734	0.002	-275.438	-75.931
SRN	4.358	0.888	0.775	4.906	0.000	2.425	6.241
(constant)	13.382	12.240		1.093	0.296	-12.566	39.330
BTS	10.714	0.309	0.665	3.560	0.003	4.335	17.092
(constant)	109.957	13.467		8.165	0.000	81.408	138.506
Abrasion resistance	-2.149	0.503	-0.730	-4.273	0.001	-3.216	-1.083
(constant)	-81.676	29.537		-2.765	0.014	-144.292	-19.060
Young's Modulus	5.145	1.108	0.758	4.645	0.000	2.797	7.493
(constant)	-103.166	29.478		-3.500	0.003	-105.656	-40.676
Poisson's ratio	614.580	114.174	0.803	5.383	0.000	372.543	856.618

Table 4.8: Regression Models' Summary of SE with Spherical button bit

Predictor	r	r ²	Adjusted r ²	Standard Error of Estimate
Density	0.592	0.350	0.309	18.46727
UCS	0.726	0.527	0.497	15.75405
Hardness (SRN)	0.768	0.590	0.564	14.67202
BTS	0.727	0.529	0.499	15.72365
Abrasion resistance	-0.783	0.613	0.589	14.24115
Young's Modulus	0.794	0.630	0.607	13.92827
Poisson's ratio	0.850	0.723	0.705	12.06371

Table 4.9: ANOVA Results of SE with Spherical button bit

Predictor	Sum of squares		df	Mean squares	F	p value
Density	Regression	2937.236	1	2937.236	8.613	0.010
	Residual	5456.643	16	341.040		
	Total	8393.879	17			
UCS	Regression	4422.835	1	4422.835	17.820	0.001
	Residual	3971.044	16	248.190		
	Total	8393.879	17			
Hardness (SRN)	Regression	4949.164	1	4949.164	22.988	0.00
	Residual	3444.715	16	215.205		
	Total	8393.879	17			
BTS	Regression	4438.146	1	4438.146	17.951	0.00
	Residual	3955.733	16	247.233		
	Total	8393.879	17			
Abrasion resistance	Regression	5148.914	1	5148.917	25.388	0.00
	Residual	3244.965	16	202.810		
	Total	8393.879	17			
Young's Modulus	Regression	5289.930	1	5289.930	27.268	0.00
	Residual	3103.949	16	193.997		
	Total	8393.879	17			
Poisson's ratio	Regression	6065.348	1	6065.308	41.6777	0.00
	Residual	2328.531	16	145.533		
	Total	8393.879	17			

Table 4.10: Significance of model components and confidence intervals of SE with Spherical button bit

Regression Model	Unstandardized coefficients		Standardized coefficients	t	Sig of t	95% Confidence interval for B	
	B	Std. Error				Beta	Lower bound
(constant)	-366.883	142.294		-2.578	0.020	-668.533	-65.232
Density	156.476	53.319	0.592	2.935	0.010	43.445	269.506
(constant)	5.188	11.361		0.457	0.654	-18.897	29.274
UCS	1.210	0.287	0.726	4.221	0.001	0.602	1.817
(constant)	-179.771	48.155		-3.733	0.002	-281.856	-77.687
SRN	4.359	0.909	0.768	4.795	0.000	2.432	6.286
(constant)	5.037	11.356		0.444	0.663	-19.036	29.110
BTS	11.828	2.792	0.727	4.237	0.001	5.916	17.746
(constant)	110.494	12.368		8.934	0.000	84.276	136.713
Abrasion resistance	-2.328	0.462	-0.783	-5.039	0.000	-3.307	-1.348
(constant)	-93.573	27.788		-3.367	0.004	-152.481	-34.665
Young's Modulus	5.441	1.042	0.794	5.222	0.000	3.232	7.650
(constant)	-118.123	26.277		-4.495	0.000	-173.827	-62.419
Poisson's ratio	657.037	101.775	0.850	6.456	0.000	441.283	872.791

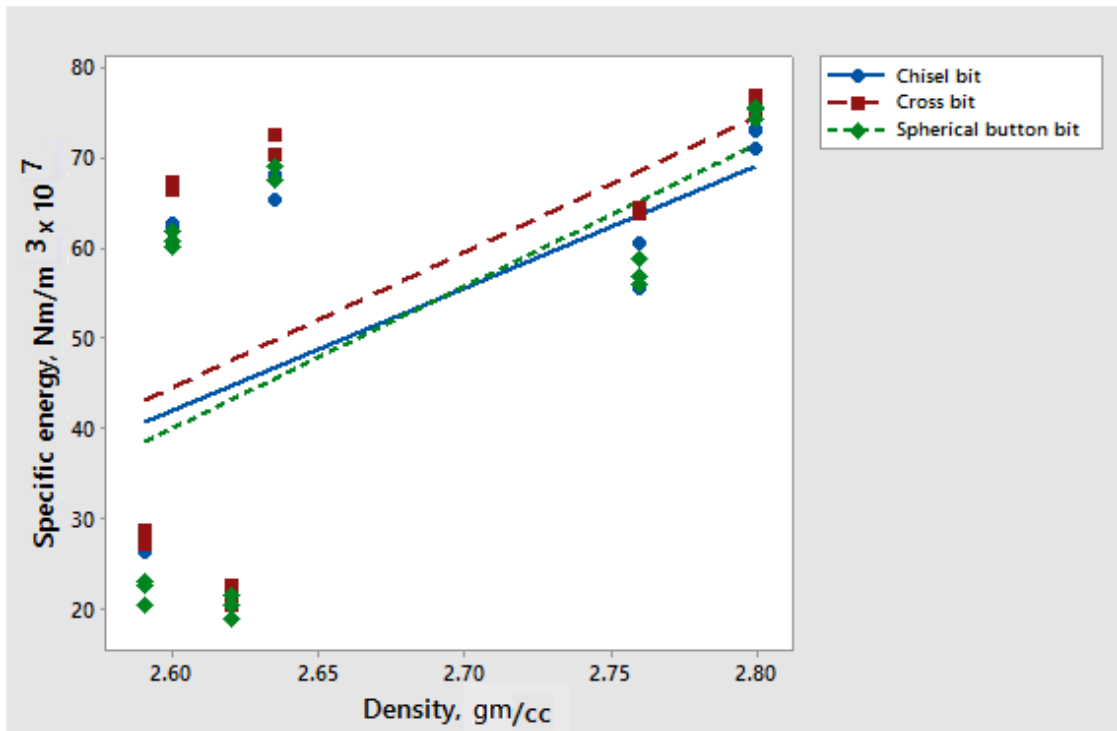


Figure 4.4 Relationship between density and Specific energy

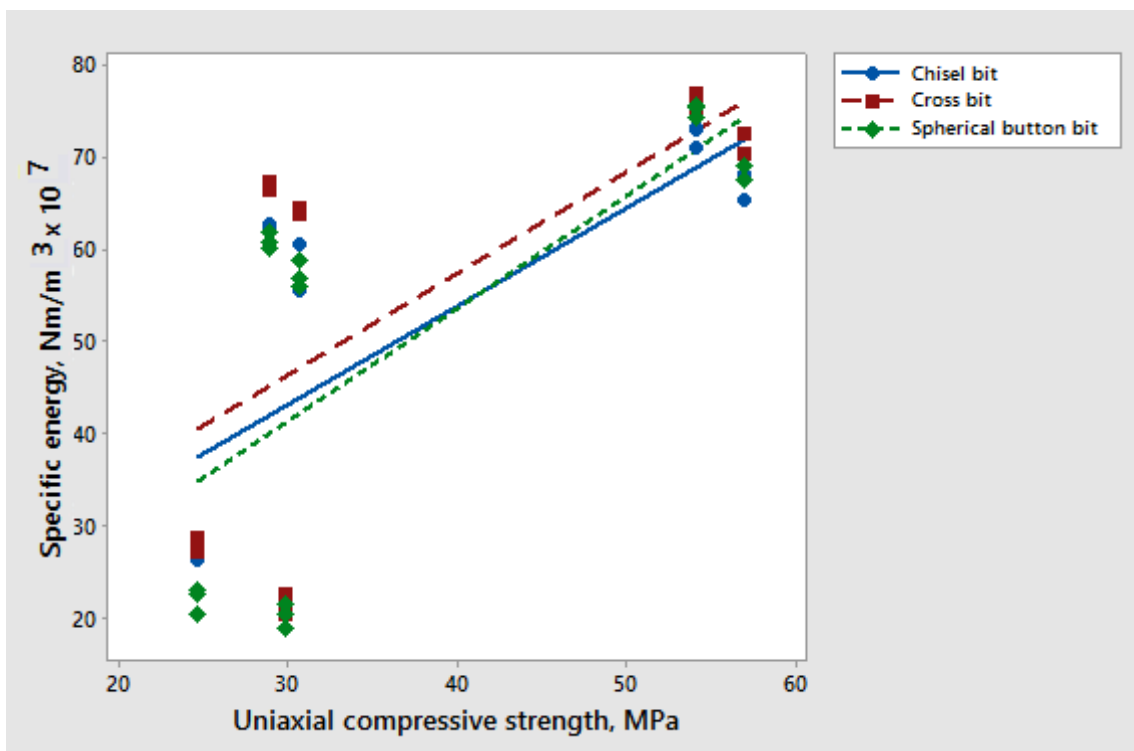


Figure 4.5 Relationship between uniaxial compressive strength and Specific energy

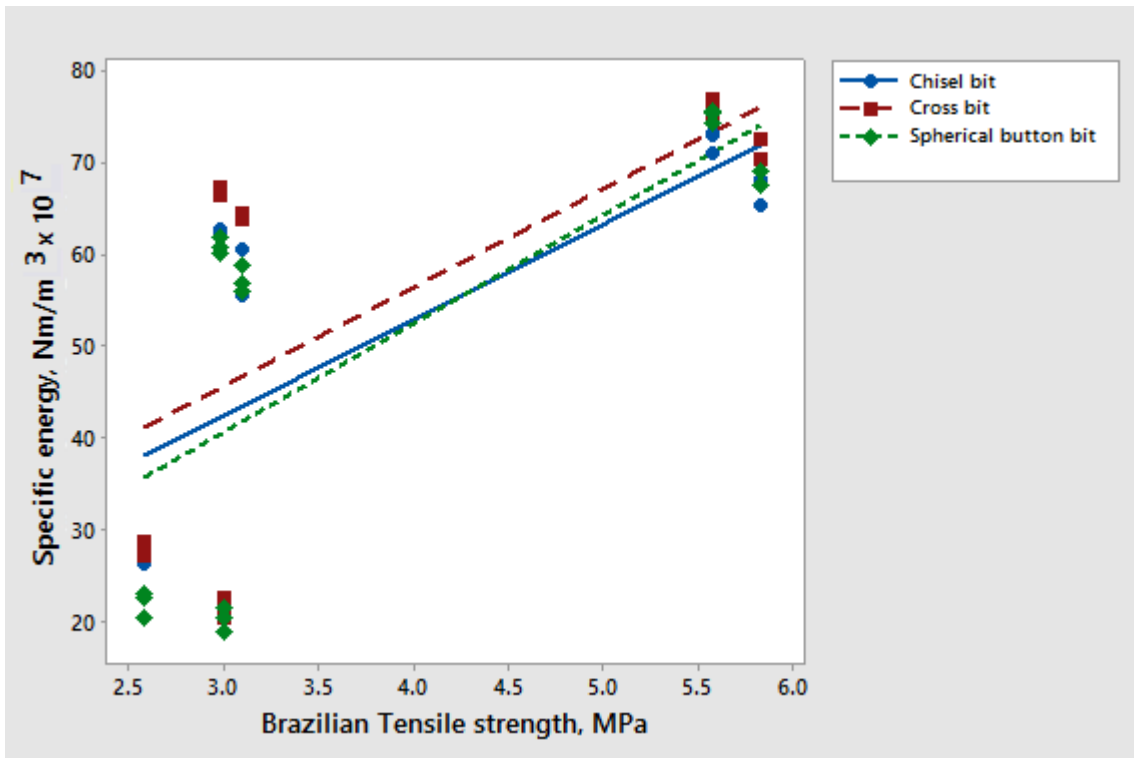


Figure 4.6 Relationship between Brazilian tensile strength and Specific energy

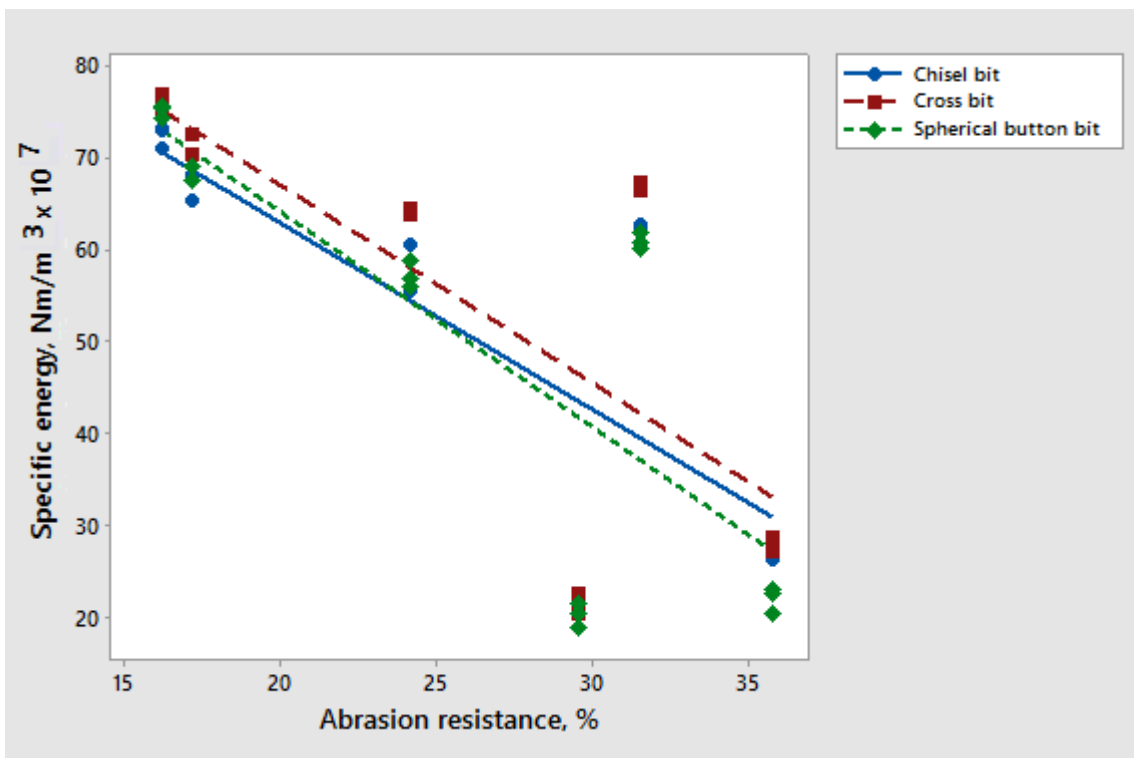


Figure 4.7 Relationship between abrasion resistance and Specific energy

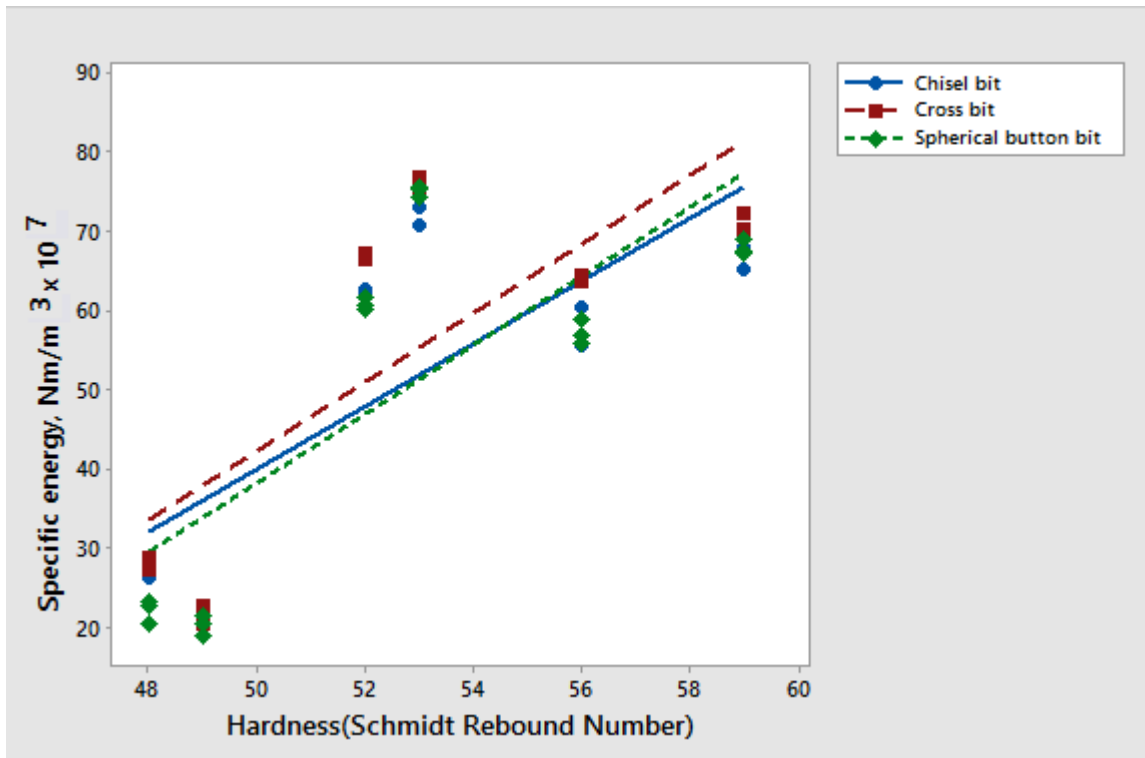


Figure 4.8 Relationship between hardness (SRN) and Specific energy

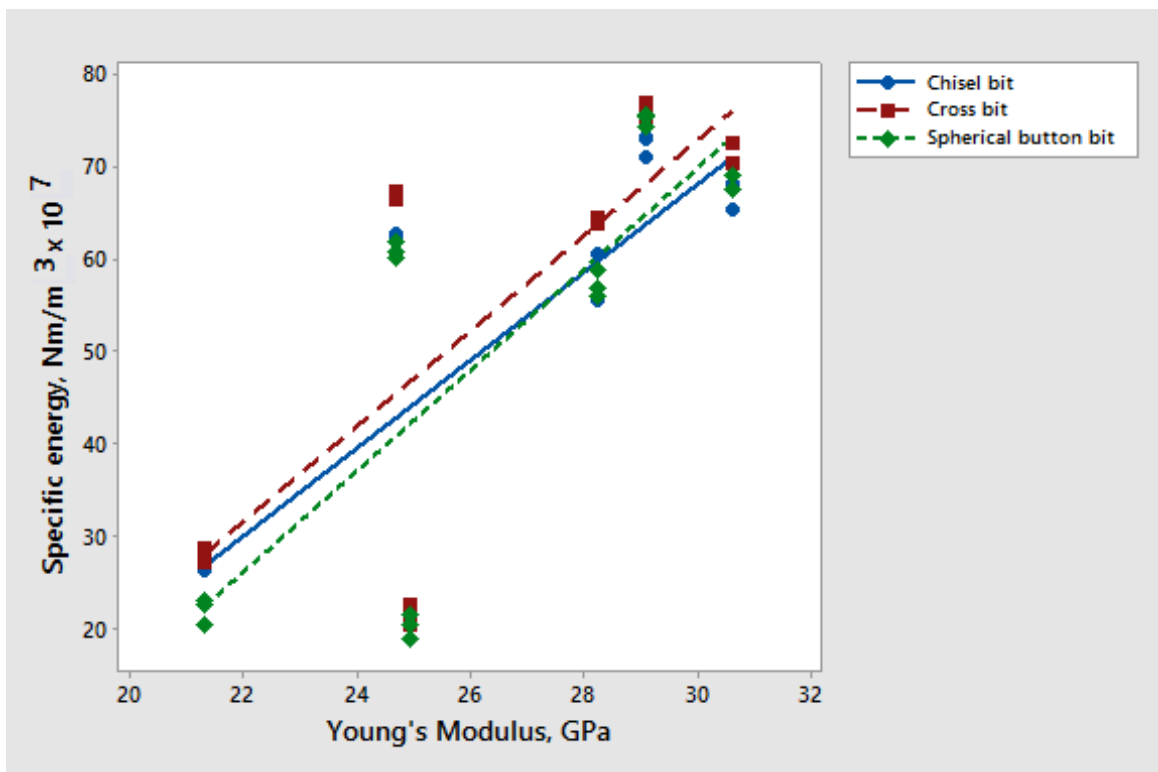


Figure 4.9 Relationship between Young's Modulus and Specific energy

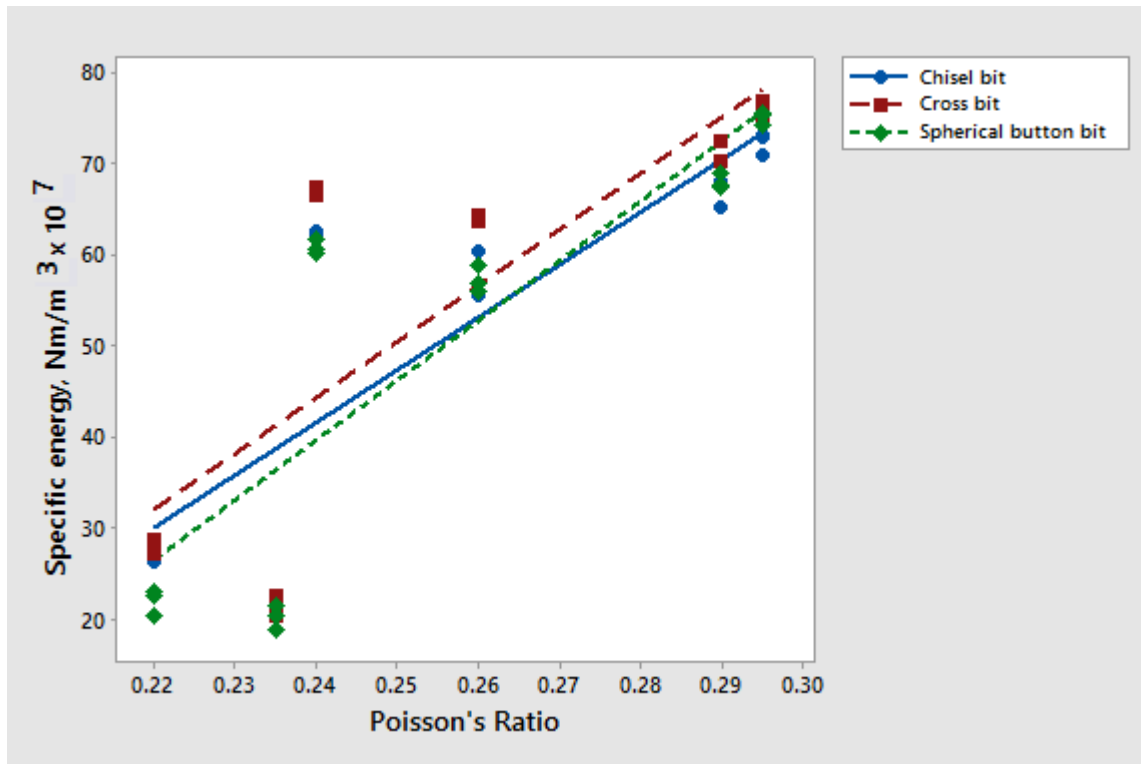


Figure 4.10 Relationship between Poisson's ratio and Specific energy

4.2.5 ANALYSIS OF RESULTS

Correlation coefficients are significant and considered at the 0.01 level. Similarly, the bivariate correlation was done in Minitab 17 software and found the values of 'p' for all the independent variables are 0.00. As per the Cohen (1988) mentioned SPSS survival manual, if 'r' value between 0.5 to 1, there is large correlation. So, the 'r' values obtained in the present study are more than 0.5, therefore all the independent parameters used in the analysis are statistically significant.

Density correlated with SE with a correlation coefficient of 0.551 for chisel bit, 0.569 for cross bit and 0.592 for spherical button bit (Table 4.2, 4.5 and 4.8) at 99% confidence level. According to regression analysis, an increase can be expected in SE as density of rocks increases. This is in agreement with earlier studies (Tiryaki and Dikmen, 2006).

UCS correlated well with SE with a correlation coefficient of 0.690 for chisel bit, 0.663 for cross bit and 0.726 for spherical button bit (Table 4.2, 4.5 and 4.8) at 99%

confidence level. According to regression analysis, a linear increase can be expected in SE as UCS increases, complying with the most of the previous studies (Rostami et al., 1993; Speight, 1997; Balci, Dermircin and Copur and Tuncdemir, 2004; Tiryki and Dikmen, 2006; Irfan Celal, Fatih Bayram and Nazmi Erhan Yasitli, 2013). UCS is the one of the major rock properties affecting rock cuttability/drillability because a considerable amount of the cutting/ drilling energy is consumed in overcoming the UCS of rock for producing a crushed zone under the pick tip at the beginning of the rock cutting/drilling process.

Correlation coefficient between BTS and SE is 0.693 for chisel bit, 0.665 for cross bit and 0.727 for spherical button bit (Table 4.2, 4.5 and 4.8) at 99% confidence level. This result is in line with the previous studies in this area. In the present study, as per regression analysis, with increase in tensile strength there is increase in SE. It is very well known from previous investigations that as UTS increases, a corresponding increase occurs in SE for most of the rocks (Balci, Dermircin and Copur and Tuncdemir, 2004; Tiryki and Dikmen, 2006; Irfan Celal, Fatih Bayram and Nazmi Erhan Yasitli, 2013) Brittle rocks were reported to show tensile failure, whilst tougher rocks fail in shear mode. However, the failure cracks in a rock forced by a pick are tensile in nature regardless of the rock type (Evans and Pomeroy, 1973; Roxborough, 1973; Nishimatsu, 1979; Hood and Roxborough, 1992).

SE increased as the Schmidt hammer hardness value increased with a correlation coefficient of 0.757 for chisel bit, 0.775 for cross bit and 0.768 for spherical button bit (Table 4.2, 4.5 and 4.8) at 99% confidence level as per the correlation and regression analysis made. This confirms the earlier findings (Balci, Dermircin and Copur and Tuncdemir, 2004; Tiryki and Dikmen, 2006; Irfan Celal, Fatih Bayram and Nazmi Erhan Yasitli, 2013).

Similarly, a strong negative correlation (r for chisel bit: - 0.736, r for cross bit: - 0.730 and r for spherical button bit: -0.783) was found between the abrasion resistance of rocks and SE (Table 4.2, 4.5 and 4.8). Relying upon these findings, a decrease can be

expected in SE, as abrasion resistance of rocks increases. This confirms the earlier finding of Irfan Celal, Fatih Bayram and Nazmi Erhan Yasitli, 2013.

SE increased as the Young's Modulus value increased with a correlation coefficient of 0.750 for chisel bit, 0.758 for cross bit and 0.794 for spherical button bit (Table 4.2, 4.5 and 4.8) at 99% confidence level as per the correlation and regression analysis made. This confirms the earlier findings (Balci, Dermircin and Copur and Tuncdemir, 2004).

Similarly SE increased as the Poisson's Ratio value increased with a correlation coefficient of 0.812 for chisel bit, 0.775 for cross bit and 0.850 for spherical button bit (Table 4.2, 4.5 and 4.8) at 99% confidence level as per the correlation and regression analysis made.

So properties of rocks exhibited linear correlations with SE of chisel and cross and spherical button bits viz density, SRN, UCS, BTS, Young's Modulus and Poisson's ratio which were in positive correlations, whereas abrasion resistance was in negative correlation and all are statistically significant with SE at 99% confidence interval.

Therefore, rock properties were found statistically significant in estimating SE individually, depending on the results obtained from linear regression analysis, ANOVA and Student's t-tests, and r^2 values.

The analysis showed that the some properties considered for the present study influence the specific energy. The influence of rock properties (like density, UCS, BTS, Young's Modulus, Poisson's ratio) on the specific energy required is shown in the graphical form, from Figure 4.4 to 4.10.

It was observed, except in the case of abrasion resistance, that with the increase in the value of properties of rock, the specific energy required increases i.e increase in strength of rock, the specific energy increases. This is because of the fact that, with the increase in the strength, the resistance to indentation increases. But limestone possessed slightly higher values than marble but comparatively lower specific energy values were

recorded. The reason is that the indentations were made perpendicular to the bedding plane in limestone. The specific energies for penetrations made perpendicular to the bedding plane in limestone were found to be less than penetrations made parallel to the bedding plane. This confirms the earlier finding by Paul B, Sikarskie D.L. (1965) and Benjumea R, Sikarskie D.L. (1969). Further it was observed that in case of limestone, less penetrations were obtained as compared to marble but the formation of chips (crater volume) was more than the marble due to break over of rock between subsequent indentations. Therefore, the specific energy also, in case of sedimentary rocks, apart from physico-mechanical properties, depends on the structural (bedding planes) properties also.

The basalt possessed slightly less strength properties as compared to black galaxy granite, but higher specific energy were found, and it offered much resistance to penetration due to high interlocking of very fine grained (40 microns) Pyroxene + amphibole minerals. The volume of rock material formed is less in every indentation as compared to black galaxy granite therefore high specific energy values were found.

Similarly the Moon white granite possessed less strength properties as compared to steel gray granite, but offered much resistance to penetration. And also the volume of chips formed were less, so high specific energy values were found for Moon white granite, because it contains high percentage of quartz with high degree of interlocking. This confirms earlier finding of Bell, 1978; Barbour et al., 1979).

4.3 INFLUENCE OF MINERALOGICAL PROPERTIES ON SPECIFIC ENERGY

4.3.1 INTRODUCTION

In order to find the influence of mineralogical properties on specific energy, different models were developed by considering the common minerals like quartz, feldspar, hornblende, pyrite, magnetite and biotite mica present in all the rocks under study.

4.3.2 EXPERIMENTAL WORK

A few lumps were selected from the samples and thin sections were prepared to study the mineralogical composition and textural features. The remaining sample was crushed and ground to minus 65 mesh size. Subsequently minus 65 plus 200 mesh size fraction was studied under the microscope. The result of the samples are given in Table 3.14 to 3.19.

4.3.3 BI-VARIATE CORRELATION

Bi-variate correlation was carried between specific energy (SE) obtained in chisel bit of 38 mm diameter at 20⁰ index angle and the common minerals present in percentage in the rocks were tested. Similarly, SE values obtained in cross bit of 48 mm at 10⁰ index angle, SE values obtained in spherical bit of 35mm diameter at 40⁰ index angle and the common minerals present in percentage in the rocks tested were considered for correlation. Correlation coefficients between independent (selected minerals in percentage) and dependent variables (SE) were determined through bivariate correlation techniques by using Windows version of SPSS 15 software. In this analysis, the correlation coefficients between SE (dependent variable) and selected mineral (independent variables) were investigated. Pearson's correlation coefficients were obtained after applying bivariate correlation technique to the test data, and the results are given in Table 4.11.

Table 4.11: Pearson's correlation coefficients (SE with mineralogical composition)

S. No	Independent variable	Chisel bit	Cross bit	Spherical button bit
		r	r	r
1	Quartz	0.848	0.862	0.832
2	Feldspar	- 0.9689	- 0.984	- 0.970
3	Hornblende	0.759	0.77	0.787
4	Pyrite	0.448	0.438	0.463
5	Magantite	0.532	0.521	0.566
6	Biotite mica	0.323	0.384	0.327

4.3.4 SIMPLE REGRESSION OF SE AND MINERALS

4.3.4.1 SIMPLE REGRESSION OF SE (CHISEL BIT) AND MINERALS

Simple regression was carried out between specific energy(SE) obtained in chisel bit of 38 mm diameter at 20° index angle and the common minerals present in rocks tested by using Microsoft Excel 13 software. All the relationships like linear, exponential and power were tested between dependent and independent variables. The relationships between specific energy (y) and mineralogical properties(x) are given in Table 4.12.

Table 4.12: Relationship between specific energy (chisel bit) and mineralogical properties

Mineralogical property	Regression equation	r ²
Quartz	$y = 2.1537x^{0.8744}$	0.8133
Feldspar	$y = -4.9749x + 350.81$	0.9389
Hornblende	$y = 7.4797\ln(x) + 37.48$	0.8452
Pyrite	$y = 47.449x^{0.2335}$	0.3023
Magnetite	$y = 10.293\ln(x) + 44.297$	0.3267
Biotite mica	$y = 29.793x^{0.3238}$	0.2923

4.3.4.2 SIMPLE REGRESSION OF SE (CROSS BIT) AND MINERALS:

Simple regression was carried out between SE obtained in cross bit and common mineral properties. All the relationships like linear, exponential and power were tested between dependent and independent variables. The relationships between specific energy (y) and mineralogical properties(x) are given in Table 4.13.

Table 4.13: Relationship between specific energy (cross bit) and mineralogical properties

Mineralogical property	Regression equation	r ²
Quartz	$y = 2.0704x^{0.9032}$	0.8313
Feldspar	$y = -4.0013x + 299.49$	0.9598
Hornblende	$y = 8.168\ln(x) + 39.659$	0.8729
Pyrite	$y = 50.5x^{0.2414}$	0.3096
Magnetite	$y = 11.239\ln(x) + 47.104$	0.3373
Biotite mica	$y = 30.207x^{0.3472}$	0.3304

4.3.4.3 SIMPLE REGRESSION OF SE (SPHERICAL BUTTON BIT) AND MINERALS

Simple regression was carried out between SE obtained in spherical bit and common mineral properties. All the relationships like linear, exponential and power were tested between dependent and independent variables. The relationships between specific energy (y) and mineralogical properties(x) are given in Table 4.14.

Table 4.14: Relationship between specific energy (spherical button bit) and mineralogical properties

Mineralogical property	Regression equation	r ²
Quartz	$y = 1.3642x^{0.9944}$	0.8475
Feldspar	$y = -6.0851x + 415.14$	0.9668
Hornblende	$y = 30.525x^{0.2071}$	0.8811
Pyrite	$y = 12.007\ln(x) + 51.903$	0.4025
Magnetite	$y = 11.821\ln(x) + 42.657$	0.3662
Biotite mica	$y = 26.086x^{0.3954}$	0.3512

4.3.5 ANALYSIS OF RESULTS

Correlation coefficients are significant and considered at the 0.01 level. As per the Cohen (1988) mentioned SPSS survival manual, if 'r' value between 0.5 to 1 then there is large correlation, medium correlation if r value between 0.3 and 0.49 and small correlation if r value between 0.1 and 0.29. So, the 'r' values obtained in the present study are medium to high, therefore all the independent parameters used in the analysis are statistically significant. The equations developed through regression for SE vs minerals like quartz, feldspar and hornblende are statistically highly significant and the minerals like pyrite, magnetite and biotite mica are statistically low to medium significant.

A strong positive correlation (r for chisel bit: 0.848, r for cross bit: 0.862 and r for spherical button bit: 0.832) was found between the quartz content of thin section of rocks and SE. And also the relationships (models) were established between quartz content and SE. The models were statistically significant (r² for chisel bit- 0.8133, r² for cross bit- 0.8313 and r² for spherical button bit- 0.8475). The specific energy for the rocks considered for study increased with increased percentage of quartz content (Table 4.12 to 4.14).

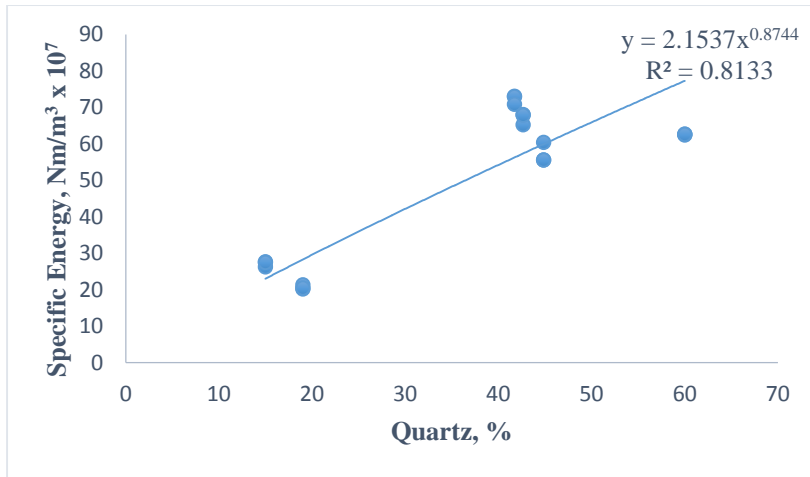


Figure 4.11 Relationship between specific energy of chisel bit and quartz mineral in various rocks

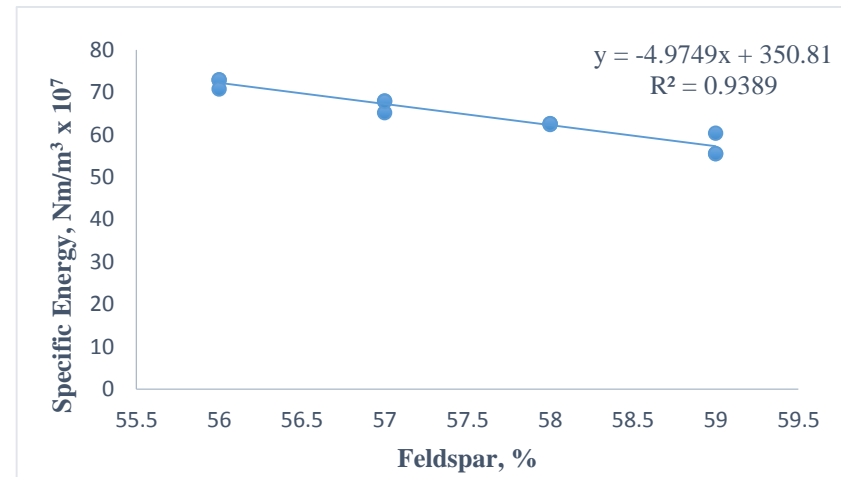


Figure 4.12 Relationship between specific energy of chisel bit and feldspar mineral in various rocks

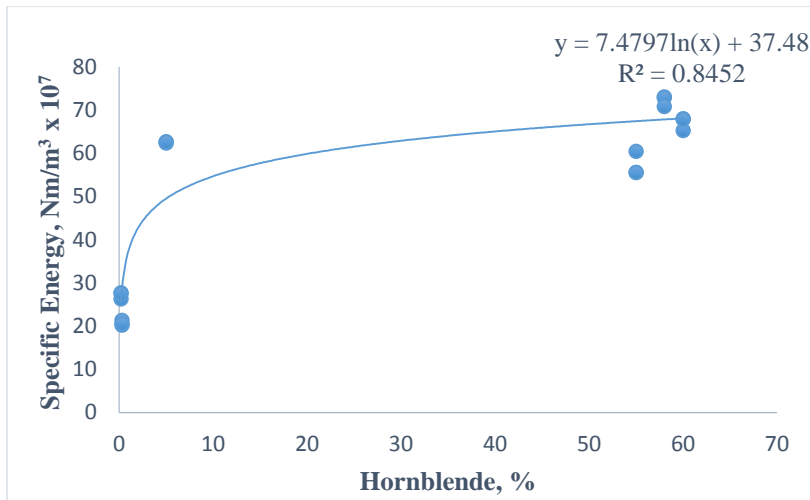


Figure 4.13 Relationship between specific energy of chisel bit and hornblende mineral in various rocks

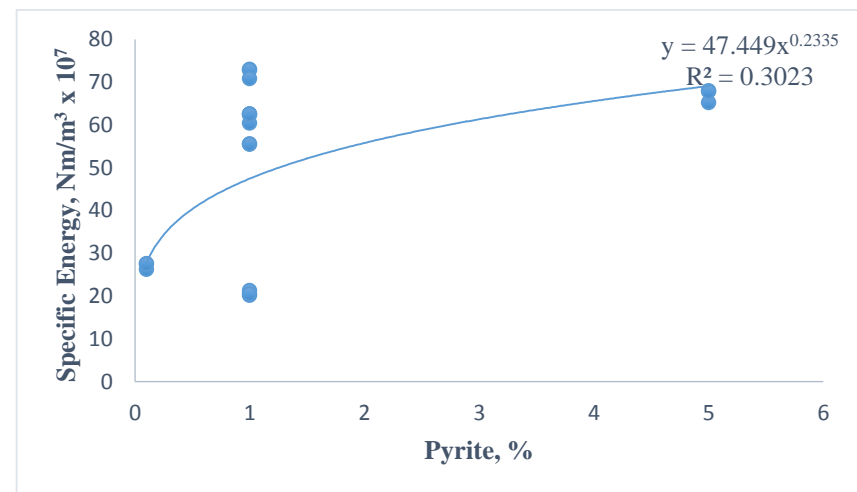


Figure 4.14 Relationship between specific energy of chisel bit and pyrite mineral in various rocks

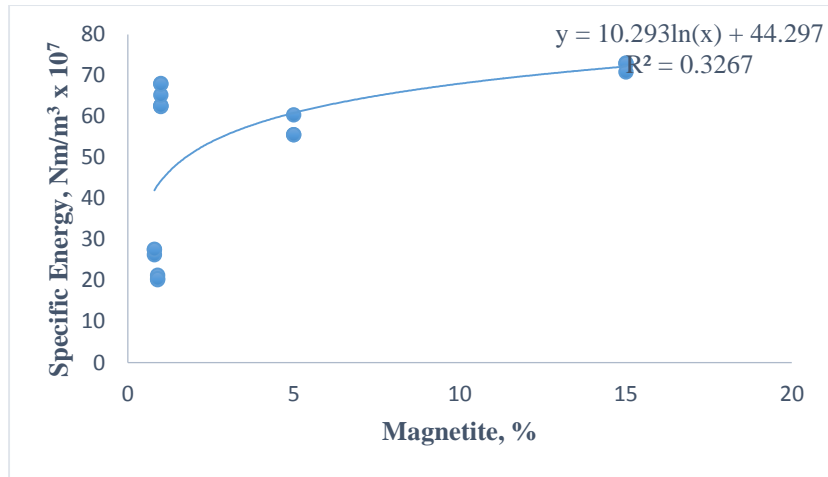


Figure 4.15 Relationship between specific energy of chisel bit and magnetite mineral in various rocks

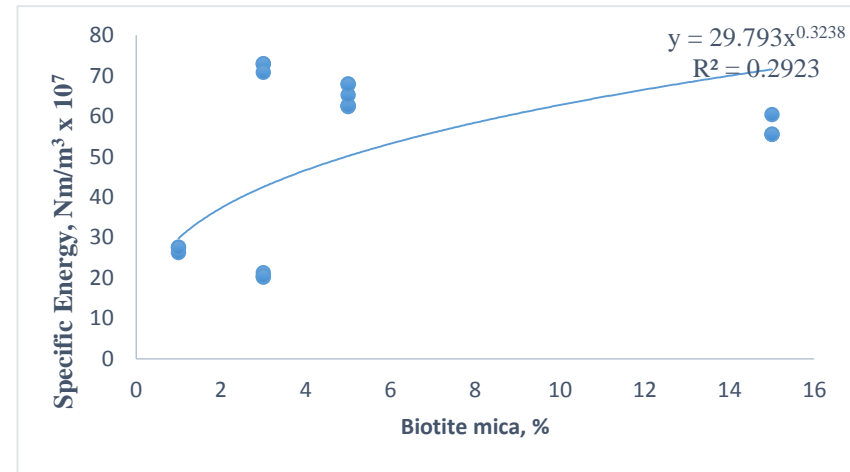


Figure 4.16 Relationship between specific energy of chisel bit and biotite mica mineral in various rocks

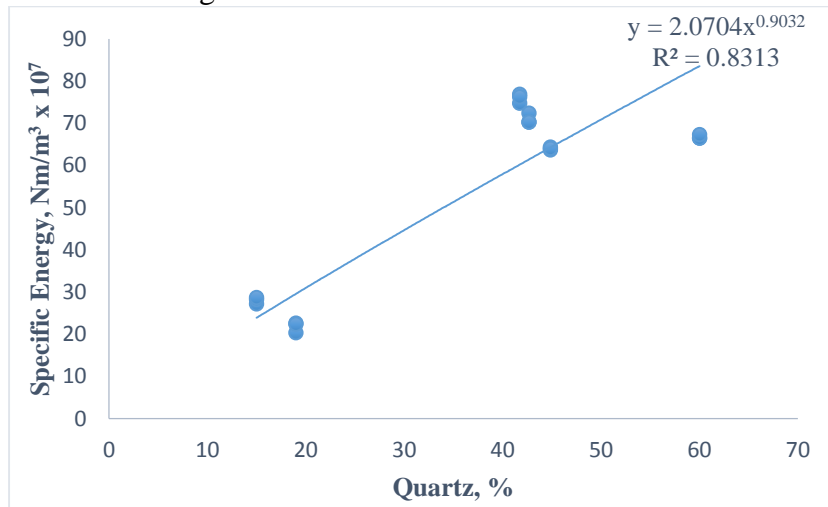


Figure 4.17 Relationship between specific energy of cross bit and Quartz mineral in various rocks

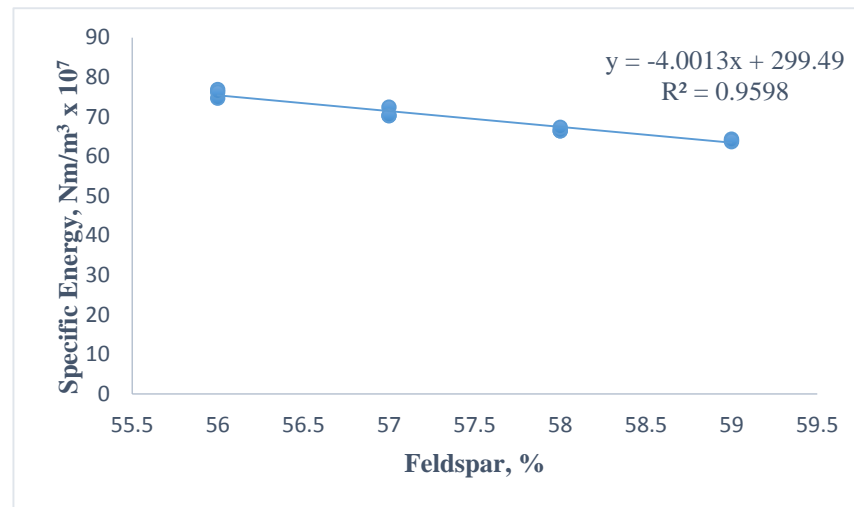


Figure 4.18 Relationship between specific energy of cross bit and feldspar mineral in various rocks

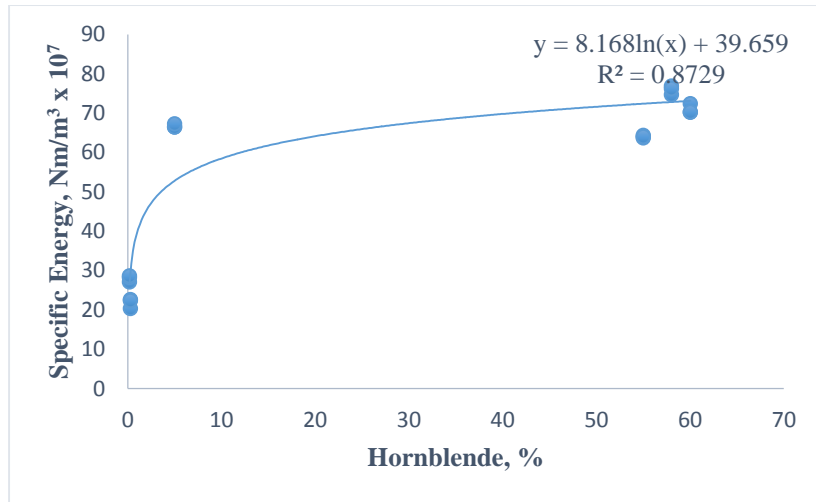


Figure 4.19 Relationship between specific energy of cross bit and hornblende mineral in various rocks

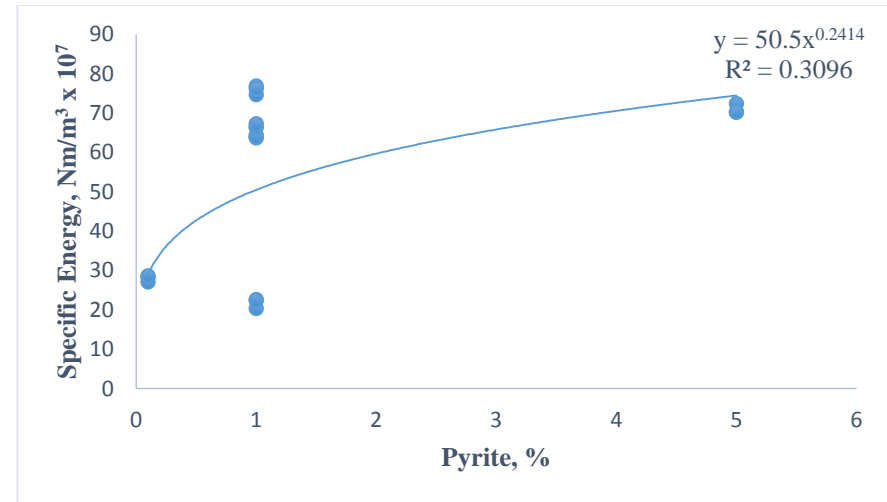


Figure 4.20 Relationship between specific energy of cross bit and pyrite mineral in various rocks

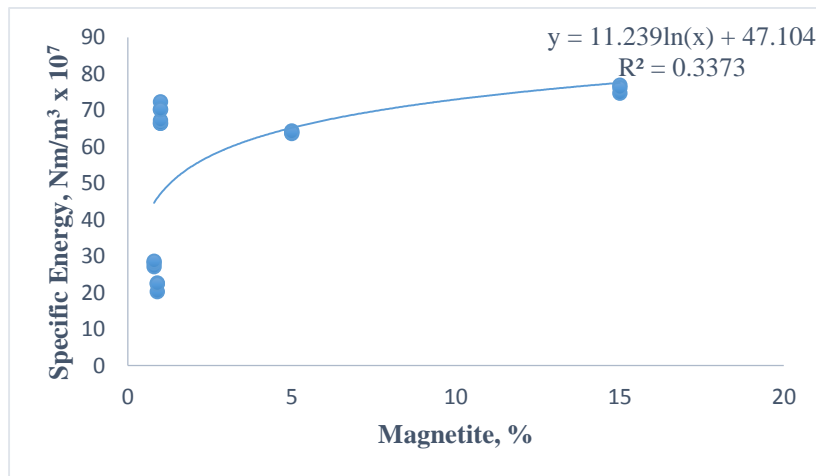


Figure 4.21 Relationship between specific energy of cross bit and magnetite mineral in various rocks

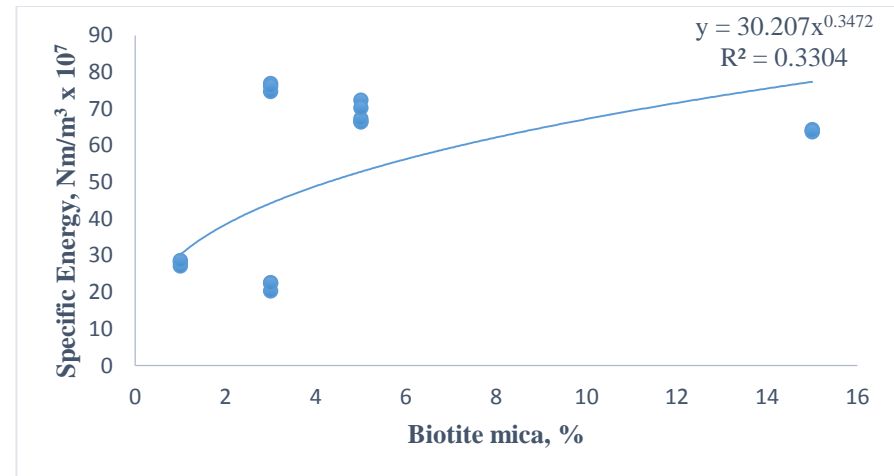


Figure 4.22 Relationship between specific energy of cross bit and biotite mica mineral in various rocks

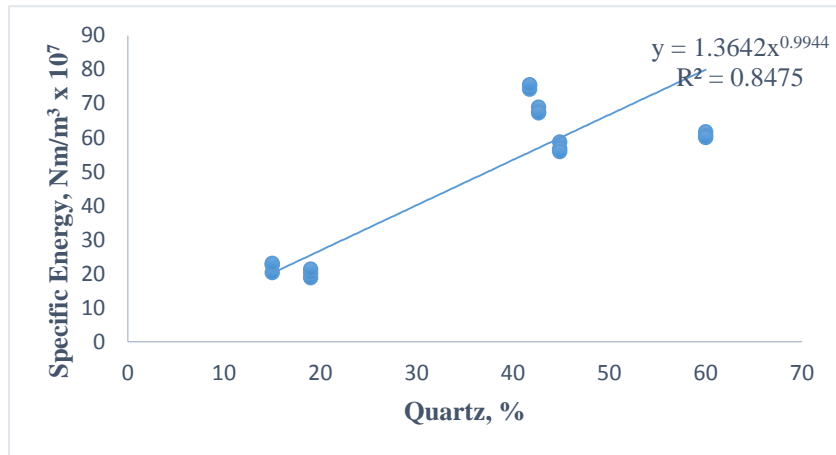


Figure 4.23 Relationship between specific energy of spherical button bit and quartz mineral in various rocks

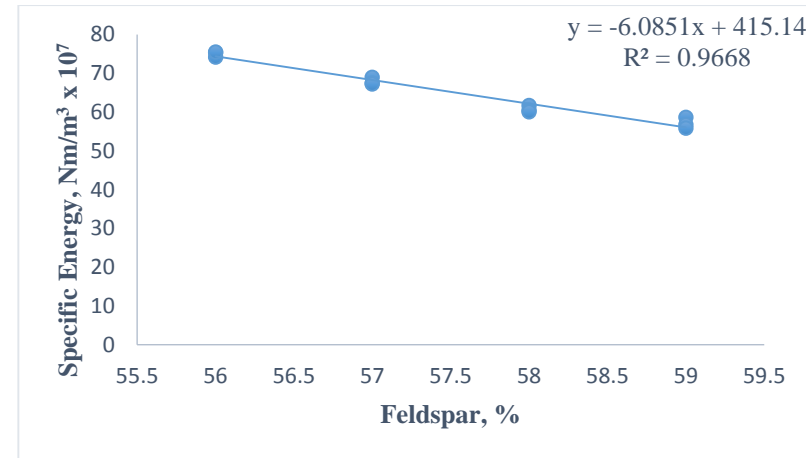


Figure 4.24 Relationship between specific energy of spherical button bit and feldspar mineral in various rocks

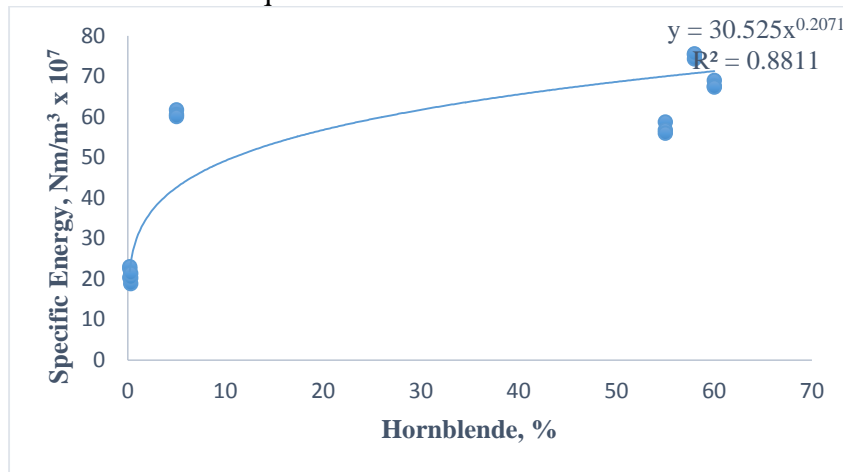


Figure 4.25 Relationship between specific energy of spherical button bit and hornblende mineral in various rocks

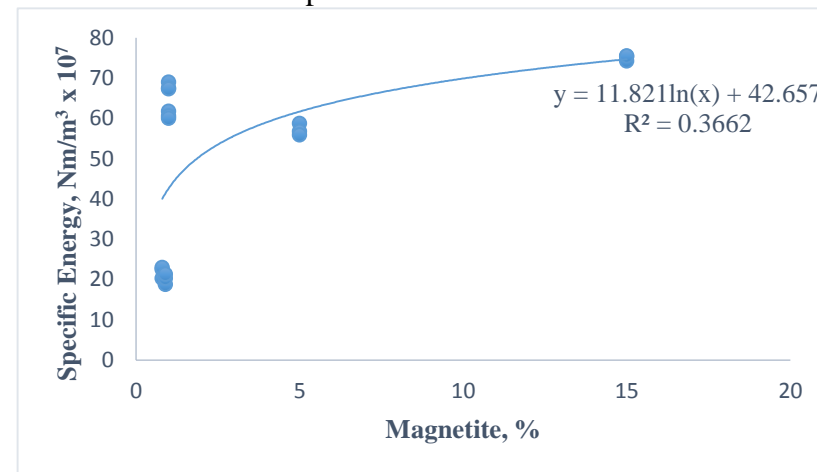


Figure 4.26 Relationship between specific energy of spherical button bit and magnetite mineral in various rocks

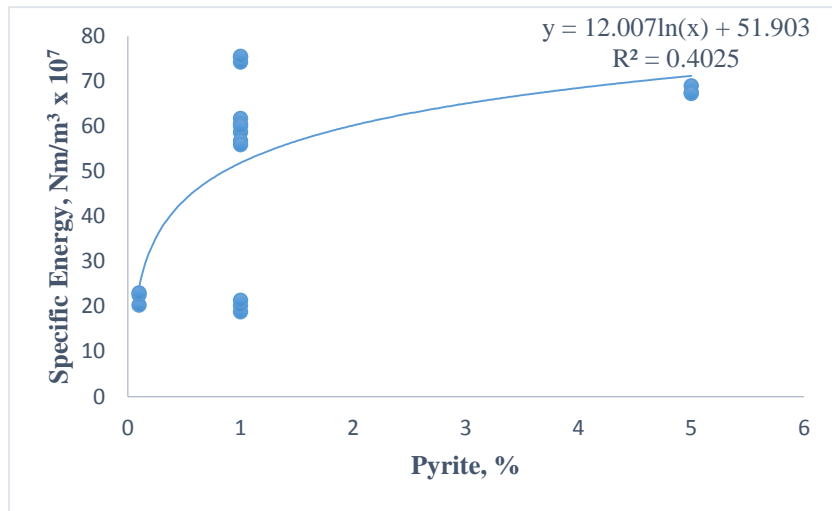


Figure 4.27 Relationship between specific energy of spherical button bit and pyrite mineral in various rocks

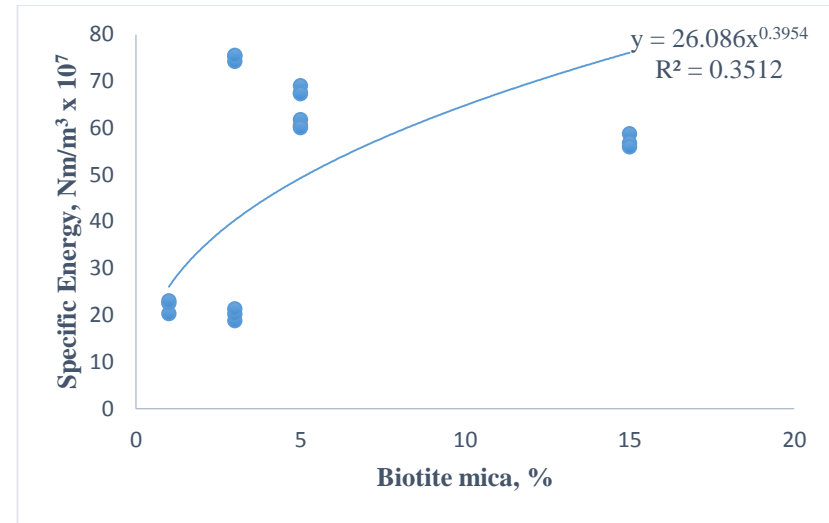


Figure 4.28 Relationship between specific energy of spherical button bit and biotite mica mineral in various rocks

The quartz content is the most widely known parameter in searching for the effects of rock composition on mechanical strength, drillability, and cuttability characteristics of rocks (West, 1986). Fahy and Guccione (1979) and Shakoor and Bonelli (1991) have found a considerable relationship between UCS and quartz content of sandstones. Tugrul and Zarif (1999) reported that as the quartz content of granites increased, their measures of strength also increased. It was proposed that degree of interlocking with quartz particles is much more effective on mechanical rock properties than their percentage in rock (Bell, 1978; Barbour et al., 1979).

Based on the earlier findings and results of the present study, it is conclude that a remarkable increase can be expected in SE, as the percentage of quartz increases (Figure 4.11, 4.17 and 4.23).

Similarly, a strong negative correlation (r for chisel bit: - 0.9689, r for cross bit: - 0.984 and r for spherical button bit: -0.970) was found between the feldspar content of thin sections of rocks and SE. This correlation is meaningful, as feldspars are reported to play important role in reducing the strength of rocks (Tugrul and Zarif, 1999; Tiryaki and Dikmen., 2006). And also the relationships (models) were established between feldspar content and SE. The models were statistically significant (r^2 for chisel bit- 0.9389, r^2 for cross bit- 0.9598 and r^2 for spherical button bit- 0.9668) (Table 4.12 to 4.14)). Relying upon these findings, decrease can be expected in SE, as the percentage of feldspar increases (Figure 4.12, 4.18 and 4.24).

A strong positive correlation (r for chisel bit: 0.759, r for cross bit: 0.77 and r for spherical button bit: 0.787) was found between the hornblende content of thin section of rocks and SE. And also the relationships (models) were established between hornblende content and SE. The models were statistically significant (r^2 for chisel bit- 0.8452, r^2 for cross bit- 0.8729 and r^2 for spherical button bit- 0.8811). The specific energy for the rocks considered for study increased with increased percentage of hornblende content from (Figure 4.13, 4.19 and 4.25). Relying upon these findings, increase can be expected in SE, as the percentage of hornblende increases.

A medium correlation (r for chisel bit: 0.448, r for cross bit: 0.438 and r for spherical button bit: 0.463) was found between the pyrite content of thin section of rocks and SE. And also the relationships (models) were established between pyrite content and SE. The models were statistically significant (r^2 for chisel bit: 0.3023, r^2 for cross bit: 0.3096 and r^2 for spherical button bit: 0.4025). The specific energy for the rocks considered for study increased with increased percentage of pyrite content (Figure 4.14, 4.20 and 4.27). Relying upon these findings, increase can be expected in SE, as the percentage of pyrite increases (Table 4.12 to 4.14).

A medium to large correlation (r for chisel bit: 0.532, r for cross bit: 0.521 and r for spherical button bit: 0.566) was found between the magnetite content of thin section of rocks and SE. And also the relationships (models) were established between magnetite content and SE. The models were statistically significant (r^2 for chisel bit: 0.4025, r^2 for cross bit: 0.3373 and r^2 for spherical button bit: 0.3662). The specific energy for the rocks considered for study increased with increased percentage of magnetite content (Figure 4.15, 4.21 and 4.26). Relying upon these findings, increase can be expected in SE, as the percentage of magnetite increases (Table 4.12 to 4.14).

A medium correlation (r for chisel bit: 0.323, r for cross bit: 0.384 and r for spherical button bit: 0.327) was found between the biotite mica content of thin section of rocks and SE. And also the relationships (models) were established between biotite mica content and SE. The models were statistically significant (r^2 for chisel bit: 0.2923, r^2 for cross bit: 0.3304 and r^2 for spherical button bit: 0.3512). The specific energy for the rocks considered for study increased with increased percentage of biotite mica content from Figure 4.16, 4.22 and 4.28. Relying upon these findings, increase can be expected in SE, as the percentage of biotite mica increases (Table 4.12 to 4.14).

4.4 INFLUENCE OF ELEMENTS/MINERALS IN OXIDES FORM OBTAINED FROM XRF TEST ON SPECIFIC ENERGY

4.4.1 INTRODUCTION

In order to find the influence of elements/minerals in oxide form on specific energy, different models have been developed by considering the common elements/minerals in oxide form like Al_2O_3 , SiO_2 , SO_3 , Cl, K_2O , CaO present in all the rocks under study.

4.4.2 BI-VARIATE CORRELATION

Bi-variate correlation was carried between specific energy (SE) obtained in chisel bit of 38 mm diameter at 20° index angle and the common elements/minerals in oxide form present in percentage in the rocks tested. Similarly SE values obtained in cross bit of 48 mm at 10° index angle, SE values obtained in spherical bit of 35mm diameter at 40° index angle and the common minerals present in percentage in the rocks tested were considered for correlation. Correlation coefficients between independent (selected elements/minerals in oxide form in percentage) and dependent variables (SE) were determined through bivariate correlation techniques by using Windows version of SPSS 15 software. In this analysis, the correlation coefficients between SE (dependent variable) and selected mineral (independent variables) were investigated. Pearson's correlation coefficients were obtained after applying bivariate correlation technique to the test data and results are given Table 4.15.

Table 4.15: Pearson's correlation coefficients (SE with minerals/elements)

S.No	Independent variable	Chisel bit	Cross bit	Spherical button bit
		R	r	r
1	Al_2O_3	0.799	0.82008	0.8216
2	SiO_2	0.8676	0.8841	0.86503
3	SO_3	-0.06506	-0.0935	-0.0879
4	Cl	0.28878	0.28847	0.2458
5	K_2O	0.27732	0.3191	0.24799
6	CaO	-0.84499	-0.86188	-0.86775

4.4.3 SIMPLE REGRESSION OF SE (CHISEL BIT) AND ELEMENTS /MINERALS IN OXIDES FORM

Simple regression was carried out between specific energy(SE) obtained in chisel bit of 38 mm diameter at 20° index angle and the common elements/minerals in oxide form present in rocks tested by using Microsoft Excel 13 software. All the relationships like linear, exponential and power were tested between dependent and independent variables. The relationship between specific energy (y) and mineralogical properties(x) is given in Table 4.16.

Table 4.16: Relationship between specific energy (chisel bit) and elements/minerals in oxide form

Mineralogical property	Regression equation	r ²
Al ₂ O ₃	y = 3.259x + 18.482	0.6725
SiO ₂	y = 1.167x + 13.318	0.7817
SO ₃	y = -5.9616x + 53.648	0.0042
Cl	y = 53.901x ^{0.2036}	0.269
K ₂ O	y = 39.768e ^{0.0421x}	0.1108
CaO	y = -1.3553x + 81.119	0.7428

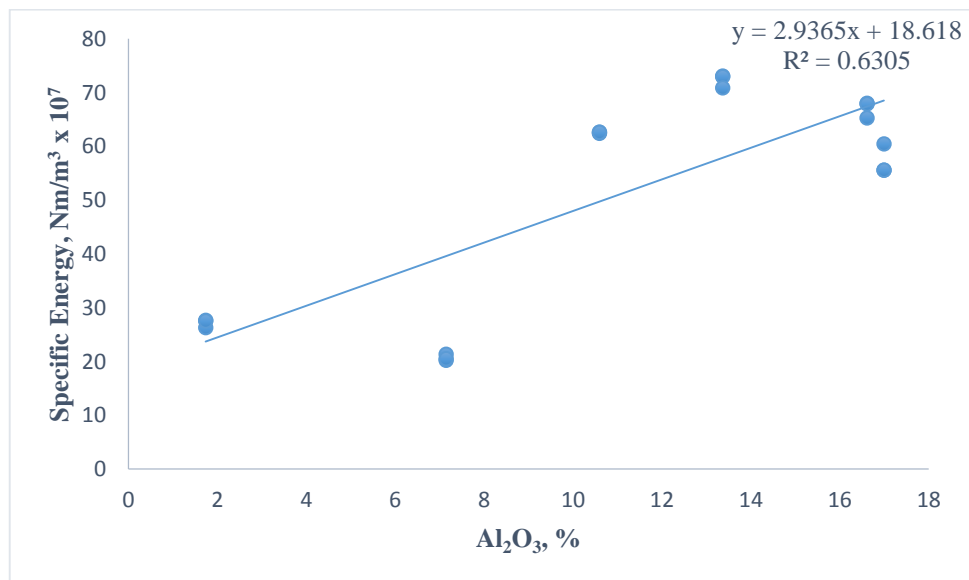


Figure 4.29 Relationship between specific energy of chisel bit and Al₂O₃ in various rocks

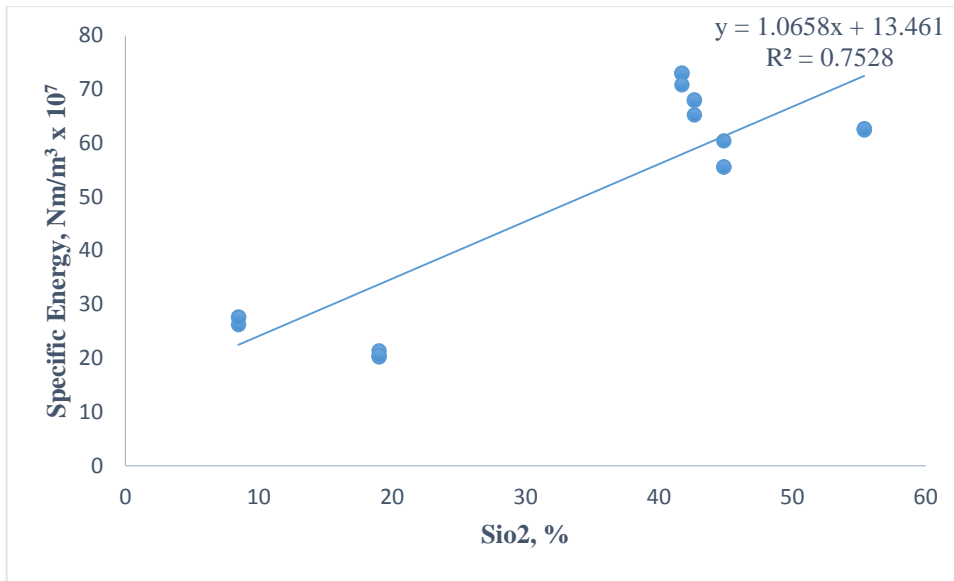


Figure 4.30 Relationship between specific energy of chisel bit and SiO₂ in various rocks

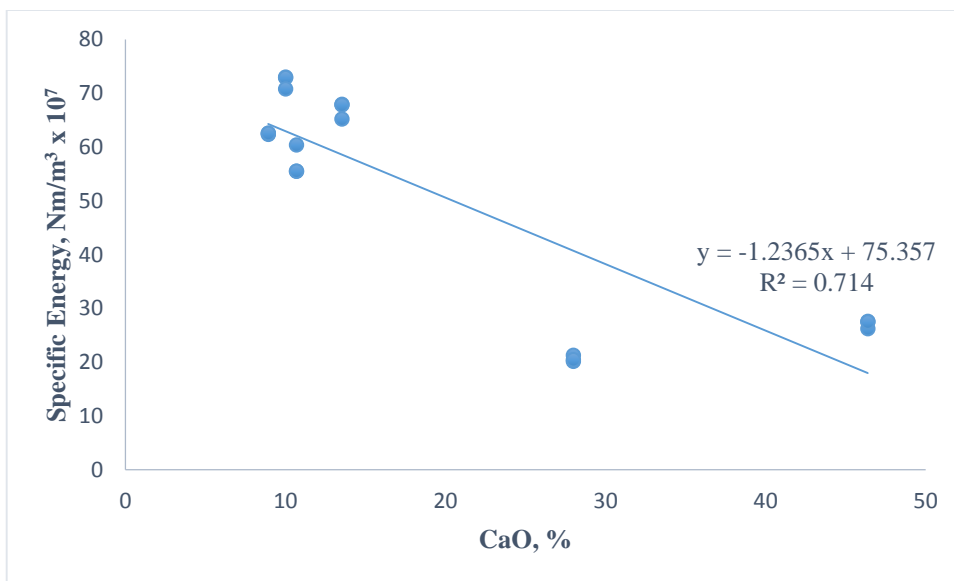


Figure 4.31 Relationship between specific energy of chisel bit and CaO in various rocks

4.4.4 SIMPLE REGRESSION OF SE (CROSS BIT) AND ELEMENTS /MINERALS IN OXIDES FORM

Simple regression was carried out between SE obtained in cross bit and common elements/minerals in oxide form. All the relationships like linear, exponential and

power were tested between dependent and independent variables. The relationship between specific energy (y) and mineralogical properties(x) is given in Table 4.17.

Table 4.17: Relationship between specific energy (cross bit) and elements/minerals in oxide form

Mineralogical property	Regression equation	r ²
Al ₂ O ₃	y = 3.259x + 18.482	0.725
SiO ₂	y = 1.167x + 13.318	0.7817
SO ₃	y = -9.2144x + 58.453	0.0088
Cl	y = 57.557x ^{0.2092}	0.2719
K ₂ O	y = 41.594e ^{0.0467x}	0.1309
CaO	y = -1.3553x + 81.119	0.7428

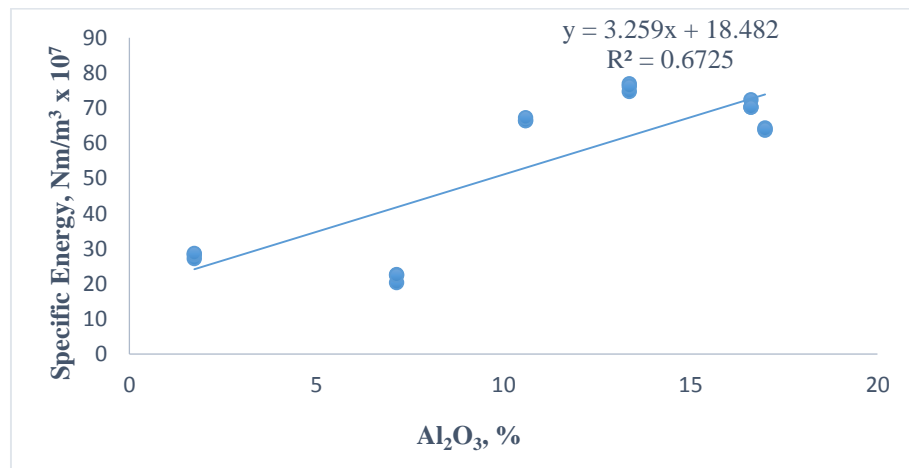


Figure 4.32 Relationship between specific energy of cross bit and Al₂O₃ in various rocks

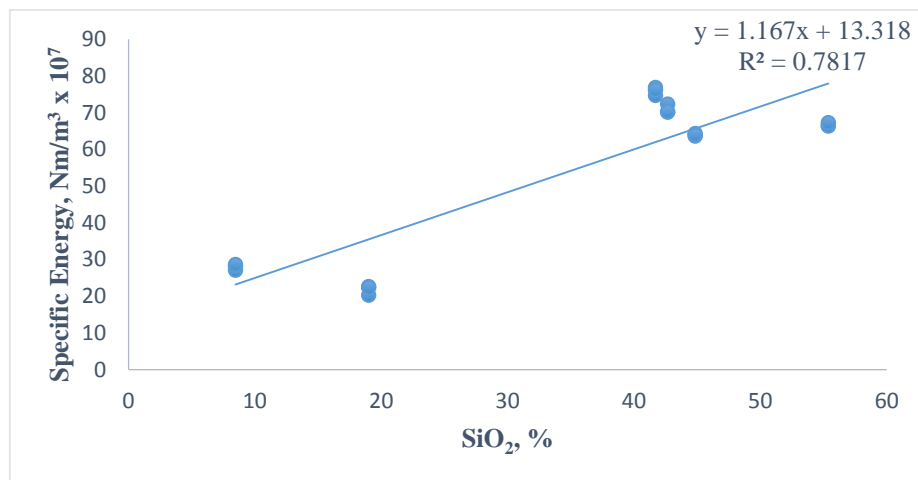


Figure 4.33 Relationship between specific energy of cross bit and SiO₂ in various rocks

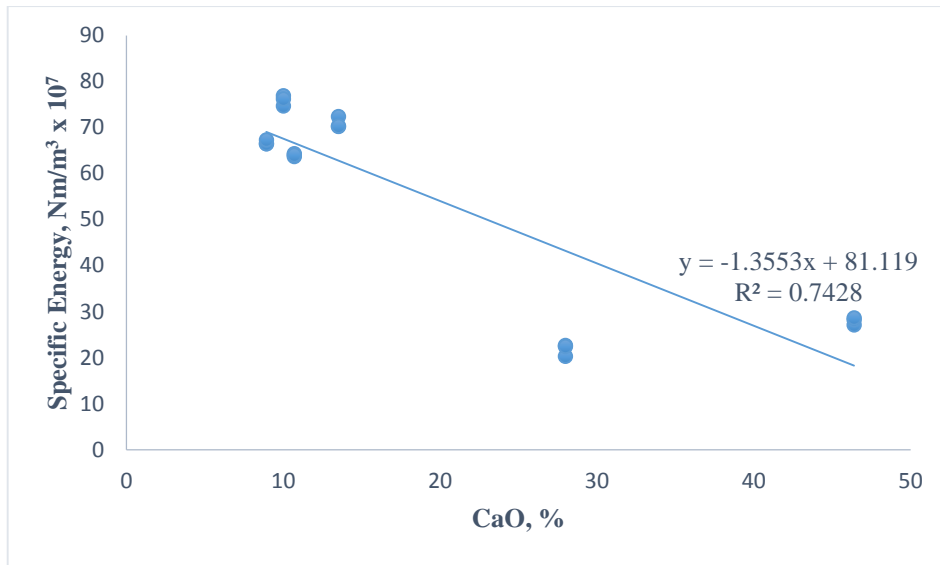


Figure 4.34 Relationship between specific energy of cross bit and CaO in various rocks

4.4.5 SIMPLE REGRESSION OF SE (SPHERICAL BUTTON BIT) AND ELEMENTS/MINERALS IN OXIDES FORM:

Simple regression was carried out between SE obtained in spherical bit and common elements/minerals in oxide form. All the relationships like linear, exponential and power were tested between dependent and independent variables. The relationship between specific energy (y) and mineralogical properties(x) is given in Table 4.18.

Table 4.18: Relationship between specific energy (spherical button bit) and elements/minerals in oxide form

Mineralogical property	Regression equation	r ²
Al ₂ O ₃	y = 3.296x + 14.012	0.6751
SiO ₂	y = 1.1526x + 9.7664	0.7483
SO ₃	y = 50.557e ^{-0.3x}	0.0146
Cl	y = 52.588x ^{0.2185}	0.2495
K ₂ O	y = 37.714e ^{0.0469x}	0.1109
CaO	y = -1.3774x + 77.492	0.758

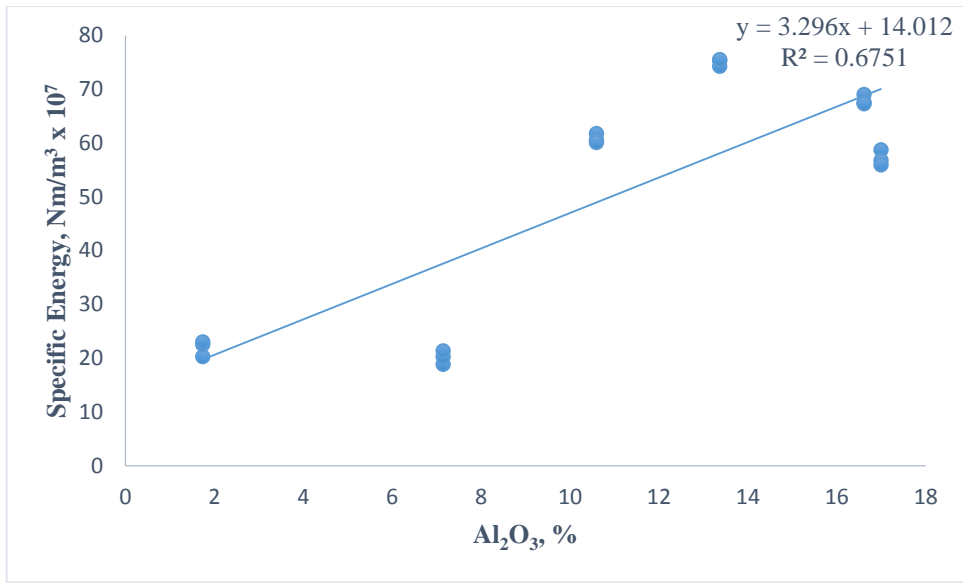


Figure 4.35 Relationship between specific energy of spherical button bit and Al₂O₃ in various rocks

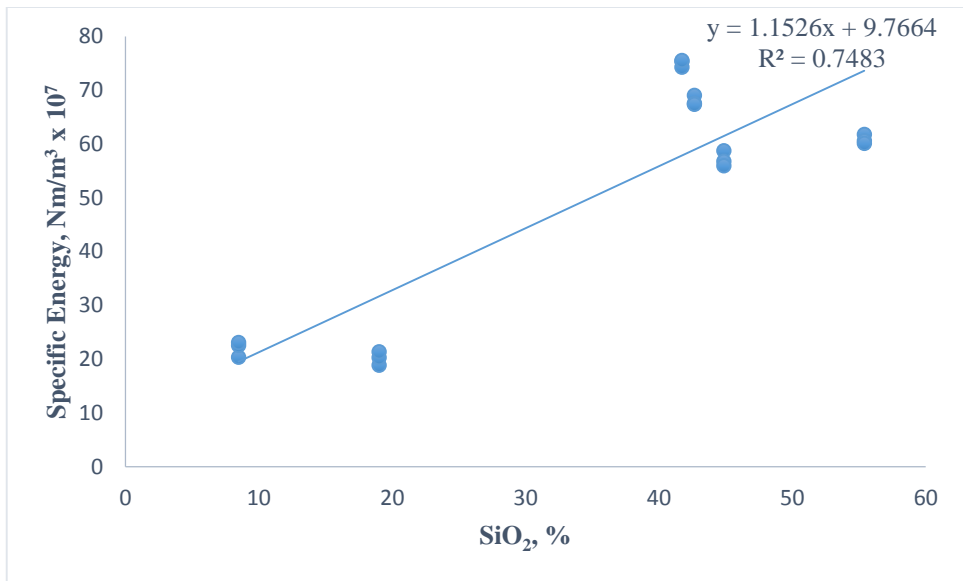


Figure 4.36 Relationship between specific energy of spherical button bit and SiO₂ in various rocks

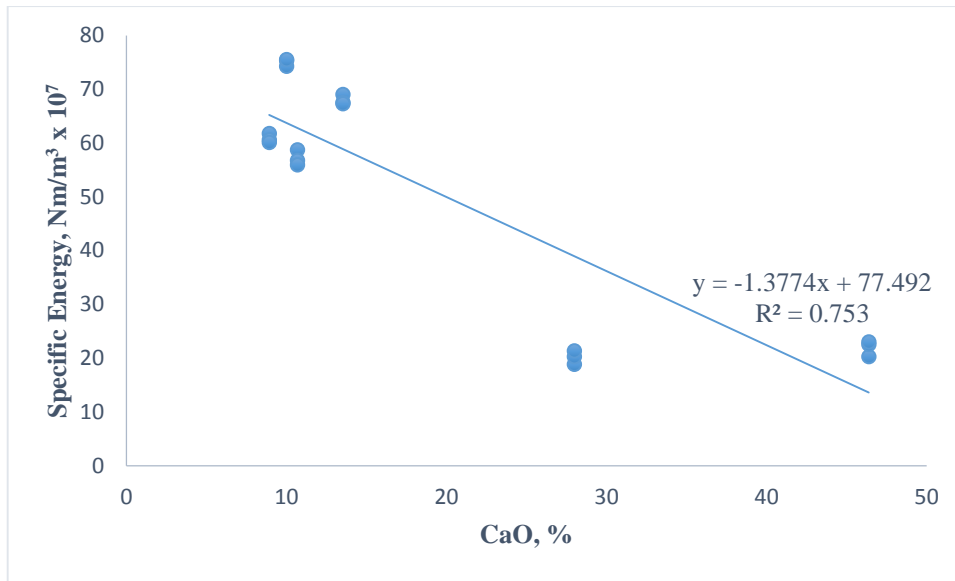


Figure 4.37 Relationship between specific energy of spherical button bit and CaO in various rocks

4.4.6 ANALYSIS OF RESULTS

A strong positive correlation (r for chisel bit: 0.799, r for cross bit: 0.82008 and r for spherical button bit: 0.8216) was found between the Al_2O_3 content of XRF test of rocks and SE. And also the relationships (models) were established between Al_2O_3 content and SE. The models were statistically significant (r^2 for chisel bit 0.6725, r^2 for cross bit 0.725 and r^2 for spherical button bit 0.6751). The specific energy for the rocks considered for study increased with increased percentage of Al_2O_3 content (Figure 4.29, 4.32 and 4.35).

A strong positive correlation (r for chisel bit: 0.8676, r for cross bit: 0.8841 and r for spherical button bit: 0.86503) was found between the SiO_2 content of XRF test of rocks and SE. And also the relationships (models) were established between SiO_2 content and SE. The models were statistically significant (r^2 for chisel bit- 0.7817, r^2 for cross bit- 0.7817 and r^2 for spherical button bit- 0.7483). The specific energy for the rocks considered for study increased with increased percentage of SiO_2 content (Figure 4.30, 4.33 and 4.36).

Similarly, a strong negative correlation (r for chisel bit: -0.84499, r for cross bit: -0.86188 and r for spherical button bit: -0.86775) was found between the CaO content

of XRF test of rocks and SE. The models were statistically significant (r^2 for chisel bit- 0.7428, r^2 for cross bit- 0.7428 and r^2 for spherical button bit- 0.758). Relying upon these findings, a decrease can be expected in SE, as the percentage of CaO increases (Figure 4.31, 4.34 and 4.37).

But, the low correlations were found between SO_3 (r for chisel bit: 0.0042, r for cross bit: 0.0088 and r for spherical button bit: 0.0146) content of XRF test of rocks and SE, between Cl content of XRF test of rocks and SE (r for chisel bit: 0.269, r for cross bit: 0.2719 and r for spherical button bit: 0.2495) and between K_2O content of XRF test of rocks and SE (r for chisel bit: 0.1108, r for cross bit: 0.1309 and r for spherical button bit: 0.1109). Therefore all these are not significant. However relationships (models) were developed which showed low values of r^2 which are not significant.

4.5 ANALYSIS OF PREDICATIVE (REGRESSION) MODELS:

The regression models were developed based on the technical papers published by Gokhan Aydin et al.(2012) and B. Tiryaki et al.(2005). When developing the models, initially the statistical significance of each property with SE was verified by carrying out correlation as per the earlier findings of B. Tiryaki et al.(2005). All variables were statistically significant as per correlation. In this study, as an example the SE increases with increase in UCS. But while in regression model, it is giving opposite result. This is due BTS has stronger influence than UCS. The findings are similar to the findings of Gokhan Aydin et al.(2012). This is due to influence of other variables used in the regression model. Therefore when we are using multiple regression, one factor influences other. To obtain positive relation of UCS, BTS etc we need to consider some others factors which was not possible in this research to decide upon. Because of this reason, an attempt was made to find out the influence of each property on SE to understand the how much each variable influence SE as per earlier findings of B. Tiryaki et al.(2005). Finally it can be concluded that statistical methods constrain the data along a particular geometry which may not always be favourable to capture non-linear relationships existing between various parameters. But the problems encountering in real engineering applications are more complex and therefore other

technologies are required to carry out more scientific analysis to understand the relation between various parameters.

4.5.1 Residual Plots for Specific energy

Histogram of the Residuals is an exploratory tool to show general characteristics of the residuals including typical values, spread, and shape. A long tail on one side may indicate a skewed distribution. If one or two bars are far from the others, those points may be outliers. All models showed equal distribution and no outliers which indicate the regression models developed are good (Figure 3.73 (a), (b), 3.75 (a), (b) 3.77 (a) and (b)).

Normal Probability Plot of residuals. The points in this plot should form a straight line indicating that the residuals are normally distributed. If the points on the plot depart from a straight line, the normality assumption may be invalid. All models showed the above trends which indicate the regression models developed are good Figure 3.73 (a), (b), 3.75 (a), (b) 3.77 (a) and (b).

Residuals versus Fitted Values. This plot showed a random pattern of residuals on both sides of 0. If a point lies far from the majority of points, it may be an outlier. There should not be any recognizable patterns in the residual plot. For instance, if the spread of residual values tend to increase as the fitted values increase, then this may violate the constant variance assumption. All models showed the above trends which indicate the regression models developed are good (Figure 3.73 (a), (b), 3.75 (a), (b) 3.77 (a) and (b)).

Residuals versus Order of Data. This is a plot of all residuals in the order that the data was collected and can be used to find non-random error, especially of time-related effects. This plot helps you to check the assumption that the residuals are uncorrelated with each other. All models showed the above trends which indicate the regression models developed are good (Figure 3.73 (a), (b), 3.75 (a), (b) 3.77 (a) and (b)).

The experimental to predicted and testing values for all the models are shown in Figure 3.72 (a), (b), 3.74 (a), (b) 3.76 (a) and (b) with R^2 values 0.92, 0.94 and 0.95 for spherical button bit, chisel bit and cross bit, respectively which shows that the models are good.

4.5.2 Performance prediction of the derived models

In fact, the coefficient of correlation between the measured and predicted values is a good indicator to check the prediction performance of the model. However, in this study, Variation Account For (VAF) and Root Mean Square Error (RMSE) indices were calculated to compare the performance of the prediction capacity of predictive models developed (Alvarez and Babuska 1999, Finol et al. 2001, Gokceoglu 2002, Yilmaz and Yuksek 2008, Yilmaz and Yuksek 2009, Yilmaz and Kaynar 2011).

$$VAF = \left[1 - \frac{\text{var}(y - y')}{\text{var}(y)} \right] \times 100 \quad \dots\dots(4.1)$$

$$RMSE = \sqrt{\frac{1}{N} \sum_{i=1}^N (y - y')^2} \quad \dots\dots(4.2)$$

Where y and y' are the measured and predicted values, respectively. If the VAF is 100 and RMSE is 0, then the model will be excellent. Mean absolute percentage error (MAPE) which is a measure of accuracy in a fitted series value was also used to check the prediction performances of the models. MAPE usually expresses accuracy as a percentage as shown in equation

$$MAPE = \frac{1}{N} \sum_{i=1}^N \left| \frac{A_i - P_i}{A_i} \right| \times 100 \quad \dots\dots(4.3)$$

Where A_i is the actual value and P_i is the predicted value. Lower values of MAPE indicate that there will be a better correlation between predicted values and experimental results.

Using the developed regression models for bits, performance prediction indices for training as well as test data were calculated and are given in Table 4.19. From the table

it is evident that the developed models for predicting SE are statistically significant and good.

Table 4.19: Values of performance indices of regression models of all bits

Performance Indices		Spherical button bit	Chisel bit	Cross bit
Training data	VAF	95.407	95.350	95.152
	RMSE	4.425	4.781	4.427
	MAPE	0.161	0.106	0.084
Test data	VAF	90.189	93.186	95.171
	RMSE	6.581	5.872	6.859
	MAPE	0.194	0.121	0.112

4.6 ANALYSIS OF ARTIFICIAL NEURAL NETWORK RESULTS

The neural network architecture, network training tool and network training regression of chisel bit have been shown in Figure 3.80 (a), Figure 3.80 (b) and Figure 3.80 (c) respectively. Similarly, neural network architecture, network training tool and network training regression of cross bit have been shown in Figure 3.81(a), Figure 3.81(b) and Figure 3.81(c) respectively. In the same manner neural network architecture, network training tool and network training regression of spherical button bit have been shown in Figure 3.82(a), Figure 3.82(b) and Figure 3.82(c) respectively.

It was understood that all the ANN models for SE have given predicted SE values close to the measured ones. This indicates that all ANN models have quite similar performances and are good choices to predict SE values. In fact, the coefficient of determination between the measured and predicted values is a good indicator to check the prediction performance of the model.

The variance account for (VAF) and root mean square error (RMSE) indices were also calculated to control the performance of the prediction capacity of predictive models developed by Alvarez Grima and Babuska (1999), Finol et al. (2001) and Gokceoglu (2002) shown in equation 4.1 and 4.2.

Where y and y' are the measured and predicted values, respectively. If the VAF is 100 and RMSE is 0, then the model will be excellent. Mean absolute percentage error (MAPE), which is a measure of accuracy in a fitted series value, was also used to check the prediction performances of the models. MAPE usually expresses accuracy as a percentage as shown in equation 4.3. Where A_i is the actual value and P_i is the predicted value. Lower values of MAPE, indicate that there will be a better correlation between predicted values and experimental results. Using the developed regression models for bits, performance prediction indices for training as well as test data were calculated and are given in Table 4.20.

Table 4.20: Values of performance indices of ANN models of all bits

Performance Indices		Spherical button bit	Chisel bit	Cross bit
Training data	VAF	99.956	99.961	99.999
	RMSE	1.349	0.402	0.491
	MAPE	0.011	0.007	0.011
Validation data	VAF	97.620	99.507	99.159
	RMSE	2.947	1.800	1.976
	MAPE	0.104	0.043	0.034
Test data	VAF	99.051	99.516	99.481
	RMSE	2.165	1.663	1.721
	MAPE	0.055	0.031	0.028

Table 4.21: Comparison of Regression and ANN models of all bits

Performance Indices		Spherical button bit		Chisel bit		Cross bit	
		Regression	ANN	Regression	ANN	Regression	ANN
Training data	VAF	95.407	99.956	95.350	99.961	95.152	99.999
	RMSE	4.425	1.349	4.781	0.402	4.427	0.491
	MAPE	0.161	0.011	0.106	0.007	0.084	0.011
Test data	VAF	90.189	99.051	93.186	99.516	95.171	99.481
	RMSE	6.581	2.165	5.872	1.663	6.859	1.721
	MAPE	0.194	0.055	0.121	0.031	0.112	0.028

The respective VAF, RMSE and MAPE indices for predicting SE were obtained as 90.18883, 6.581418, 0.193766 from multiple regression model(testing); but the values

for VAF, RMSE and MAPE indices were obtained in neural network model (testing) are 99.05135, 2.164868, 0.055091 for spherical button bit, the respective VAF, RMSE and MAPE indices for predicting SE were obtained as 93.18637, 5.872092, 5.872092 from multiple regression model (testing); but the values for VAF, RMSE and MAPE indices obtained in neural network model (testing) are 99.51557, 6.858609, 0.112072 which higher than multiple regression model for chisel bit and The respective VAF, RMSE and MAPE indices for predicting SE were obtained as 95.17123, 6.858609, 0.112072 from multiple regression model (testing); but the values for VAF, RMSE and MAPE indices obtained in neural network model (testing) are 99.4812, 1.721213, 0.028481 which are higher than multiple regression model for (Table 4.21).

The conclusion from all the above ANN modeling methods is that the prediction performances of neural network model are higher than those of multiple regression equations. This finding confirms the earlier findings (Meulenkamp and Alvarez Grima, 1999); Singh et al., 2001; Kripamoy Zorlu et al., 2008; Tiryaki, 2008; Sarkar et al., 2010; Isik Yilmaz et al., 2011; Ibrahim et al., 2012).

4.7 ANALYSIS OF NUMERICAL MODELLING RESULTS

4.7.1 Results of Compressive Stress Field

The results of compressive stress field as obtained from FEM analysis for each bit-rock combination (six rock types and three bits) considered in the present theoretical investigation are given in Figure 4.38 to 4.43). The magnitude of compressive stress developed along X- axis and Z- axis for all rock types considered under chisel, cross and spherical button are given in Table 4.40 to 4.45 (Appendix-II). Theses represent of the variation of the stresses in different rock types. It is observed that there is maximum compressive stress near the tip of the bit.

The ANSYS analysis presents for each step of loading, the state of displacement in the rock blocks during the static indentation tests (Table 4.28 to 4.33 in Appendix-II).

4.7.2 Comparison of Static Indentation results obtained from experimental and FEM Analysis

The results of indentation of FEM 3-D static analysis (single indentation) for each bit-rock combination considered in the present theoretical investigation in accordance with the variables considered in the static indentation tests are shown in Figure 4.45 to 4.50 and Table 34 to 39. These figures represent the nodal displacement contours along X, Y and Z directions for the loading conditions mentioned therein, which correspond to the peak loading in the static indentation tests. From these figures, it can be inferred that in all the directions, displacement is decreasing from the loading axes towards the boundary. The magnitude of indentation and details of the crater formed, as obtained from the FEM analysis, under the chisel, cross and spherical button bits of 48 mm diameter of all rocks considered are given in Table 4.34 to 4.39 and Figure 4.44.

The comparative values of Force- Displacement of the indenter as obtained from FEM analysis and static indentation tests are presented together in a graphical form (Figure 4.51(a) to 4.51(c)) for all rocks for clarity of representation. Comparison of the results, at the peak load, as obtained from FEM analysis and static indentation tests for all the bit-rock combinations considered are given in the Table 4.22 to 4.27. For all the rocks under study, the comparative values of displacements, under the three types of indenters, as obtained from the FEM analysis and static indentation tests, for all the twelve stages of loading, are given in Table 4.28 to 4.33. It is observed, from both the analysis, that in all the rock types investigated, displacement is maximum under spherical button bit followed by chisel and cross bits. From these studies, it may be inferred that the rock penetration as well as the volume of crater formed under a bit does not depend on the applied energy alone, but also depends on its geometry. Therefore, it is implied that the energy needed to cause breakage depends on bit geometry.

The relationship between the physico-mechanical properties of rocks and displacement as obtained, for the three bit geometries, from the static indentation tests and FEM (ANSYS) analysis, are presented together, for the purpose of comparison (Figure

4.52(a) to 4.52(g)). It is observed that the static indentation test results follow a similar trend (displacement decreasing linearly with the increase in the respective rock properties), except in abrasion resistance (Figure 4.52(c)) as obvious from the FEM analysis.

The above mentioned comparison indicates that even with the coarse meshing adopted in the FEM analysis, the theoretical nature of variation is in agreement with that obtained from static indentation test results. The present numerical value indicates that experimental values are higher than FEM analysis and generally range from 10 to 19% (except few). This can be attributed to the coarseness of the mesh, the homogeneity and ideal conditions considered in the FEM analysis. It also needs to be pointed out that even though the geometry of chisel and cross (wedge shaped) bits is actually somewhat curved, in FEM analysis, line loading along one axis for chisel and two line loads along two mutually perpendicular axis for cross bit was considered. In addition, at the contact points between the bit and the rock, the friction was also not taken into account. A more refined mesh with non-homogenous, non-linear and an-isotropic formulation of the FEM analysis will bring better agreement with the experimental values.

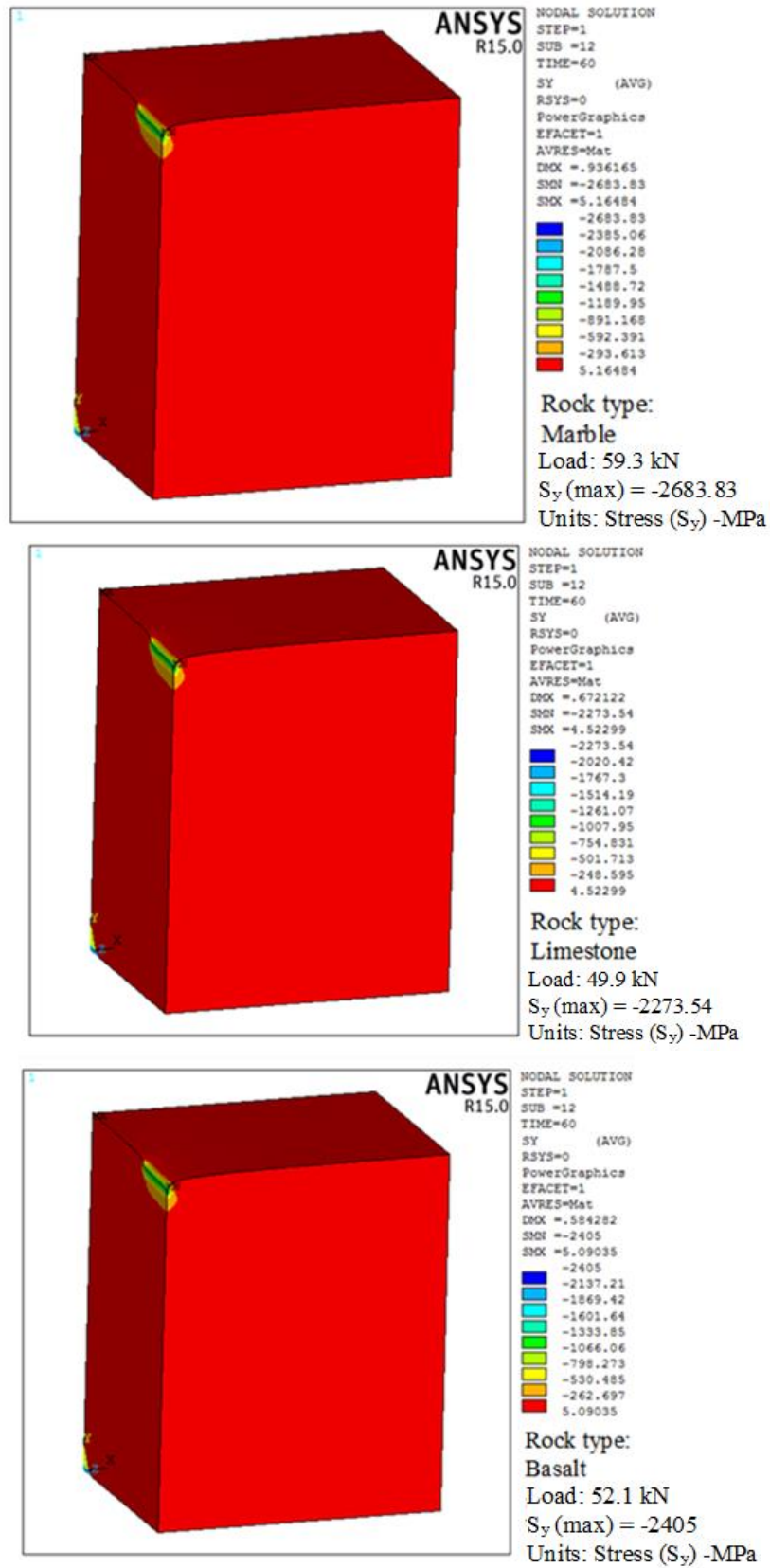


Figure 4.38 Compressive stress contours for chisel bit of 48 mm diameter in three rock types

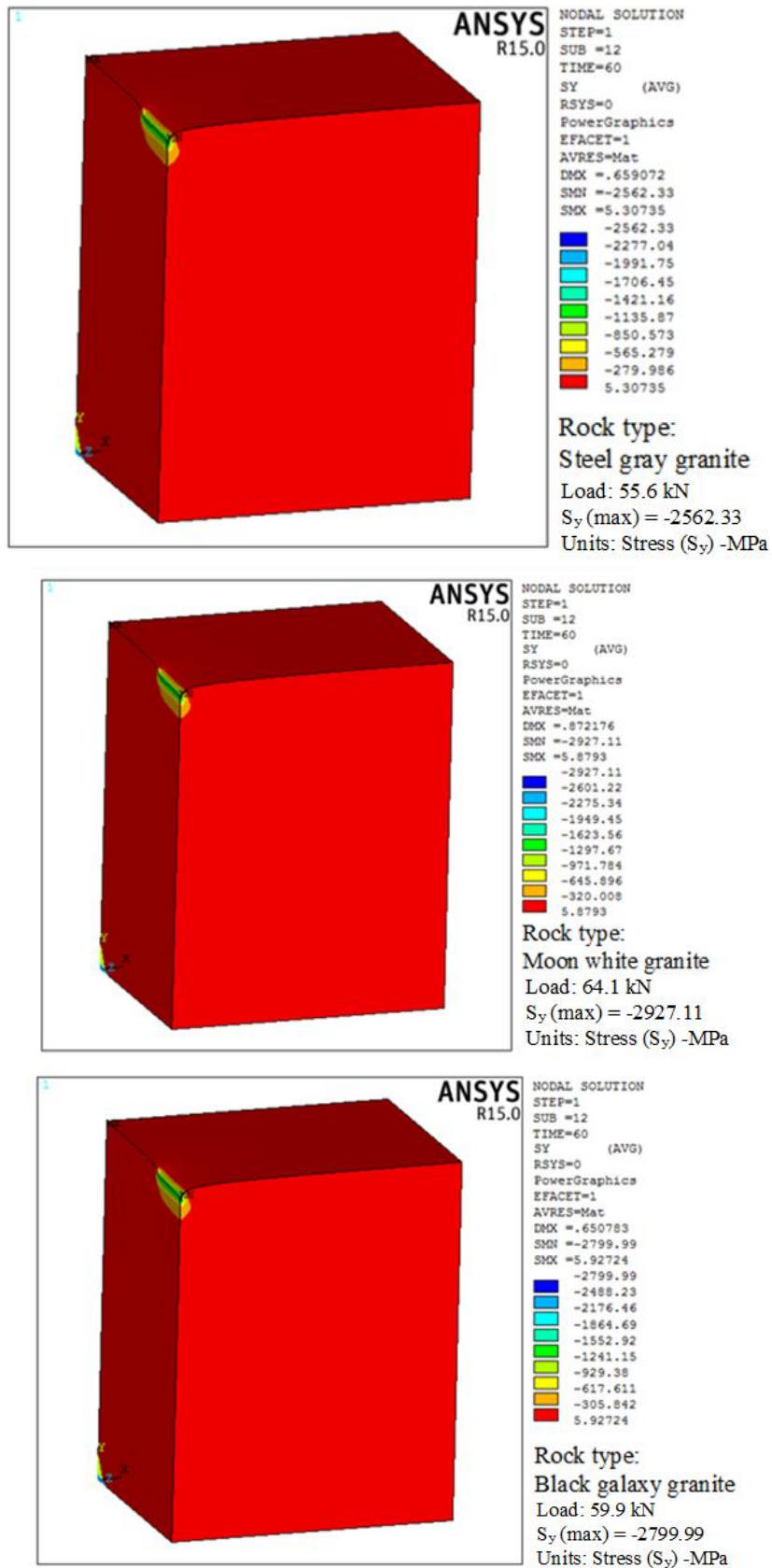


Figure 4.39 Compressive stress contours for chisel bit of 48 mm diameter in three types of granite rocks

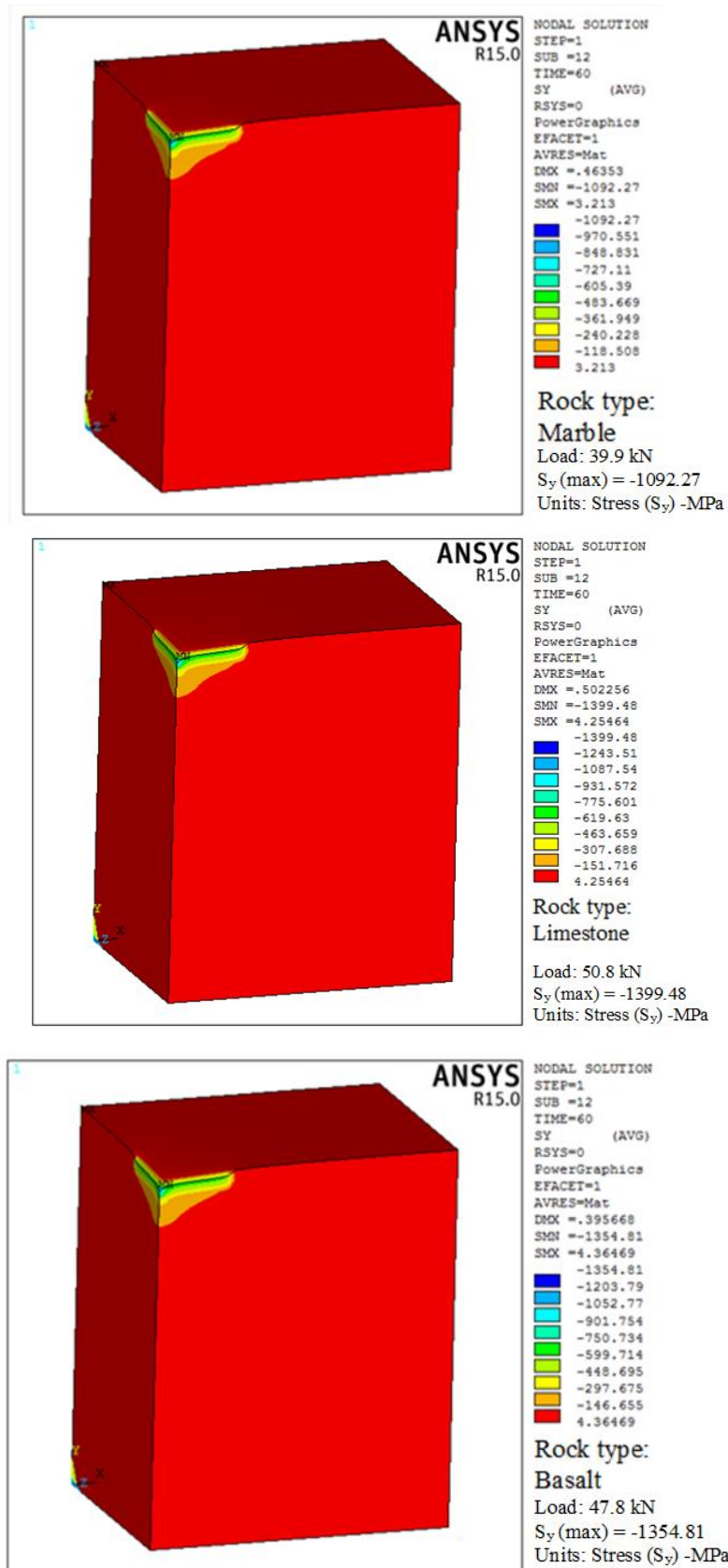


Figure 4.40 Compressive stress contours for cross bit of 48 mm diameter in three rock types

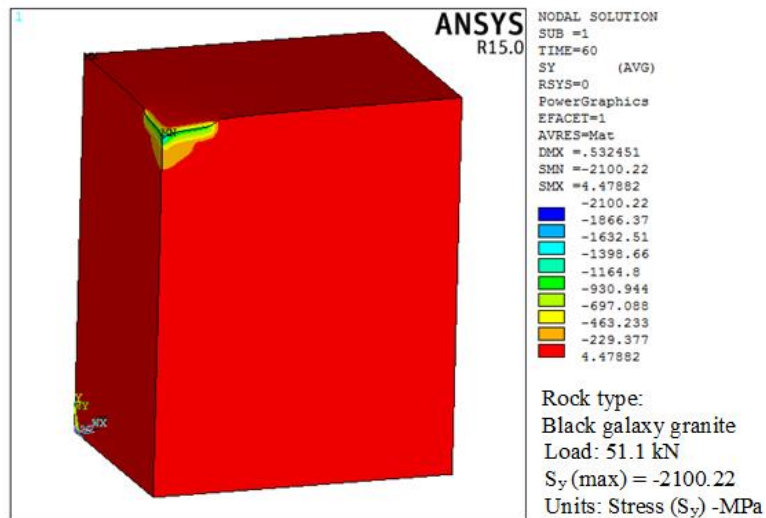
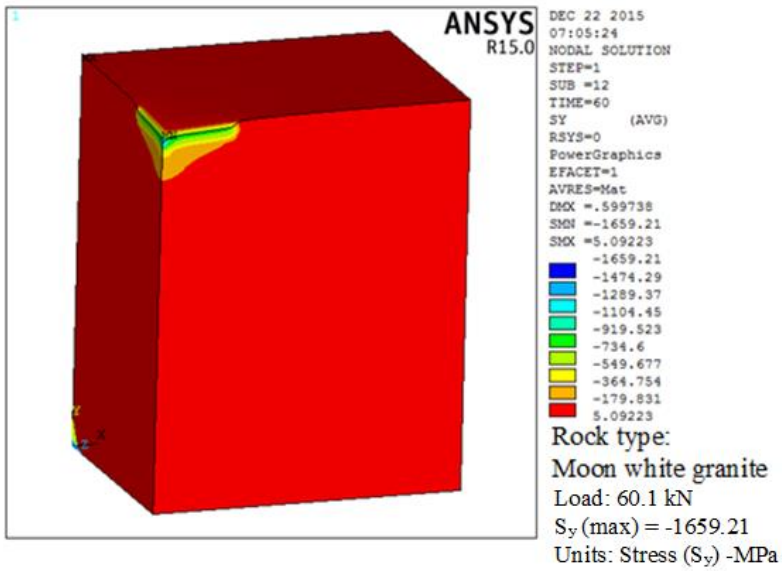
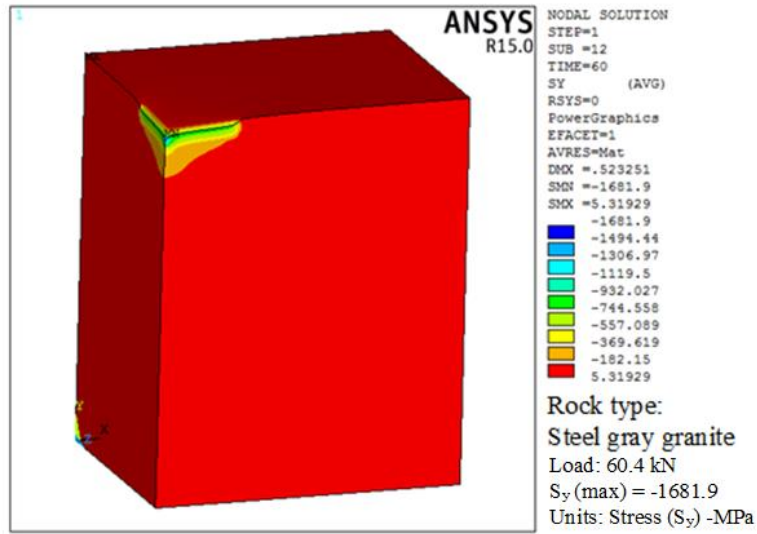


Figure 4.41 Compressive stress contours for cross bit of 48 mm diameter in three types of granite rocks

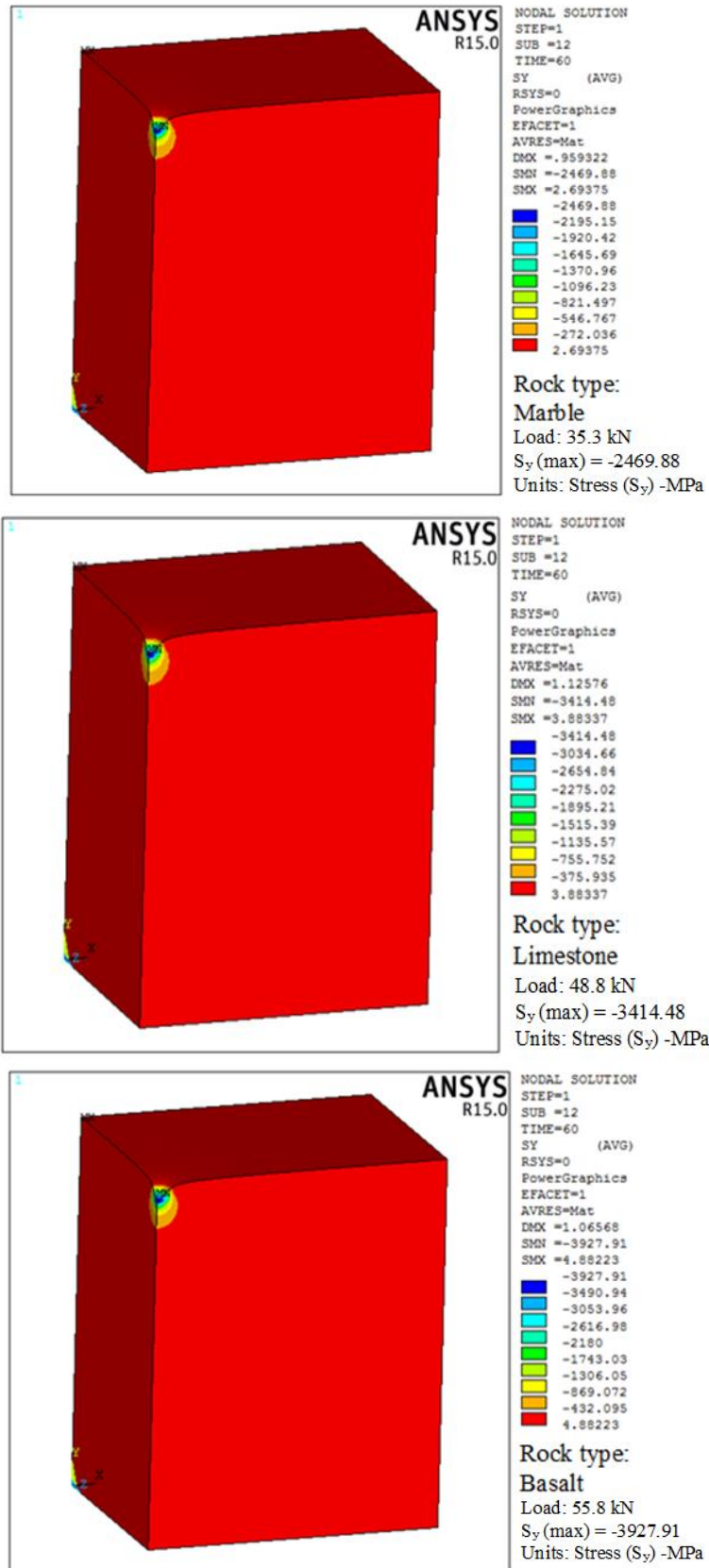


Figure 4.42 Compressive stress contours for spherical button bit of 48 mm diameter in three rock types

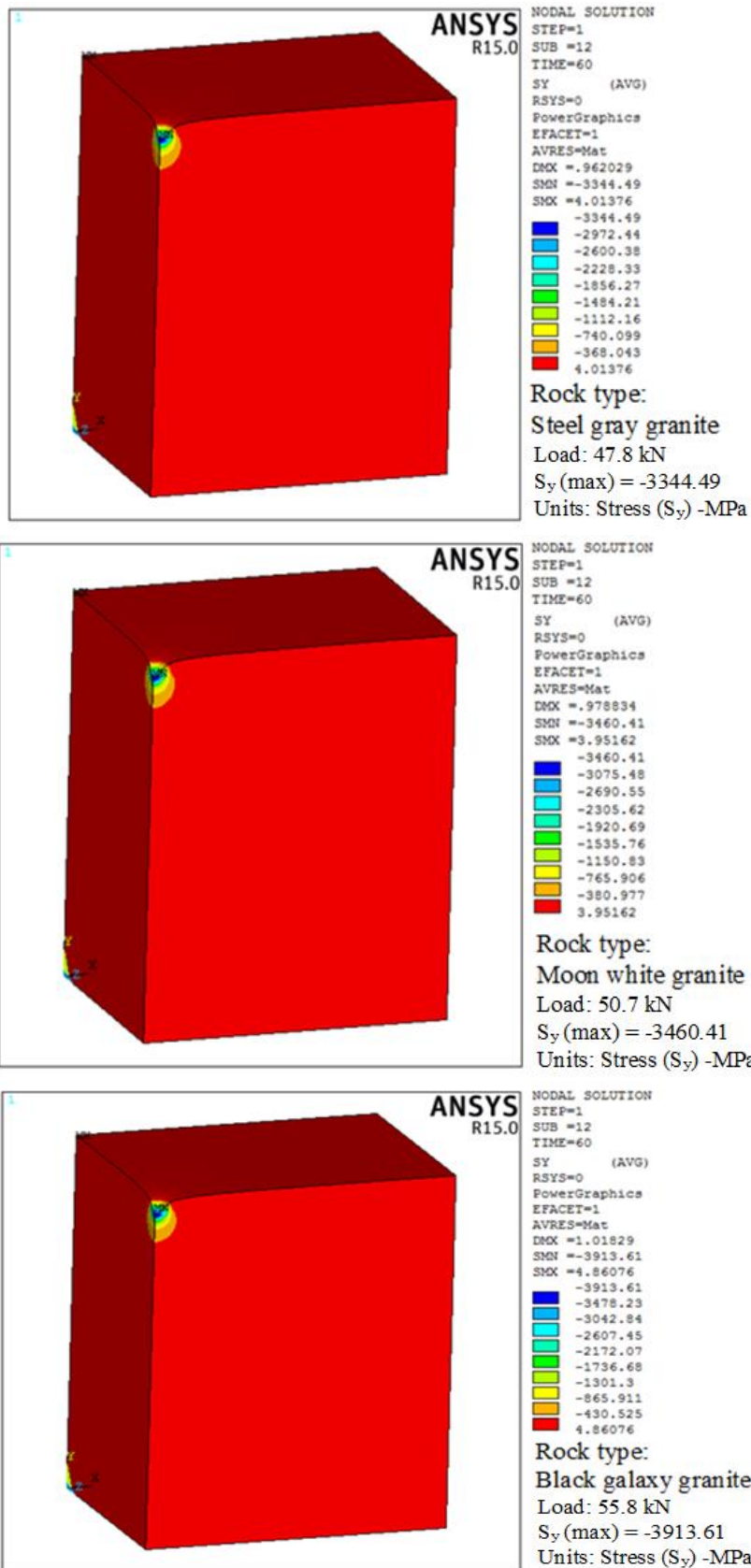
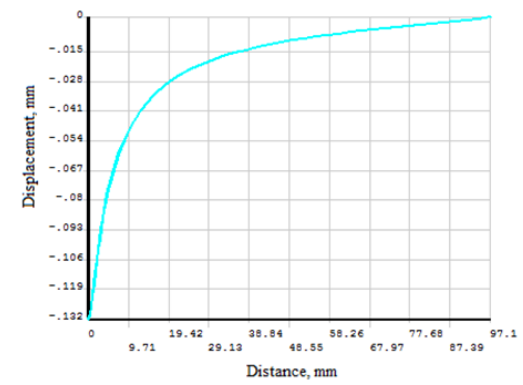
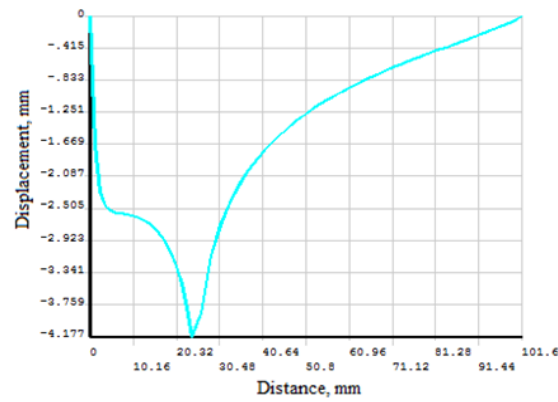
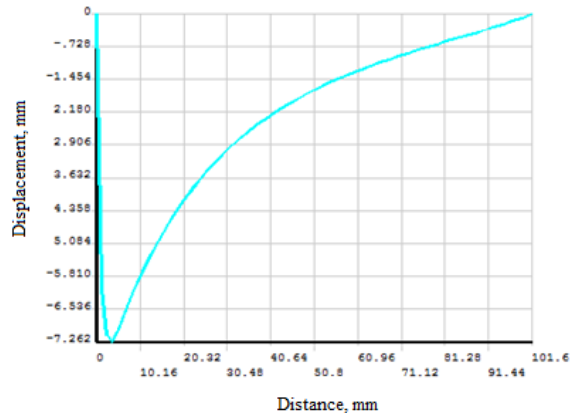
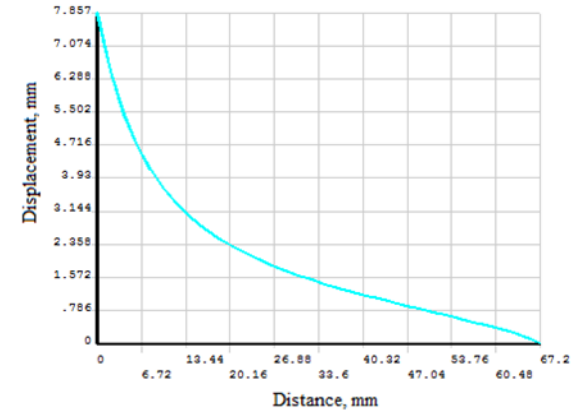
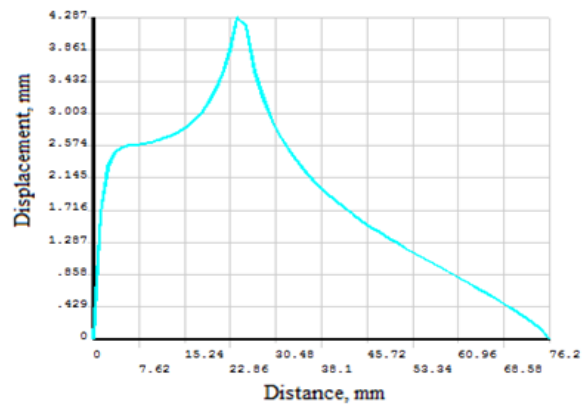
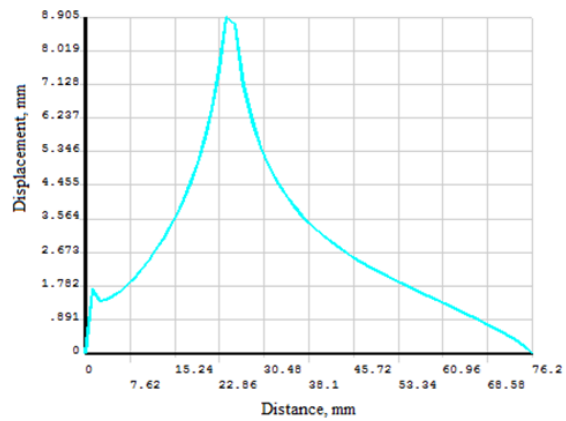


Figure 4.43 Compressive stress contours for spherical button bit of 48 mm diameter in three types of granite rocks



Displacement along X-axis



Displacement along Z-axis

Bit geometry: Chisel

Bit geometry: Cross

Bit geometry: Spherical button

Figure 4.44 Relationship between indentation depth and displacement in X and Z- axes for chisel, cross and spherical button bits of 48 mm diameter in marble.

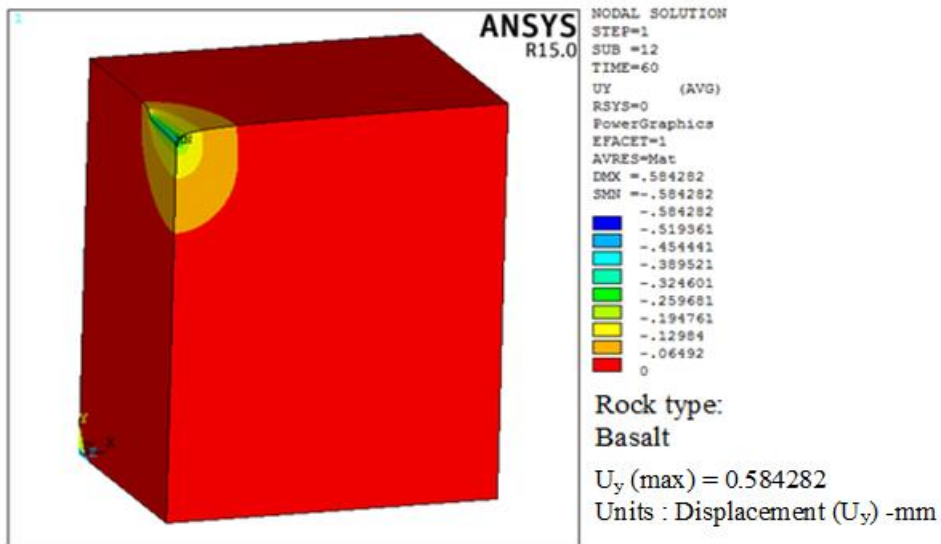
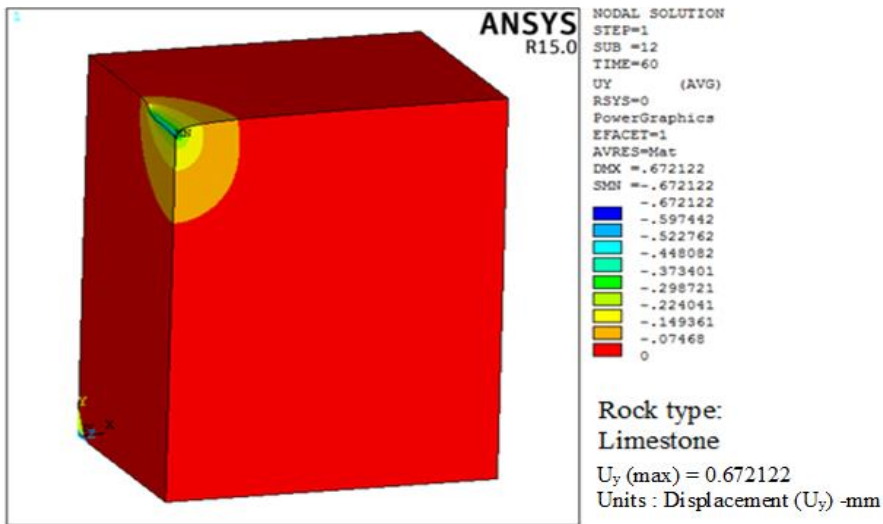
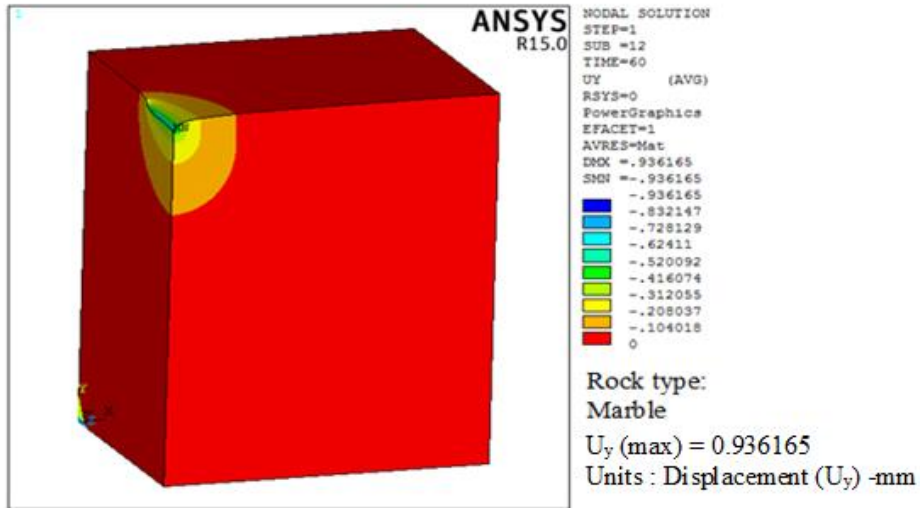


Figure 4.45 Displacement contours for chisel bit of 48 mm diameter in three types of rocks

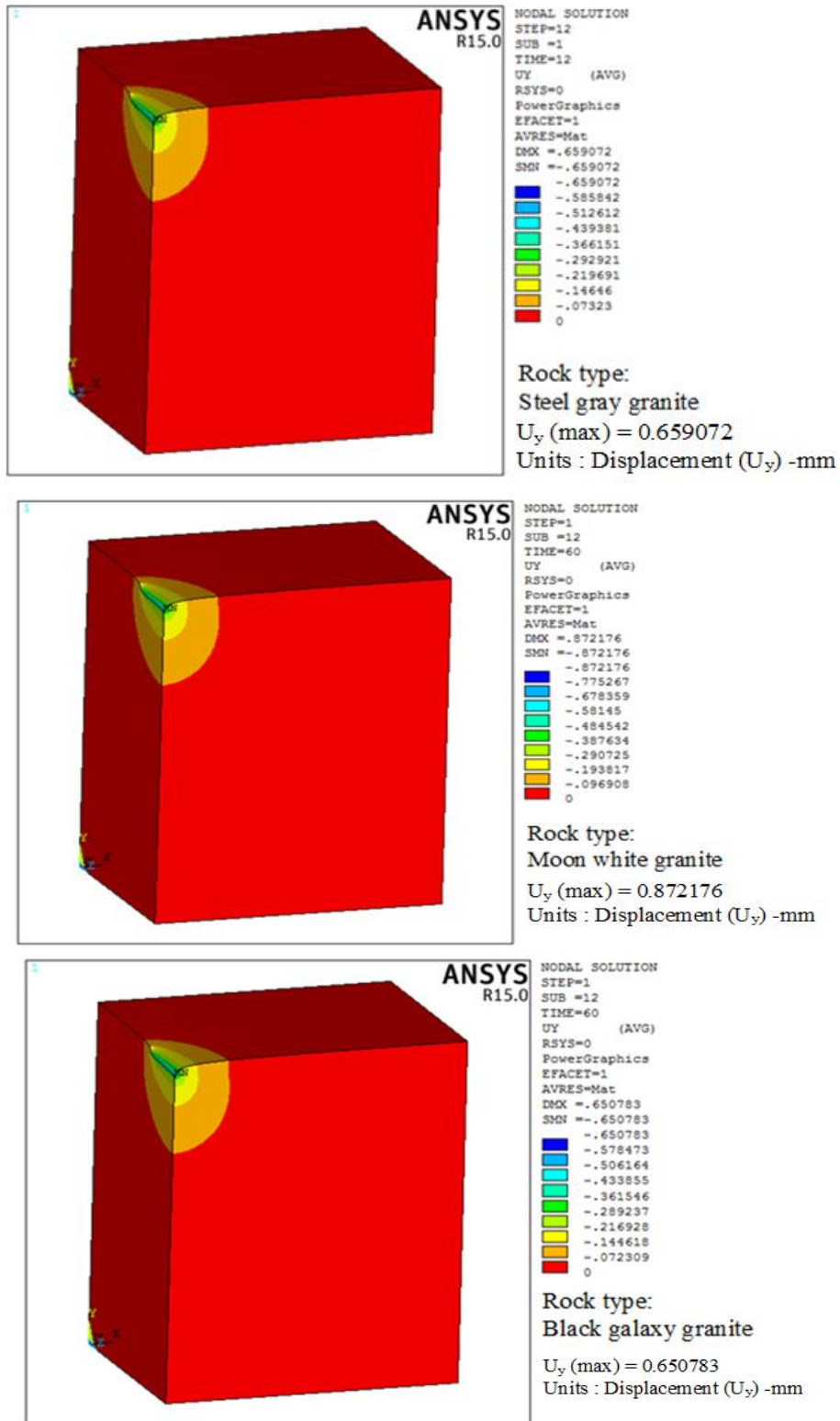


Figure 4.46 Displacement contours for chisel bit of 48 mm diameter in three types of granite rocks

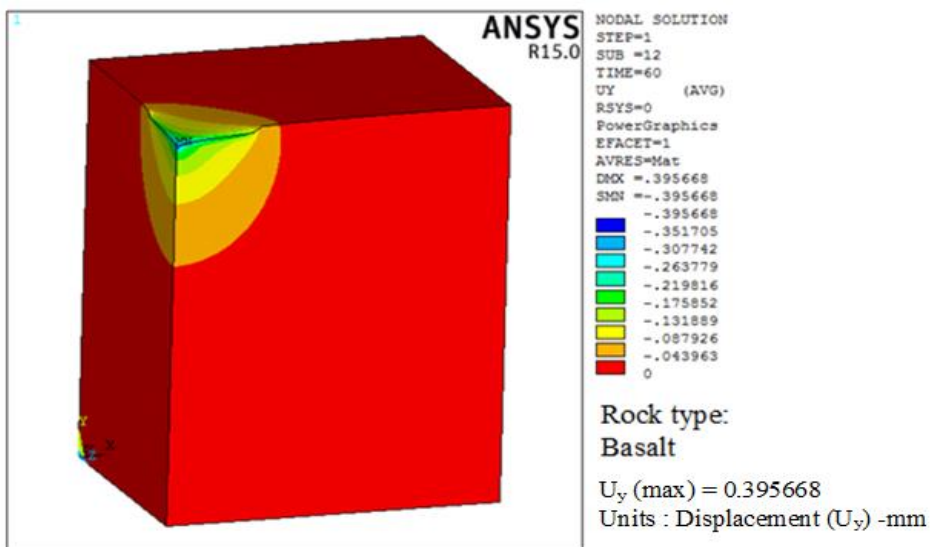
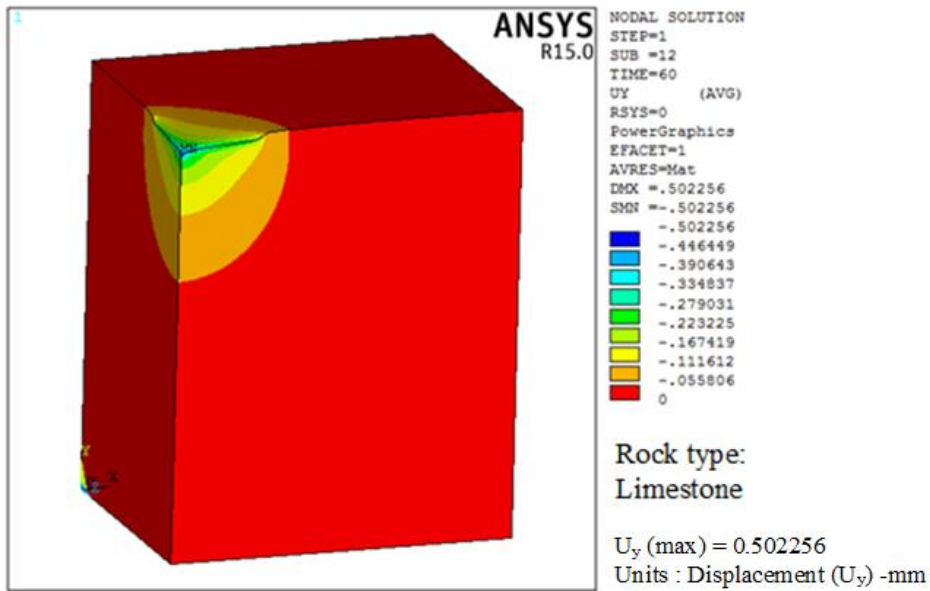
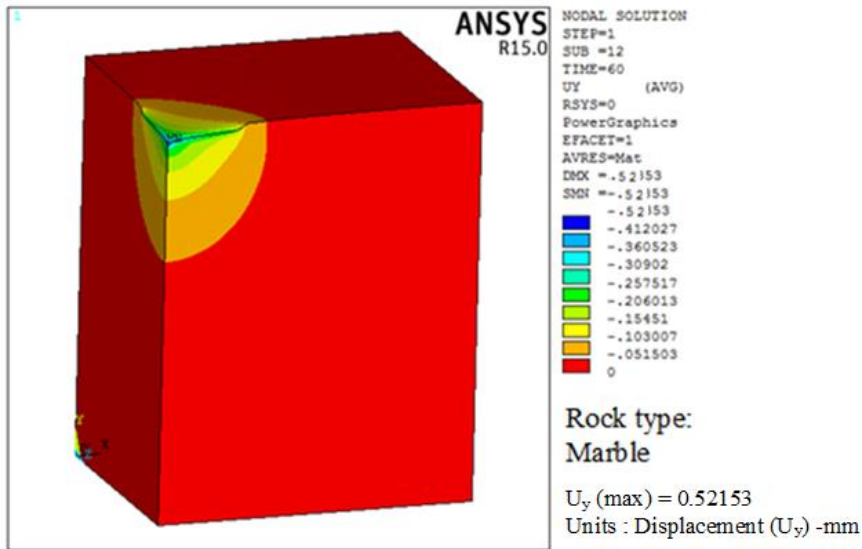


Figure 4.47 Displacement contours for cross bit of 48 mm diameter in three types of rocks

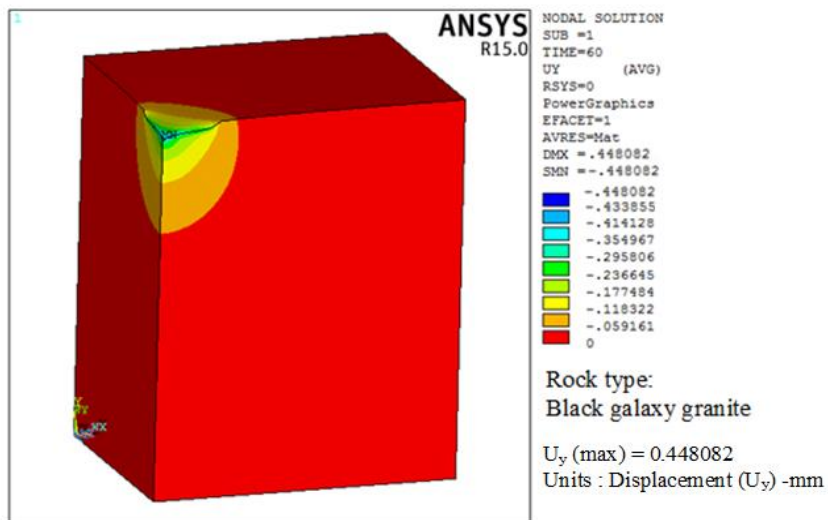
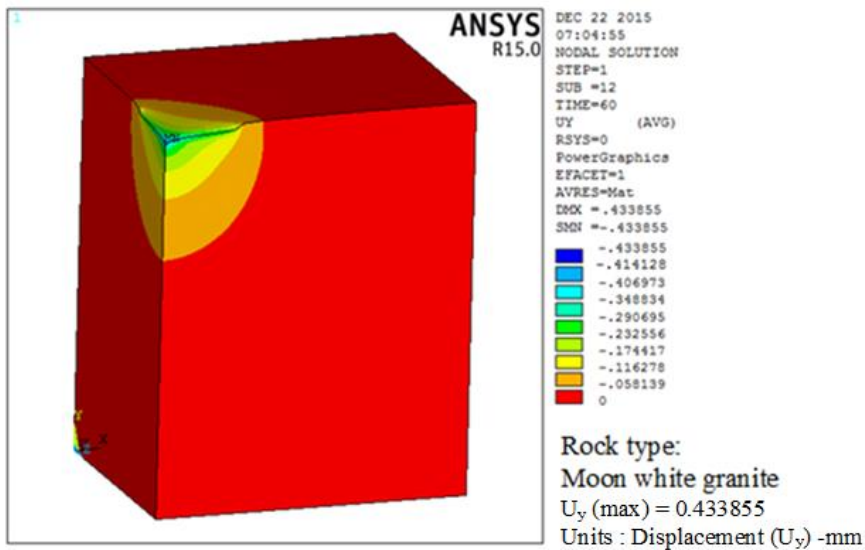
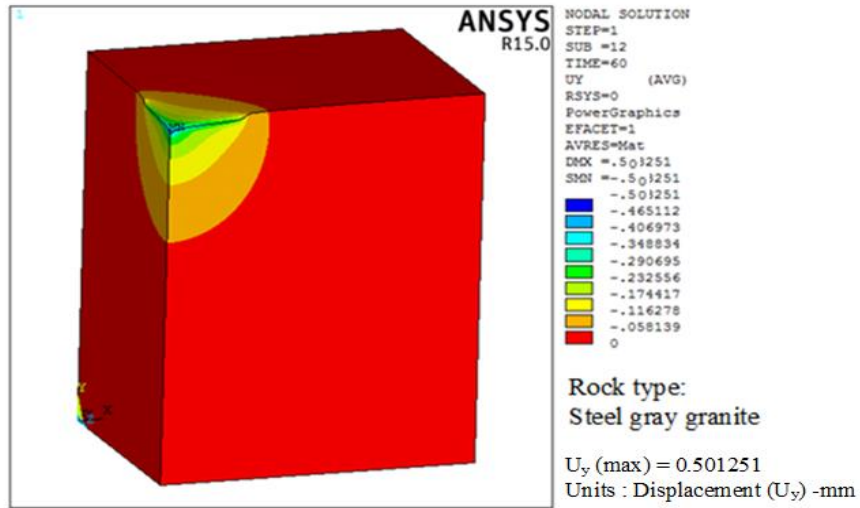


Figure 4.48 Displacement contours for cross bit of 48 mm diameter in three types of granite rocks

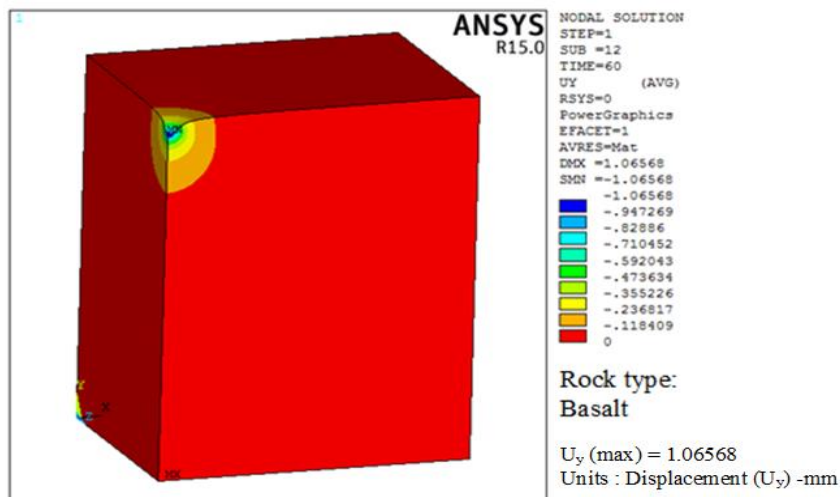
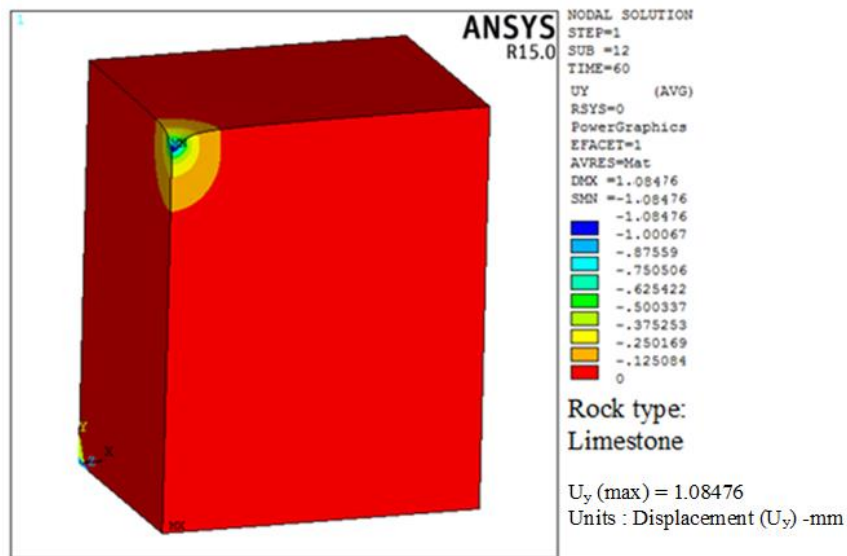
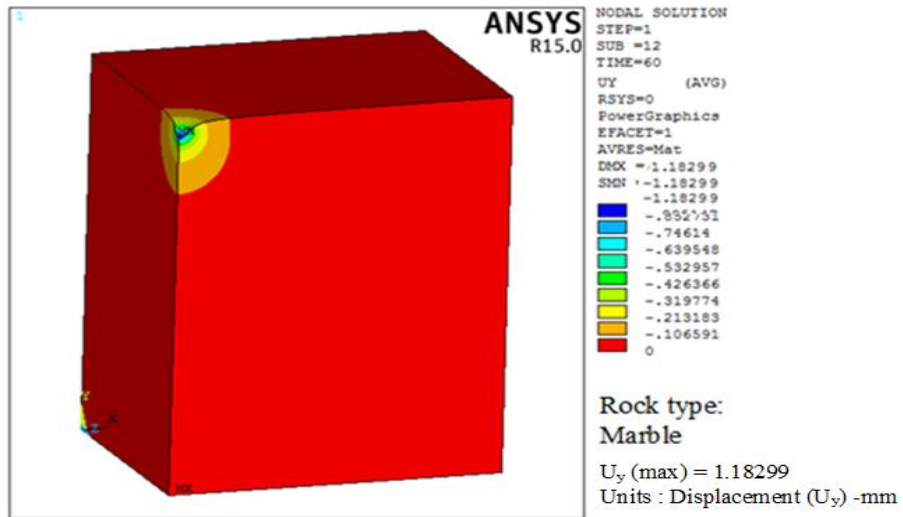


Figure 4.49 Displacement contours for spherical button bit of 48 mm diameter in three types of rocks

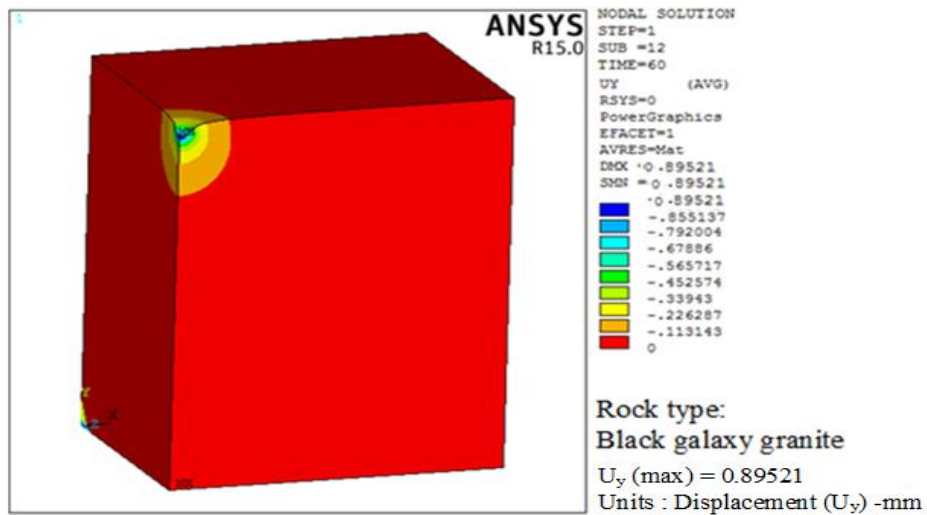
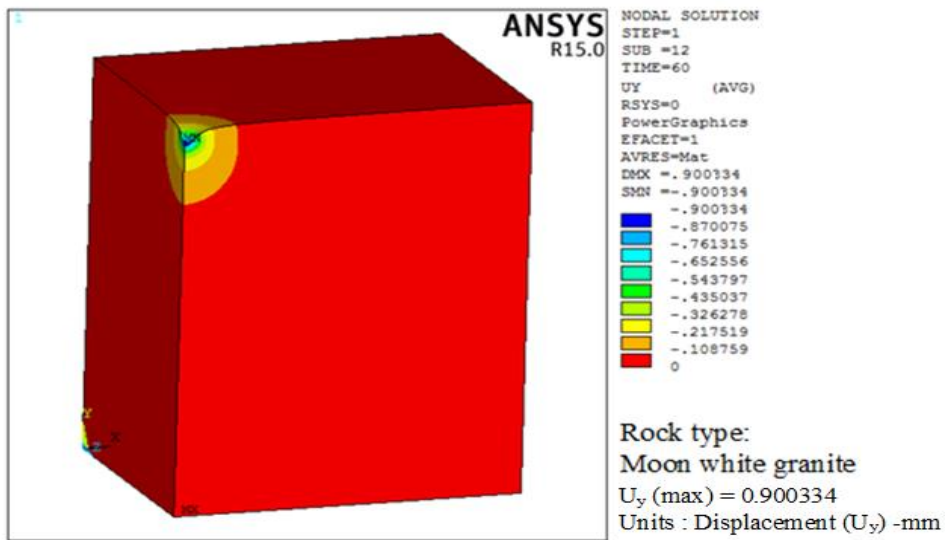
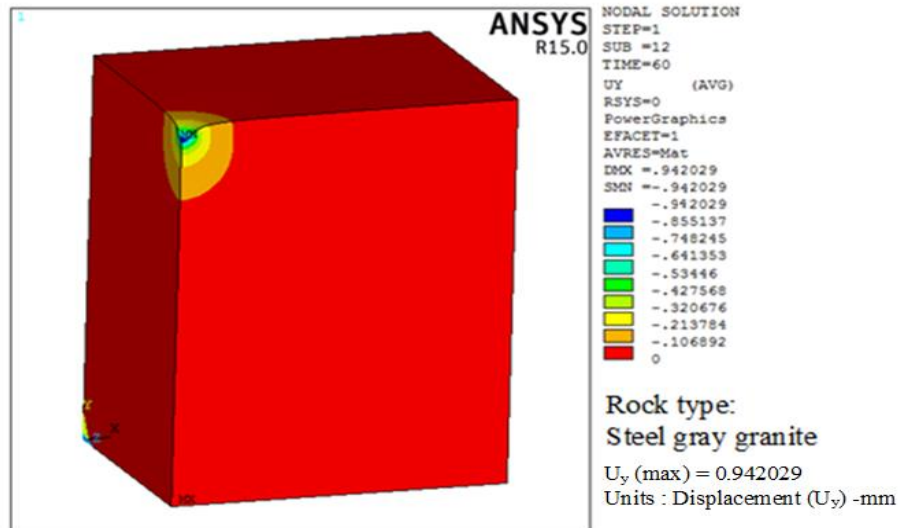


Figure 4.50 Displacement contours for spherical button bit of 48 mm diameter in three types of granite rocks

5. CONCLUSIONS AND SCOPE FOR FUTURE WORK

5.1 CONCLUSIONS

In the present work, the energy required to remove unit volume of rock (specific energy) using commercial drill bits with different geometry of bits in static indentation tests on various rock at different index angles has been studied. Basically this study evaluates the influence of index angle on specific energy and performances of various bits. This study also evaluates influence of physico-mechanical properties and mineralogical properties on specific energy. The predictive models (regression and ANN) developed evaluate the estimation of specific energy in rock indentation and influencing parameters like operating variables and the rock properties. The following conclusions are drawn from the current study:

- Results of indentation (F-P curves) revealed that bit penetration into rocks occurs by both crushing and chipping of the rock (limestone, basalt, steel gray granite, moon white granite and black galaxy granite). However, for some bit-rock combinations, penetrations occurs only by crushing (marble). The chipping was mostly observed in basalt and granite group of rocks.
- It was observed that spherical button bit required minimum SE as compared to chisel and cross bits in static indentation of rocks. So spherical button bit can be used extensively to the similar type of rocks under study to obtained good results.
- The SE varies with diameter of the bit, index angle the optimum index angle at which SE is minimum for the group of rocks like basalt, steel gray granite, moon white granite and black galaxy granite and for group of rocks such as limestone and pink marble, are around 20° and 30° respectively. The index angle during percussive drilling influences the SE values.
- The rock properties (like density, UCS, BTS, Abrasion resistance, Young's Modulus, Poisson's ratio) influence the SE. It was observed, except in the case of abrasion resistance, that with the increase in the density, UCS, BTS, Young's Modulus, Poisson's ratio of the rock, the SE increases. This is because of the fact that, with the increase in the strength of the rock, the resistance to indentation increases. However in case of abrasion resistance, when it increases, SE decreases.

- The regression models shown in equations 3.1, 3.2 and 3.3 were developed and can be used to estimate the specific energy during rock indentation have high potentials as a guidance for practical applications.
- The developed regression model results showed that the significant operating variables affecting the SE were index angle, diameter of indenter (drill bit) and other variables are physico-mechanical properties of the rock. The results of the current study can provide opportunities to evaluate the drillability of granitic rocks without drilling tests involving complicated testing procedures.
- The developed models presented in this thesis can be used to assess the specific energy in rock indentation from the physic-mechanical properties of rocks. Hence, the proposed investigation has the potential to serve the mining, civil and geotechnical industries during drilling.
- The simple regression equations developed between SE and mineralogical properties (thin section analysis and XRF) indicates that the SE not only depends on physico-mechanical properties but also on mineralogical properties.
- The performance indices like VAF, RMSE and MAPE revealed that prediction performance of ANN model are higher than those of multiple regression equations. The performance comparison also showed that the ANN is a good approach for minimizing the uncertainties in the area of rock mechanics. The ability to adapt or continue learning the use of neural network may provide new approaches and methodologies, and minimize the potential inconsistency of correlations.
- The experimental values of displacement are higher than that of FEM analysis (95% of values are between 10 to 19.5% variation). It is observed that maximum compressive stress is generated near the tip of the bit and the magnitude of compressive stress developed at any point away from vertical axis depends on the geometry of the indenter.

5.2 SCOPE FOR FUTURE WORK

- In the present study, no continuous data logging equipment was used to record force and penetrations in indentation tests. So, to record force and penetrations easily continuous data logging equipment may be used in future studies.

- In the present study limited number of indenters (drill bits -12) were used. More number of indenters may be used to obtain huge data to carry out regression and ANN modelling.
- In future studies, newly designed drill bits with any new geometry may be used to carry out same research work to assess the performance of the bit which will be useful to drill bit manufacturing companies.

REFERENCES

- Acaroglu, O; Ozdemir, L & Asbury B (2008). "A Fuzzy Logic Model to Predict Specific Energy Requirement for TBM Performance Prediction", *Tunnelling and Underground Space Technology.*, 23, 600-608.
- Adnan Aydin (2015), "ISRM Suggested Method for Determination of the Schmidt Hammer Rebound Hardness: Revised Version", *The ISRM Suggested Methods for Rock Characterization, Testing and Monitoring: 2007-2014*, Ulusay13, 293-298.
- Alberto Carpinteri, Bernardino Chiaia, Stefano Invernizzi (2004) "Numerical analysis of indentation fracture in quasi-brittle materials" *Engineering Fracture Mechanics*, 567-577.
- Alehossein H, Detournay E, Huang H. (2000). "An analytical model for the indentation of rocks by blunt tools". *Rock Mech Rock Eng.*, 33(4), 267-84.
- Alehossein, H., Hood, M. (1996) "State of the art review of rock models for disk roller cutters". In: *Aubertin, M., Hassani, F., Mitri, H. (eds.), 2nd NARMS, Rock Mechanics Tools and Techniques, Montreal. Balkema, Rotterdam.*
- Altindag, R. (2002). "Correlation of Specific Energy with Rock Brittleness Concepts or Rock Cutting." *The Journal of the South African Institute of Mining and Metallurgy*, 0, 163-172.
- Altindag, R. (2003). "Correlation of specific energy with rock brittleness concepts on rock cutting", *The J. of the South African Inst. of Min. and Metall.*, 163.
- Alvarez, G.M. and Babuska, R. (1999). "Fuzzy model for the prediction of unconfined compressive strength of rock samples." *Int. J. Rock Mech. Min. Sci.*, 36, 339-349.
- Anderson, J.A. (1995). "An Introduction to Neural Networks." *MIT Press, Cambridge, M A.*, ISBN: 10: 0262011441, 672.
- Atici, U., Ersoy, A. (2009). "Correlation of Specific Energy of Cutting Saws and Drilling Bit with Rock Brittleness and Destruction Energy." *Journal of Materials Processing Technology*, 209, 2602-2612.
- Balci, C., Dermircin, M.A., Copur, H. and Tundemir, H. (2004). "Estimation of Optimum Specific Energy Based on Rock Properties for Assessment of Roadheader Performance." *The Journal of the South African Institute of Mining and Metallurgy.*, 0, 633-642.

- Barbour, T. G., Atkinson, R. H., Ko, H. Y. (1979). "Relationship of mechanical, index and mineralogical properties of coal measures rock". *20th Symp. on Rock Mech., Austin, Texas, USA*, 189–198.
- Becker, H., Lemmes, F., and Schommer, M. (1984). "Testing of rock mechanics as a basis for improved cutting technology", *Glückauf Translation*, 120 (8), 122–124.
- Bell, F. G. (1978). "The physical and mechanical properties of Fell sandstones, Northumberland, England". *Engng. Geol.* 12, 1–29.
- Benardos, A.G., Kaliampakos, D.C. (2004). "Modelling TBM performance with artificial neural networks", *Int. j. rock mech.min.sci.*, 19, 597-605.
- Benjumea, R. and Sikarskie, D.L. (1969). "A note on the penetration of a rigid wedge into a nonisotropic brittle material". *International Journal of Rock Mechanics and Mining Sciences & Geomechanics Abstracts*, 6, 343–352.
- Bilgin, N. and Shahriar, K.(1988). "The development of a rock cutting rig for rapid excavation systems and its application to Amasra Coalfield (in Turkish)". *Proceedings of 6th Coal Congress of Turkey, (Zonguldak, Turkey, May 2327)*, 13–28.
- Blokhin V.S. (1982). "Improvement of drilling tool efficiency", *Kiev Teknika*.
- Brooks, Z., Ulm, F.J., Einstein, H.H., Abousleiman, Y. (2010). "A nanomechanical investigation of the crack tip process zone". *44th US Rock Mechanics Symposium and 5th U.S.-Canada Rock Mechanics Symposium 2010, ARMA*, 10–309.
- Brown, E.T.(1981), " ISRM Rock characterization Testing and Monitoring Suggested methods", *Pergamon Pres*.
- Carlo Lopez Jimeno, Emilio Lopez Jimeno and Carcedo, F.J.A. (1995). "Drilling and Blasting of rocks" *A.A. Balkema Publishers, U.S.A.*
- Cheatham, J.B., Gnirk, P.F. (1967). "The mechanics of rock failure associated with drilling at depth". *In Proceedings of the 8th US Symposium on Rock Mechanics*, 410-439.
- Chen, L., Labuz, J. (1998). "Normal wedge indentation of rocks by a wedge-shaped tool III": Experimental evidence. *Int. J. Rock Mech. Min. Sci. Geomech. Abstr.* Submitted.
- Chiang, L. (2004). "Dynamic force–penetration curves in rock by matching theoretical to experimental wave response". *J Exp Mech*, 2, 167–175.

- Chiang, L. and Stamm, E. (1998). "Design Optimization of Valveless DTH Pneumatic Hammers by a Weighted Pseudo-Gradient Search Method," *Journal of Mechanical Design*, 120, 687-694.
- Cohen, J. W. (1988). "Statistical power analysis for the behavioral sciences (2nd edn)." Hillsdale, NJ: Lawrence Erlbaum Associates, 79-81.
- Cook, N.G.W., Hood, M., Tsai, F., (1984)." Observation of crack growth in hard rock loaded by an indenter. *Int. J. Rock Mech. Min. Sci. Geomech. Abstr.* 21, 97 104.
- Copur, H., Bilgin, N., Tuncdemir, H. and Baci, C. (2003)." A Set of Indices Based on Indentation Tests for Assessment of Rock Cutting Performance and Rock Properties." *The Journal of the South African Institute of Mining and Metallurgy.*, 0, 589-599.
- Copur, H., Tuncdenir, H., Bilgin, N. and Dincer, T. (2001)." Specific Energy as a Criterion for Use of Rapid Excavation Systems in Turkish Mines." *The Institution of Mining and Metallurgy*, 110, 1-10.
- Curry, D., Fear, M., Govzitch, A. and Aghazada, L.(2005)." Technical Limit Specific Energy-An Index to Facilitate Drilling Performance Evaluation," paper SPE/IADC 92318 presented at the SPE/IADC Drilling Conference, Amsterdam, The Netherlands, 23-25 February.
- Dehghan,S., Sattari, Gh., Chehreh Chelgani, S., Aliabadi, M. A.(2010)." Prediction of Uniaxial Compressive Strength and Modulus of Elasticity for Travertine samples using Regression and Artificial Neural Networks". *Mining Science and Technology*, 20, 0041–0046.
- Deketh, H..J.R. (1998). "Towards the prediction of rock excavation machine performance". *Bull. Eng. Geol. Env.*, 57, 3–15.
- Dollinger, G.L. (1977). "Choosing cutters for the best boreability". *Compressed Air Magazine*, Sept., 15–19.
- Dollinger, G.L., Handewith, H.J. and Breeds, C.D. (1998). "Use of the indentation tests for estimating TBM performance". *Canadian Tunneling, The Annual Publication of The Tunneling Association of Canada*, Lo, K. Y. (ed.), 27–33.

- Dollinger, G.L., Handewith, H.J., Breeds, C.D. (1998). "Use of the punch test for estimating TBM performance." *Tunn Undergr Space Technol*, 13(4), 403–408.
- Dunn, P., Roberts, C., and Ballardin, B. (1993). "The use of specific energy as a drillability index, Proceedings of geotechnical instrumentation and monitoring open pit and underground mining (Eds. Szwedzicki)", 125–132.
- Dupriest, F. E. and Koederitz, W. L. (2005). "Maximizing Drill Rate with Real-Time Surveillance of Mechanical Specific Energy," paper SPE/IADC 92194 presented at the SPE/IADC Drilling Conference, Amsterdam, The Netherlands.
- Ellis, G.W., Yao, C, Zhao, R. (1992). "Neural network modelling of the mechanical behaviour of sand". *In: Proceedings of the Ninth Conference on ASCE Eng. Mech. ASCE, New York*, 421–424.
- Ersoy, A. Atici, U. (2007). "Correlation of P and S-waves with Cutting Specific Energy and Dominant Properties of Volcanic and Carbonate Rocks." *Rock Mechanics and Rock Engineering.*, 40(5), 491-504.
- Ersoy, A., Buyuksagic S, Atici U. (2005). "Wear characteristics of circular diamond saws in the cutting of different hard abrasive rocks." *Wear 2005*, 258(9), 1422-1436.
- Evans, A.G., Wilshaw, T.R. (1977). "Dynamic solid particle damage in brittle materials: an appraisal". *J. Mater. Sci.* 12, 97-116.
- Evans, I. (1962). "A theory of the basic mechanics of coal ploughing. Int. Symp. on Mining Research, 2, ,761–798.
- Evans, I. (1984). "Basic mechanics of the point-attack pick". *Colliery Guardian*, 189–193.
- Evans, I.,Pomeroy C.D. (1973). "The strength, fracture and workability of coal". *Pergamon press limited., London*.
- Fahy, M.P Guccione, M.J. (1979). "Estimating strength of sandstones using photographic thin section data". *Bulletin of the association of engineering geologists*, 16(4), 467-485.
- Falcao Neves, P., Costa e Silva, M., and Navarro, V.F. Torres. (2012). "Evaluation of elastic deformation energy in stone cutting of Portuguese marbles with a diamond saw." *The Southern African Institute of Mining and Metallurgy*, 112, 413-418.
- Finol, J., Guo, Y.K. and Jing, X.D. (2001). "A rule based fuzzy model for the prediction of petrophysical rock parameters." *J. Pet. Sci. Eng.*, 29, 97-113.

- Fowell, R.J, McFeat-Smith, I. (1976). "Factors influencing the cutting performance of a selective tunnelling machine. In: Jones JM, editor. Proceedings of the First International Symposium on Tunnelling '76. London: IMM, 301–309.
- Fowell, R.J. (1993). "The mechanics of rock cutting". *Comprehensive rock engineering*, 4, 155–175.
- Ghabousi, J., Garret Jr., J.H., Wu, X. (1991)." Knowledge based modelling of material behaviour with neural networks". *J. Eng. Mech. ASCE*, 117(1), 132–153.
- Gill, D.E., Pichette, C., Rochon, P., Dube A, P.B. (1980). "Relation between some of the methods for predicting the penetration rate of full-face boring machines". In: *Proceedings of the 13th Canadian Symposium Rock Mechanics*, 22, 1103-1110.
- Gnirk, P.F. (1966)." An experimental study of indexed single bit-tooth penetration into dry rock at confining pressures of 0 to 7500 psi. In: Proceedings of the First Congress International Society on Rock Mechanics", 2, p. 121–129.
- Gnirk, P.F. and Cheatham, J.B. (1963). "Indentation Experiments on Dry Rocks Under Pressure." *Journal of Petroleum Technology.*, 1031–1039.
- Gokceoglu, C. (2002). "A fuzzy triangular chart to predict the uniaxial compressive strength of the Ankara Agglomerates from their petrographic composition." *Eng. Geol.*, 66, 39-51.
- Gokhan Aydin., Izzet Karakent., Kerim Aydiner. (2012)." Development of Predictive Models for Specific Energy of Diamond Saw Blades Concerning Operating Variables." *Jestech*, 15(4), 155-161.
- Gokhan Aydin., Izzet Karakert., Kerim Aydim. (2013). "Development of Predictive Models for the Specific Energy of Circular Diamond Saw Blades in the Sawing of Granitic Rocks." *Rock Mechanics and Rock Eng.*, 46, 767-783.
- Goktan, R.M. (1991) " Brittleness and micro-scale rock cutting efficiency, Mining Science and Technology", 13, 237–241.
- Guney, A. (2011)." Performance prediction of large-diameter circular saws based on surface hardness tests for Mugla (Turkey) marbles." *Rock Mech Rock Eng*, 44, 357–366.
- Guney, A., Altindag, R., Yavuz, H., and Sarac, S. (2005)." Evaluation of the Relationships between Schmidt Hardness Rebound Number and Other (Engineering) Properties of Rocks", *The 19th International Mining Congress and Fair of Turkey, IMCET2005, İzmir, Turkey.*

- Guy Lebel, J.R. (1984). “An investigation to evaluate the relationship between Rock Quality Index(RQI) and Poder Factor for Surface Mining” M.A.Sc. Thesis, University of British Columbia.
- Hamilton, H.W., Handewith, H.J. (1970). “Apparatus and method for testing rock”. United State Patent Office, no: 3618369. Patented November 9, 1971
- Handewith, H.J. (1970). “Predicting the economic success of continuous tunneling and hard rock”. *71st annual general meeting of the CIM*, 63, 595–599.
- Hao Zhang., Ganyun Huang., Haipeng song and Yilan Kang.(2012). “Experimental Investigation of Deformation and Failure Mechanisms in Rock under Indentation by Digital Image Correlation.” *Engineering Fracture Mechanics.*, 96, 667-675.
- Hartman, H.L. (1966). “The effectiveness of indexing in percussive and rotary drilling”. *Int J Rock Mech Min Sci*, 3, 265–278.
- Haykin, S. (1998). “Neural Networks: A Comprehensive Foundation”, *Prentice-Hall, Englewood Cliffs*.
- Hood, M. (1996). “State of the art review of rock models for disk roller cutters”, *Proc., 2nd NARMS, Rock Mechanics Tools and Techniques, Montreal, Balkema*.
- Hood, M. C., Roxborough, F. F. (1992).” Rock breakage. In: Hartman, H. L. (Sen Ed.), *SME Mining Engineering Handbook.*”, 2nd edn. Society for Mining, Metallurgy and Exploration, Littleton, CO, 1, 680–721.
- Hood, M., (1993). “Rock breakage technologies for the mines of tomorrow”. *AMIRA Annual Meeting, Kalgoorlie*.
- Huang, H., Damjanac, B. and Detournay, E. (1998) “Normal wedge indentation in rocks with lateral confinement”. *Rock Mechanics and Rock Engineering*, 31(2), 81–94.
- Huang, H., Damjanac, B., and Detournay, E. (1997).” Numerical Modeling of Normal Wedge Indentation in Rocks with Lateral Confinement.” *Int. J. RockMech. &Min. Sci.*, 34, 3-4.
- Hustrulid, W.A. and Fairhurst, C. (1971),”A Theoretical and Experimental Study of the Percussive drilling of rock Part II—force-penetration and specific energy determinations”, *International Journal of Rock Mechanics and Mining Sciences & Geomechanics Abstracts*, 8(4), 335-340, and 341-356.
- Ibrahim Ocak, Sadi Evren Seker (2012).” Estimation of Elastic Modulus of Intact Rocks by Artificial Neural Network.” *Rock Mech Rock Eng*, 45, 1047–1054.

- Irfan Celal Engin, Fatih Bayram., Nazmi Erhan Yasitli. (2013). “Experimental and Statistical Evaluation of Cutting Methods in Relation to Specific Energy and Rock Properties.” *Rock Mechanics and Rock Eng.*, 46, 755-766.
- Izquierdo, L.E. and Chiang, L.E. (2004). “A Methodology for Estimation of Specific Rock Energy Index Using Corrected Down-The-Hole Drill Monitoring Data,” *Mining Technology: Transaction of the Institute of Mining & Metallurgy*, 113, A225-A236.
- Jean Sulema, Miguel Cerrolazab (2002).” Finite element analysis of the indentation test on rocks with microstructure.” *Computers and Geotechnics*, 29, 95–117.
- Jefferson Mateus., Saavendra, N.F., Zuly Calderon-Carnillo and Darwin Mateus. (2007).”Correlation Development between Indentation Parameters and Uniaxial Compressive Strength for Colombian Sandstones.” *CT&F- Clecia Tecnologia y Futura.*, 3, 125-135.
- Jing, L.A. (2003).”A review of techniques, advances and outstanding issues in numerical modelling for rock mechanics and rock engineering.” *International Journal of Rock Mechanics & Mining Sciences*, 40, 283–353.
- Julie Pallant., (2007) SPSS Survival Manual
- Kahraman, S. and Gunaydin, O. (2006), “Indentation Hardness Test to Estimate the Sawability of Carbonate Rocks “, *Bull Eng Geol and Environ*, 67, 2008, 507-511.
- Kahraman, S., (2002). “Correlation of TBM and drilling machine performances with rock brittleness.” *Engineering Geology*, 65,269–283.
- Kahraman, S., Altun, H., Tezekici. B.S.Fener, M. (2006). “Sawability prediction of carbonate rocks from shear strength parameters using artificial neural networks”. *Int. j. rock mech.min.sci.*, 43, 157-164.
- Kahraman, S., Balç, C., Yazıcı, S. & Bilgin, N. (2000). “Prediction of the penetration rate of rotary blast hole drills using a new drillability index”, *Int. J. Rock Mech. Min. Sci.*, 37, 729-743.
- Kahraman, S. Bilgin, C. and Feridunoglu, C. (2003). “Dominant Rock Properties Affecting Penetration Rate of Percussive Drills”, *International Journal of Rock Mechanics and Mining Scienc*, 40(2), 711 -723.
- Kahraman,S., Fener, M. and Kozman, E.(2012).” Predicting the Compressive and Tensile Strength of Rocks from Indentation Hardness Index.” *The Journal of the South African Institute of Mining and Metallurgy.*, 112, 331-339

- Kahramana, S., Balci, C., Yazici, S., Bilgin, N. (2000).” Prediction of the penetration rate of rotary blast hole drills using a new drillability index.” *International Journal of Rock Mechanics and Mining Sciences* 37, 729-743.
- Kothari, C. R (2004). “Research Methodology, Methods & Techniques “, New Age International (P) Ltd., Publishers
- Kou, S. Q., Huang, Y., Tan, X.C., Lindqvist, P.A. (1995). “Identification of the governing parameters related to rock indentation depth by using similarity analysis”. *Engng Geol.*, 49, 261-269.
- Kou, S., Lindquist, P.-A., Tan, X. (1995). “An analytical and experimental investigation of rock indentation fracture”. *In: Proc., 8th International Congress on Rock Mechanics, Tokyo*, 181-184.
- Kou, S.Q. (1998). “Identification of governing factors related to the rock indentation depth by using similarity analysis”. *Engineering geology*, 49, 261-269.
- Kou, S.Q. (1999). “Numerical simulation of the cutting of homogenous rocks” *Int. j. rock mech.min.sci.*, 36(5), 711-717.
- Kripamoy Sarkar and Avyaktanand Tiwary. (2010).” Estimation of strength parameters of rock using Artificial Neural Networks.” *Bull Eng Geol Environ.*, 69, 599-606.
- Kumano, A., Goldsmith, W., (1982). ”An analytical and experimental investigation of the effect of impact on coarse granular rocks”. *Rock Mechanics*, 15, 67-97.
- Kutter, H., Sanio, H. P. (1982). “Comparative study of performance of new and worn disc cutters on a full-face tunnelling machine”. *In: Tunnelling'82, IMM, London*, 127-133.
- Lawn B, Wilshaw R. (1975).” Review Indentation Fracture: Principles and Applications”. *Journal of Material Science*; 10:1049–81.
- Lawn, B. R., Evans, A. (1977). “A model for crack initiation in elastic/plastic indentation fields.” *J. Mater. Sci.*, 12, 2195–2199.
- Lawn, B. R., Wilshaw, R. (1975). “Review indentation fracture: principles and applications”. *J. Mater. Sci.* 10, 1049-1081.
- Lawn, B., Fuller, E. (1975). “Equilibrium penny-like cracks in indentation fracture.” *J. Mater. Sci.*, 10, 2016–2024.
- Lawn, B., Marshall, D. (1979). “Hardness, toughness, and brittleness: an indentation analysis.” *J. Am. Ceramic Society*, 62 (7), 347–350.

- Lawn, B., Swain, M. (1975). "Microfracture beneath the point indentation in brittle solids." *J. Mater. Sci.*, 10, 113–122.
- Lawn, B., Wilshaw, R. (1975)." Review indentation fracture: principles and applications." *J. Mater. Sci.*, 10, 1049–1081.
- Lawn, B.R., Evans, A.G.(1977)"A Model for Crack Initiation in Elastic/Plastic Indentation Fields," *J. Muter. Sci.*, 12 [11], 2195-2199.
- Legget, R.F. and Hatheway, A.W. (1988). "Geology and Engineering. "(3rd ed). New York, McGraw-Hill Inc.
- Leite, M.H. and Ferland, F. (2001)." Determination of Unconfined Compressive Strength and Young's Modulus of Porous Materials by Indentation Test." *Engineering Geology*. 59, 267-280.
- Lindqvist, P.A., (1982). "Rock Fragmentation by Indentation and Disc Cutting". Ph.D. Thesis, 20D, Lulea, University of Technology, Lulea, Sweden.
- Lindqvist, P.A., Suarez del Rio, L.M., Montoto, M., Tan, X., Kou, S., (1994). "Rock Indentation Database-testing Procedures, Results and main Conclusions". SKB Project Report, PR 44-94-023.
- Liu, H.Y., Kou, S.Q., Lindqvist, P.A. Tang, C.A. (2002)." Numerical simulation of the rock fragmentation process induced by indenters. *Int J Rock Mech Min Sci*, 39, 491–505.
- Lundberg, B. (1974)."Penetration of Rock by Conical Indenters." *International Journal of Rock Mechanics and Mining Sciences & Geomechanics Abstracts.*, 11, 209-214.
- Magnenet, V., Auvray, C., Djordem, S., and Homand, F. (2009)." On the estimation of elastoplastic properties of rocks by indentation tests." *International Journal of Rock Mechanics & Mining Sciences*, 46, 635–642.
- MATLAB, 2006. Statistics Toolbox for use with MATLAB, User's Guide Version 5. The MathWorks Inc.
- Maurer, W.C. (1966). "The state of rock mechanics knowledge in drilling." *Proceedings of the Eighth Symposium on Rock Mechanics, University of Minesota*, 355–95.
- Maurer, W.C. (1967) "The state of rock mechanics knowledge in drilling". *8th Symp. on Rock Mechanics, New York*, 355–395.

McFeat Smith I. (1977). “Rock Property testing for the Assessment of Tunneling Machine Performance”. *Tunnels and Tunnelling*, 29-31 (1977).

McFeat-Smith, I and Fowell, R.J. (1977). “Correlation of Rock Properties and the Cutting Performance of Tunnelling Machines”. *Proceeding: Conference on Rock Engineering, New Castle upon Tyne, England*, 581-602,

McFeat-Smith, I. (1977),” Rock Property Testing For the Assessment of Tunnelling Machine Performance”, *Tunnels and Tunnelling*, 9(2), 29–33.

Mellor M. (1972). “Normalization of specific energy values.” *Int J Rock Mech Min Sci*, 9, 661–663.

Meulenkamp. F., Alvarez grima, M., (1999). “Application of neural networks for the prediction of the unconfined compressive strength (UCS) from equotip hardness”. *Int. j. rock mech.min.sci.*, 36, 29-39.

Michael L. Orlov (1996).” Multiple Linear Regression Analysis Using Microsoft Excel Chemistry Department, Oregon State University

Miller,M.H., and Sikarskie, D.L.,(1968),”On the Penetration of Rock by Three-Dimensional Indentors”, *International Journal of Rock Mechanics and Mining Science*, 5, 375-398.

Minitab 17.0 software help

Mishnaevsky, L.L. (1995).” Physical mechanisms of hard rock fragmentation under mechanical loading: A review.” *Int J Rock Mech Min Sci & Geomech Abstr*, 32(8), 763– 766.

Mohammad Haftani, Bahman Bohloli, MahdiMoosavi, Alireza Nouri, MajidMoradi, and Mohammad Reza Maleki Javan (2014).” Influence of Penetration Rate and indenter Diameter in Strength Measurement by Indentation Testing on Small Rock Specimens.” *Rock Mech Rock Eng*, DOI, 10.1007/s00603-014-0563-3.

Mohammad Haftani, Bahman Bohloli, MahdiMoosavi, Alireza Nouri, MajidMoradi, and Mohammad Reza Maleki Javan(2013).”A new method for correlating rock strength to indentation tests.” *Journal of Petroleum Science and Engineering*, 112, 24–31.

Mohd For Mohd Amin, Chan Sook Huei, Azman Kassim, Mushairry Mustaffa & Edy Tonizam Mohammad (2009) “Excavatability of Unclassified Hard Materials (LPPIM: CREAM/ UPP03-02-060111) “, Final Report, CIDB-CREAM, Kuala Lumpur.

- Murat Yurdakul., Hurriyet Akdas.(2012). “Prediction of Specific Cutting Energy for Large Diameter Circular Saws during Natural Stone Cutting.” *International Journal of Rock Mechanics and Mining Science.*, 53, 38-44.
- Murthy, Ch.S.N. (1998). “Experimental and Theoretical Investigations of Some Aspects of Percussive Drilling”, *Ph.D. Thesis (unpublished)*, Indian Institute of Technology, Kharagpur.
- Nelson, P. P., Ingraea, A. R., O'Rourke, T. D. (1985). “TBM performance prediction using rock fracture parameters”. *Int. J. Rock Mech. Min. Sci. Geomech. Abstr.* 22(3), 189-192.
- Nishimatsu, Y. (1972).”The Mechanics of Rock Cutting”. *International Journal of Rock Mechnics and Mining Sciences & Geomechnics Abstracts*, 9, 261-270.
- Nishimatsu, Y. (1979). “On the effect of tool velocity in the rock cutting”. *Proc., Int. Conf. on Mining and Machinery, Brisbane*, 314–319.
- Nishimatsu, Y. (1979). “On the effect of tool velocity in the rock cutting.” *Proc., Int. Conf. on Mining and Machinery, Brisbane*, 314–319.
- Okuchaba, B.J. (2008).”Development of a model to calculate mechanical specific energy for air hammer drilling systems” M.S.Thesis, Texas A&M University
- Olgay Yarali and Eren Soyer. (2013). “Assessment of relationships between drilling rate index and mechanical properties of rocks”, *Tunnelling and Underground Space Technology*”, 33, 46-53.
- Ozdemir, L. (1977). “Development of theoretical equations for predicting tunnel borability.” *PhD. Thesis, T-1969, Colorado School of mines, Golden, Co*
- Ozdemir, L. (1995).” *Mechanical Mining. Short Course Notebook.* Colorado School of Mines, Mining Eng. Dept., USA.
- Paithinkar, A.G., Misra, G.B. (1976).” A critical appraisal of the protodyakonov index.” *Int J Rock Mech Min Sci*, 13, 249–251.
- Paithinkar, A.G., Misra, G.B. (1980).” Drillability of rocks in percussive drilling from energy per unit volume as determined with a microbit.” *Min Eng*, 32, 1407–1410.
- Pang, S.S., Goldsmith, W. (1990). “Investigation of crack formation during loading of brittle rock”. *Rock Mech and Rock engg*, 23, 3-63.
- Paone, J. and Madson, D. (1966). ”Drillability Studies on Impregnated Diamond Bits”. *RI-USBM 6776*, U.S. Bureau of Mines.

- Paone, J., Madson, D., and Bruce, W.E. (1969). "Drillability studies-Laboratory percussive drilling.", *Bureau of Mines* RI 7300, 22.
- Pariseau, W.G. and Fairhurst, C. (1967). "The force-penetration characteristic for wedge penetration into rock". *International Journal of Rock Mechanics and Mining Sciences & Geomechanics Abstracts*, 14, 165–180.
- Paul, B. and Sikarskie, D.L. (1965). "A preliminary theory of static penetration by a rigid wedge into a brittle material". *Society for Mining, Metallurgy and Exploration, Transactions, U.S.A.*, 372–383.
- Pessier, R.C. and Fear, M.J.(1992). "Quantifying Common Drilling Problems With Mechanical Specific Energy and a Bit-Specific Coefficient of Sliding Friction," paper SPE 24584 presented at the 1992 SPE 67th Annual Technical Conference and Exhibition, Washington, DC.
- Rao, U.M., Misra, B (1998). "Principles of Rock Drilling", Oxford & IBH Publishing Co.Pvt. Ltd,
- Ratan Raj Tatia (2004). "Surface and Underground Excavations- Methods, Techniques and Equipment." A.A. Balkema Publishers, Great Britain.
- Reddish, d.T., Ergul Yasar. (1996). "A New Portable Rock Strength Index Test based on Specific Energy of Drilling." *International Journal of Rock Mechanics and Mining Science.*, 33, 543-548.
- Ringstad, C., Lofthus, E.B., Sonstebo, E.F., Fjaer, E., Zausa, F., Fuh, G.F. (1998). "Prediction of rock parameters from micron indentation measurement: the effect of sample size." *EUROCK '98, Trondheim, Norway, SPE 47313*.
- Rostami, J., Neil, D. M., Ozdemir, L. (1993). "Roadheader application for the Yucca Mountain experimental study facility". Final Report. EMI, Colorado School of Mines, 122.
- Rostami, J., Ozdemir, L., Neil, D.M. (1994). "Performance prediction: a key issue in mechanical hard rock mining" *Min. Eng.*, November, 1263– 1267.
- Roxborough, F. F. (1973). "Cutting rock with picks". *The Mining Engineer*, 133, 445–455.
- Roxborough, F. F., Rispin, A. (1973). "A laboratory investigation into the application of picks for mechanized tunnel boring in the lower chalk". *The Mining Engineer*, 133, 1–13.

- Roxborough, F.F. and Sen, G.C. (1986). "Breaking coal and rock." Australian Coal Mining Practice. Australas. Inst. Min. Metall., Chap. 9.
- Roxborough, F.F., Phillips, H.P. (1975). "Rock excavation by disc cutter." *International Journal Rock Mechanics and Mining Science*, 12, 361–366.
- Rumelhart, D., McClelland, J. (1986). "Parallel distributed processing: explorations in the microstructure of cognition". Bradford
- Rumelhart, D.E.; Hinton, G.E. and Williams, R.J. (1986). "Learning Internal Representations By Error Propagation, in Parallel Distributed Processing: Explorations in the Microstructure of cognition", *Vol. 1, ed. by Rumelhart D.E. & McClelland J.L. Bradford Books/MIT Press.*
- Saffet Yagiz. (2009)." Discussion of the paper entitled 'Indentation Hardness Test to Estimate the Sawability of Carbonate Rocks. By S. Kahraman and O.Gunaydin. Bull Eng Geol and Environ, 67, 2008, 507-511." *Bulletin of Engineering Geology and the Environment.*, 68, 437-439.
- Saksala, T., Gomon, D., Hokka, M., and Kuokkala, V.T. (2013)." Numerical modeling and experimentation of dynamic indentation with single and triple indenters on Kuru granite" ., *Rock Dynamics and Applications – State of the Art – Zhao & Li (eds) Taylor & Francis Group*, 0, 415-421.
- Sanio, J.P. (1985). "Prediction of the performance of disc cutters in anisotropic rock". *Int J Rock Mech & Mining Sci*, 22, 153-161.
- Santarelli, F.J., Marshala, A.F., Brignoli, M., Rossi, E., Bona, N. (1996)." Formation Evaluation from logging on cuttings." *SPE Permian Basin Oil and Gas Recovery Conference, Midland, Texas, SPE 36851.*
- Schmidt, R.L. (1972). "Drillability studies- Percussive drilling in the field", *Bureau of Mines RI 7684*, 31.
- Seibi, A., Al-Alawi, S.M., (1997). "Prediction of fracture toughness using artificial neural networks (ANNs)." *Eng. Fract. Mech.*, 56, 311–319.
- Shakoor, A., Bonelli, R. E. (1991). "Relationship between petrographic characteristics, engineering index properties and mechanical properties of selected sandstones". *Bull. Assoc. Engng. Geol.* 28, 55–71.
- Shao-Quan Kou., Yi Huang., Xiang-Chun Tan and Per-Arne .(1998). "Identification of the Governing Parameters related to Rock Indentation Depth by using Similarity Analysis." *Engineering Geology.*, 49, 261-269.

- Sikarskie, D.L., Altiero, N.J., (1973). "The formation of chips in the penetration of elastic-brittle materials". *J. Appl. Mech.* 40 (3), 791-798.
- Simon, R., (1967). "Rock fragmentation by concentrated loading". *Proceedings of the 8th US Symposium on Rock Mechanics*, 440-454.
- Simpson, P. K. (1990). "Artificial neural system-foundation, paradigm, application and implementation". Pergamon Press, New York.
- Singh, P.S. (1986). "Brittleness and the mechanical winning of coal, *Min. Sci. and Tech.* ", 3, 173-180.
- Singh, T. N., Kanchan, R., Verma, A. K., Singh, S. (2003). "An intelligent approach for prediction of triaxial properties using unconfined uniaxial strength". *Min. Eng. J*, 5, 12-16.
- Singh, V.K., Singh, D., Singh, T.N. (2001). "Prediction of strength properties of some schistose rocks". *Int Rock Mech Min Sci.*, 38(2), 269-284.
- Sivanandan, S.N. and Paulraj, M. (2011). "Introduction Artificial Neural Networks", *Vikas Publishing House Private Limited*.
- Sonmez, H., Gokceoglu, C., Nefeslioglu, H.A., Kayabasi, A. (2006). "Estimation of rock modulus: for intact rocks with an artificial neural network and for rock masses with a new empirical equation." *International Journal of Rock Mechanics and Mining Sciences*, 43(2), 224-235.
- Speight, H. E. (1997). "Observations on drag tool excavation and the consequent performance of roadheaders in strong rock". *AusIMM Proc.* No 1, 17-32.
- Sua Arez-Rivera, F.R., Cook, P.J., Cook, N.G.W., Myer, L.R. (1991). "The role of wetting fluids during the indentation of porous rocks". *Proceedings of the 32nd US Symposium on Rock Mechanics*, 683-692.
- Szlavin, J., (1974). "Relationship between some physical properties of rock determined by laboratory tests." *Int. J. Rock Mech. Min. Sci. Geomech. Abst.* 11, 57-66.
- Szwedzicki, T. (1998a). "Indentation Harness Testing of Rock." *International Journal of Rock Mechanics and Mining Science.*, 35(6), 825-829.
- Szwedzicki, T. (1998b). "Draft ISRM Suggested Methods For Determining The Indentation Hardness Index Of Rock Materials." *International Journal of Rock Mechanics and Mining Sciences & Geomechanics Abstracts.*, 35, 831-835.

- Tan, X. C., Kou, S. Q., Lindquist, P.-A. (1996). "Simulation of rock fragmentation by indenters using DDM and fracture mechanics". In: *Aubertin, M., Hassani, F., Mitri, H. (eds.), 2nd NARMS, Rock Mechanics Tools and Techniques, Montreal. Balkema, Rotterdam, 685-692.*
- Tan, X., Kou, S., Lindqvist, P.A. (1996). "Simulation of rock fragmentation by indenters using DDM and fracture mechanics". *Proc., 2nd NARMS, Rock Mechanics Tools and Techniques, Montreal, Balkema.*
- Tandanand, S., Unger, H.F. (1975). "Drillability determination- A drillability index of percussive drills.", *USBM RI 8073.*
- Tang, C.A. (1997). "Numerical simulation of progressive rock failure and associated seismicity" *Int. j. rock mech.min.sci.*, 34, 249-262.
- Thiercelin, M., Cook, J., et al., (1988). "Failure mechanisms induced by indentation of porous rocks", *Proceedings of the 29th US Symposium*, 135-142.
- Tiryaki, B. (2008a). "Application of artificial neural networks for predicting the cuttability of rocks by drag tools." *Tunnelling Underground Space Technol.*, 23, 273-280.
- Tiryaki, B. (2008b). "Predicting intact rock strength for mechanical excavation using multivariate statistics, artificial neural networks and regression trees." *Eng. Geol.*, 99, 51-60.
- Tiryaki, B., Cagatay Dikmen, A. (2006). "Effects of Rock Properties on Specific Cutting Energy in Linear Cutting of Sandstones by Picks." *Rock Mechanics and Rock Engineering*. 39(2), 89-120.
- Tiryaki, B., Cagatay Dikmen, A.(2006). "Effects of Rock Properties on Specific Cutting Energy in Linear Cutting of Sandstones by Picks." *Rock Mechanics and Rock Engineering.*, 39(2), 89-120.
- Tugrul, A., Zarif, I. H. (1999) "Correlation of mineralogical and textural characteristics with engineering properties of selected granitic rocks from Turkey". *Engng. Geol*, 51, 303–317.
- Unger, H.F. and Fumanti, R.R. (1972). "Percussive drilling with independent rotation", *U.S.B.M. Report of investigation No.7692.*
- Wagner, H., Schumann, E.R.H. (1971). "The stamp-load bearing strength of rock—an experimental and theoretical investigation". *Rock Mech*, 3(4), 185–207.

- Wang, J.K., Lehnhoff, T.F. (1976).” Bit penetration into rock: a finite element study.” *Int J Rock Mech Min Sci*, 13,, 11–16.
- Wang, J.K. (1976). “Bit Penetration into rock- A finite element study, *Int.J. Rock. Mech. Min. Sci.*, 13,11-16.
- Wang, S. Y., Sloan, S. W., Liu, H. Y. and Tang, C. A.(2011).” Numerical simulation of the rock fragmentation process induced by two drill bits subjected to static and dynamic (impact) loading. ” *Rock Mech and Rock Eng.*, 44, 317–332.
- Waughman, R.J., Kenner, J.V. and Moore, R.A. (2002). “Real-Time Specific Energy Monitoring Reveals Drilling Inefficiency and Enhances the Understanding of When to Pull Worn PDC Bits,” paper IADC/SPE 74520 presented at the IADC/SPE Drilling Conference, Dallas, Texas, 26-28 February.
- Werbos, P.J. (1974). “Beyond regression: New tools for prediction and analysis in the behavioral sciences.” *Ph.D. Thesis, Harvard University*.
- West, G. (1986). “A relation between abrasiveness and quartz content for some coal measures sediments”. *Int. J. Min. Geol*, 4, 73–78.
- Yagiz, .S (2008b). ‘Assessment of brittleness using rock strength and density with punch penetration test.” *Tunn Undergr Space Technol.*, doi:10.1016/j.tust.2008.04.002 (in press)
- Yagiz, S. (2002).” Development of rock fracture and brittleness indices to quantify the effects of rock mass features and toughness in the CSM model basic penetration for hard rock tunneling machines”. Ph.D. Thesis, Colorado School of Mines, Golden, CO, USA, 289 (unpublished)
- Yagiz, S. (2006). “A model for prediction of tunnel boring machine performance.“ Substructures and underground space. Paper no. 383. Engineering geology for tomorrow’s cities in DVD, p 10. In: The 10th international association of Engineering Geologists Congress. The Geological Society of London, Nottingham, UK
- Yagiz, S. (2008 a). “Utilizing rock mass properties for predicting TBM performance in hard rock condition”. *Tunn Undergr Space Technol*, 23(3), 326–339.
- Yagiz, S. (2008 b). “Assessment of brittleness using rock strength and density with punch penetration test”. *Tunn Undergr Space Technol*. doi:10.1016/j.tust.2008.04.002 (in press)

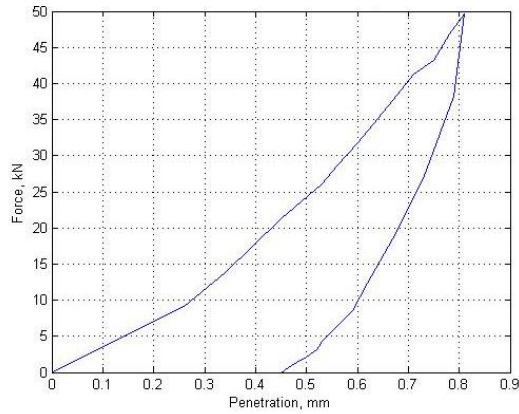
- Yagiz, S. (2009). "Assessment of brittleness using rock strength and density with punch penetration test." *Tunnelling and Underground Space Technology*, 24, 66–74.
- Yagiz, S., Ozdemir, L. (2001). "Geotechnical parameters influencing the TBM performance in various rocks." *In: Program with abstracts.44th Annual Meeting of AEG, Technical Session 10 Engineering Geology for Construction Practices, St Louis, MO, USA*
- Yarali, O., Kahraman, S. (2011)." The drillability assessment of rocks using the different brittleness values". *Tunneling Underground Space Technology*, 26, 406–414.
- Yilmaz, I, Yuksek, G. (2009)." Prediction of the strength and elasticity modulus of gypsum using multiple regression, ANN, and ANFIS models." *International Journal of Rock Mechanics and Mining Sciences*, 46, 803–810.
- Yilmaz, I. and Oguz Kaynar. (2011)." Multiple regressions, ANN (RBF, MLP) and ANFIS models for prediction of swell potential of clayey soils." *Expert systems with Applications*, 38, 5958-5966.
- Yilmaz, I. and Sendir, H. (2002) Correlation of Schmidt hardness with unconfined compressive strength and young's modulus in gypsum from Sivas (Turkey), *Engineering Geology*, 66: 211-219
- Yilmaz, I. and Yuksek, A. G. (2008)." Technical Note An Example of Artificial Neural Network (ANN) Application for Indirect Estimation of Rock Parameters". *Rock Mechanics and Rock Engineering*, 41 (5), 781–795.
- Yilmaz, I. and Yuksek, A.G. (2009). "Prediction of the strength and elasticity modulus of gypsum using multiple regression, ANN, ANFIS models and their comparison." *Int. J. Rock Mech. Min. Sci.*, 46(4), 803-810.
- Zausa, F., Santarelli, F.J. (1995). "A new method to determine rock strength from an index test on fragments of very small dimension". *VIII ISRM International Congress on rock mechanics, Tokyo, Japan*
- Zhlobinsky, B.A. (1970). "Dynamic Fracture of Rocks under Indentation", Nedra, Moscow
- Zhu, W.C., Tang, C.A. (2006). "Numerical simulation of Brazilian disk rock failure under static and dynamic loading". *Int J Rock Mech Min Sci*, 43, 236–252.

Zienkiewicz, O.C. (1968). "Continuum mechanics as an approach to rock mass problems", *Rock Mechanics in Engineering Practice, Chapter 8, 237-273*, edited by K.G. Stagg, O.C. Zienkiewicz, J. Wiley and Son.

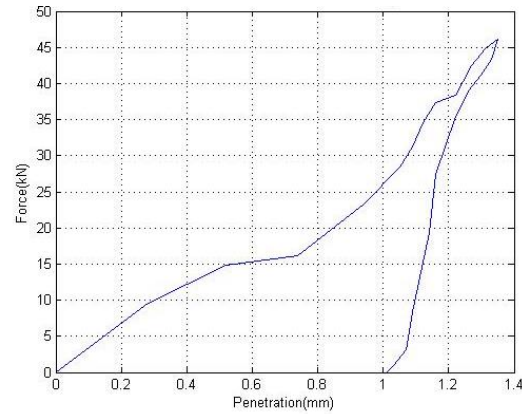
Zienkiewicz, O.C. (1968). "The Finite Element Method", McGrawhill, London

Zorlu, K. (2008). "Prediction of uniaxial compressive strength sandstones using photography-based models", *Engineering Geology*, 96,141-158.

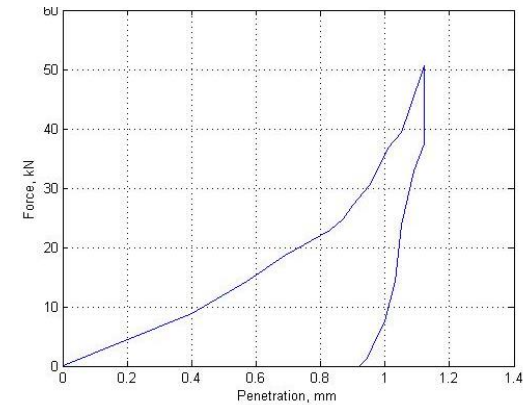
APPENDIX- I



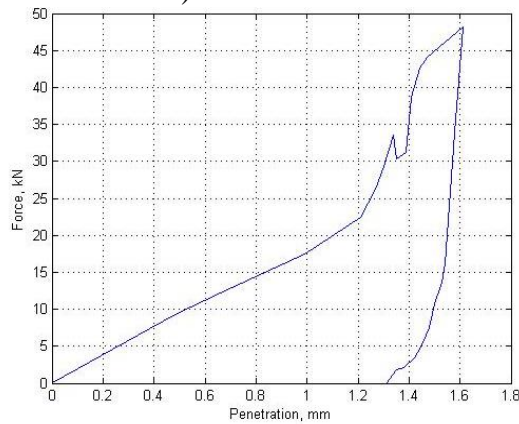
a) Marble



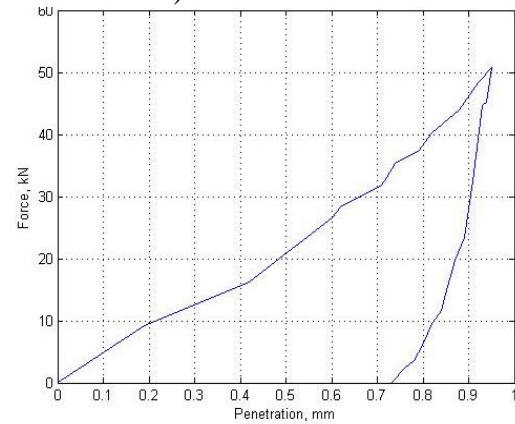
b) Limestone



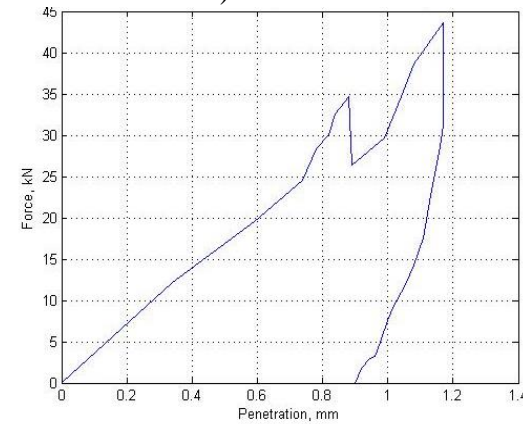
c) Basalt



d) Steel gray granite

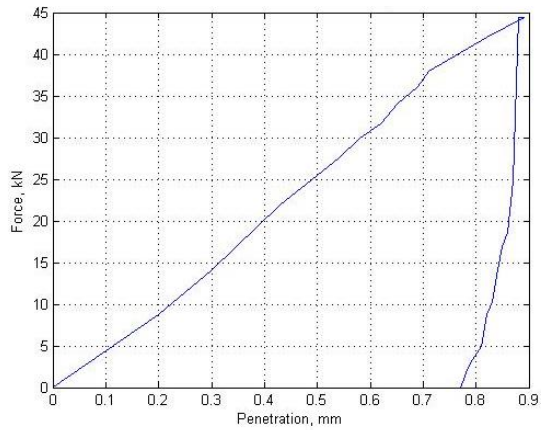


e) Moon white granite

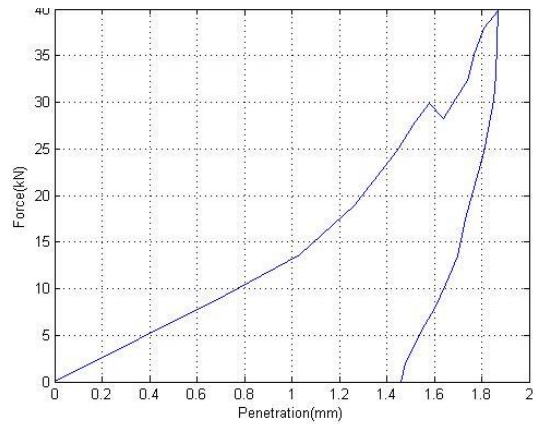


f) Black galaxy granite

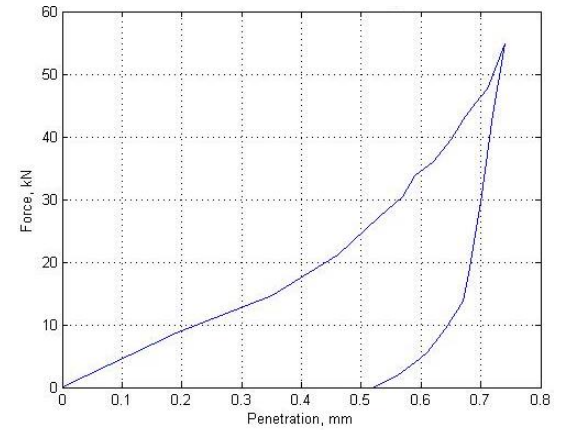
Figure 3.18 (a-f) Force–Penetration (F-P) curves for 38mm diameter chisel bit at 10° index angle for various types of rocks



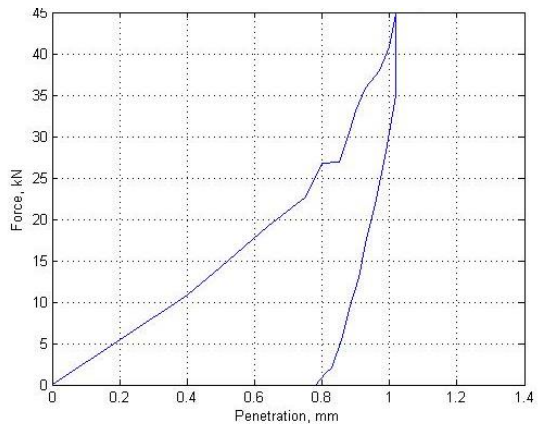
a) Marble



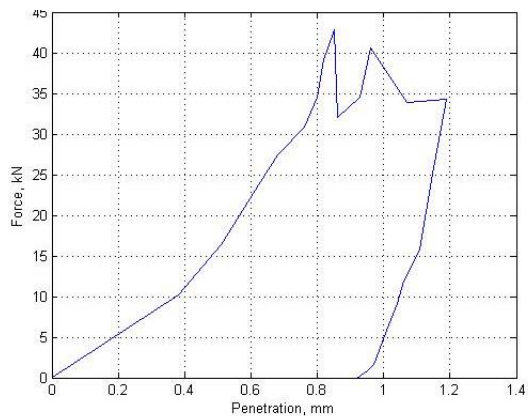
b) Limestone



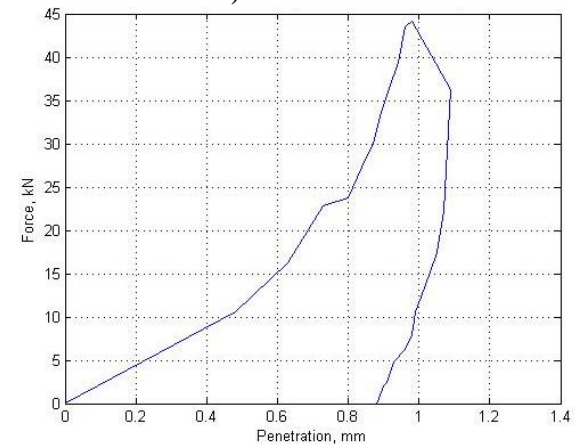
c) Basalt



d) Steel gray granite

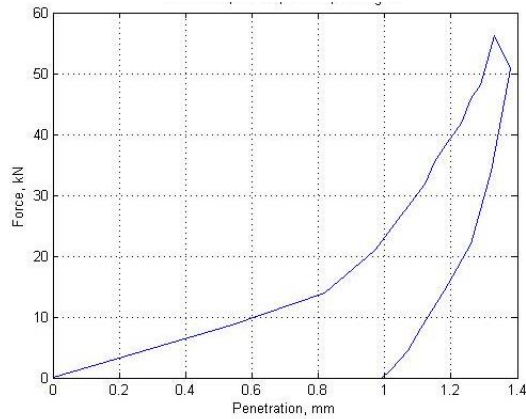


e) Moon white granite

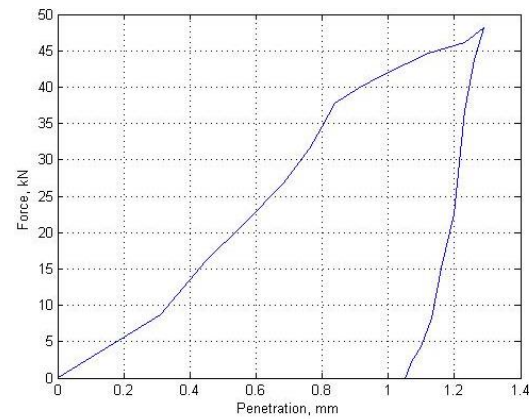


f) Black galaxy granite

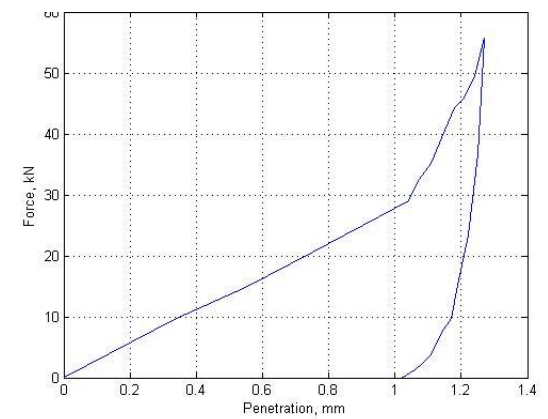
Figure 3.19 (a-f) Force–Penetration (F-P) curves for 38mm diameter chisel bit at 20° index angle for various types of rocks



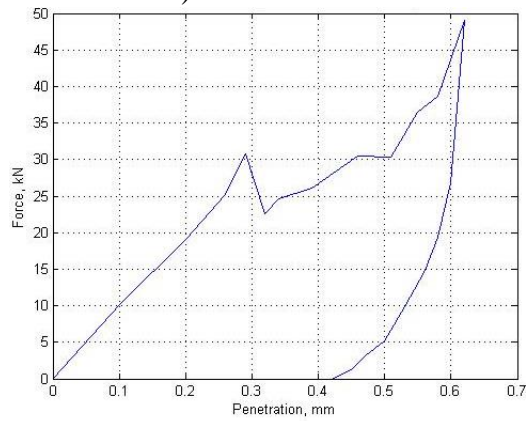
a) Marble



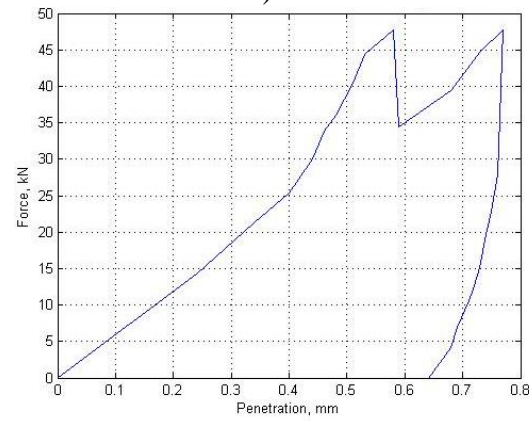
b) Limestone



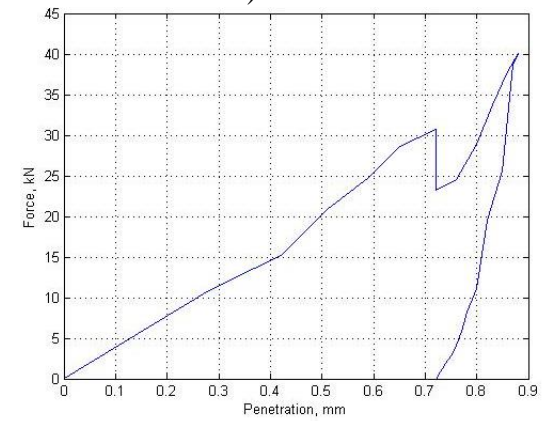
c) Basalt



d) Steel gray granite

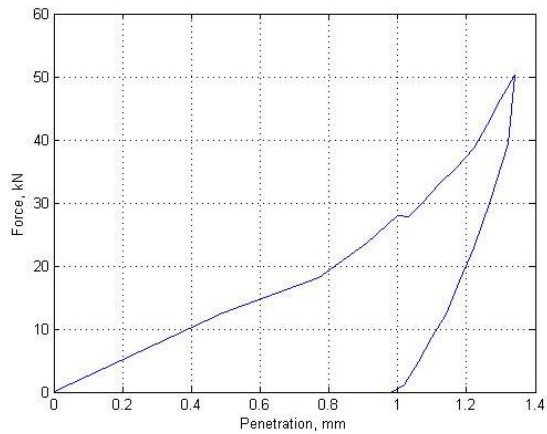


e) Moon white granite

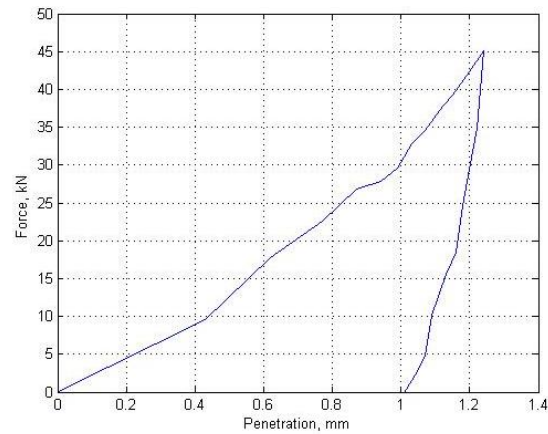


f) Black galaxy granite

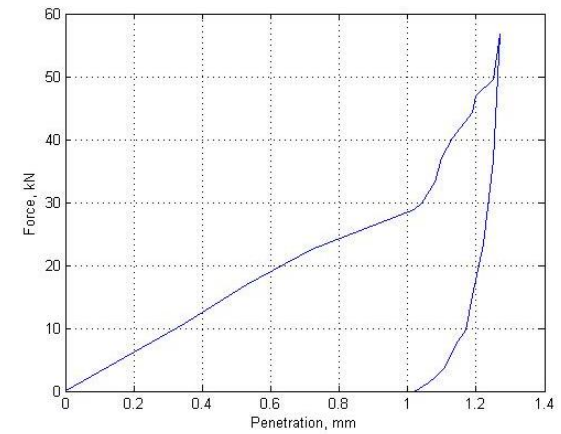
Figure 3.20 (a-f) Force–Penetration (F-P) curves for 38mm diameter chisel bit at 30° index angle for various types of rocks



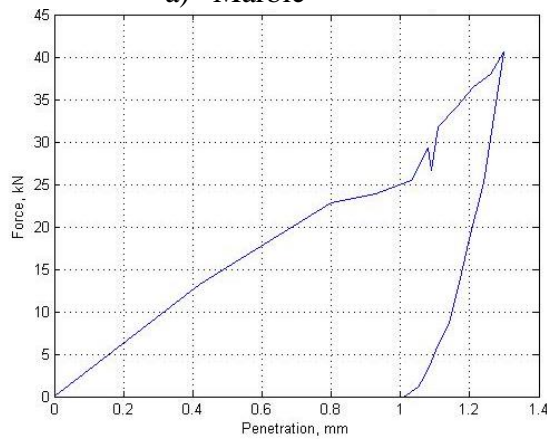
a) Marble



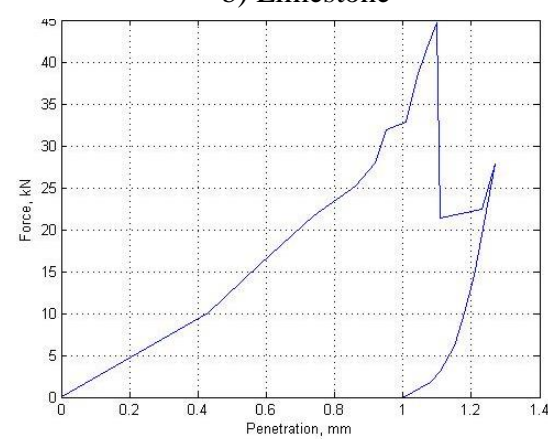
b) Limestone



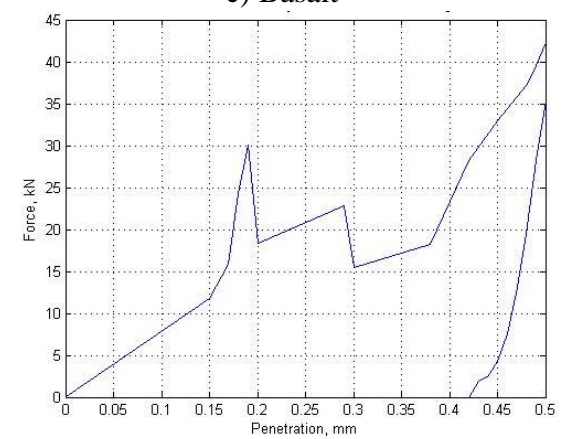
c) Basalt



d) Steel gray granite

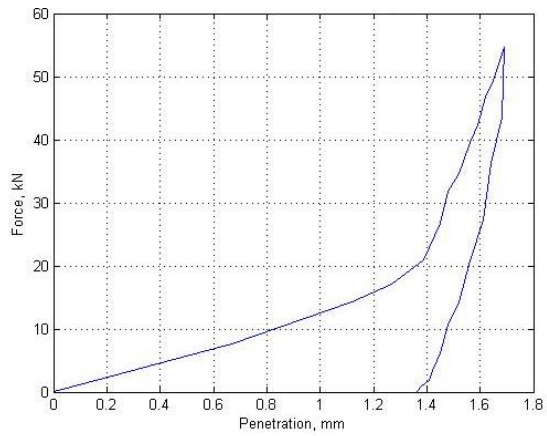


e) Moon white granite

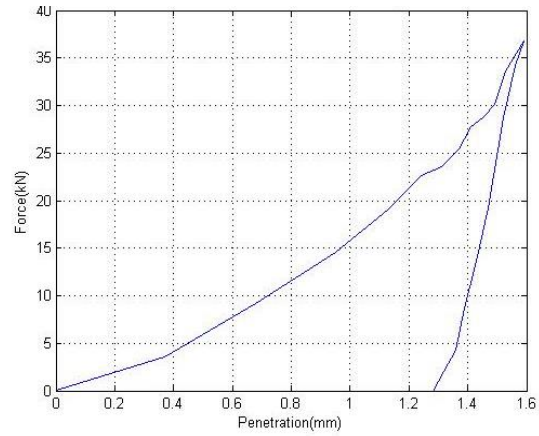


f) Black galaxy granite

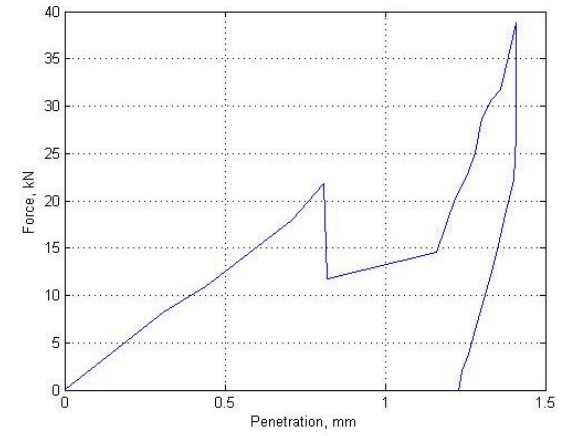
Figure 3.21 (a-f) Force–Penetration (F-P) curves for 38mm diameter chisel bit at 40° index angle for various types of rocks



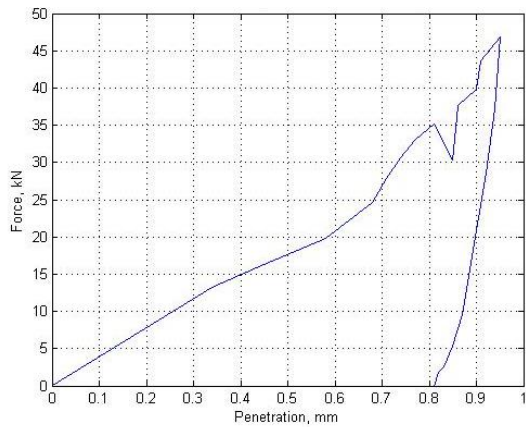
a) Marble



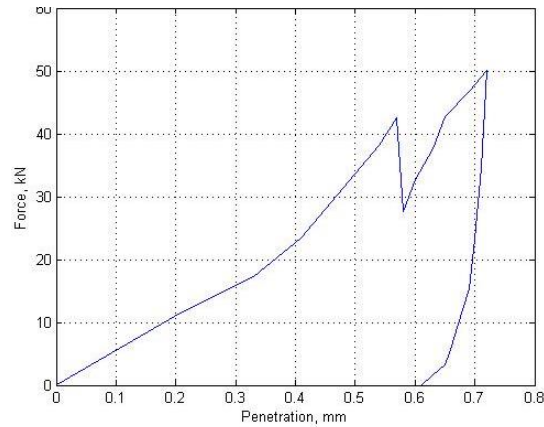
b) Limestone



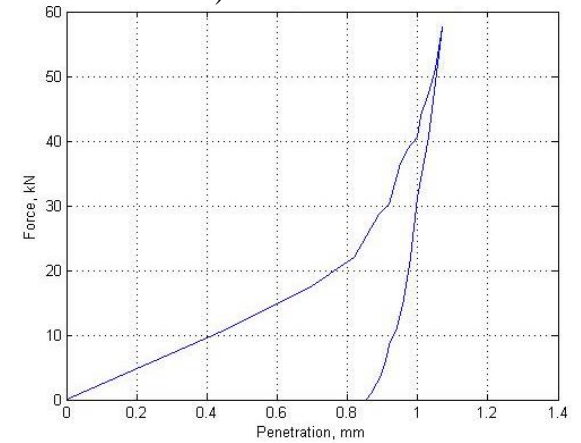
c) Basalt



d) Steel gray granite

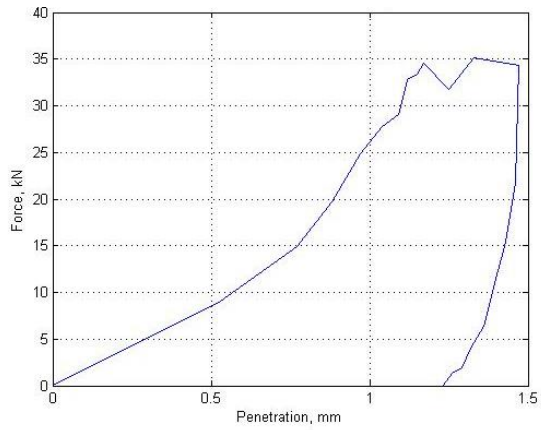


e) Moon white granite

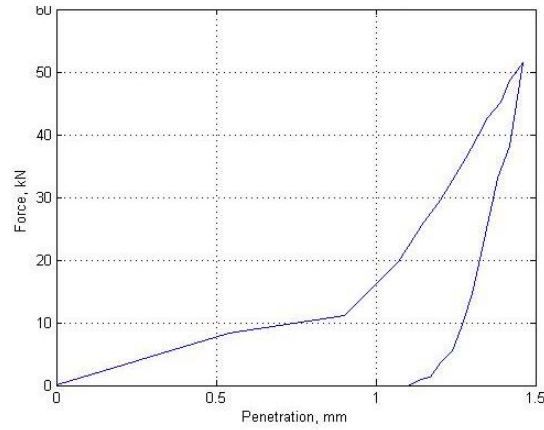


f) Black galaxy granite

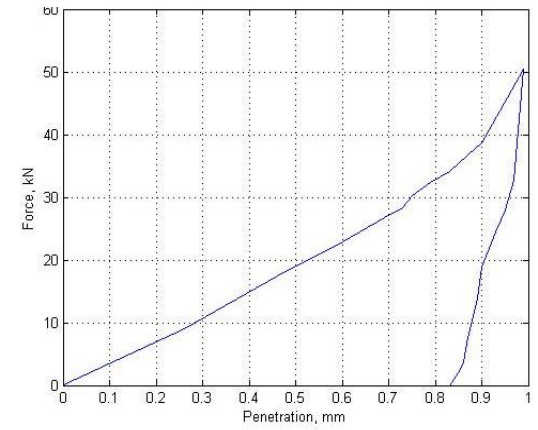
Figure 3.22 (a-f) Force–Penetration (F-P) curves for 45mm diameter chisel bit at 10^0 index angle for various types of rocks



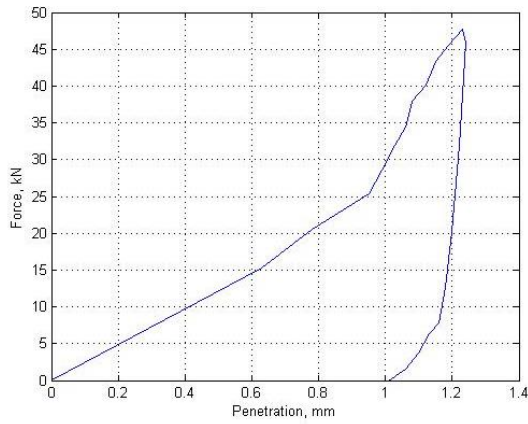
a) Marble



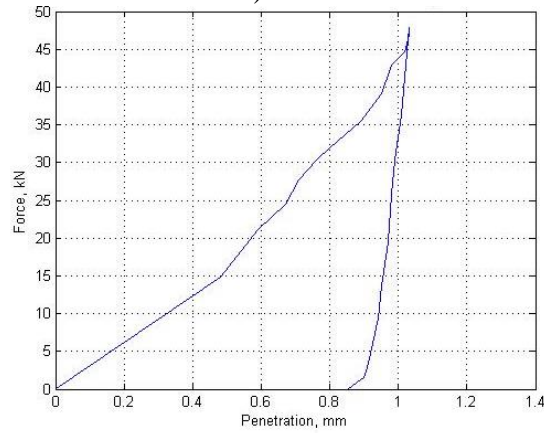
b) Limestone



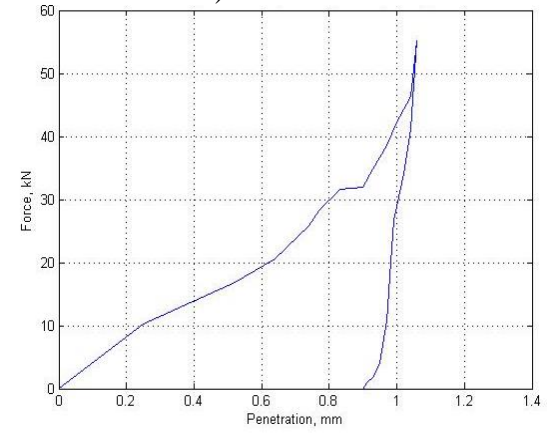
c) Basalt



d) Steel gray granite

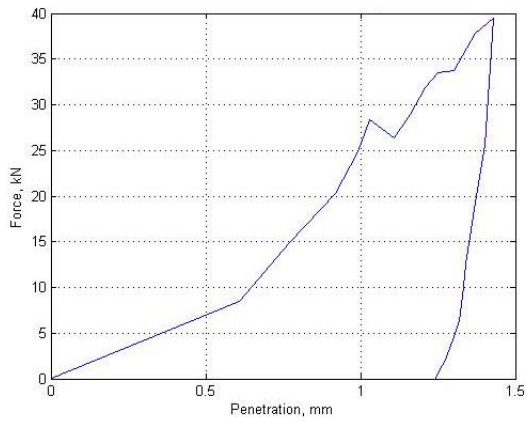


e) Moon white granite

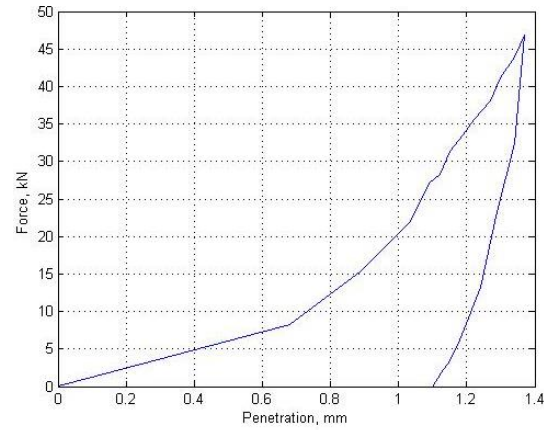


f) Black galaxy granite

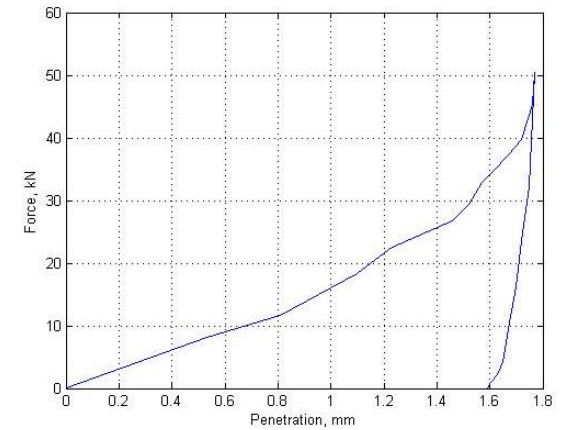
Figure 3.23 (a-f) Force–Penetration (F-P) curves for 45mm diameter chisel bit at 20° index angle for various types of rocks



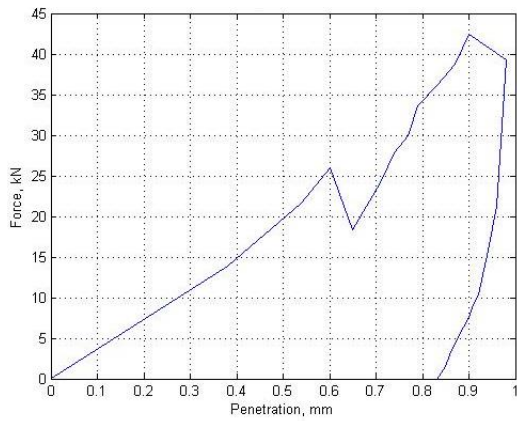
a) Marble



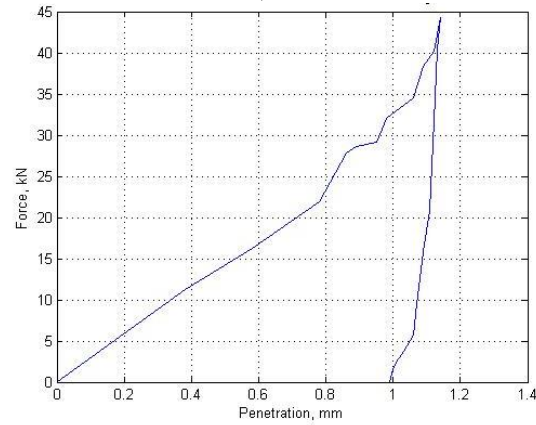
b) Limestone



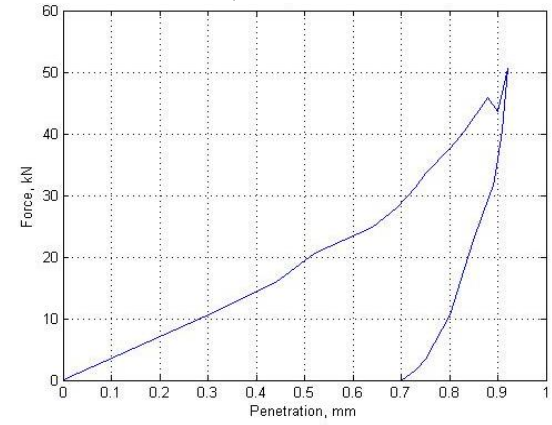
c) Basalt



d) Steel gray granite

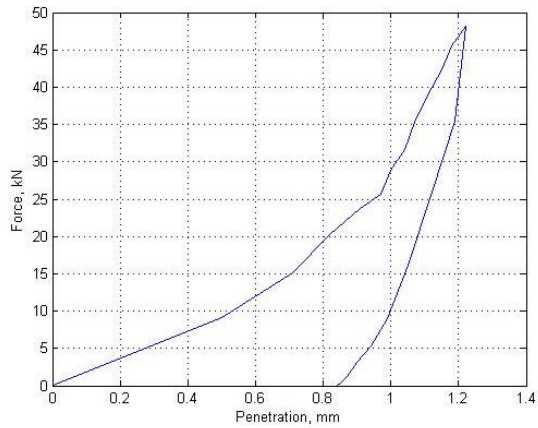


e) Moon white granite

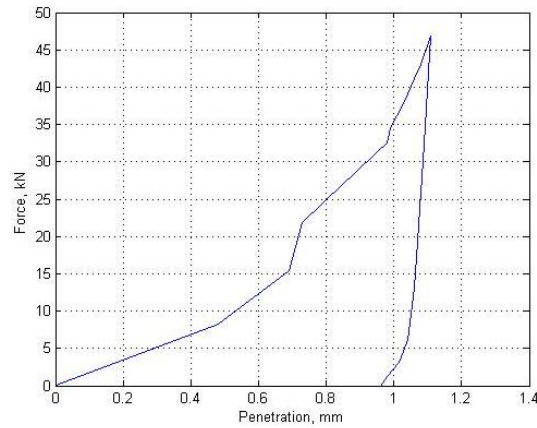


f) Black galaxy granite

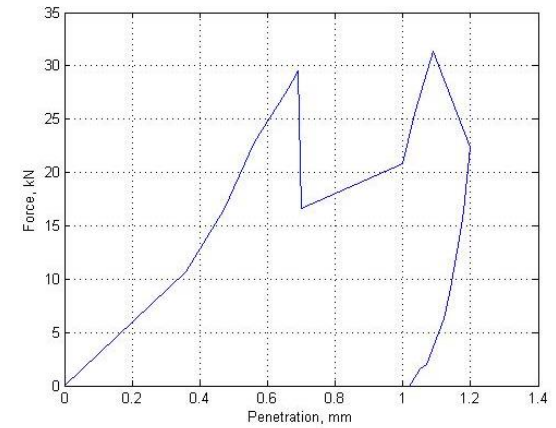
Figure 3.24 (a-f) Force–Penetration (F-P) curves for 45mm diameter chisel bit at 30° index angle for various types of rocks



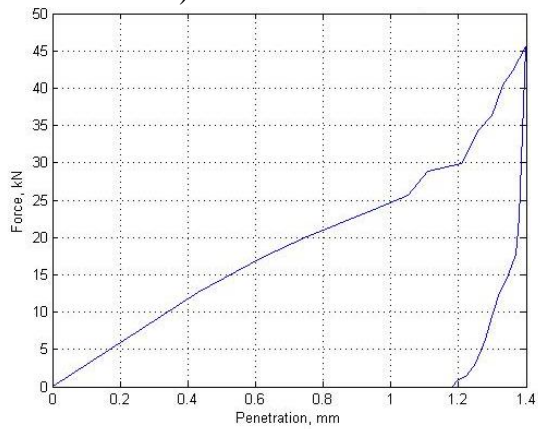
a) Marble



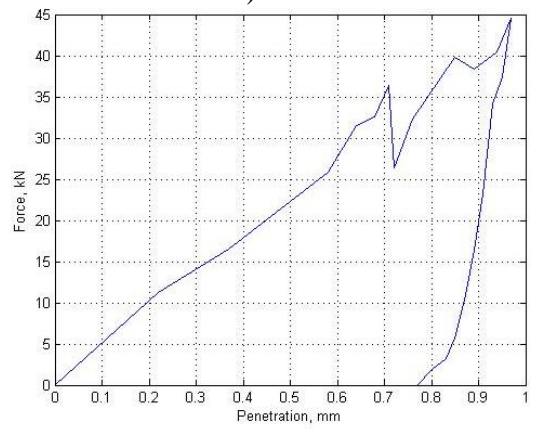
b) Limestone



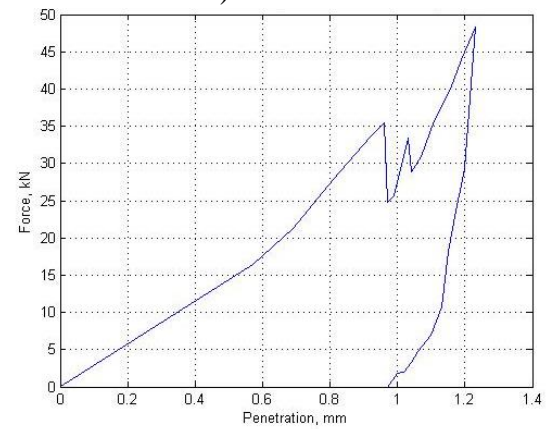
c) Basalt



d) Steel gray granite

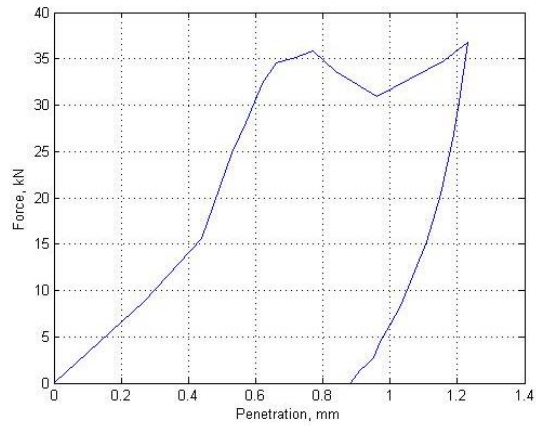


e) Moon white granite

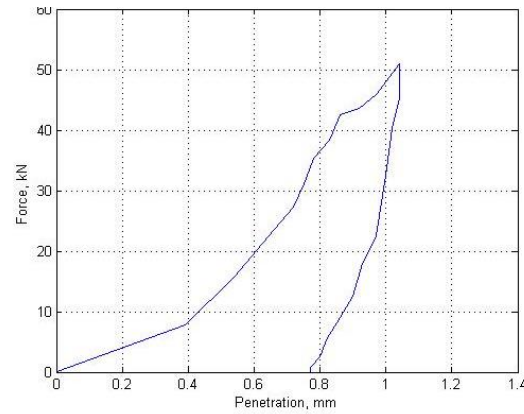


f) Black galaxy granite

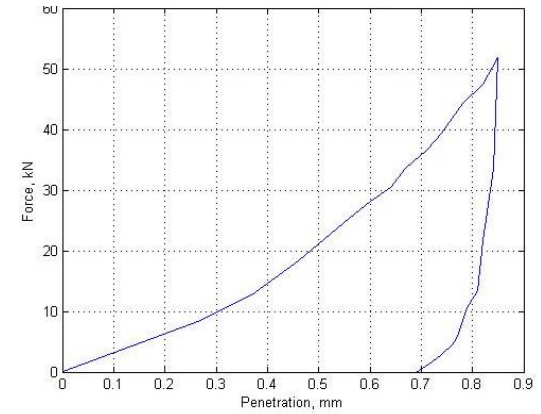
Figure 3.25 (a-f) Force–Penetration (F-P) curves for 45mm diameter chisel bit at 40° index angle for various types of rocks



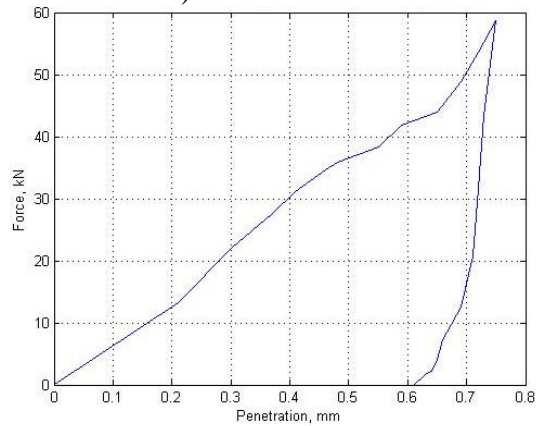
a) Marble



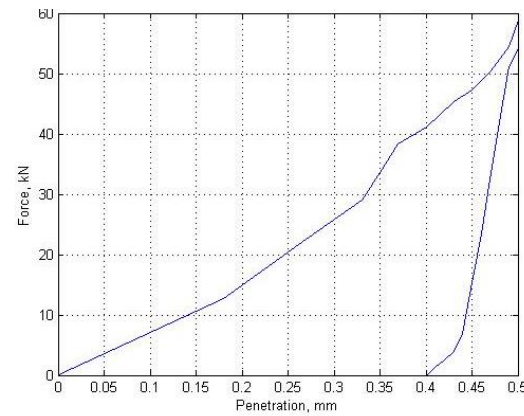
b) Limestone



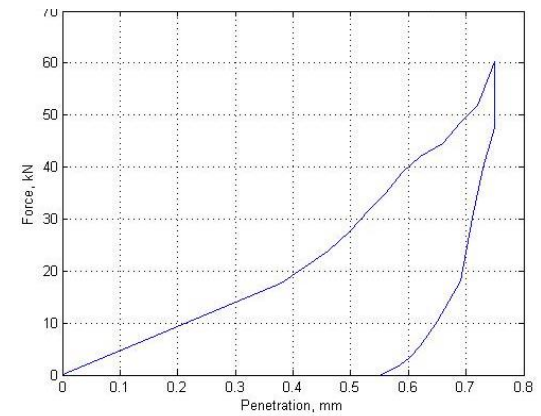
c) Basalt



d) Steel gray granite

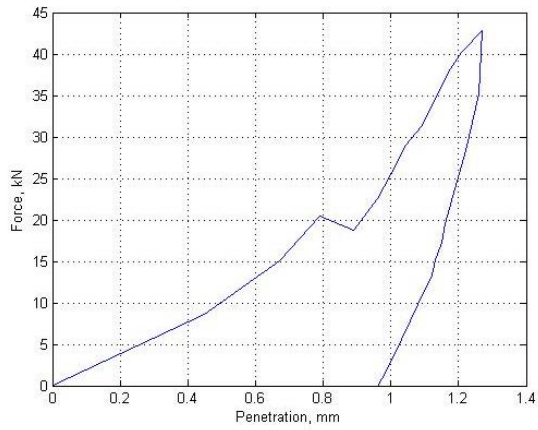


e) Moon white granite

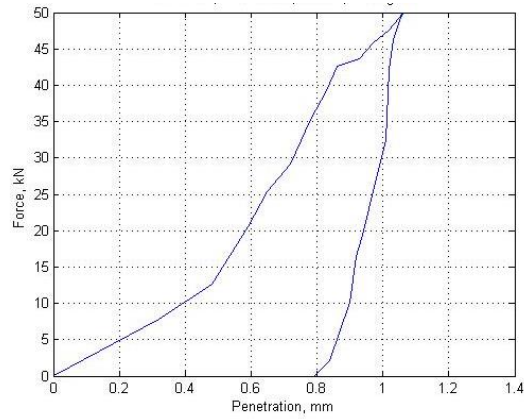


f) Black galaxy granite

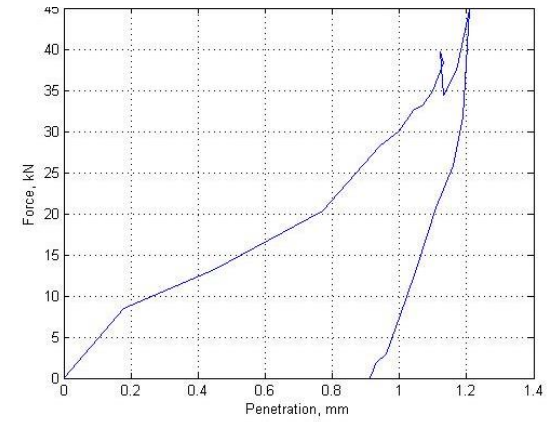
Figure 3.26 (a-f) Force–Penetration (F-P) curves for 48mm diameter chisel bit at 10^0 index angle for various types of rocks



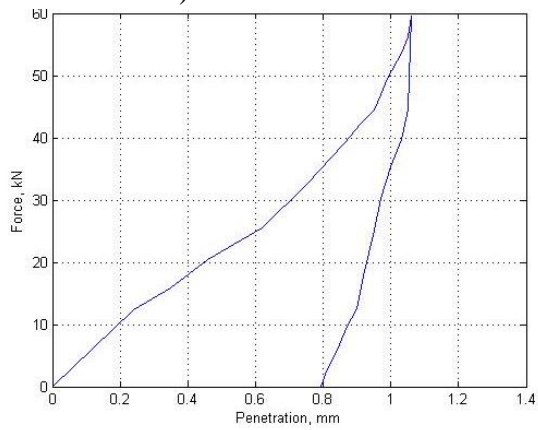
a) Marble



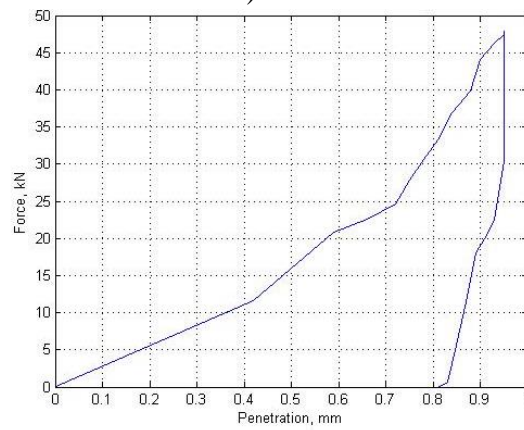
b) Limestone



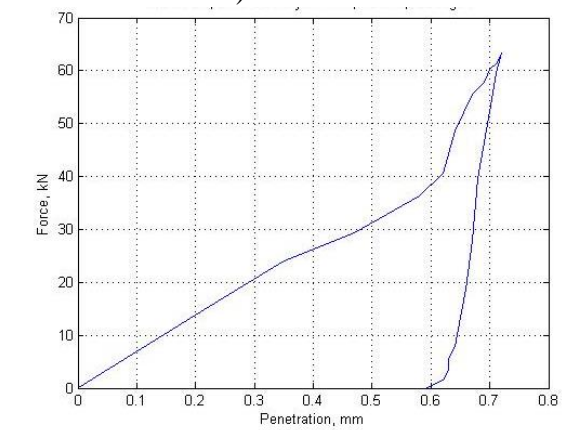
c) Basalt



d) Steel gray granite

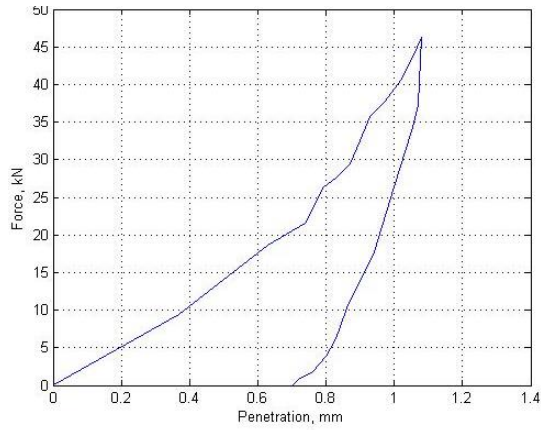


e) Moon white granite

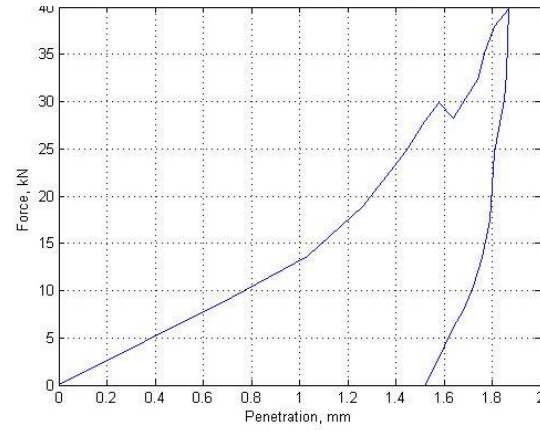


f) Black galaxy granite

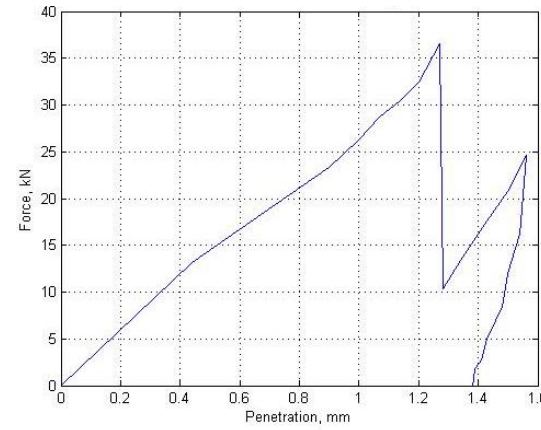
Figure 3.27 (a-f) Force–Penetration (F-P) curves for 48mm diameter chisel bit at 20° index angle for various types of rocks



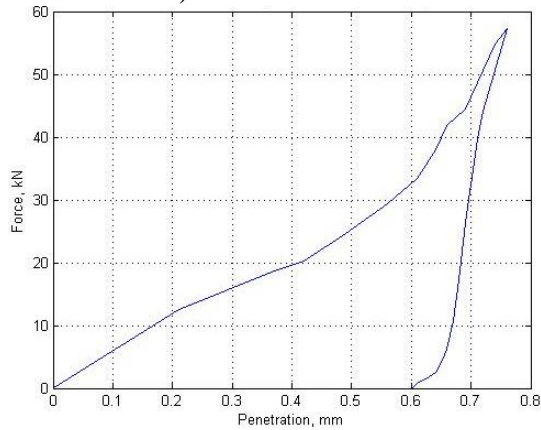
a) Marble



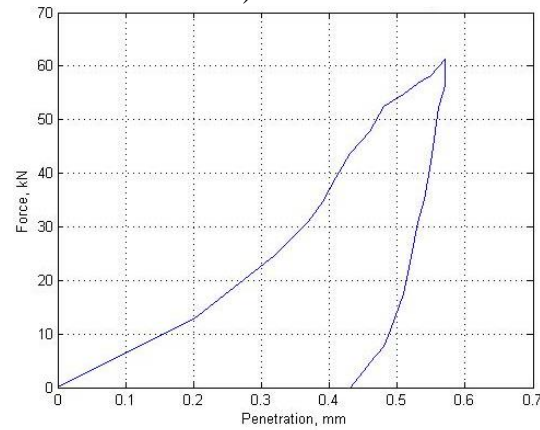
b) Limestone



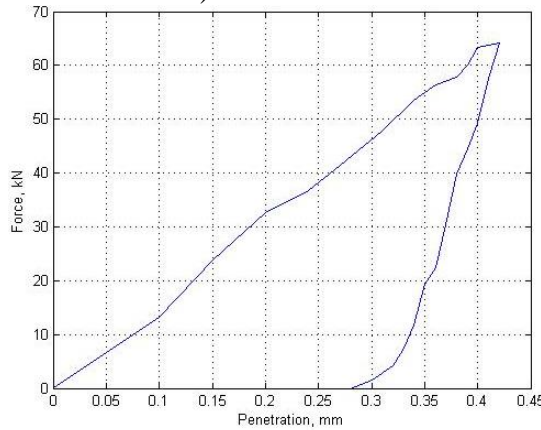
c) Basalt



d) Steel gray granite

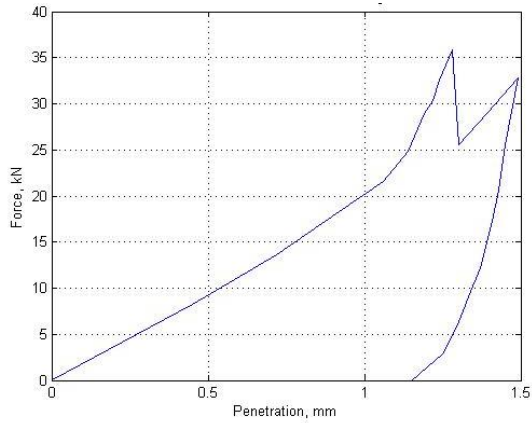


e) Moon white granite

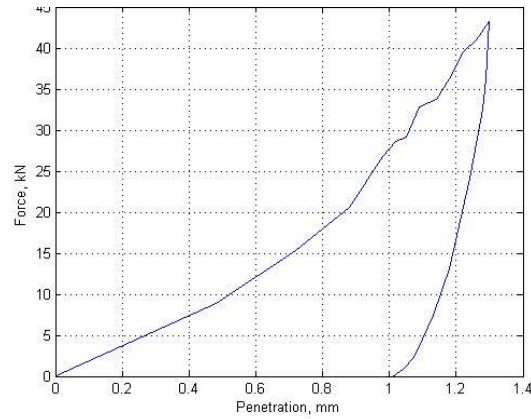


f) Black galaxy granite

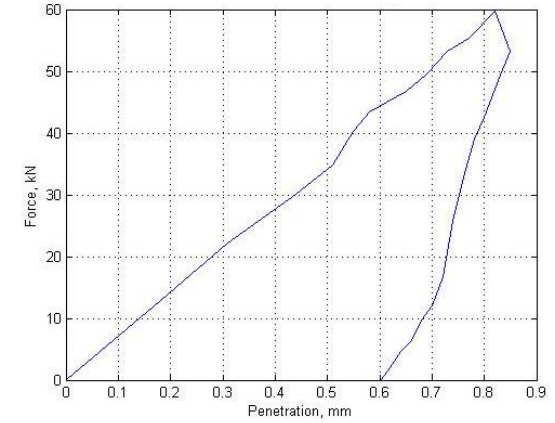
Figure 3.28 (a-f) Force–Penetration (F-P) curves for 48mm diameter chisel bit at 30° index angle for various types of rocks



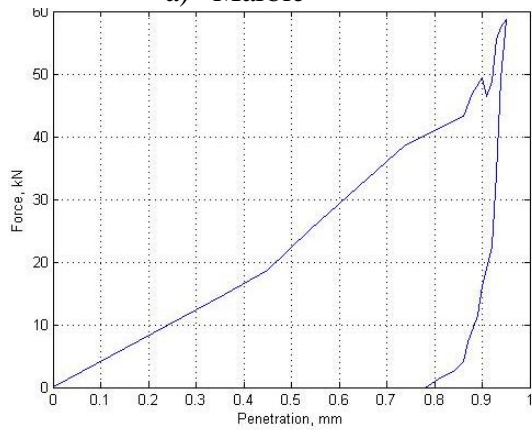
a) Marble



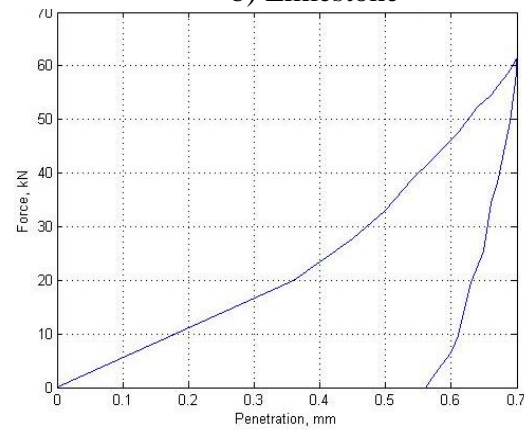
b) Limestone



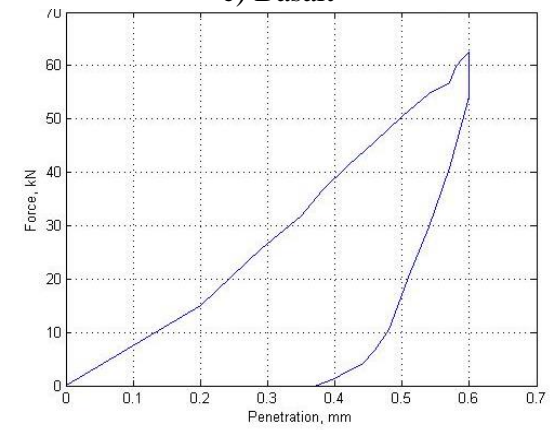
c) Basalt



d) Steel gray granite

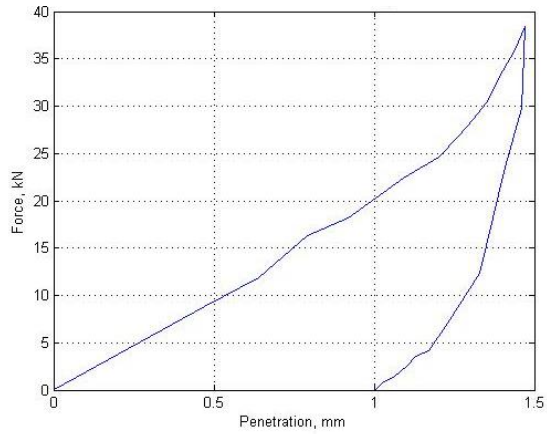


e) Moon white granite

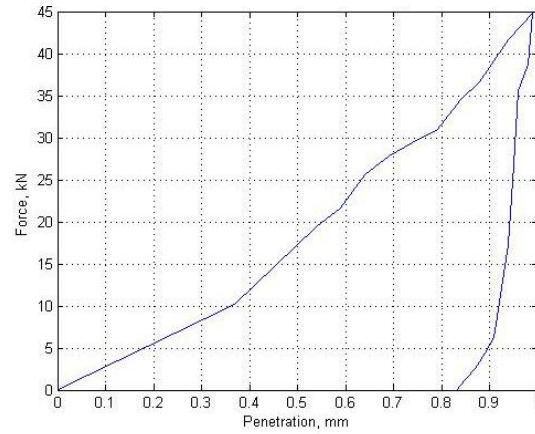


f) Black galaxy granite

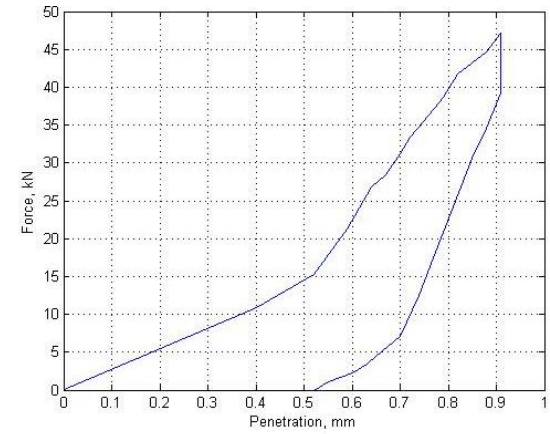
Figure 3.29 (a-f) Force–Penetration (F-P) curves for 48mm diameter chisel bit at 40° index angle for various types of rocks



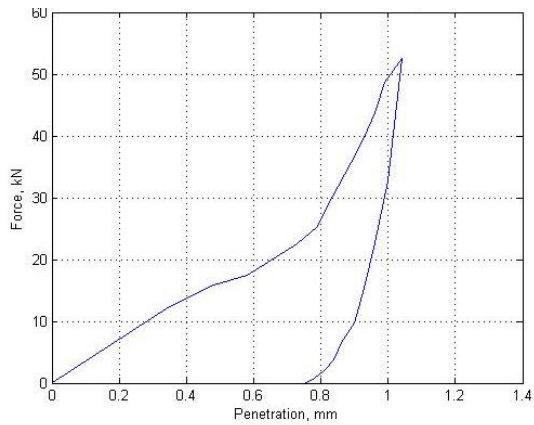
a) Marble



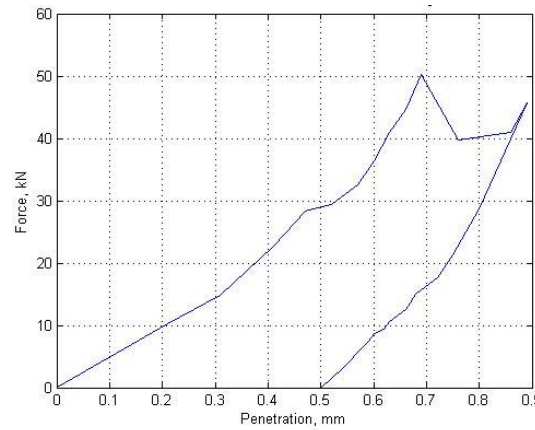
b) Limestone



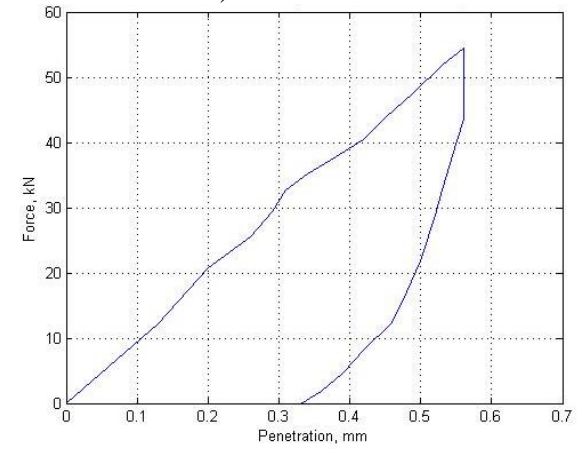
c) Basalt



d) Steel gray granite

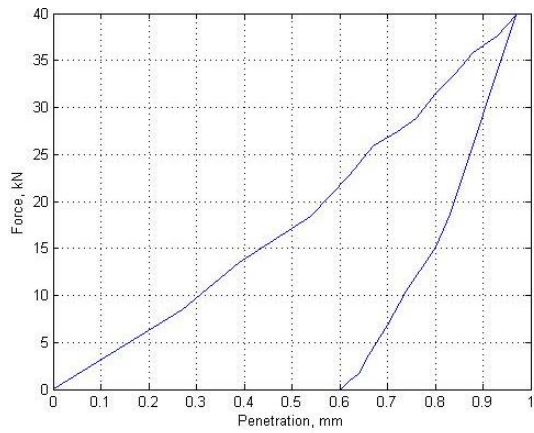


e) Moon white granite

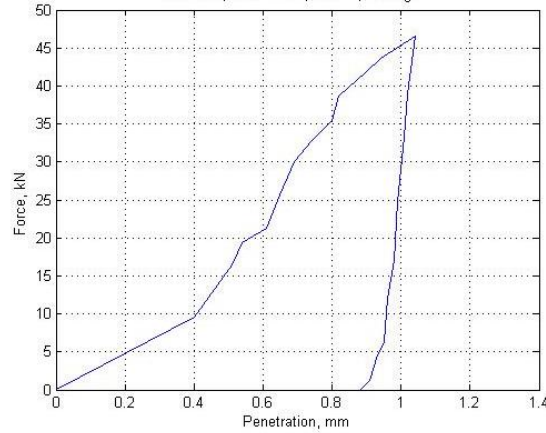


f) Black galaxy granite

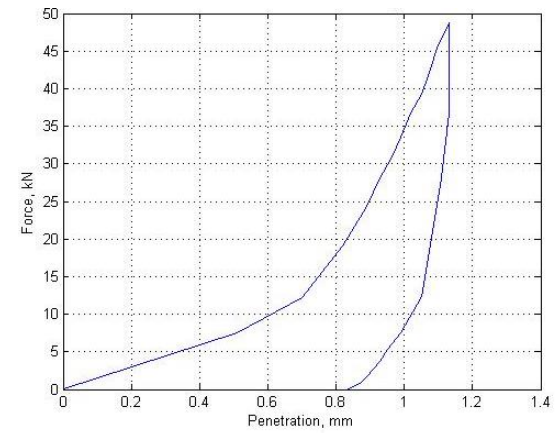
Figure 3.30 (a-f) Force–Penetration (F-P) curves for 35mm diameter cross bit at 10^0 index angle for various types of rocks



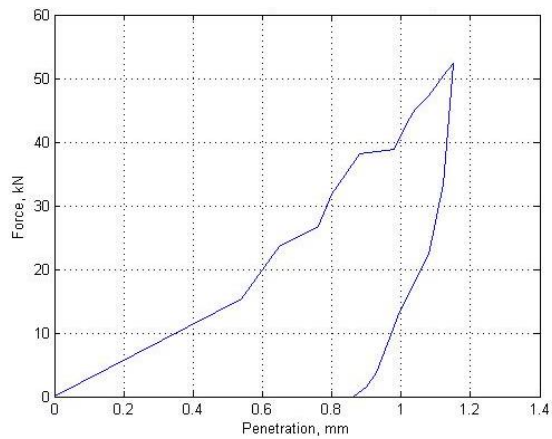
a) Marble



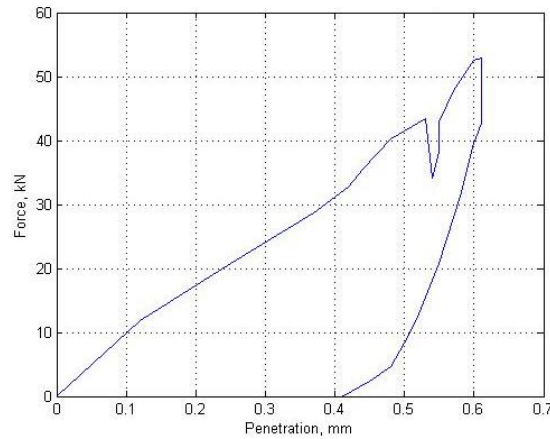
b) Limestone



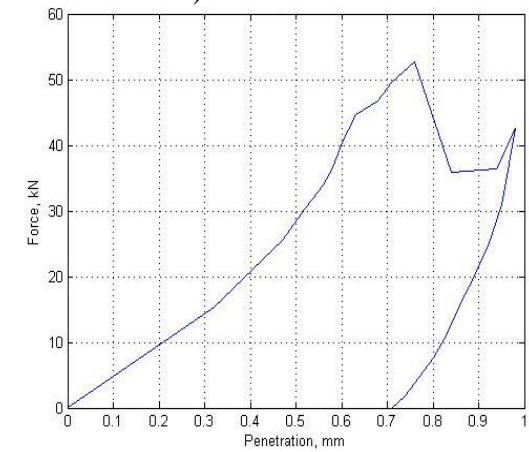
c) Basalt



d) Steel gray granite

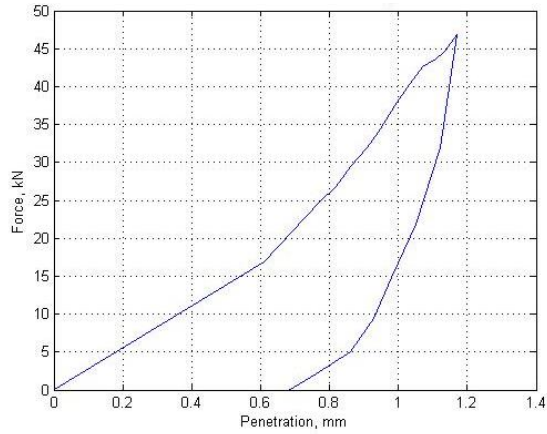


e) Moon white granite

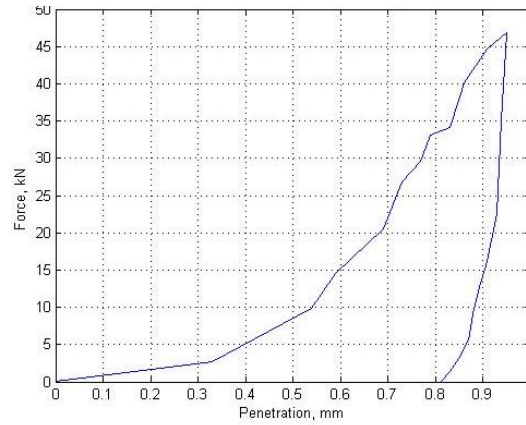


f) Black galaxy granite

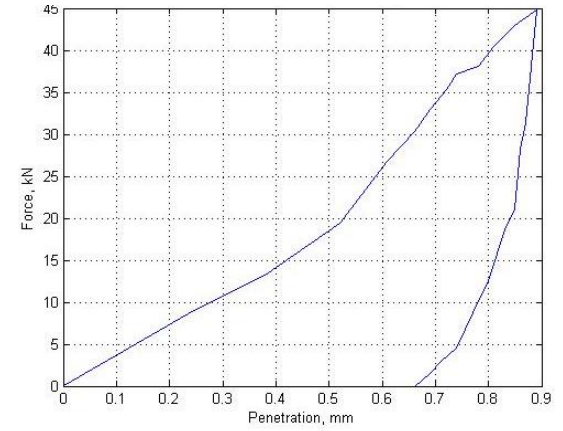
Figure 3.31 (a-f) Force–Penetration (F-P) curves for 35mm diameter cross bit at 20° index angle for various types of rocks



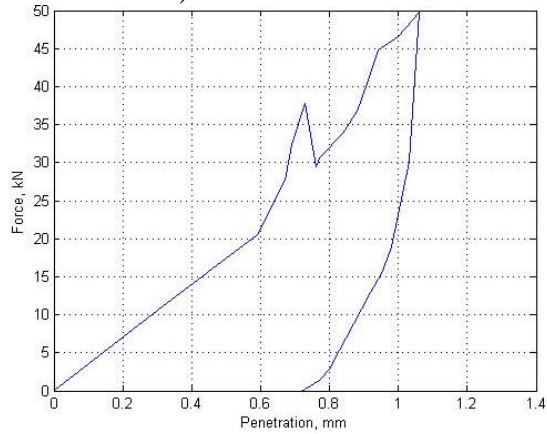
a) Marble



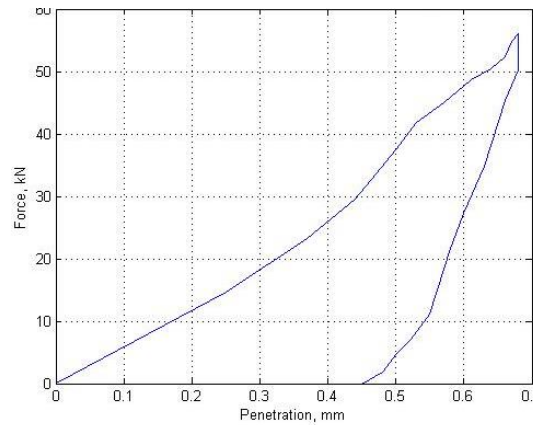
b) Limestone



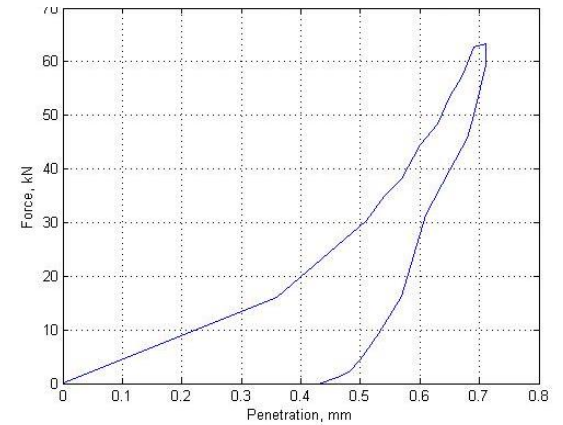
c) Basalt



d) Steel gray granite

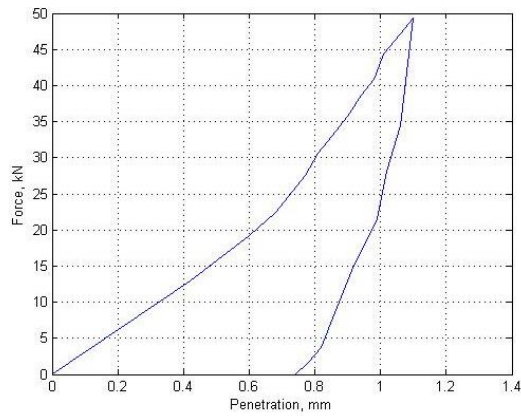


e) Moon white granite

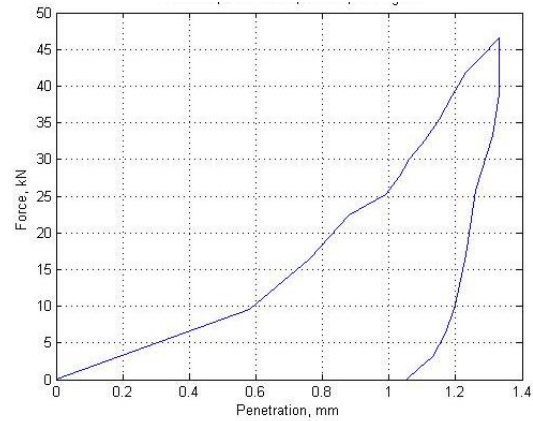


f) Black galaxy granite

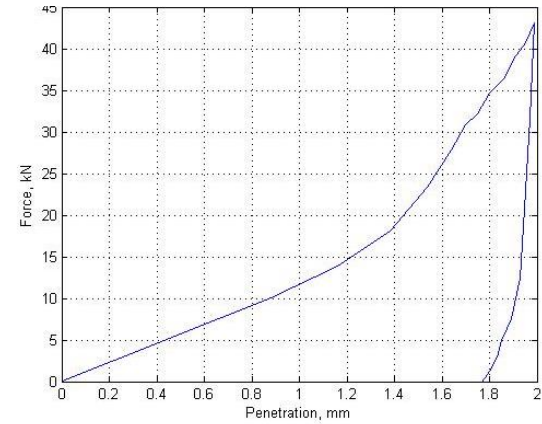
Figure 3.32 (a-f) Force–Penetration (F-P) curves for 35mm diameter cross bit at 30° index angle for various types of rocks



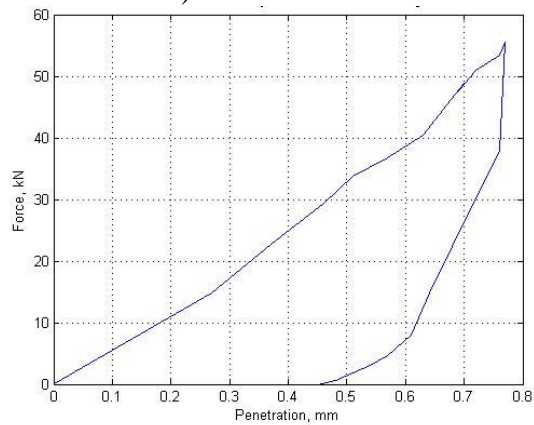
a) Marble



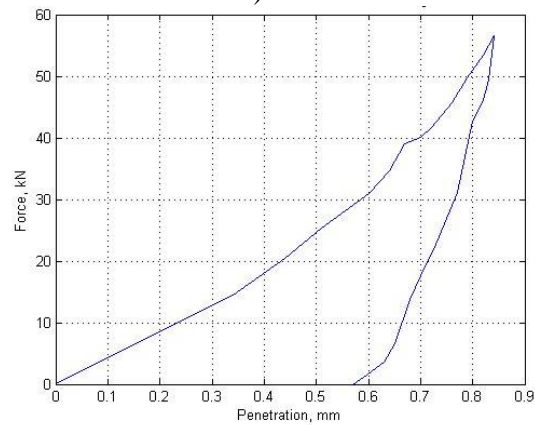
b) Limestone



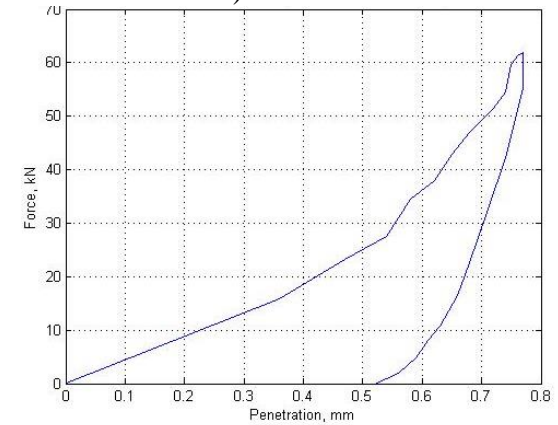
c) Basalt



d) Steel gray granite

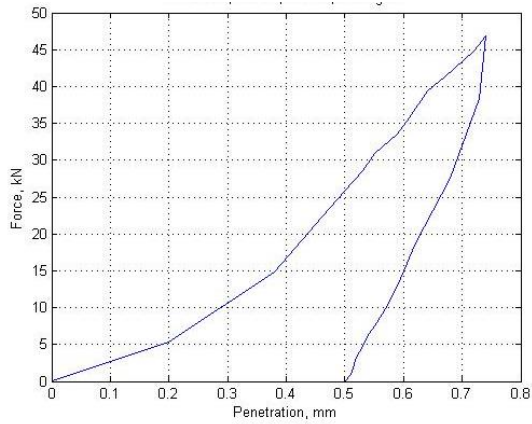


e) Moon white granite

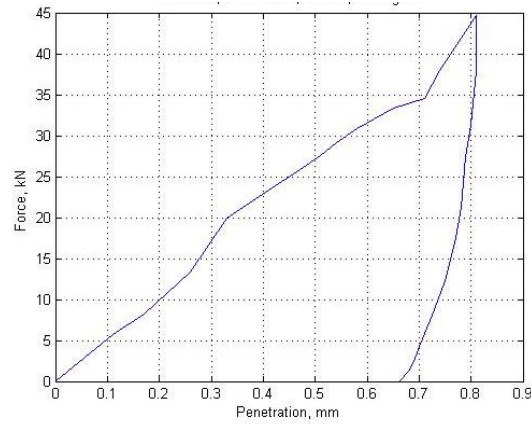


f) Black galaxy granite

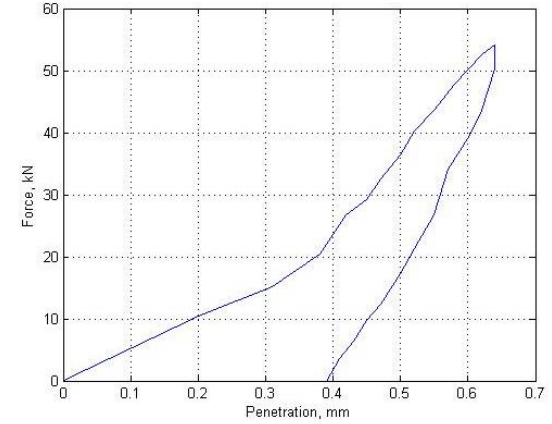
Figure 3.33 (a-f) Force–Penetration (F-P) curves for 35mm diameter cross bit at 40° index angle for various types of rocks



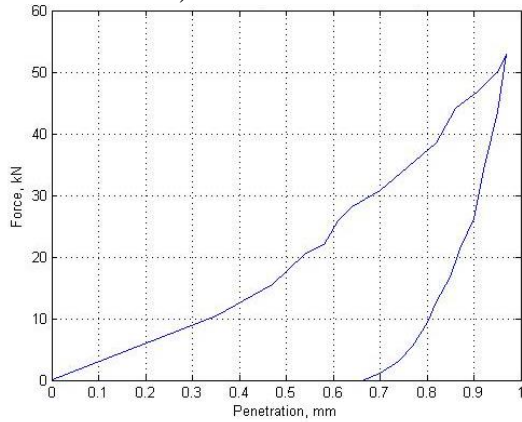
a) Marble



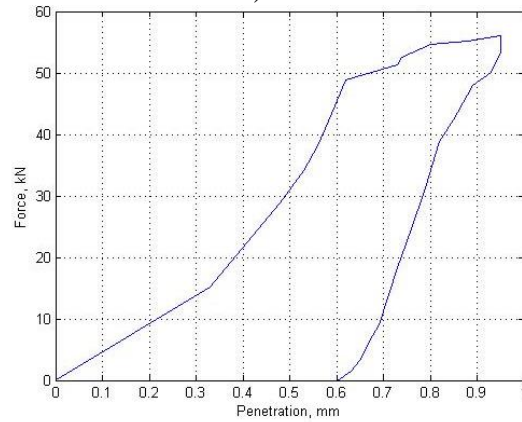
b) Limestone



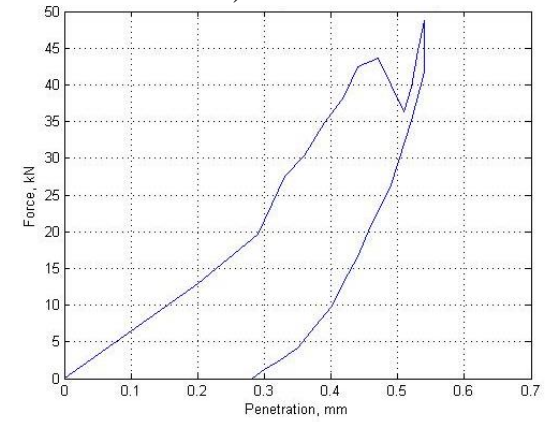
c) Basalt



d) Steel gray granite

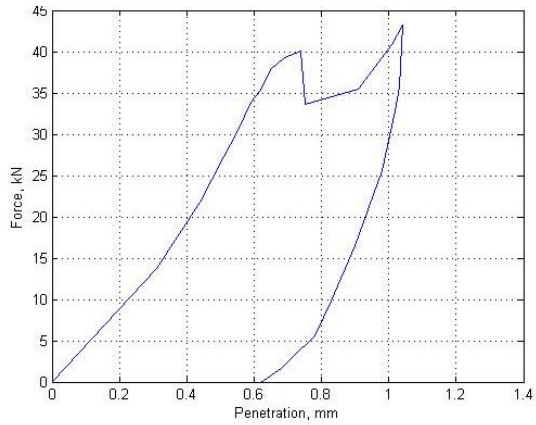


e) Moon white granite

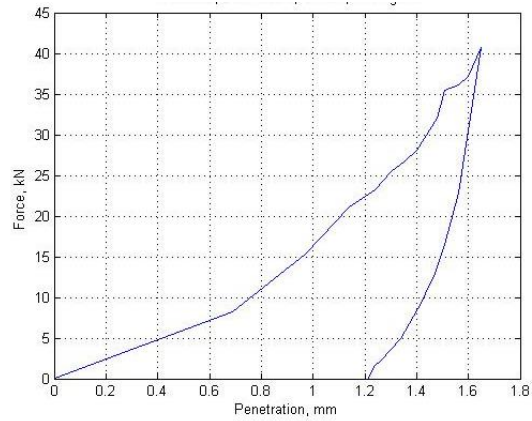


f) Black galaxy granite

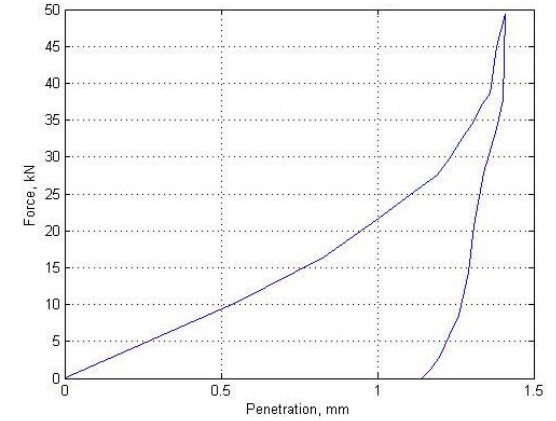
Figure 3.34 (a-f) Force–Penetration (F-P) curves for 38mm diameter cross bit at 10^0 index angle for various types of rocks



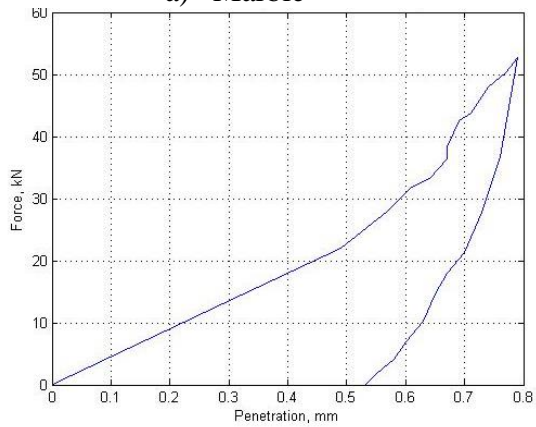
a) Marble



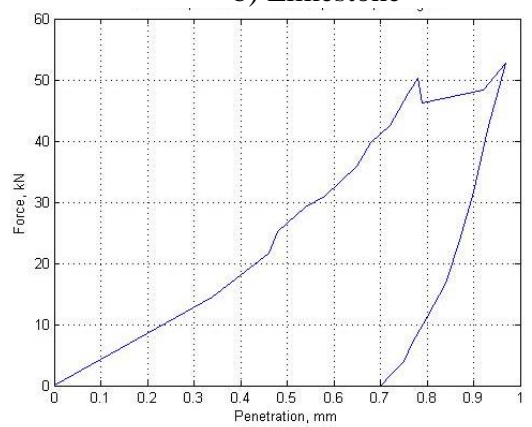
b) Limestone



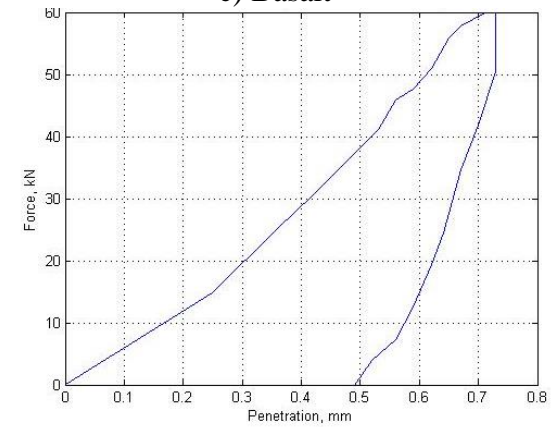
c) Basalt



d) Steel gray granite

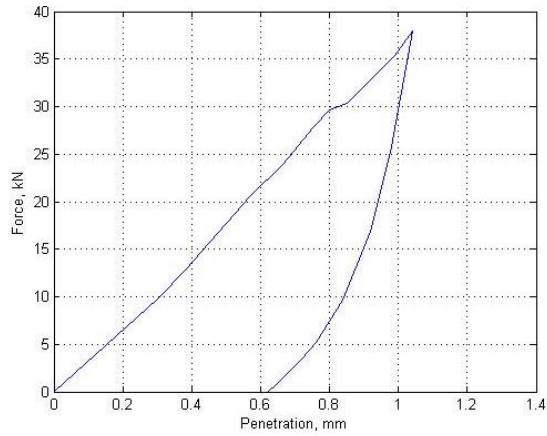


e) Moon white granite

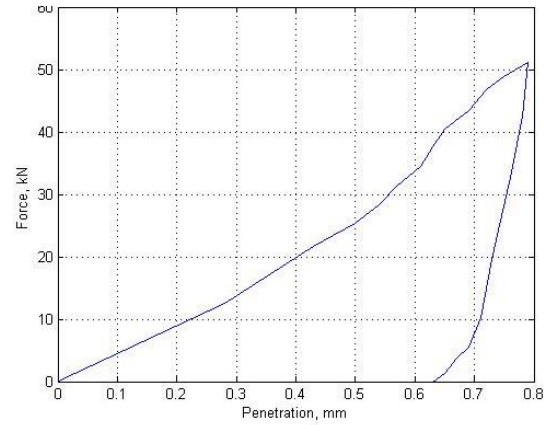


f) Black galaxy granite

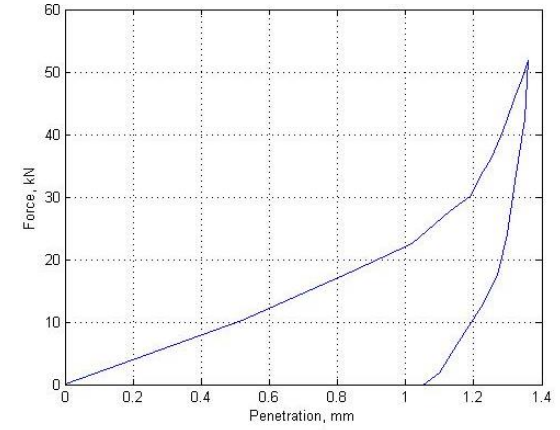
Figure 3.35 (a-f) Force–Penetration (F-P) curves for 38mm diameter cross bit at 20° index angle for various types of rocks



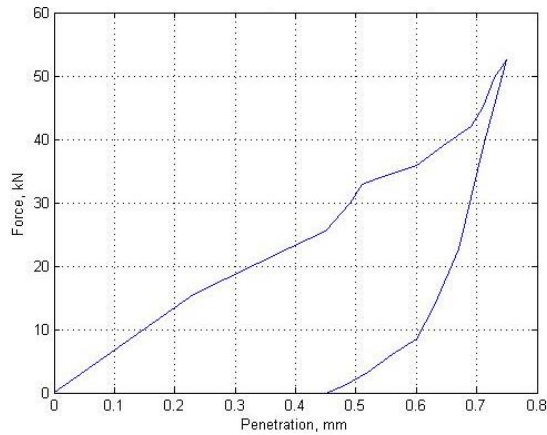
a) Marble



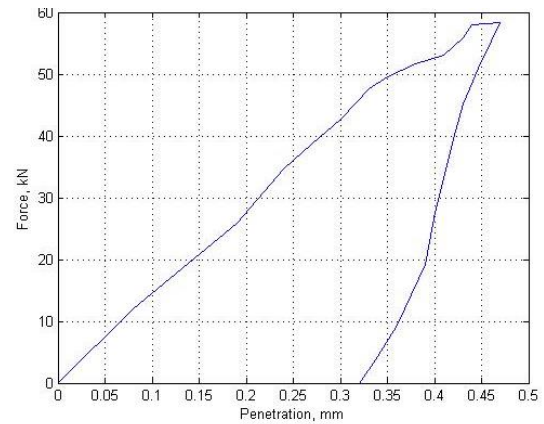
b) Limestone



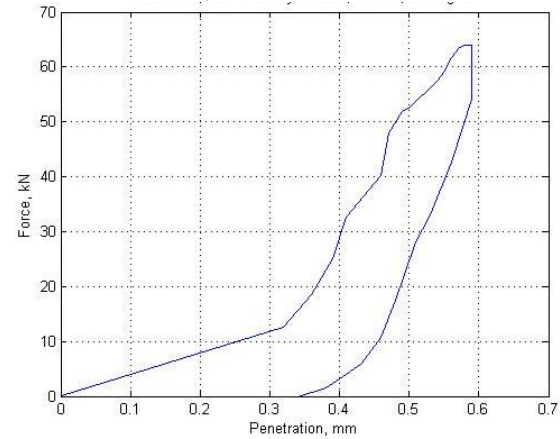
c) Basalt



d) Steel gray granite

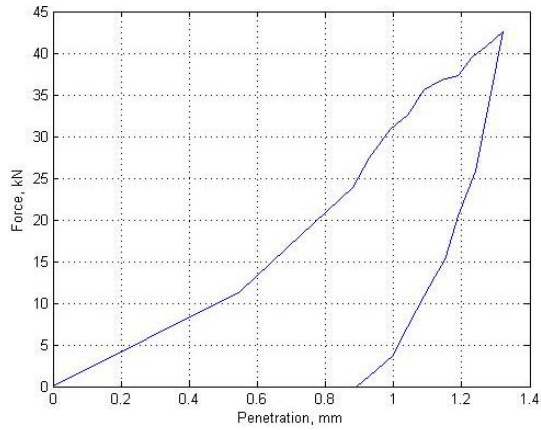


e) Moon white granite

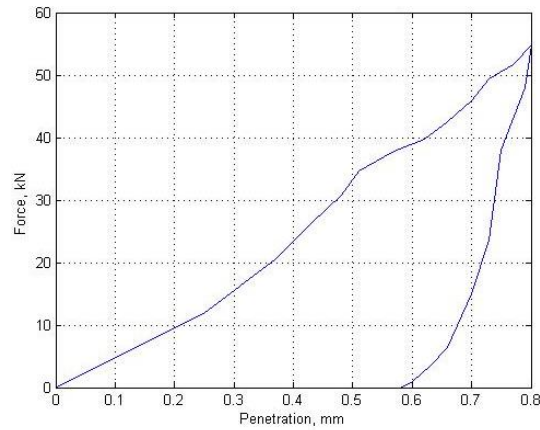


f) Black galaxy granite

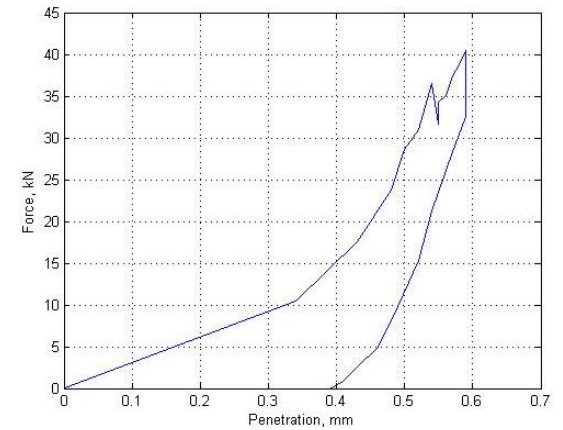
Figure 3.36 (a-f) Force–Penetration (F-P) curves for 38mm diameter cross bit at 30° index angle for various types of rocks



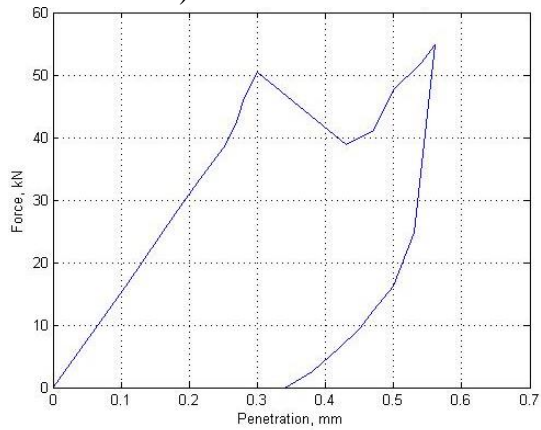
a) Marble



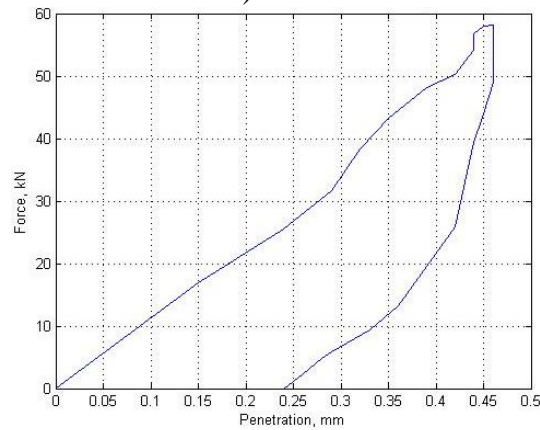
b) Limestone



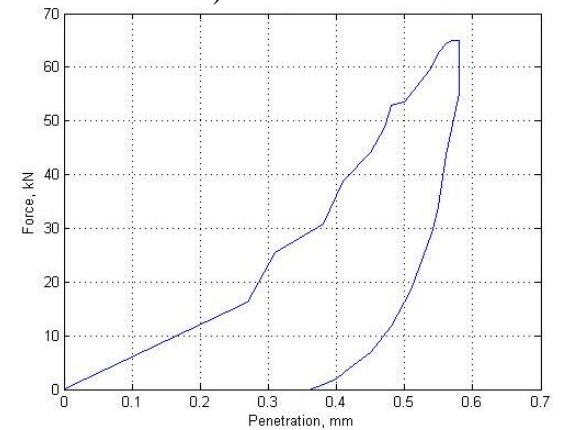
c) Basalt



d) Steel gray granite

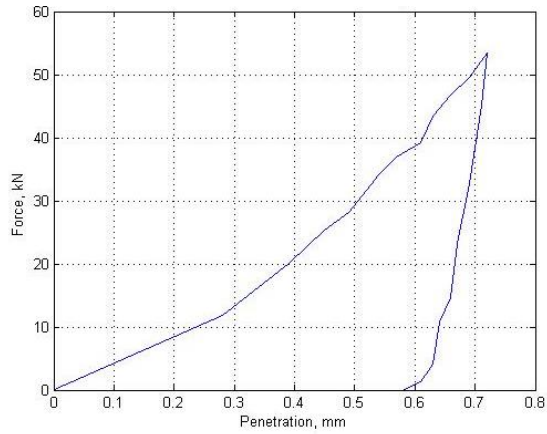


e) Moon white granite

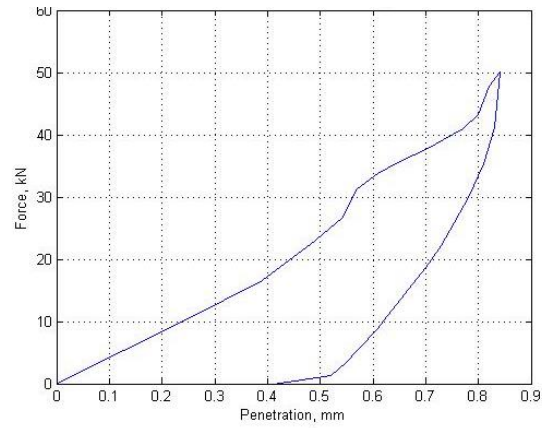


f) Black galaxy granite

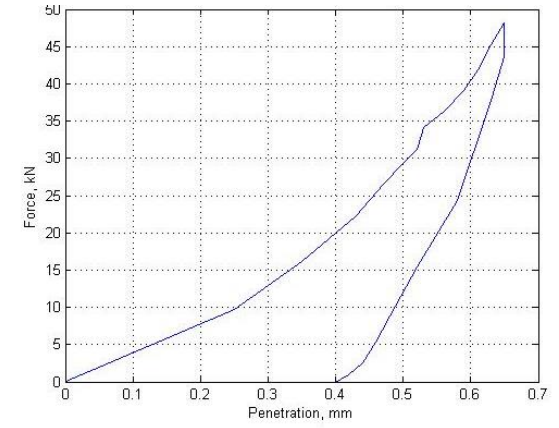
Figure 3.37 (a-f) Force–Penetration (F-P) curves for 38mm diameter cross bit at 40° index angle for various types of rocks



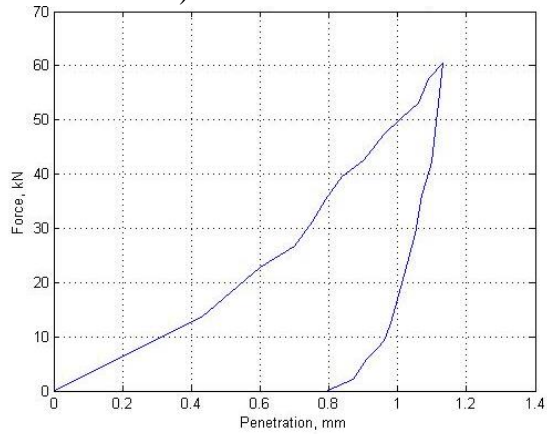
a) Marble



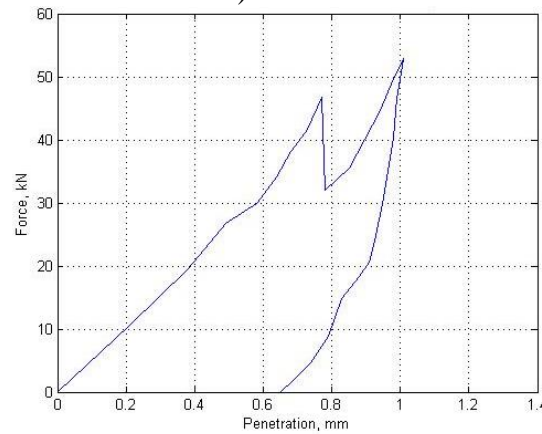
b) Limestone



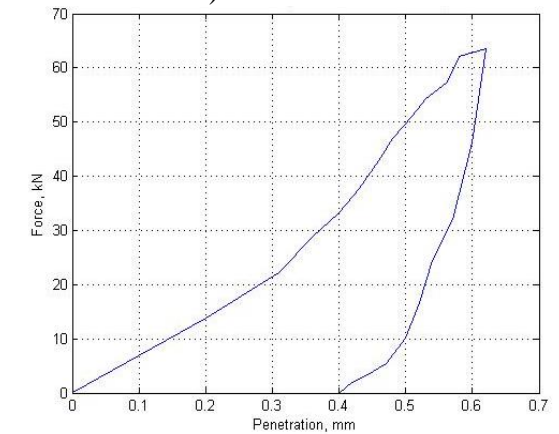
c) Basalt



d) Steel gray granite

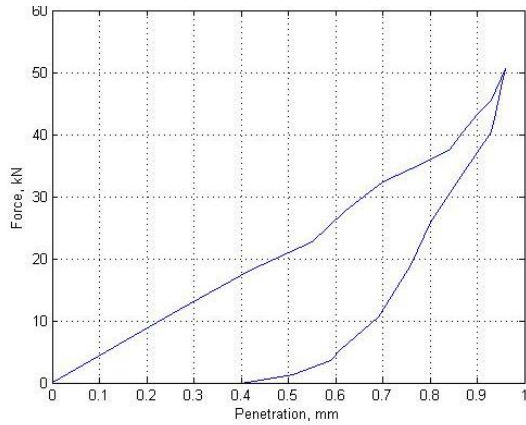


e) Moon white granite

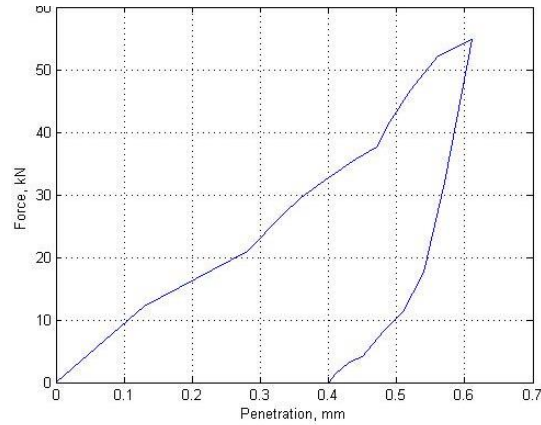


f) Black galaxy granite

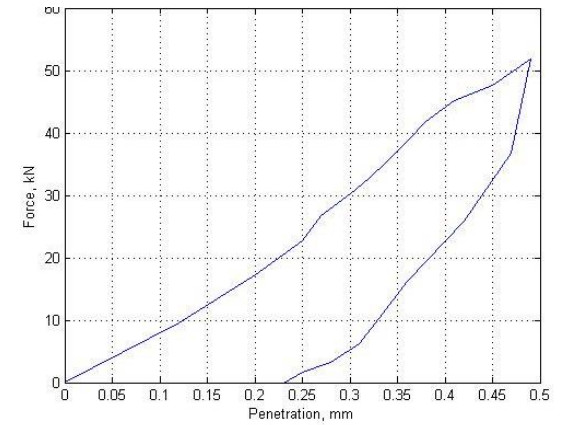
Figure 3.38 (a-f) Force–Penetration (F-P) curves for 45mm diameter cross bit at 10^0 index angle for various types of rocks



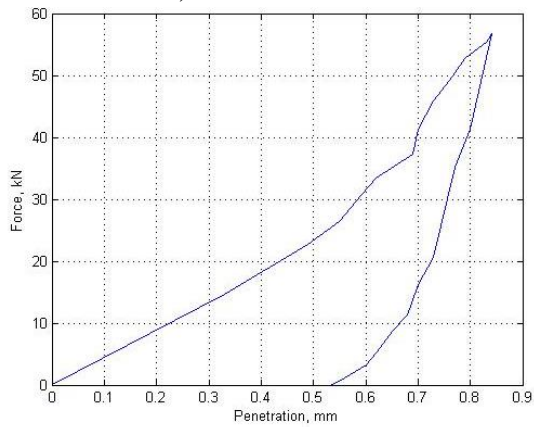
a) Marble



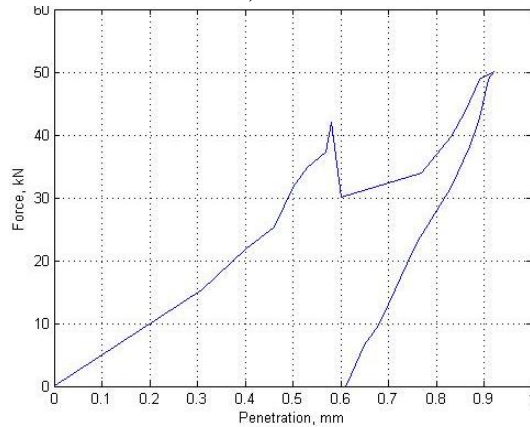
b) Limestone



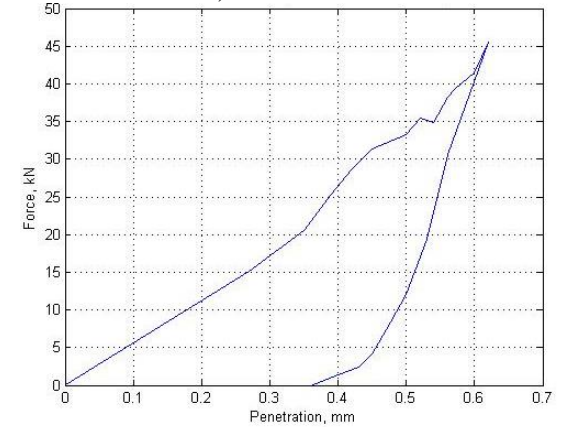
c) Basalt



d) Steel gray granite

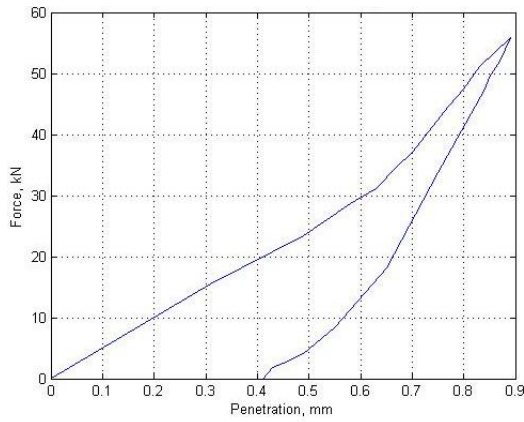


e) Moon white granite

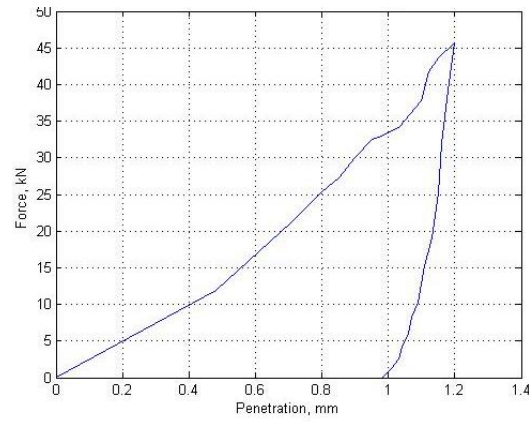


f) Black galaxy granite

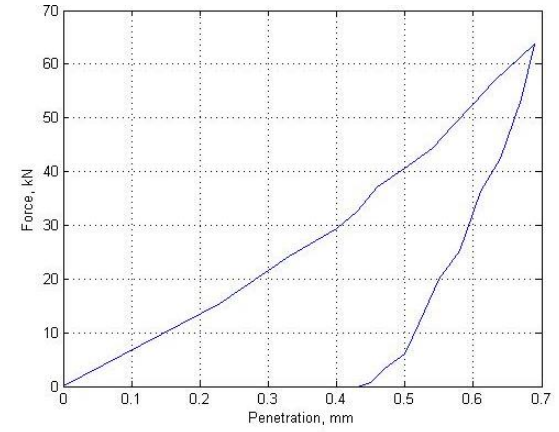
Figure 3.39 (a-f) Force–Penetration (F-P) curves for 45mm diameter cross bit at 20⁰ index angle for various types of rocks



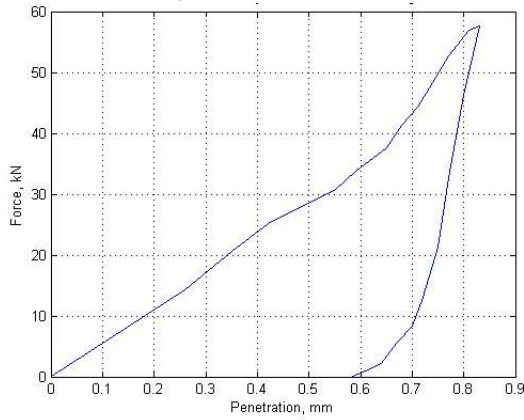
a) Marble



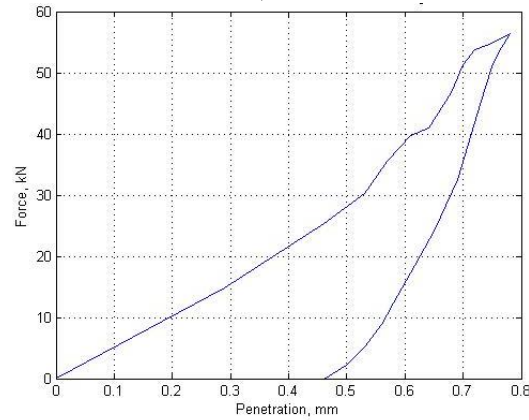
b) Limestone



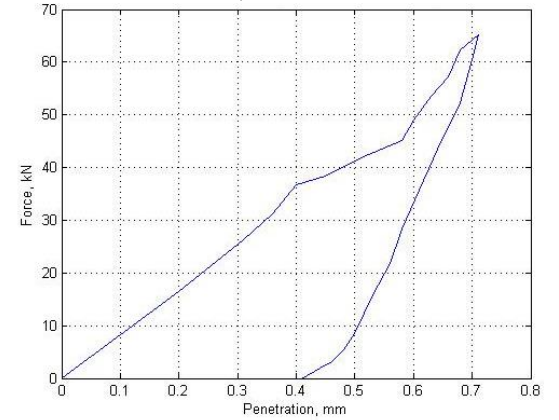
c) Basalt



d) Steel gray granite

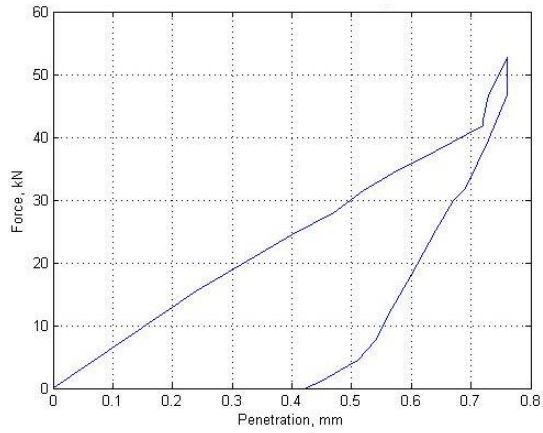


e) Moon white granite

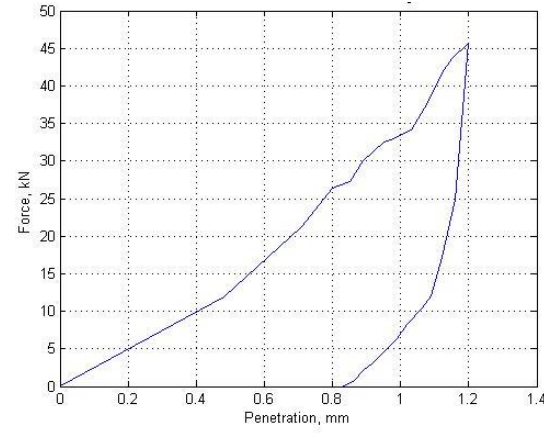


f) Black galaxy granite

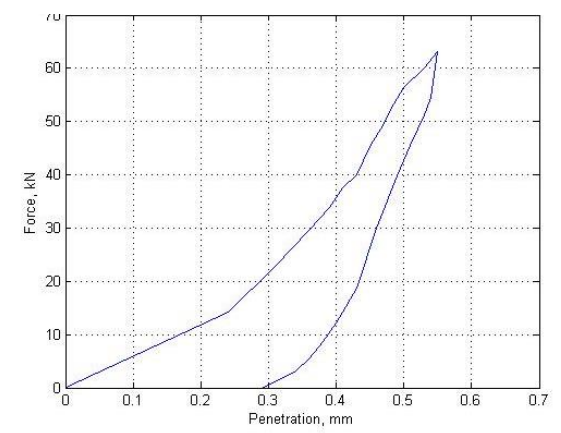
Figure 3.40 (a-f) Force–Penetration (F-P) curves for 45mm diameter cross bit at 30° index angle for various types of rocks



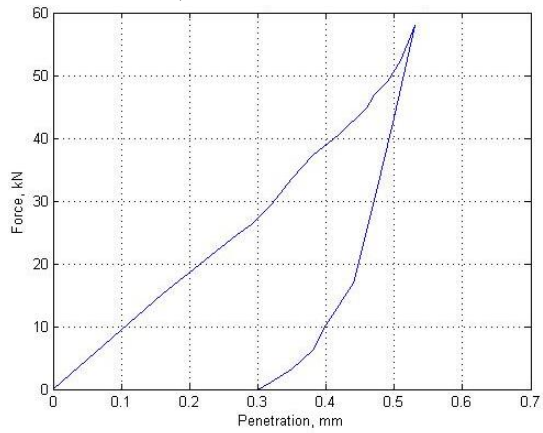
a) Marble



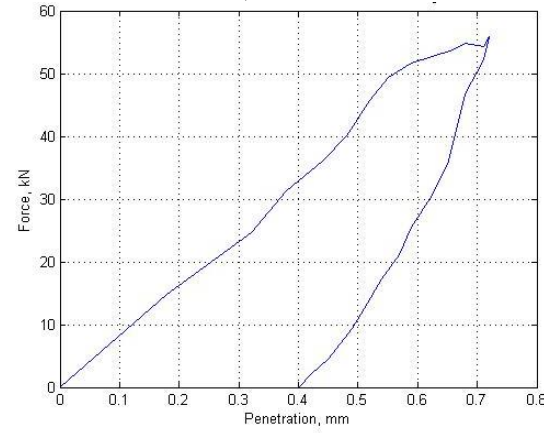
b) Limestone



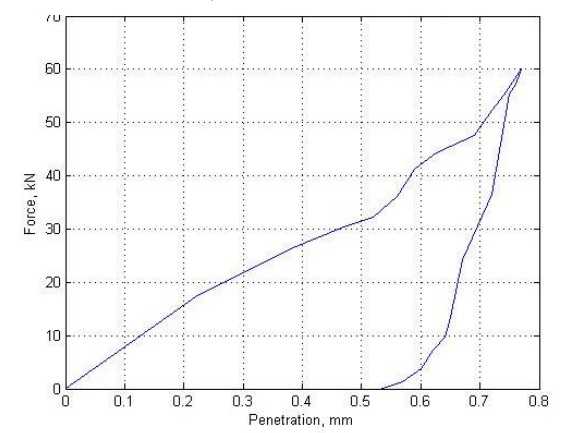
c) Basalt



d) Steel gray granite

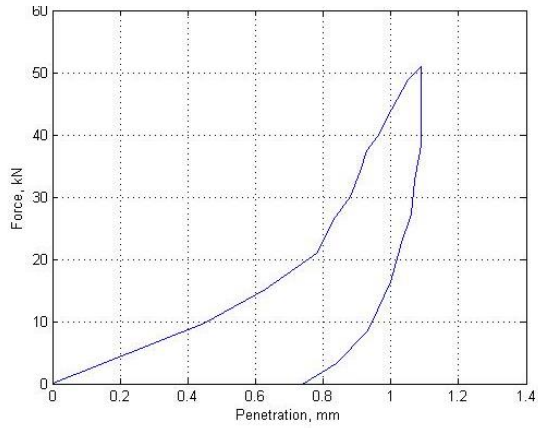


e) Moon white granite

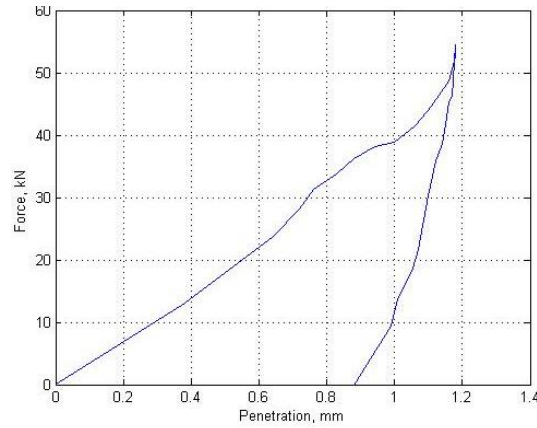


f) Black galaxy granite

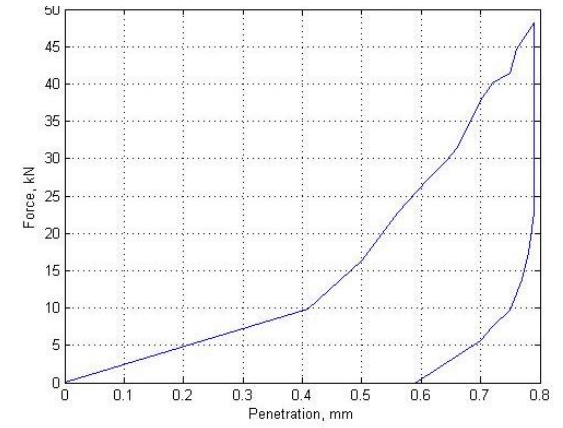
Figure 3.41 (a-f) Force–Penetration (F-P) curves for 45mm diameter cross bit at 40° index angle for various types of rocks



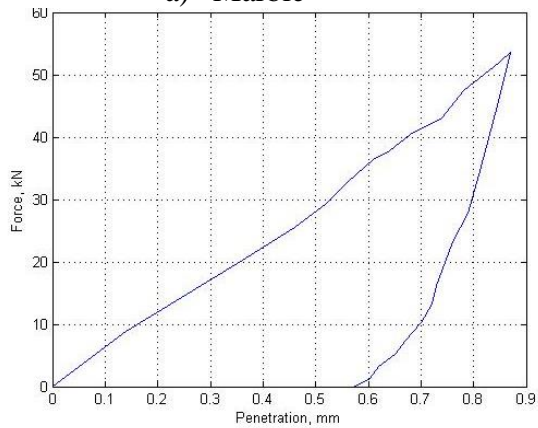
a) Marble



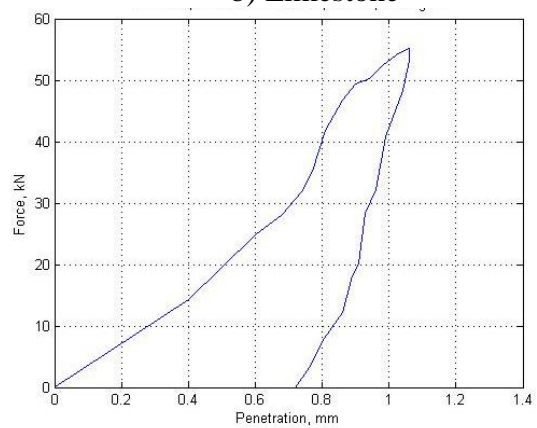
b) Limestone



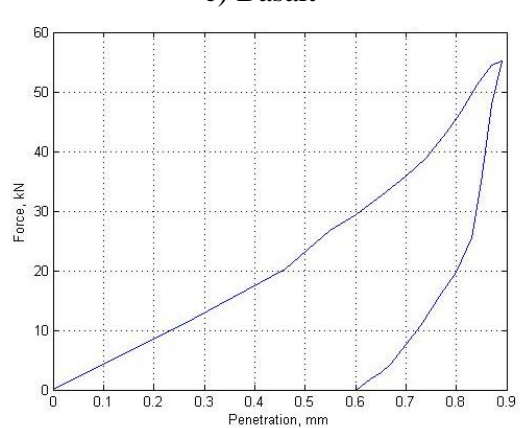
c) Basalt



d) Steel gray granite

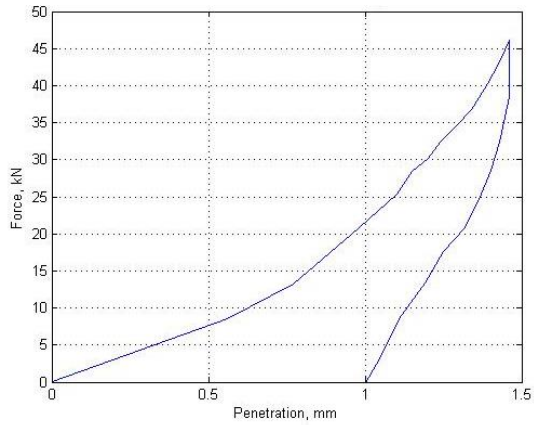


e) Moon white granite

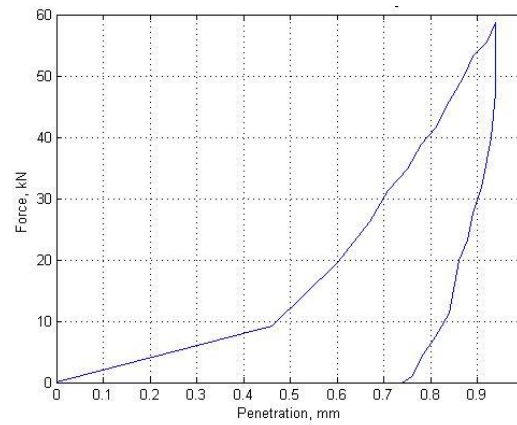


f) Black galaxy granite

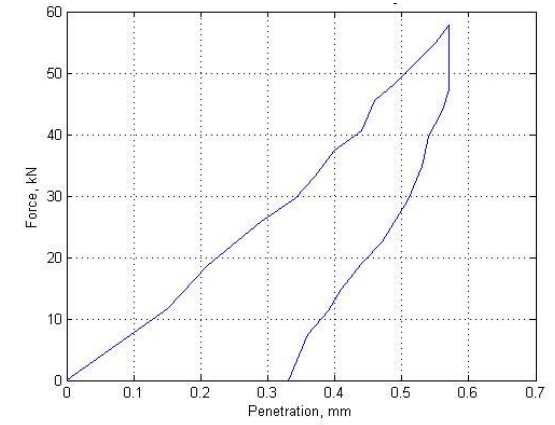
Figure 3.42 (a-f) Force–Penetration (F-P) curves for 48mm diameter cross bit at 10^0 index angle for various types of rocks



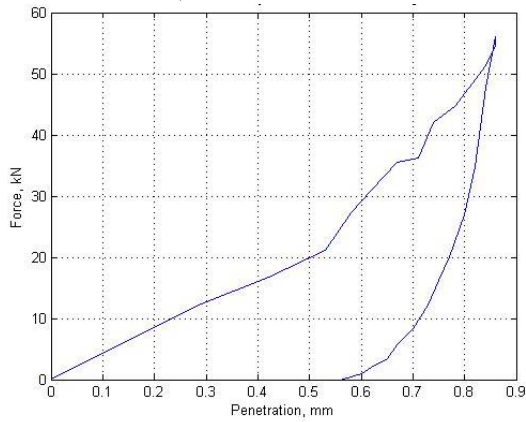
a) Marble



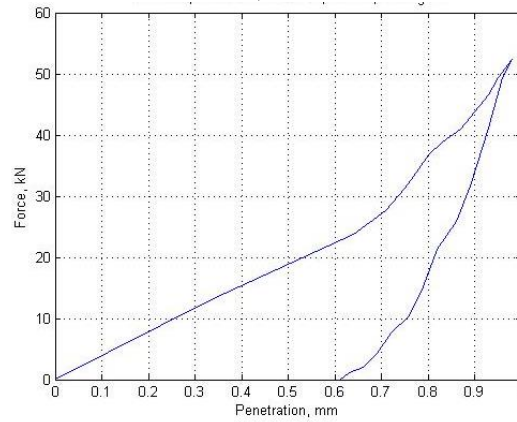
b) Limestone



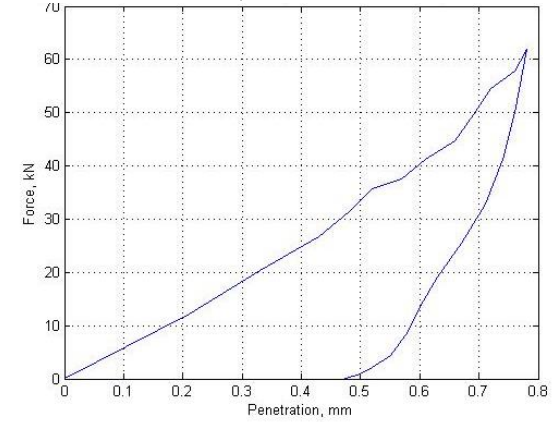
c) Basalt



d) Steel gray granite

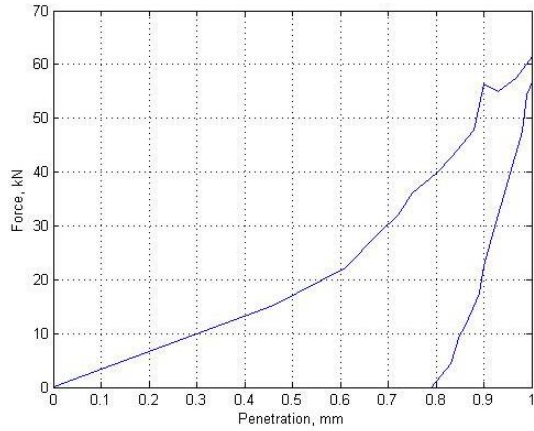


e) Moon white granite

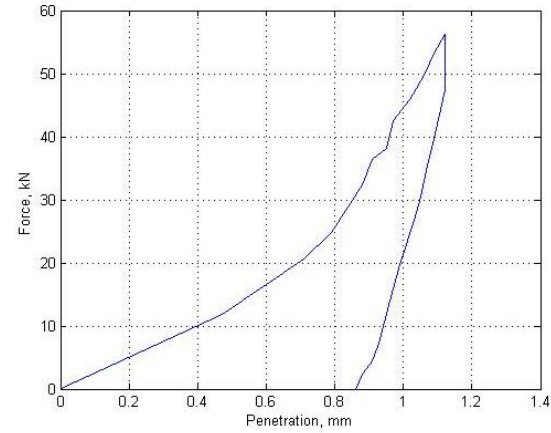


f) Black galaxy granite

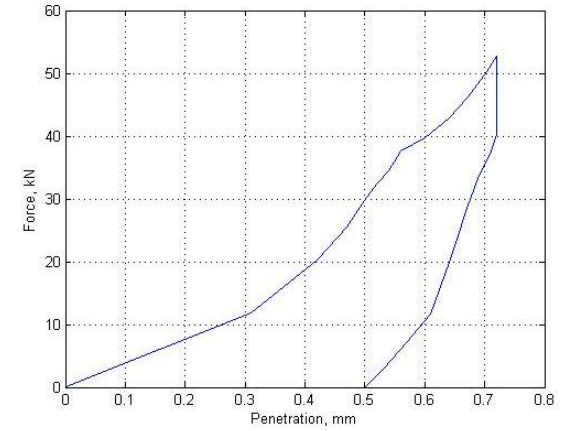
Figure 3.43 (a-f) Force–Penetration (F-P) curves for 48mm diameter cross bit at 20° index angle for various types of rocks



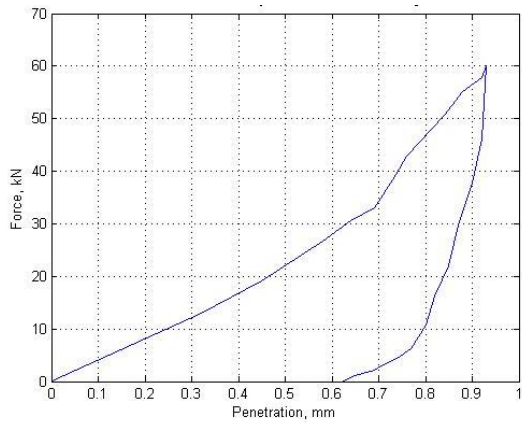
a) Marble



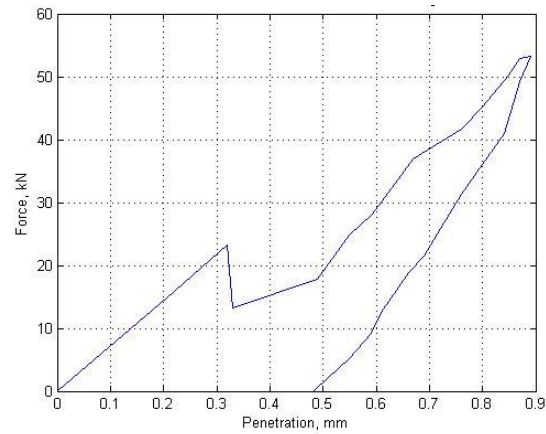
b) Limestone



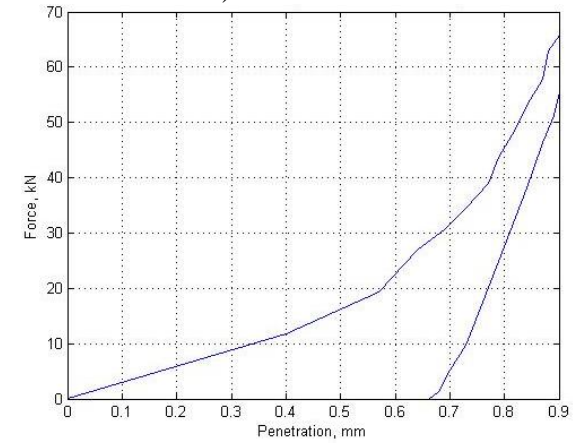
c) Basalt



d) Steel gray granite

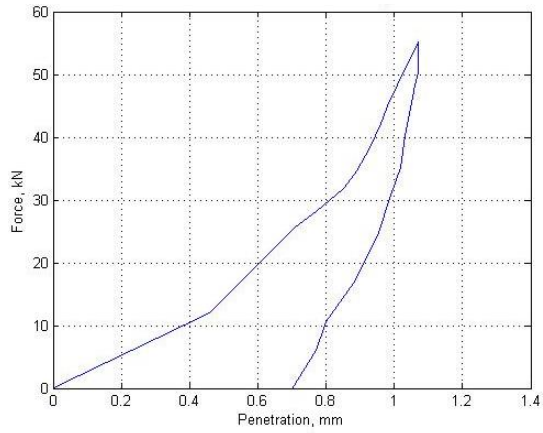


e) Moon white granite

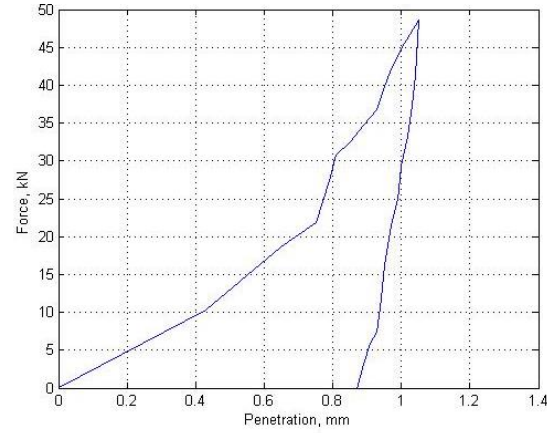


f) Black galaxy granite

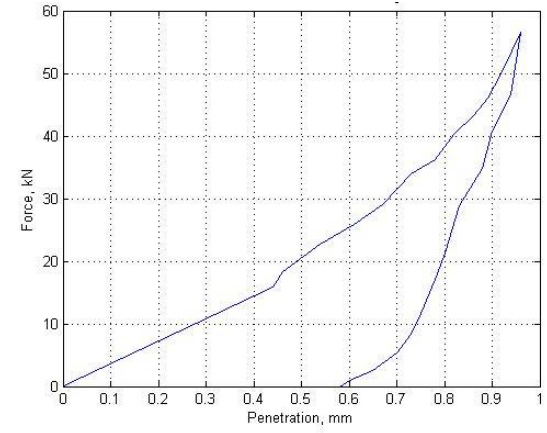
Figure 3.44 (a-f) Force–Penetration (F-P) curves for 48mm diameter cross bit at 30° index angle for various types of rocks



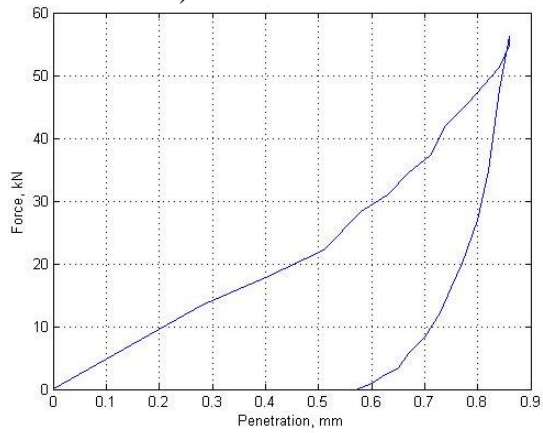
a) Marble



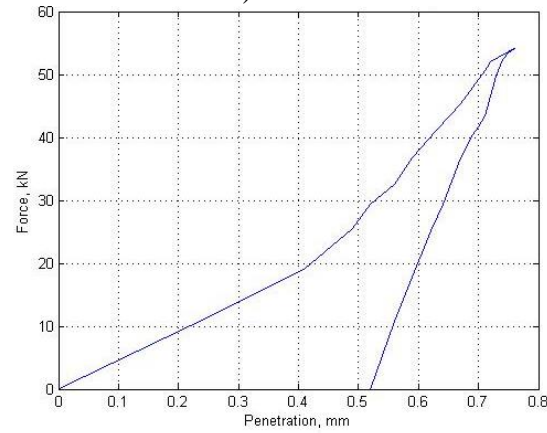
b) Limestone



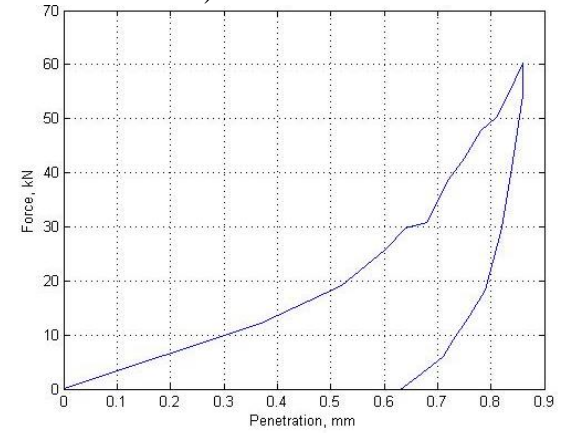
c) Basalt



d) Steel gray granite

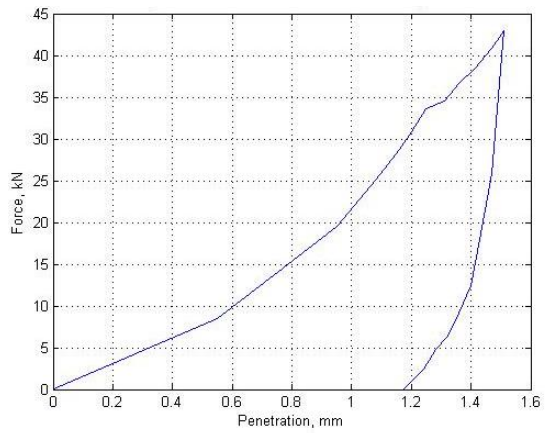


e) Moon white granite

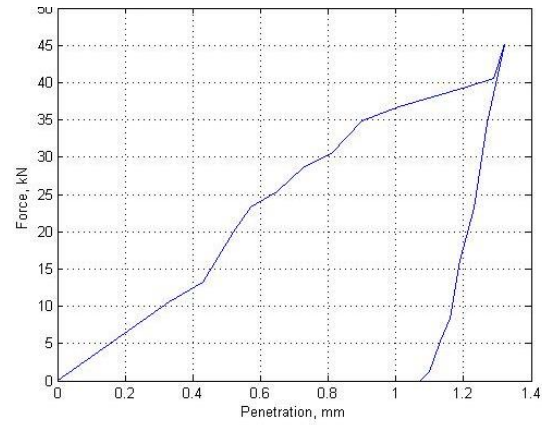


f) Black galaxy granite

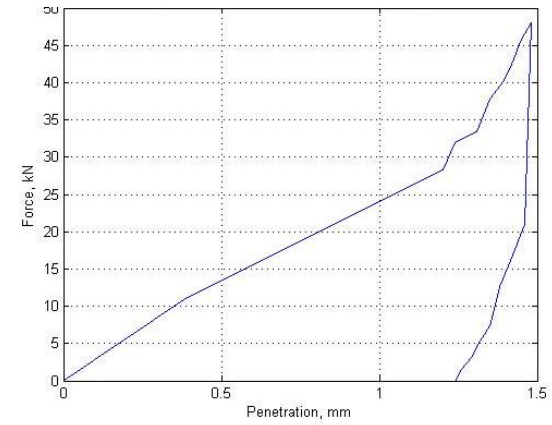
Figure 3.45 (a-f) Force–Penetration (F-P) curves for 48mm diameter cross bit at 40° index angle for various types of rocks



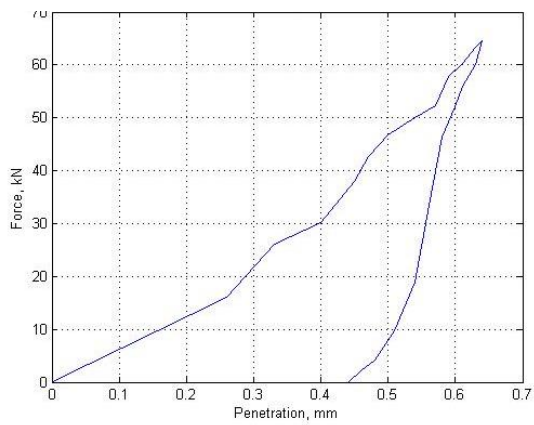
a) Marble



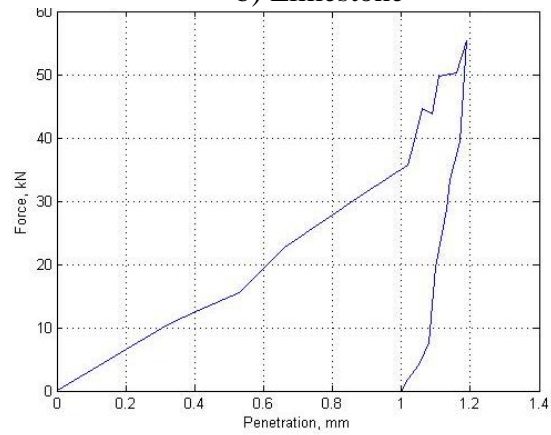
b) Limestone



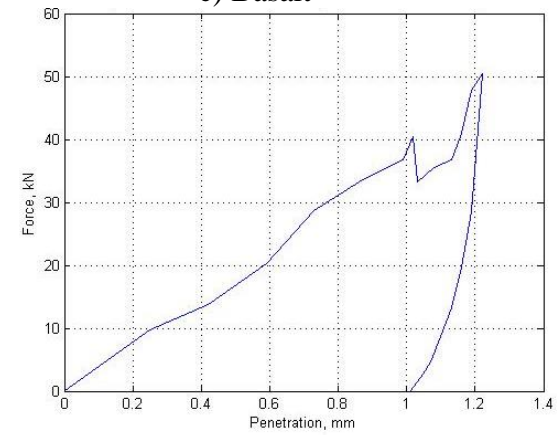
c) Basalt



d) Steel gray granite

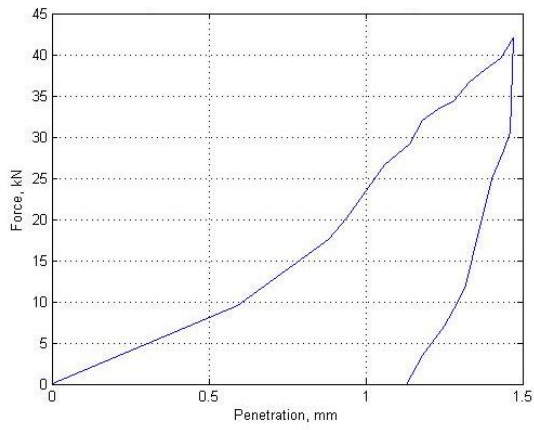


e) Moon white granite

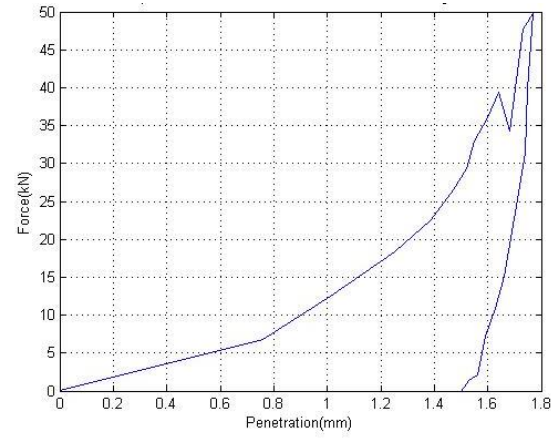


f) Black galaxy granite

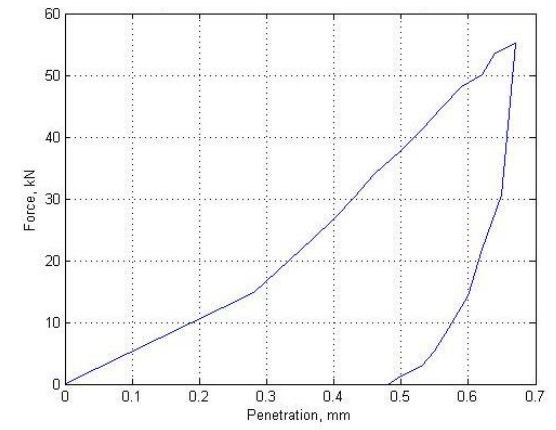
Figure 3.46 (a-f) Force–Penetration (F-P) curves for 35mm diameter spherical button bit at 10^0 index angle for various types of rocks



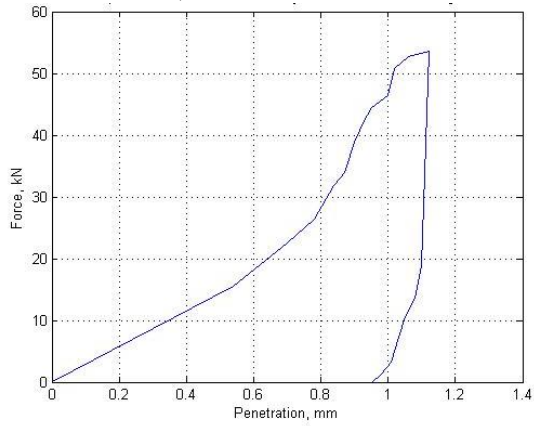
a) Marble



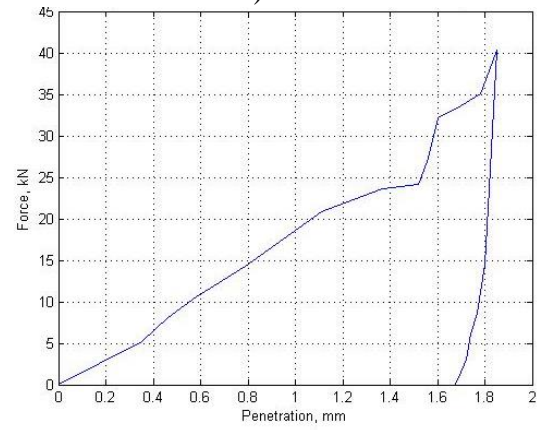
b) Limestone



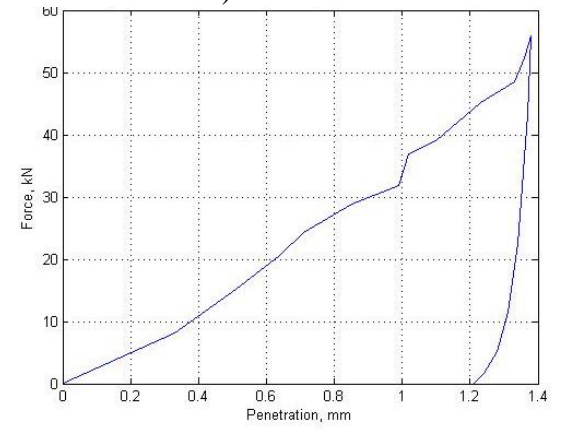
c) Basalt



d) Steel gray granite

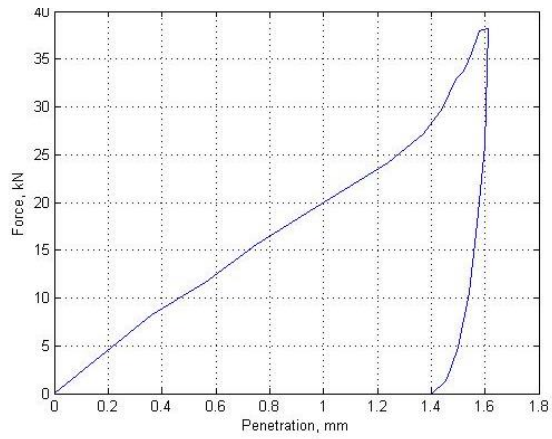


e) Moon white granite

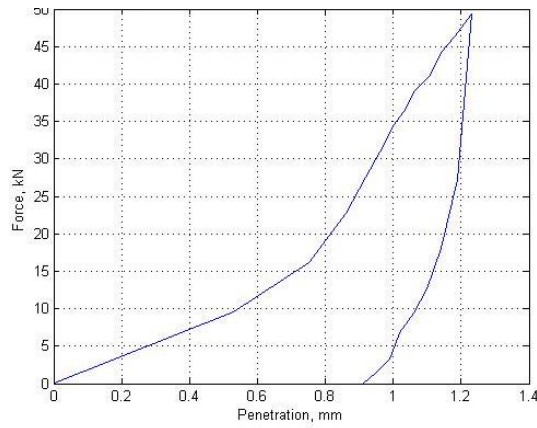


f) Black galaxy granite

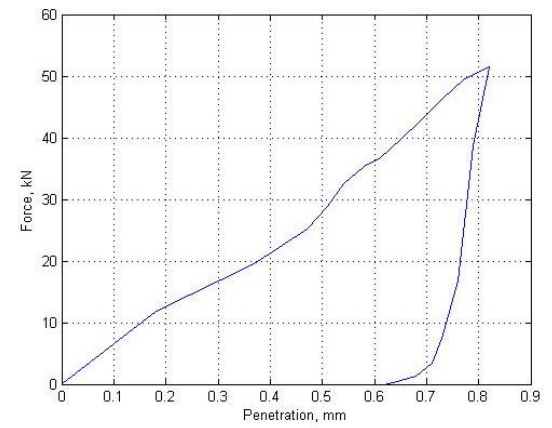
Figure 3.47 (a-f) Force–Penetration (F-P) curves for 35mm diameter spherical button bit at 20° index angle for various types of rocks



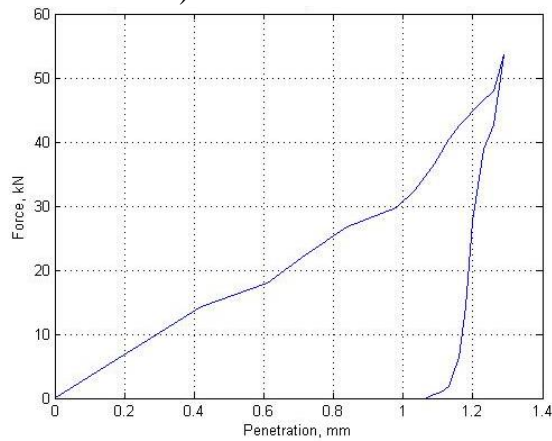
a) Marble



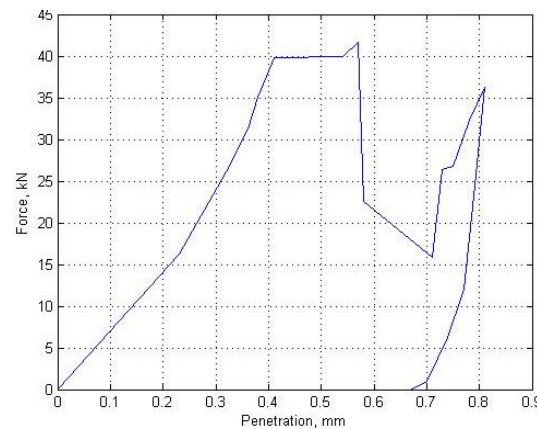
b) Limestone



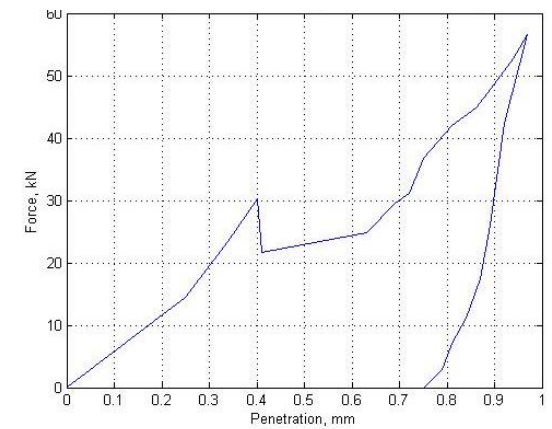
c) Basalt



d) Steel gray granite

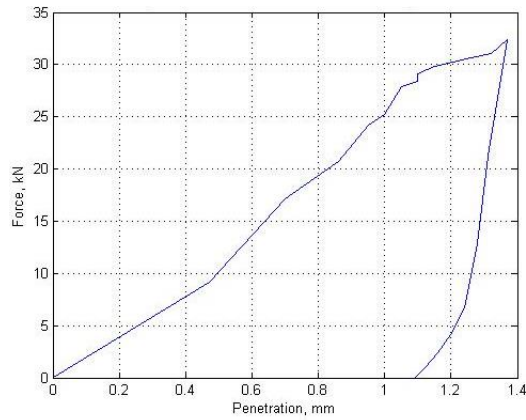


e) Moon white granite

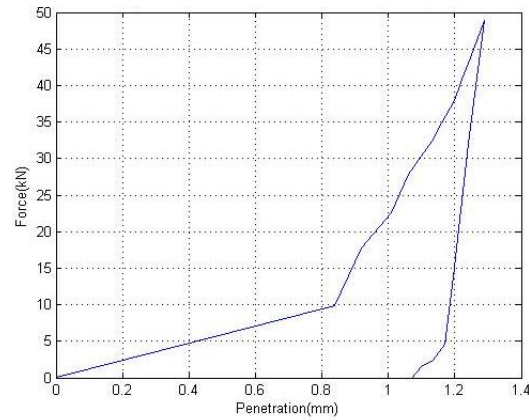


f) Black galaxy granite

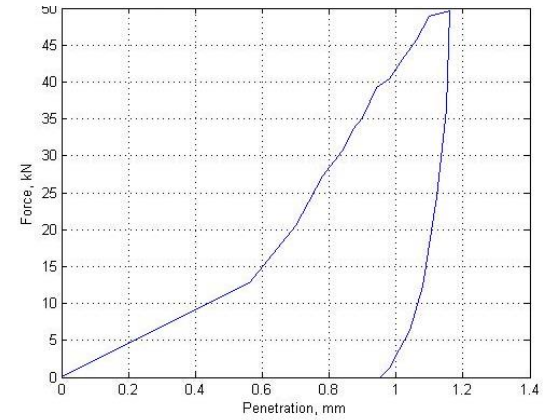
Figure 3.48 (a-f) Force–Penetration (F-P) curves for 35mm diameter spherical button bit at 30° index angle for various types of rocks



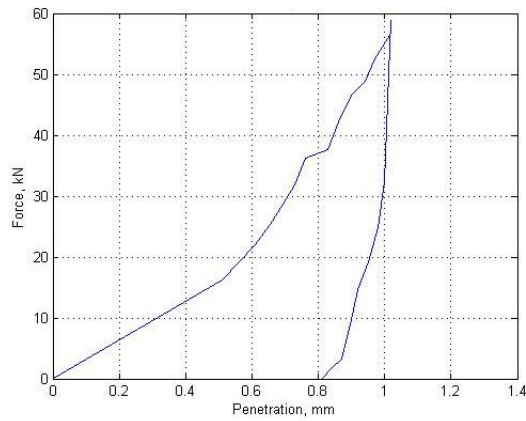
a) Marble



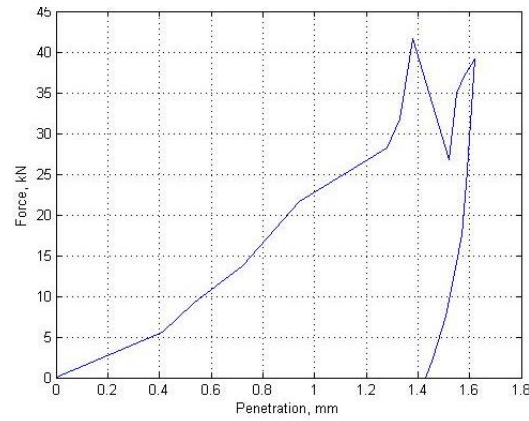
b) Limestone



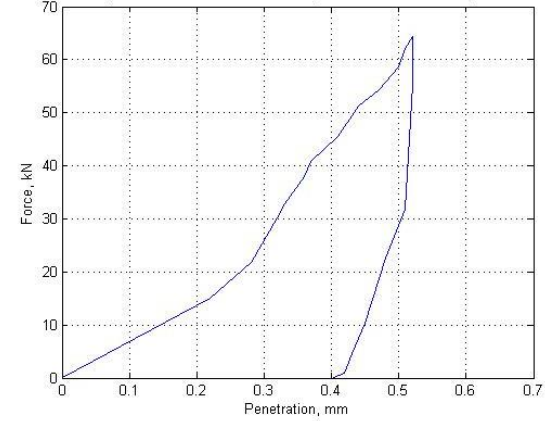
c) Basalt



d) Steel gray granite

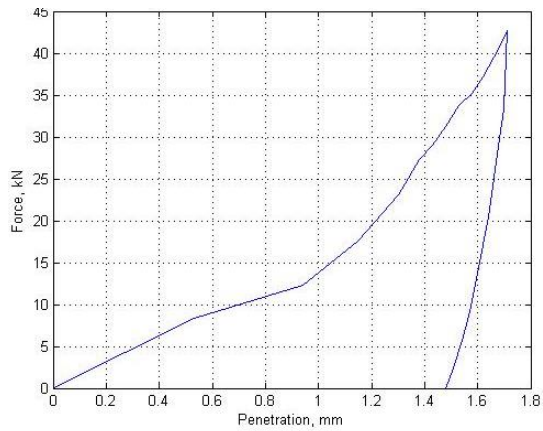


e) Moon white granite

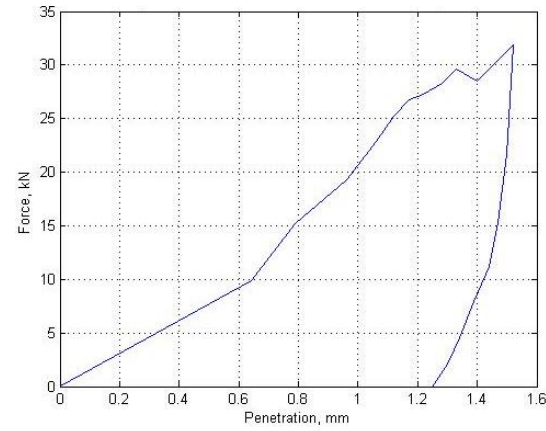


f) Black galaxy granite

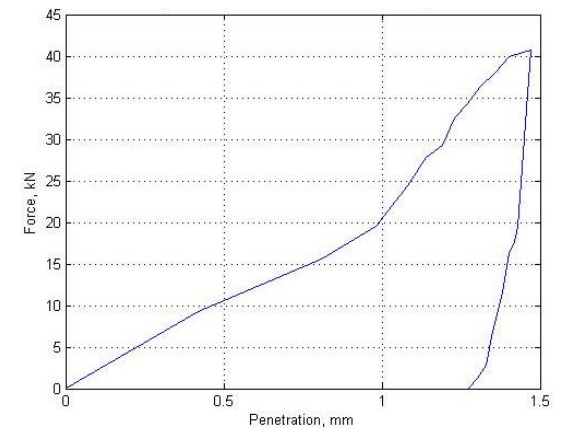
Figure 3.49 (a-f) Force–Penetration (F-P) curves for 35mm diameter spherical button bit at 40° index angle for various types of rocks



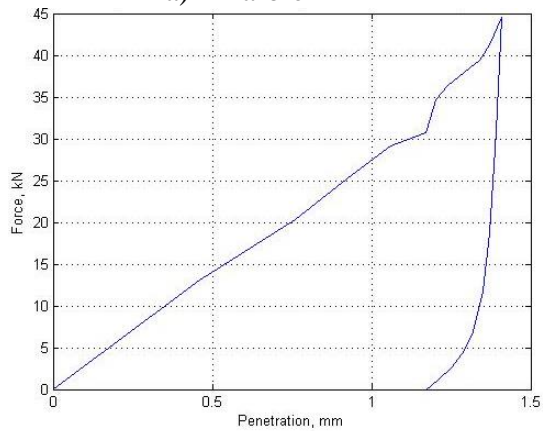
a) Marble



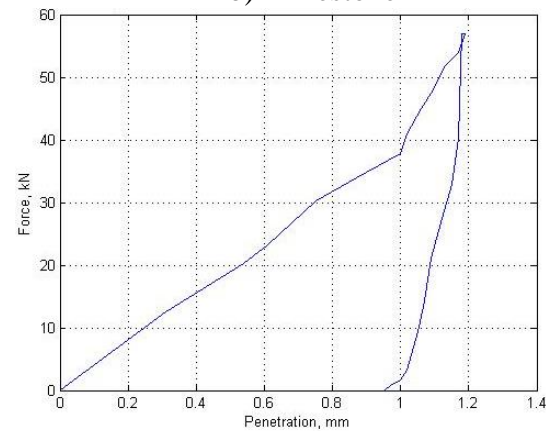
b) Limestone



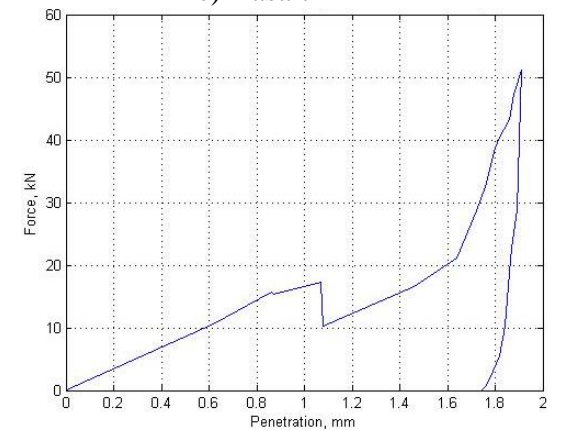
c) Basalt



d) Steel gray granite

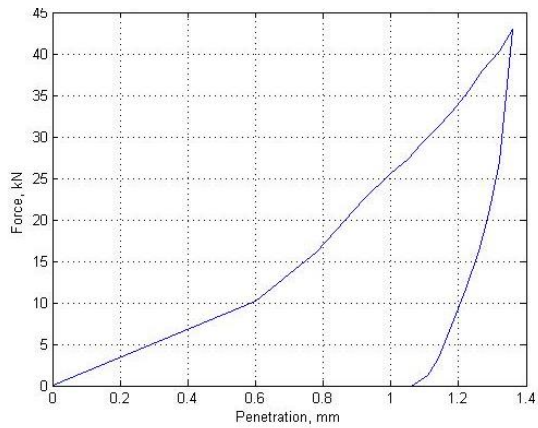


e) Moon white granite

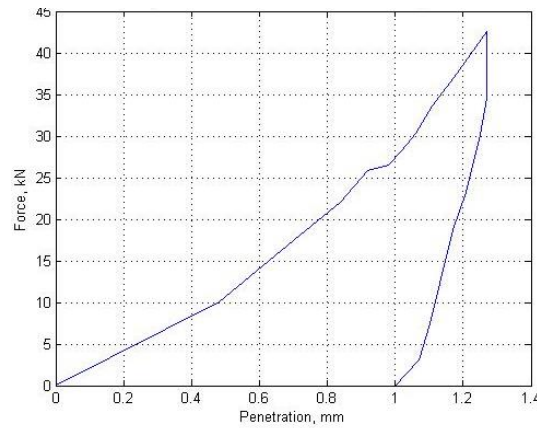


f) Black galaxy granite

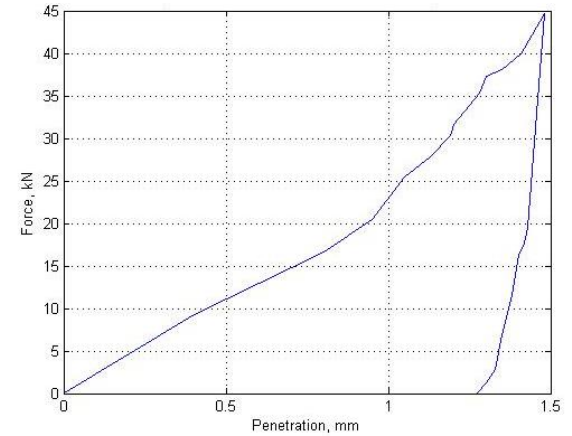
Figure 3.50 (a-f) Force–Penetration (F-P) curves for 38mm diameter spherical button bit at 10^0 index angle for various types of rocks



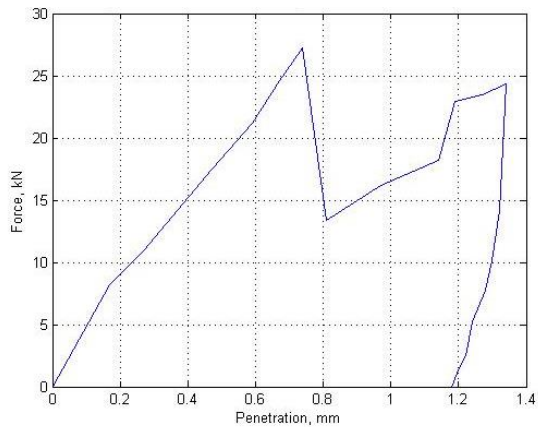
a) Marble



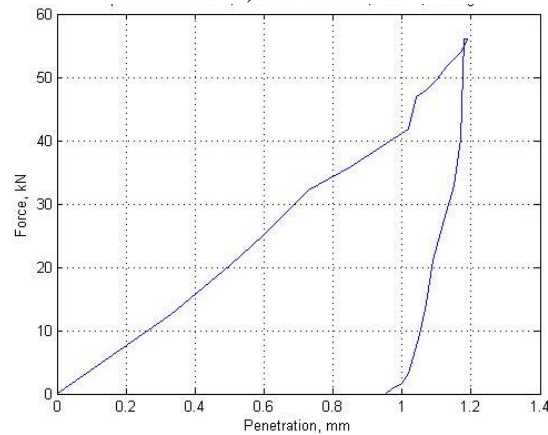
b) Limestone



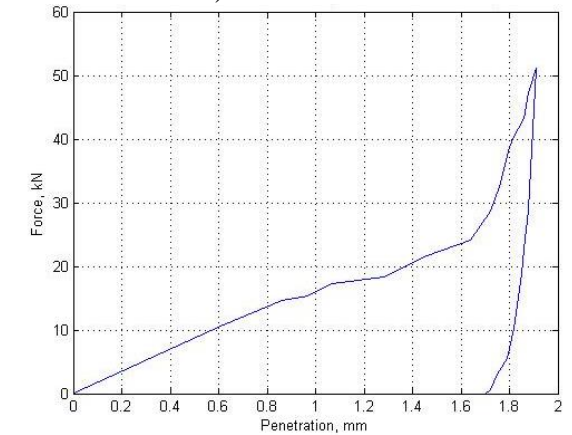
c) Basalt



d) Steel gray granite

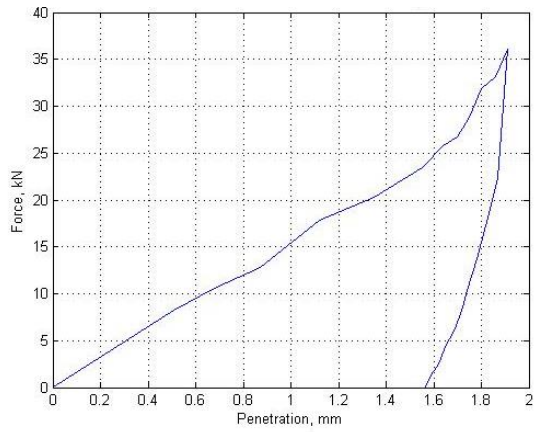


e) Moon white granite

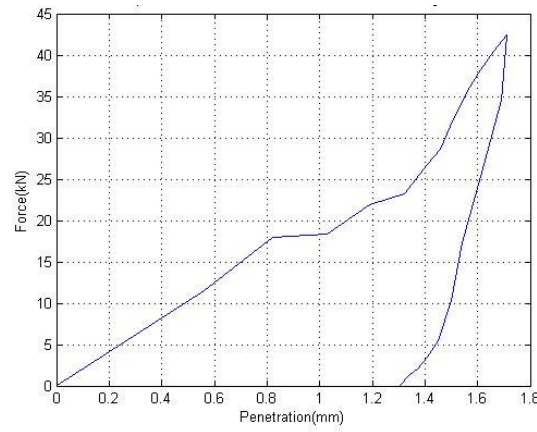


f) Black galaxy granite

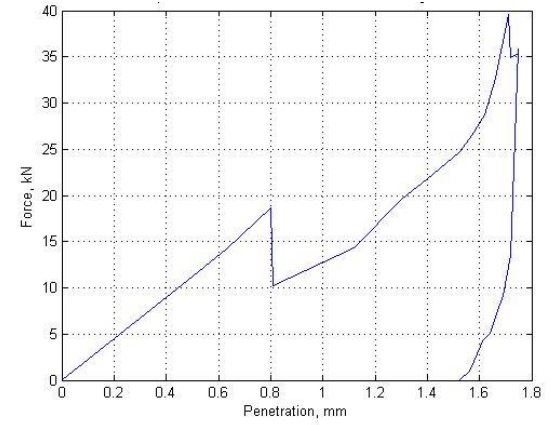
Figure 3.51 (a-f) Force–Penetration (F-P) curves for 38mm diameter spherical button bit at 20° index angle for various types of rocks



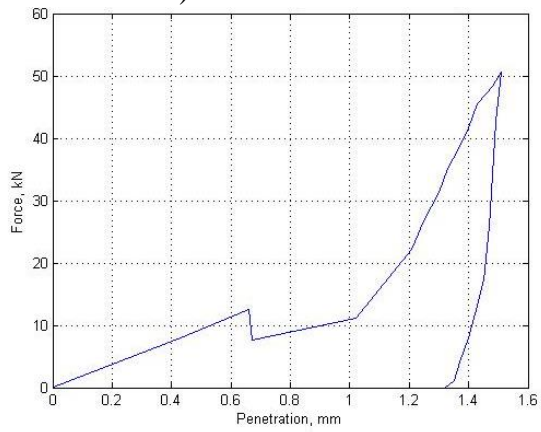
a) Marble



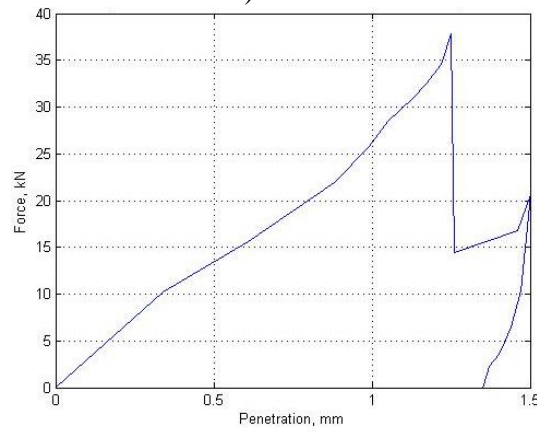
b) Limestone



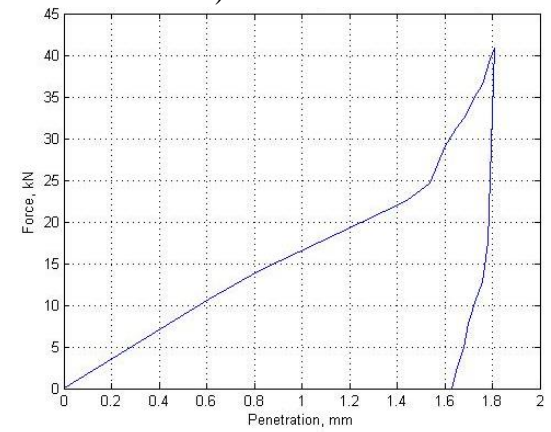
c) Basalt



d) Steel gray granite

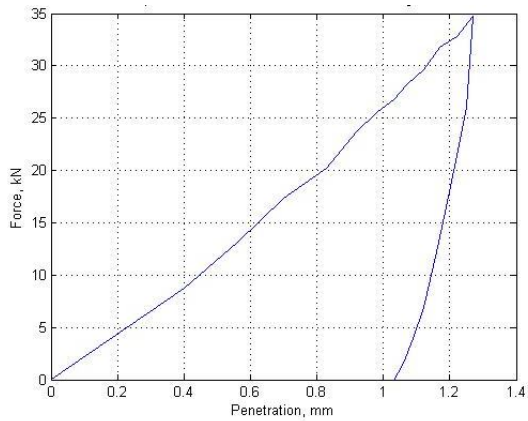


e) Moon white granite

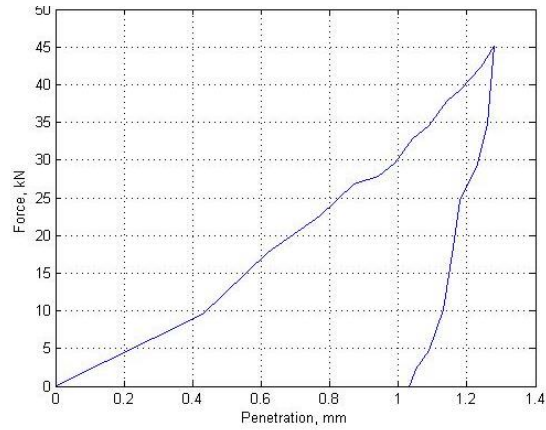


f) Black galaxy granite

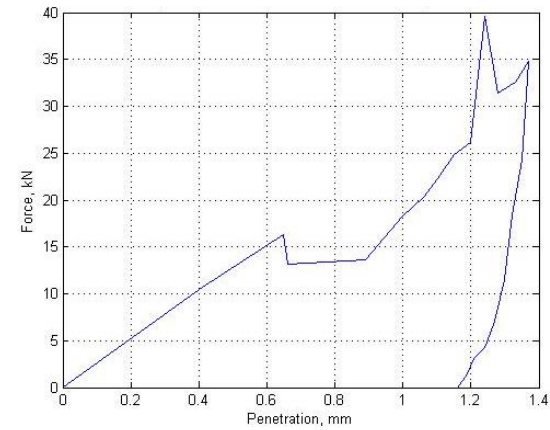
Figure 3.52 (a-f) Force–Penetration (F-P) curves for 38mm diameter spherical button bit at 30° index angle for various types of rocks



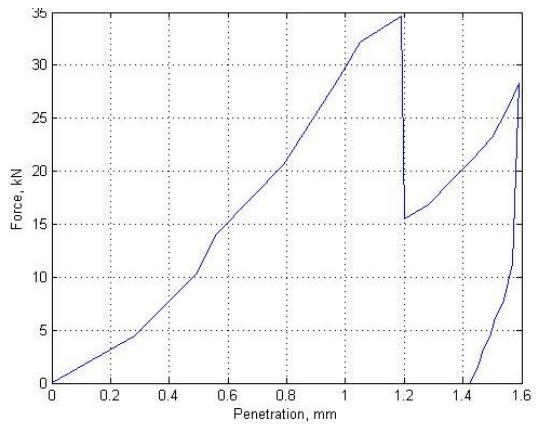
a) Marble



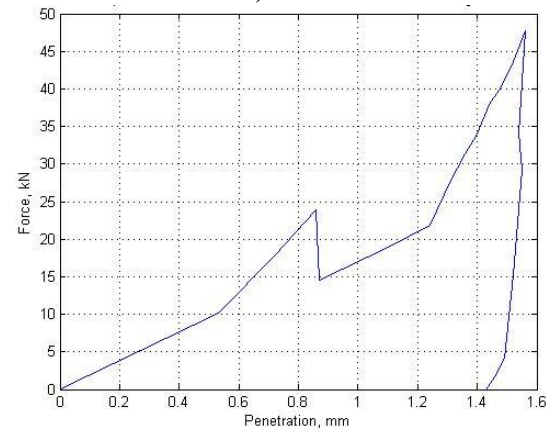
b) Limestone



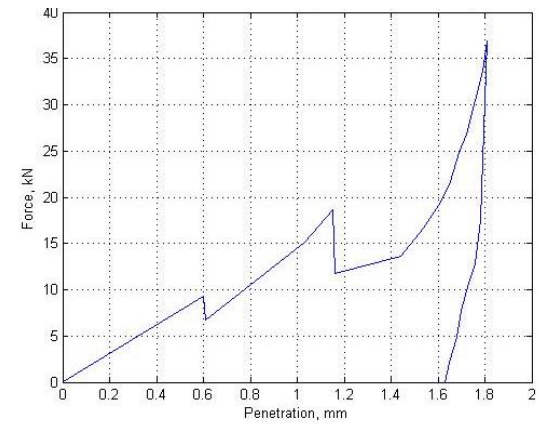
c) Basalt



d) Steel gray granite

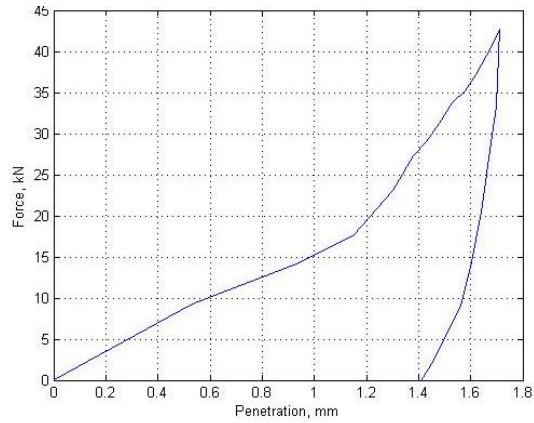


e) Moon white granite

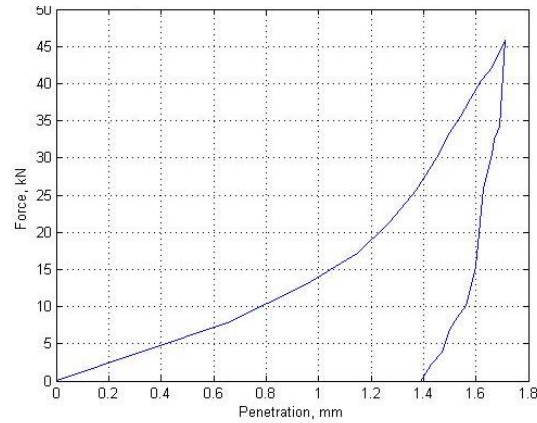


f) Black galaxy granite

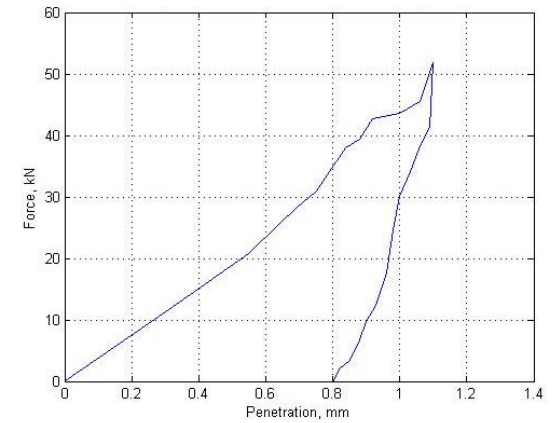
Figure 3.53 (a-f) Force–Penetration (F-P) curves for 38mm diameter spherical button bit at 40° index angle for various types of rocks



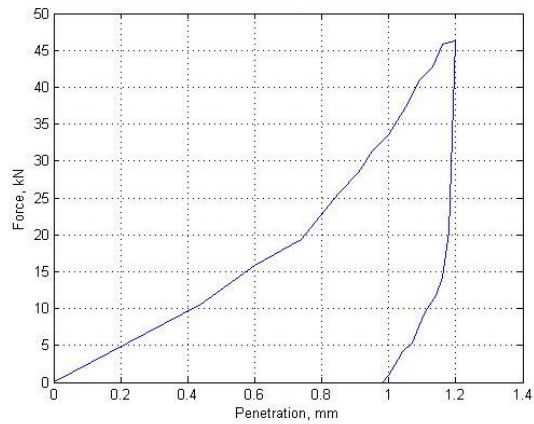
a) Marble



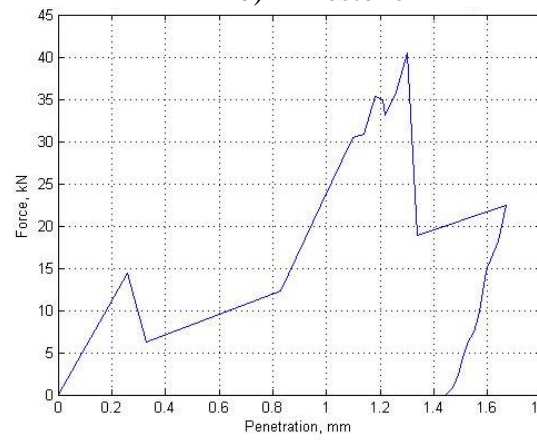
b) Limestone



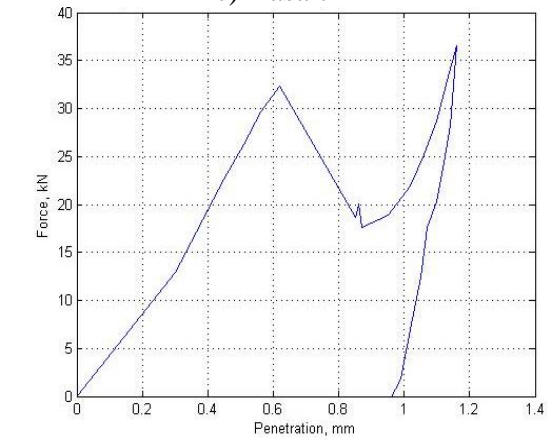
c) Basalt



d) Steel gray granite

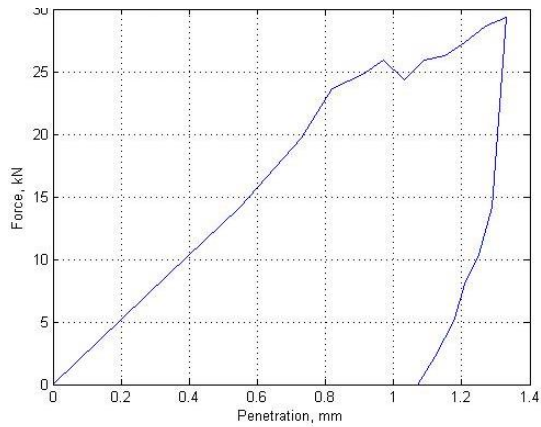


e) Moon white granite

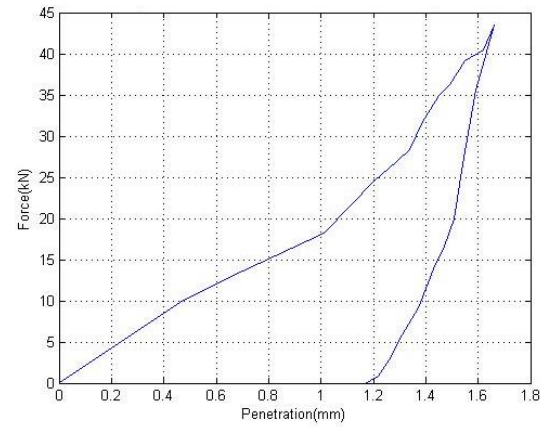


f) Black galaxy granite

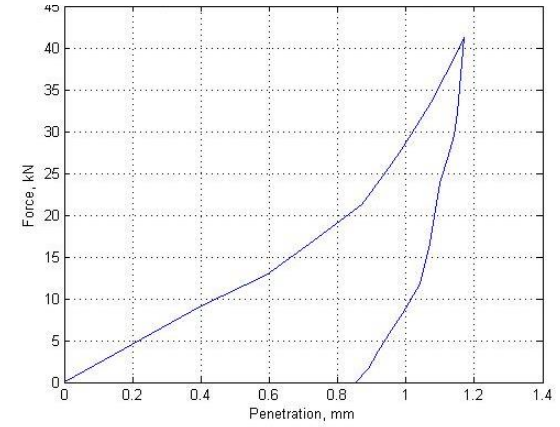
Figure 3.54 (a-f) Force–Penetration (F-P) curves for 45mm diameter spherical button bit at 10° index angle for various types of rocks



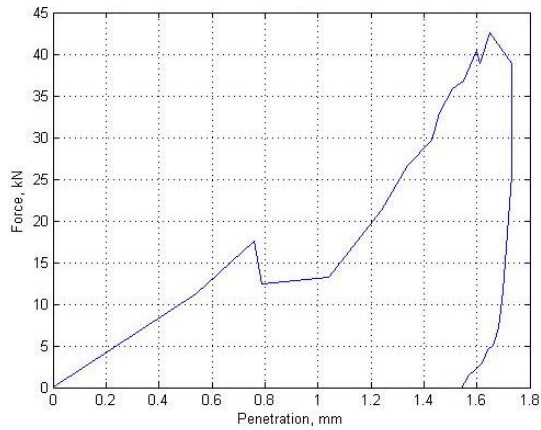
a) Marble



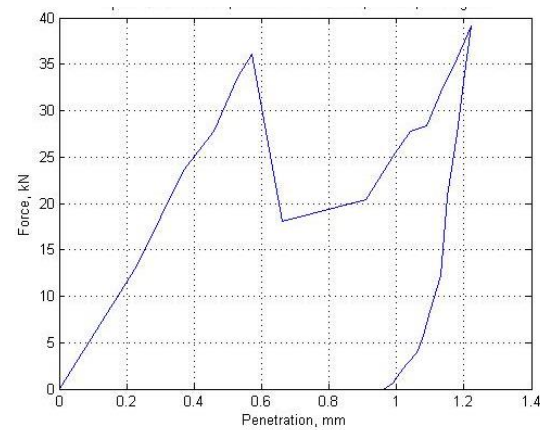
b) Limestone



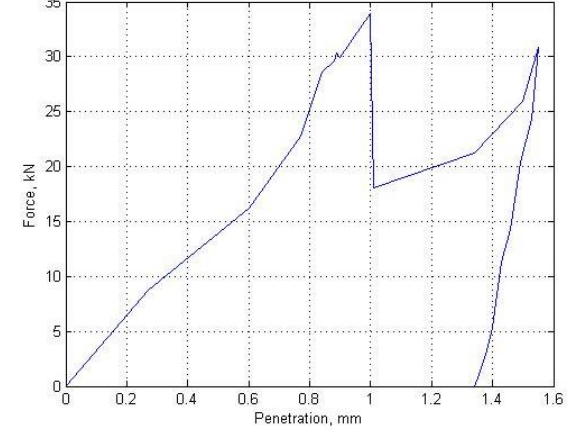
c) Basalt



d) Steel gray granite

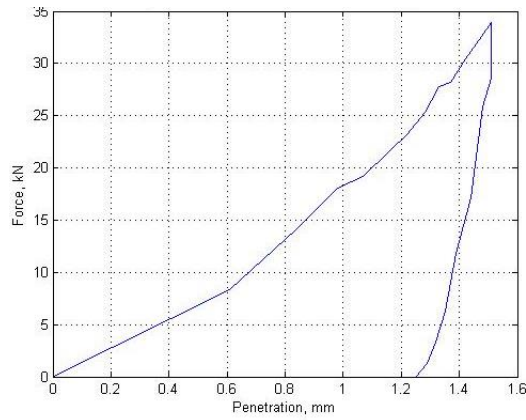


e) Moon white granite

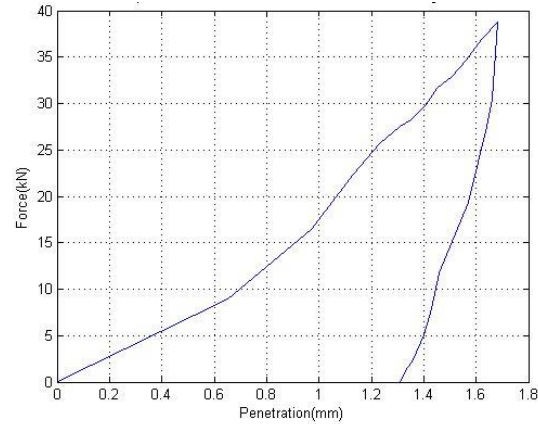


f) Black galaxy granite

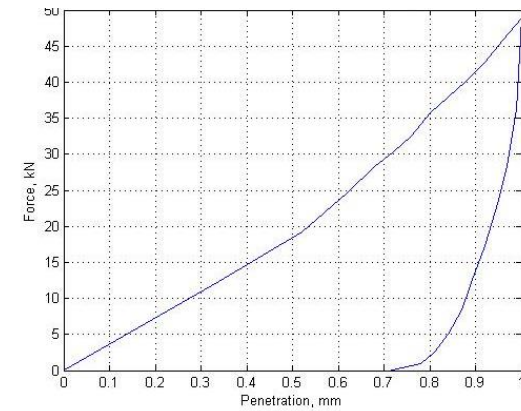
Figure 3.55 (a-f) Force–Penetration (F-P) curves for 45mm diameter spherical button bit at 20° index angle for various types of rocks



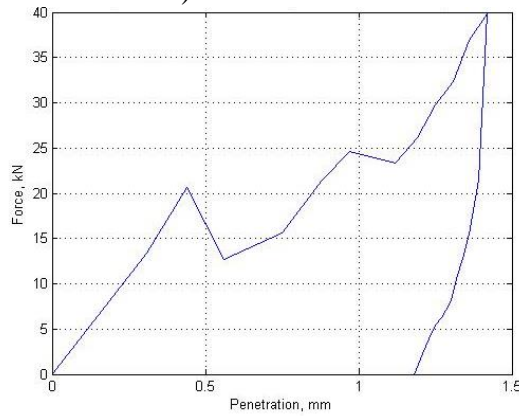
a) Marble



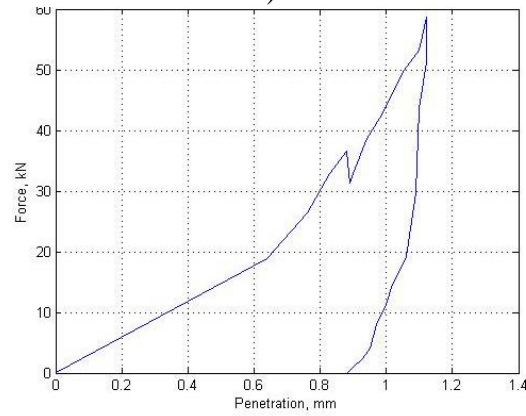
b) Limestone



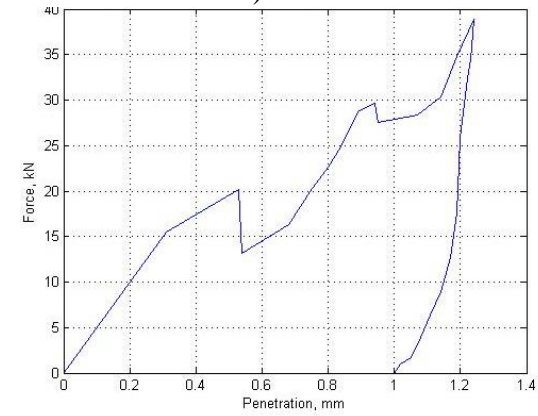
c) Basalt



d) Steel gray granite

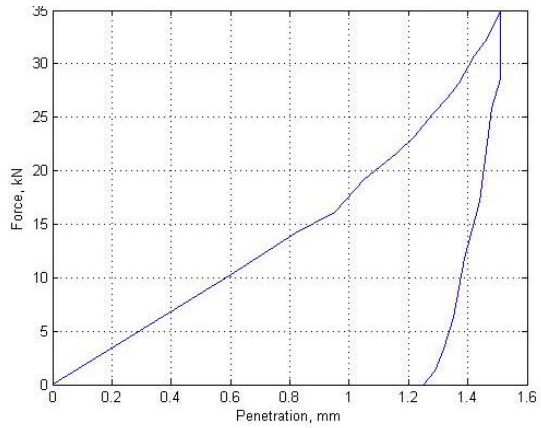


e) Moon white granite

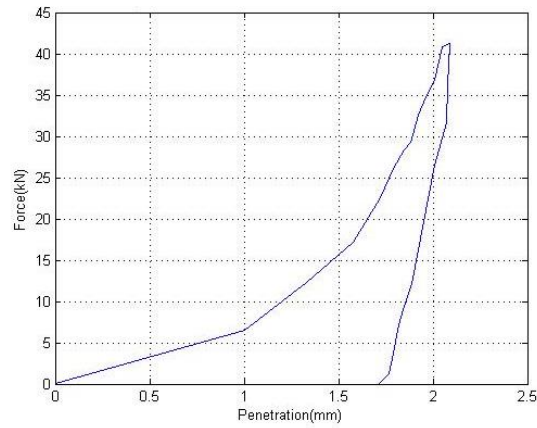


f) Black galaxy granite

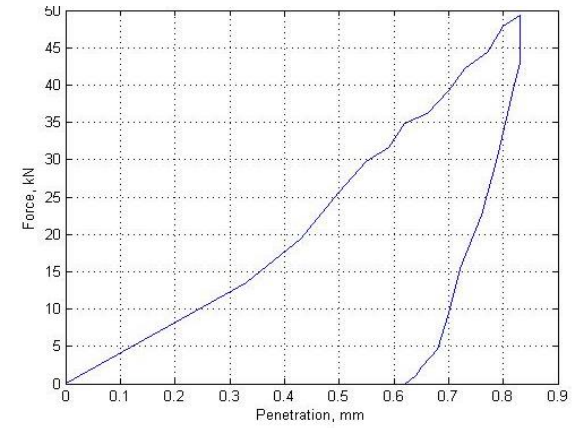
Figure 3.56 (a-f) Force–Penetration (F-P) curves for 45mm diameter spherical button bit at 30° index angle for various types of rocks



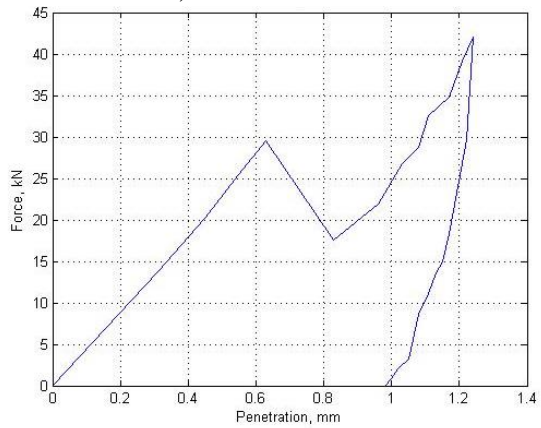
a) Marble



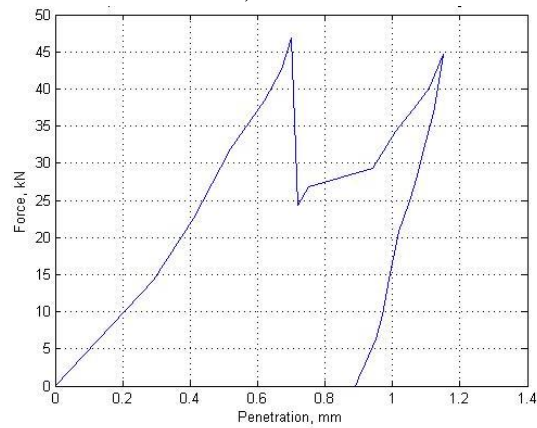
b) Limestone



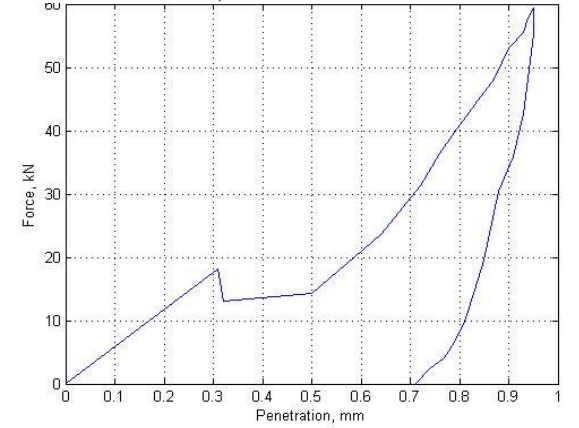
c) Basalt



d) Steel gray granite

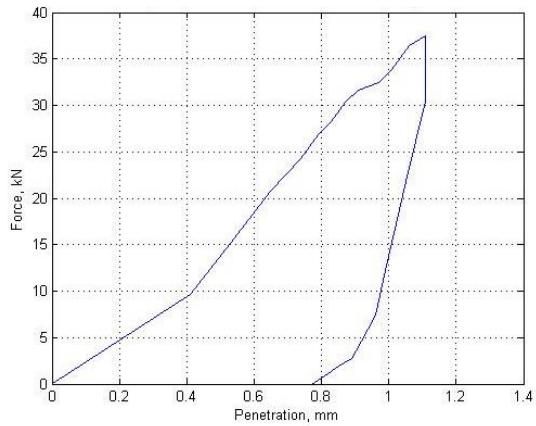


e) Moon white granite

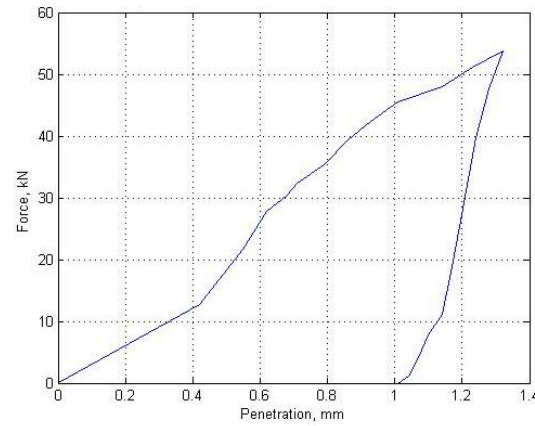


f) Black galaxy granite

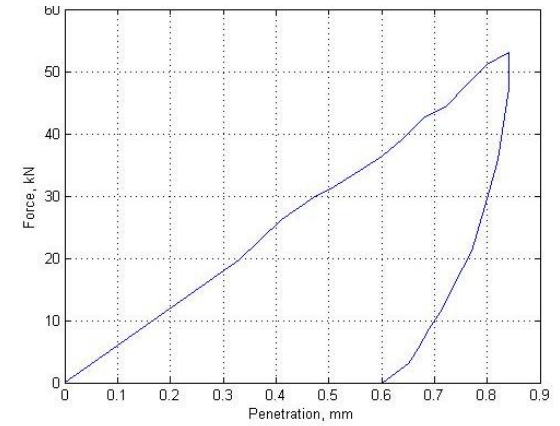
Figure 3.57 (a-f) Force–Penetration (F-P) curves for 45mm diameter spherical button bit at 40° index angle for various types of rocks



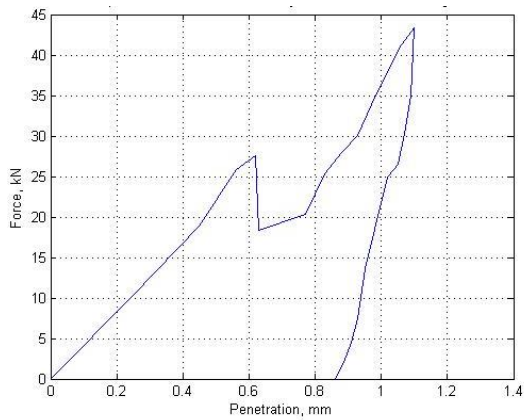
a) Marble



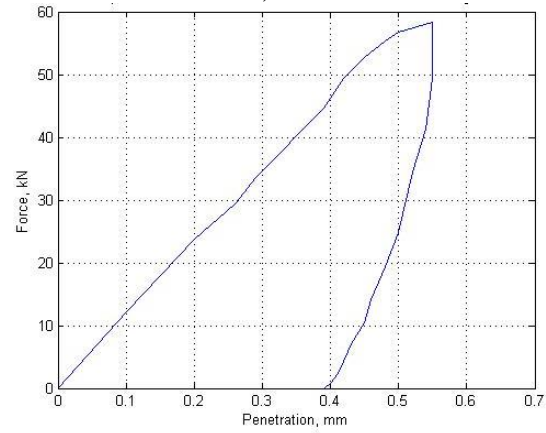
b) Limestone



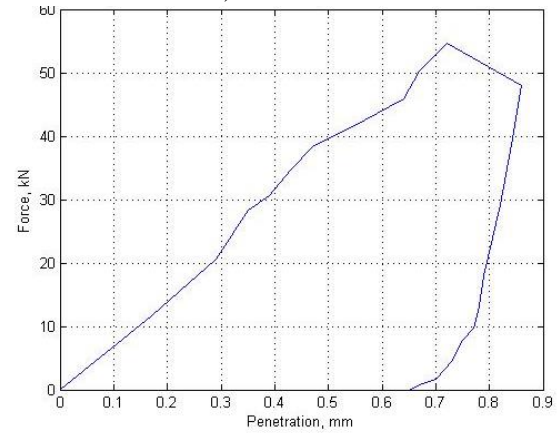
c) Basalt



d) Steel gray granite

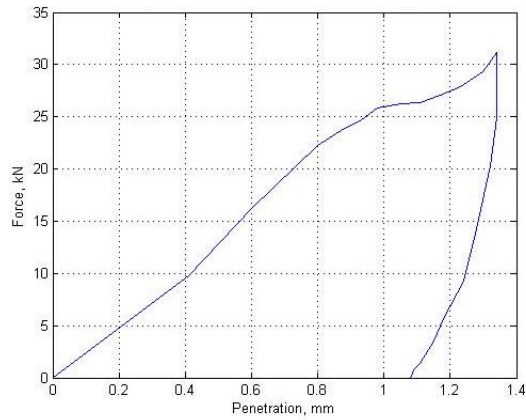


e) Moon white granite

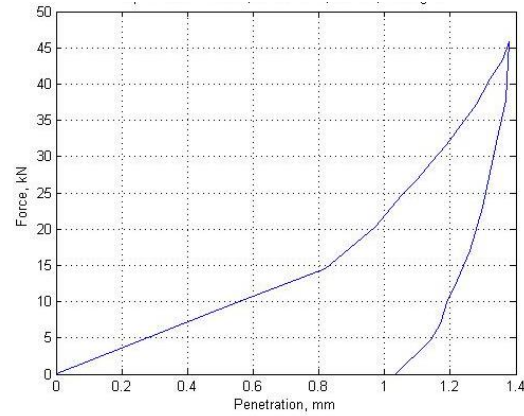


f) Black galaxy granite

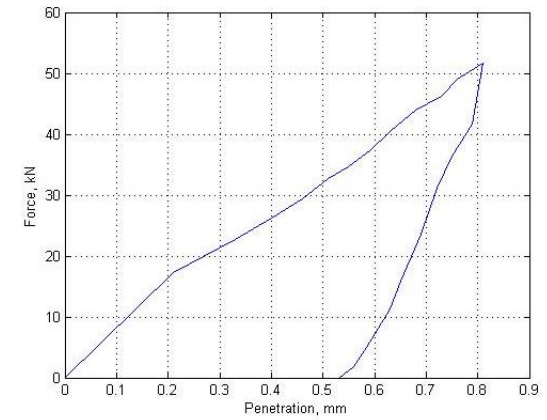
Figure 3.58 (a-f) Force–Penetration (F-P) curves for 48mm diameter spherical button bit at 10^0 index angle for various types of rocks



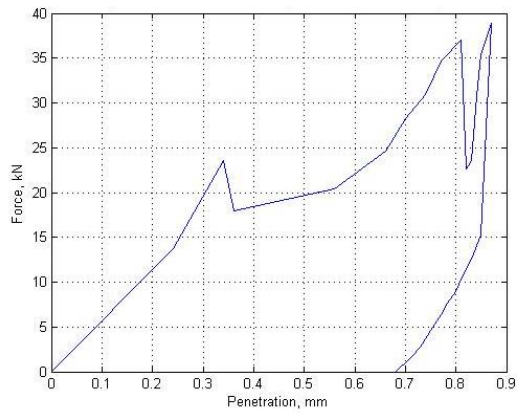
a) Marble



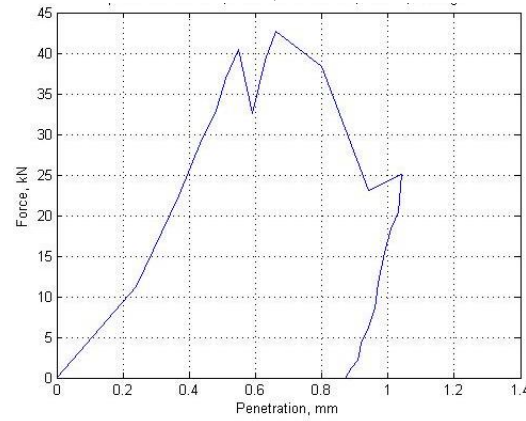
b) Limestone



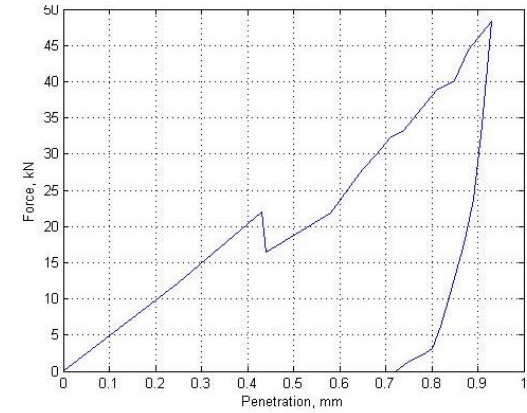
c) Basalt



d) Steel gray granite

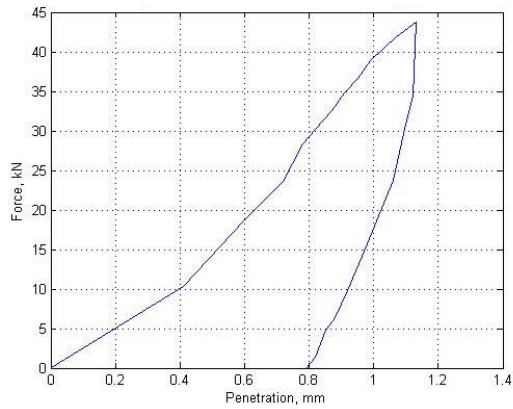


e) Moon white granite

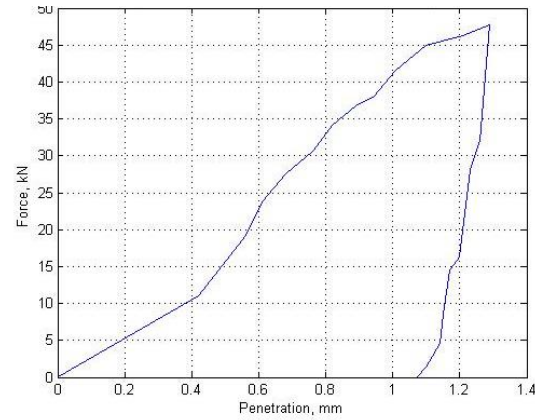


f) Black galaxy granite

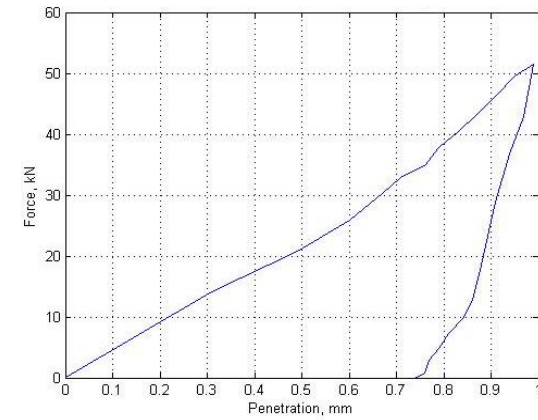
Figure 3.59 (a-f) Force–Penetration (F-P) curves for 48mm diameter spherical button bit at 20° index angle for various types of rocks



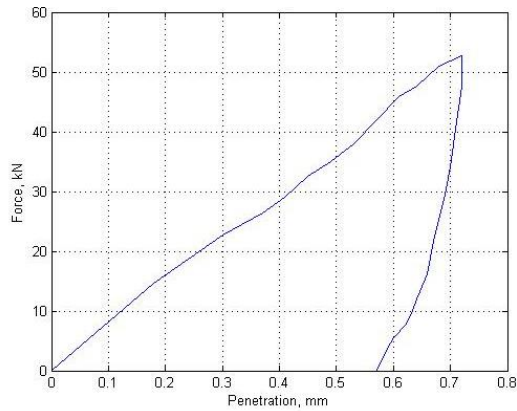
a) Marble



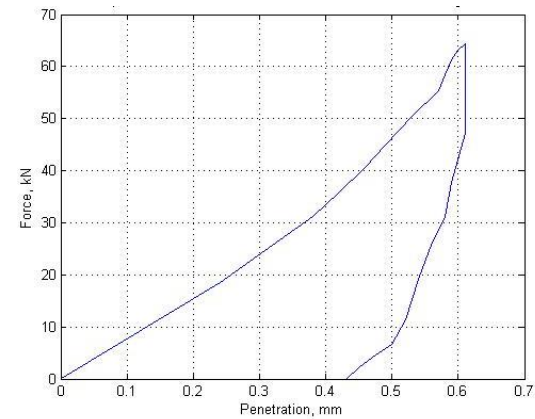
b) Limestone



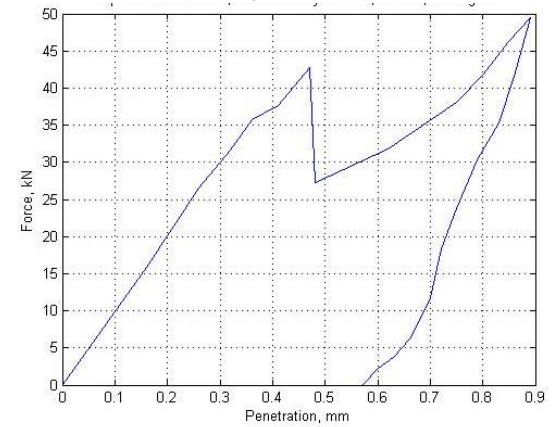
c) Basalt



d) Steel gray granite

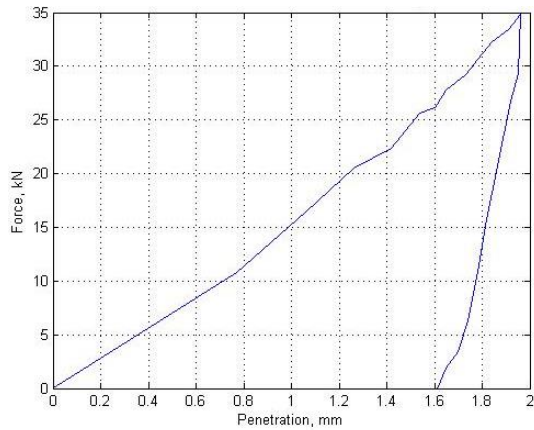


e) Moon white granite

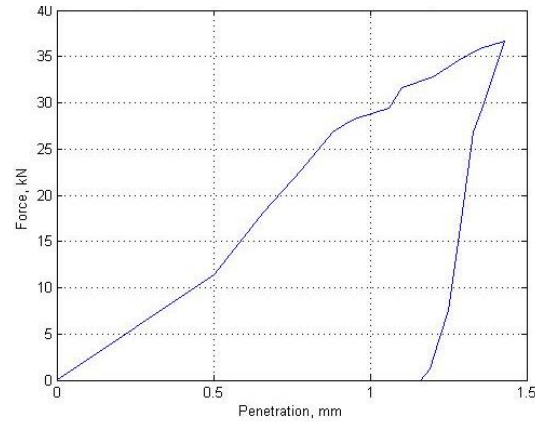


f) Black galaxy granite

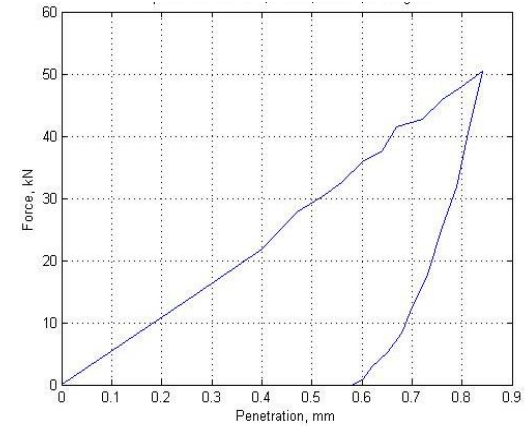
Figure 3.60 (a-f) Force–Penetration (F-P) curves for 48mm diameter spherical button bit at 30° index angle for various types of rocks



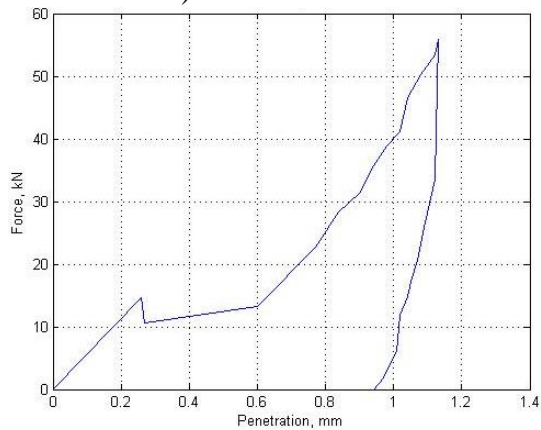
b) Marble



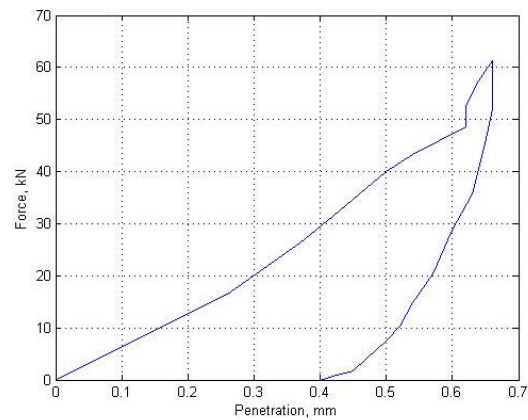
b) Limestone



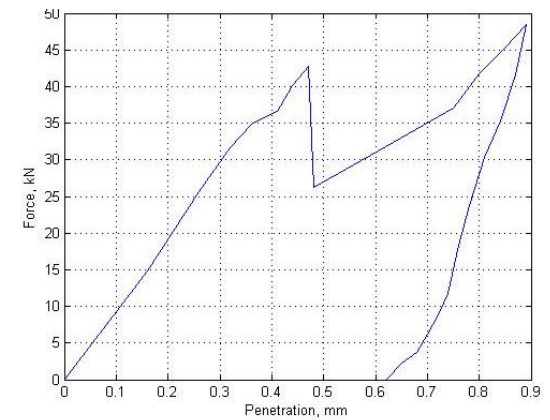
c) Basalt



d) Steel gray granite



e) Moon white granite



f) Black galaxy granite

Figure 3.61 (a-f) Force–Penetration (F-P) curves for 48mm diameter spherical button bit at 40° index angle for various types of rocks

Table 3.8: Specific energy values for chisel type 35, 38, 45 and 48 mm diameters

Type of Rock	Index angle (degrees)	Specific energy(Nm/m ³) x 10 ⁷			
		35mm dia	38mm dia	45mm dia	48mm dia
Marble	10	38.36	30.57	27.74	22.46
	20	33.84	27.14	23.32	18.62
	30	30.89	24.29	19.33	15.51
	40	39.23	31.34	25.36	22.62
Limestone	10	31.78	22.13	19.70	18.88
	20	27.10	20.67	17.64	15.90
	30	23.67	19.53	15.39	14.19
	40	32.57	24.90	20.86	17.21
Basalt	10	80.02	78.55	77.17	63.16
	20	72.83	72.26	69.72	56.47
	30	82.67	79.40	77.78	65.04
	40	90.79	87.67	85.69	70.52
Steel gray granite	10	68.37	66.47	64.12	56.14
	20	61.56	57.18	55.61	47.50
	30	69.62	66.97	64.59	53.69
	40	78.26	75.62	73.45	60.47
Moon white granite	10	72.94	69.13	67.50	57.34
	20	64.91	62.54	60.39	50.10
	30	73.58	70.02	68.46	58.36
	40	81.13	77.93	76.56	63.96
Black galaxy granite	10	76.19	75.48	71.95	61.11
	20	68.31	67.04	64.52	53.92
	30	76.35	76.37	74.32	60.91
	40	85.01	83.42	79.32	66.17

Table 3.9: Specific energy values for cross type 35, 38, 45, and 48 mm diameters

Type of Rock	Index angle (degrees)	Specific energy(Nm/m ³) x 10 ⁷			
		35mm dia	38mm dia	45mm dia	48mm dia
Marble	10	43.84	33.51	33.22	28.01
	20	39.54	29.23	26.98	22.95
	30	35.28	25.94	22.61	19.70
	40	44.54	34.69	30.93	28.04
Limestone	10	36.55	27.64	25.79	21.79
	20	33.17	24.23	23.03	18.95
	30	30.73	22.74	21.30	18.15
	40	39.58	28.73	26.13	22.39
Basalt	10	89.19	83.57	78.52	75.94
	20	80.52	72.68	68.50	64.42
	30	90.82	83.88	79.75	74.19
	40	98.32	92.88	86.44	80.28
Steel gray granite	10	75.31	69.36	67.96	64.01
	20	66.64	60.60	58.01	54.06
	30	77.36	69.89	67.67	62.50
	40	84.84	78.05	76.19	68.45
Moon white granite	10	79.96	75.18	74.31	66.74
	20	71.74	65.70	63.06	57.20
	30	81.85	76.21	72.45	65.86
	40	87.27	85.07	80.89	72.65
Black galaxy granite	10	84.18	79.24	75.05	70.97
	20	76.11	69.74	66.94	61.81
	30	83.57	80.36	76.51	70.36
	40	91.29	89.49	84.68	75.94

Table 3.10: Specific energy values for spherical button type 35, 38, 45 and 48 mm diameters

Type of Rock	Index angle (degrees)	Specific energy(Nm/m ³) x 10 ⁷			
		35mm dia	38mm dia	45mm dia	48mm dia
Marble	10	21.44	18.40	15.83	12.46
	20	18.01	15.77	12.52	9.42
	30	15.24	13.75	10.10	7.60
	40	21.98	18.15	14.43	12.71
Limestone	10	17.69	15.08	12.02	8.71
	20	14.07	13.05	10.32	7.86
	30	13.31	11.82	9.17	7.18
	40	20.15	16.38	12.27	9.92
Basalt	10	63.20	62.29	61.01	48.60
	20	56.83	53.78	53.61	42.53
	30	67.10	63.18	64.27	49.90
	40	75.05	69.46	71.61	55.28
Steel gray granite	10	50.28	49.20	52.49	38.94
	20	41.61	41.65	43.57	32.96
	30	49.37	49.81	49.24	37.97
	40	57.15	57.49	55.04	43.23
Moon white granite	10	53.19	53.10	55.86	42.41
	20	45.98	46.13	45.59	34.82
	30	53.68	54.96	54.04	43.10
	40	60.80	61.69	61.86	47.82
Black galaxy granite	10	61.76	59.07	58.59	45.87
	20	53.59	49.83	50.22	39.72
	30	61.08	57.64	59.37	47.92
	40	67.97	66.12	66.26	53.89

APPENDIX- II

Table 4.22 Comparison of results of FEM analysis (ANSYS) with static indentation tests for all bit-rock combinations at the peak load in marble rock.

Rock type: Marble						
Bit geometry	Diameter of bit(mm)	Load applied (kN)		Depth of penetration (mm)		Variation (%)
		Experimental	ANSYS	Experimental	ANSYS	
Chisel	48	59.3	59.3	0.98	0.93	5.10
Cross	48	39.9	39.9	0.57	0.52	8.77
Spherical button	48	35.3	35.3	1.16	1.10	5.17
Chisel	45	42.4	42.4	0.84	0.70	16.30
Cross	45	49.7	49.7	0.75	0.61	18.48
Spherical button	45	32.3	32.3	1.02	0.88	13.94
Chisel	38	43.6	43.6	1	0.82	17.93
Cross	38	49.9	49.9	0.87	0.85	1.83
Spherical button	38	24.8	24.8	0.9	0.75	16.13
Chisel	35	30.1	30.1	0.7	0.60	13.98
Cross	35	50.1	50.1	0.89	0.77	13.82
Spherical button	35	32.5	32.5	1.47	1.31	11.18

Table 4.23 Comparison of results of FEM analysis (ANSYS) with static indentation tests for all bit-rock combinations at the peak load in limestone rock.

Rock type: Limestone						
Bit geometry	Diameter of bit(mm)	Load applied (kN)		Depth of penetration (mm)		Variation (%)
		Experimental	ANSYS	Experimental	ANSYS	
Chisel	48	49.9	49.9	0.82	0.67	18.05
Cross	48	50.8	50.8	0.62	0.50	19.03
Spherical button	48	48.8	48.8	1.12	1.08	3.57
Chisel	45	44.8	44.8	0.88	0.75	14.22
Cross	45	51.5	51.5	0.78	0.72	8.25
Spherical button	45	40.8	40.8	1.12	0.94	15.96
Chisel	38	50.2	50.2	0.9	0.80	11.46
Cross	38	39.7	39.7	0.85	0.77	9.78
Spherical button	38	37.8	37.8	1.12	0.98	12.79
Chisel	35	50.5	50.5	1.01	0.86	14.65
Cross	35	44.9	44.9	0.79	0.75	5.22
Spherical button	35	41.1	41.1	1.08	1.06	1.66

Table 4.24 Comparison of results of FEM analysis (ANSYS) with static indentation tests for all bit-rock combinations at the peak load in basalt rock.

Rock type: Basalt						
Bit geometry	Diameter of bit(mm)	Load applied (kN)		Depth of penetration (mm)		Variation (%)
		Experimental	ANSYS	Experimental	ANSYS	
Chisel	48	51.2	51.2	0.68	0.58	14.12
Cross	48	47.8	47.8	0.49	0.40	19.39
Spherical button	48	55.8	55.8	1.08	1.07	1.39
Chisel	45	44.6	44.6	0.64	0.53	16.46
Cross	45	46.7	46.7	0.48	0.41	14.69
Spherical button	45	50.2	50.2	1.01	0.96	5.25
Chisel	38	41.1	41.1	0.69	0.56	18.91
Cross	38	49.9	49.9	0.78	0.67	13.91
Spherical button	38	35.3	35.3	0.8	0.76	5.55
Chisel	35	35.5	35.5	0.63	0.51	18.47
Cross	35	53.3	53.3	0.65	0.58	10.41
Spherical button	35	31.1	31.1	0.81	0.67	17.81

Table 4.25 Comparison of results of FEM analysis (ANSYS) with static indentation tests for all bit-rock combinations at the peak load in steel grey granite

Rock type: Steel gray granite						
Bit geometry	Diameter of bit(mm)	Load applied (kN)		Depth of penetration (mm)		Variation (%)
		Experimental	ANSYS	Experimental	ANSYS	
Chisel	48	55.6	55.6	0.68	0.66	3.09
Cross	48	60.4	60.4	0.53	0.50	5.66
Spherical button	48	47.8	47.8	0.98	0.94	4.08
Chisel	45	43.6	43.6	0.66	0.54	17.75
Cross	45	58.9	58.9	0.65	0.54	16.86
Spherical button	45	37.8	37.8	0.9	0.76	15.48
Chisel	38	39.1	39.1	0.68	0.55	18.72
Cross	38	55.5	55.5	0.65	0.59	9.14
Spherical button	38	26.7	26.7	0.72	0.60	16.38
Chisel	35	39.8	39.8	0.7	0.60	14.57
Cross	35	52.6	52.6	0.71	0.60	15.37
Spherical button	35	38.2	38.2	1.02	0.86	15.56

Table 4.26 Comparison of results of FEM analysis (ANSYS) with static indentation tests for all bit-rock combinations at the peak load in moon white granite

Rock type: Moon white granite						
Bit geometry	Diameter of bit(mm)	Load applied (kN)		Depth of penetration (mm)		Variation (%)
		Experimental	ANSYS	Experimental	ANSYS	
Chisel	48	64.1	64.1	0.89	0.87	2.02
Cross	48	60.1	60.1	0.51	0.43	15.69
Spherical button	48	50.7	50.7	0.96	0.90	6.25
Chisel	45	52.1	52.1	0.89	0.74	16.34
Cross	45	49.7	49.7	0.61	0.53	13.89
Spherical button	45	50.4	50.4	1.1	1.08	1.87
Chisel	38	47.9	47.9	0.91	0.78	14.54
Cross	38	66.4	66.4	0.88	0.81	7.53
Spherical button	38	39.9	39.9	1.09	0.93	14.95
Chisel	35	46.2	46.2	0.94	0.80	15.25
Cross	35	55.1	55.1	0.74	0.72	2.05
Spherical button	35	52.4	52.4	1.39	1.13	18.71

Table 4.27 Comparison of results of FEM analysis (ANSYS) with static indentation tests for all bit-rock combinations at the peak load in black galaxy granite

Rock type: Black galaxy granite						
Bit geometry	Diameter of bit(mm)	Load applied (kN)		Depth of penetration (mm)		Variation (%)
		Experimental	ANSYS	Experimental	ANSYS	
Chisel	48	59.9	59.9	0.78	0.65	16.67
Cross	48	51.1	51.1	0.5	0.44	12.00
Spherical button	48	55.8	55.8	0.95	0.89	6.32
Chisel	45	51.2	51.2	0.71	0.58	17.70
Cross	45	61.6	61.6	0.61	0.52	15.54
Spherical button	45	35.7	35.7	0.8	0.65	18.58
Chisel	38	38.8	38.8	0.61	0.52	15.45
Cross	38	55.9	55.9	0.63	0.54	13.90
Spherical button	38	50.1	50.1	1.23	1.02	16.70
Chisel	35	43.9	43.9	0.86	0.70	18.06
Cross	35	52.2	52.2	0.65	0.54	16.32
Spherical button	35	37.9	37.9	0.96	0.78	19.26

Table 4.28 Comparison of results of FEM analysis (ANSYS) with static indentation tests for twelve load steps for marble rock.

Bit type	Load step	Time (sec)	Force (kN)		Displacement (mm)	
			Experimental	ANSYS	Experimental	ANSYS
Rock Type: Marble						
Chisel	1	5	10.4	10.4	0.27	0.16
	2	10	21.5	21.5	0.38	0.34
	3	15	28.4	28.4	0.52	0.45
	4	20	32.6	32.6	0.54	0.51
	5	25	35.7	35.7	0.57	0.56
	6	30	39.3	39.3	0.66	0.62
	7	35	43.9	43.9	0.72	0.69
	8	40	47.8	47.8	0.77	0.75
	9	45	49.8	49.8	0.82	0.78
	10	50	52.1	52.1	0.87	0.82
	11	55	56.6	56.6	0.92	0.89
	12	60	59.3	59.3	0.98	0.93
Cross	1	5	9.6	9.6	0.18	0.04
	2	10	12.9	12.9	0.23	0.08
	3	15	17.5	17.5	0.25	0.12
	4	20	22.8	22.8	0.29	0.15
	5	25	27.3	27.3	0.34	0.19
	6	30	28.4	28.4	0.36	0.23
	7	35	30.1	30.1	0.38	0.27
	8	40	31.3	31.3	0.4	0.31
	9	45	33.2	33.2	0.46	0.35
	10	50	35.9	35.9	0.5	0.39
	11	55	37.5	37.5	0.55	0.42
	12	60	39.9	39.9	0.57	0.46
Spherical button	1	5	9.3	9.3	0.38	0.25
	2	10	15.6	15.6	0.54	0.42
	3	15	19.3	19.3	0.76	0.52
	4	20	24	24	0.81	0.65
	5	25	27.8	27.8	0.87	0.76
	6	30	28.9	28.9	0.89	0.79
	7	35	30.2	30.2	0.93	0.82
	8	40	32.9	32.9	0.97	0.89
	9	45	33.2	33.2	1.01	0.90
	10	50	34.7	34.7	1.05	0.94
	11	55	35.1	35.1	1.1	0.95
	12	60	35.3	35.3	1.16	0.96

Table 4.29 Comparison of results of FEM analysis (ANSYS) with static indentation tests for twelve load steps limestone rock.

Bit type	Load step	Time (sec)	Force (kN)		Displacement (mm)	
			Experimental	ANSYS	Experimental	ANSYS
Rock Type: Limestone						
Chisel	1	5	8.2	8.2	0.23	0.11
	2	10	15.9	15.9	0.34	0.21
	3	15	24.6	24.6	0.41	0.33
	4	20	27.7	27.7	0.48	0.37
	5	25	32.1	32.1	0.52	0.43
	6	30	36.3	36.3	0.55	0.49
	7	35	37.3	37.3	0.61	0.50
	8	40	42.9	42.9	0.66	0.58
	9	45	41.9	41.9	0.7	0.56
	10	50	46.2	46.2	0.75	0.62
	11	55	49.2	49.2	0.79	0.66
	12	60	49.9	49.9	0.82	0.67
Cross	1	5	12.1	12.1	0.19	0.04
	2	10	23.8	23.8	0.22	0.08
	3	15	28.7	28.7	0.27	0.13
	4	20	31.8	31.8	0.31	0.17
	5	25	33.9	33.9	0.36	0.21
	6	30	36.5	36.5	0.4	0.25
	7	35	38.7	38.7	0.45	0.29
	8	40	39.9	39.9	0.49	0.33
	9	45	41.7	41.7	0.53	0.38
	10	50	44.8	44.8	0.55	0.42
	11	55	48.9	48.9	0.58	0.46
	12	60	50.8	50.8	0.62	0.50
Spherical button	1	5	12.8	12.8	0.34	0.30
	2	10	21.8	21.8	0.53	0.50
	3	15	27.9	27.9	0.69	0.64
	4	20	30.6	30.6	0.77	0.71
	5	25	32.5	32.5	0.79	0.75
	6	30	35.5	35.5	0.88	0.82
	7	35	39.7	39.7	0.97	0.92
	8	40	43.3	43.3	1.06	1.00
	9	45	45.2	45.2	1.1	1.04
	10	50	46.5	46.5	1.15	1.07
	11	55	47.4	47.4	1.21	1.09
	12	60	48.8	48.8	1.3	1.13

Table 4.30 Comparison of results of FEM analysis (ANSYS) with static indentation tests for twelve load steps for basalt rock.

Bit type	Load step	Time (sec)	Force (kN)		Displacement (mm)	
			Experimental	ANSYS	Experimental	ANSYS
Rock Type: Basalt						
Chisel	1	5	6.8	6.8	0.1	0.08
	2	10	12.5	12.5	0.18	0.14
	3	15	19.8	19.8	0.27	0.23
	4	20	24.6	24.6	0.35	0.28
	5	25	28.7	28.7	0.4	0.33
	6	30	30.4	30.4	0.43	0.35
	7	35	32.3	32.3	0.48	0.37
	8	40	36.4	36.4	0.5	0.42
	9	45	39.5	39.5	0.54	0.45
	10	50	42.1	42.1	0.62	0.48
	11	55	48.6	48.6	0.66	0.55
	12	60	52.1	52.1	0.68	0.58
Cross	1	5	8.3	8.3	0.04	0.03
	2	10	15.3	15.3	0.12	0.06
	3	15	21.8	21.8	0.19	0.09
	4	20	25.6	25.6	0.23	0.13
	5	25	28.2	28.2	0.26	0.16
	6	30	30.2	30.2	0.29	0.20
	7	35	33.9	33.9	0.32	0.23
	8	40	36.4	36.4	0.35	0.26
	9	45	39.3	39.3	0.38	0.30
	10	50	41.9	41.9	0.43	0.33
	11	55	44.5	44.5	0.46	0.36
	12	60	47.8	47.8	0.49	0.40
Spherical button	1	5	12.8	12.8	0.53	0.43
	2	10	22.5	22.5	0.56	0.50
	3	15	27.6	27.6	0.62	0.53
	4	20	31.4	31.4	0.71	0.60
	5	25	34.2	34.2	0.79	0.65
	6	30	38.6	38.6	0.86	0.74
	7	35	40.7	40.7	0.93	0.78
	8	40	43.6	43.6	0.96	0.83
	9	45	47.8	47.8	1	0.91
	10	50	50.6	50.6	1.03	0.97
	11	55	52.9	52.9	1.05	1.01
	12	60	55.8	55.8	1.08	1.07

Table 4.31 Comparison of results of FEM analysis (ANSYS) with static indentation tests for twelve load steps for steel gray granite rock.

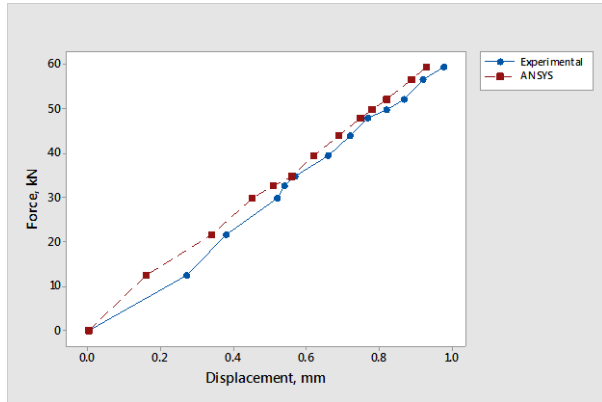
Bit type	Load step	Time (sec)	Force (kN)		Displacement (mm)	
			Experimental	ANSYS	Experimental	ANSYS
Rock Type: Steel gray granite						
Chisel	1	5	12.3	12.3	0.18	0.15
	2	10	21.4	21.4	0.29	0.25
	3	15	26.3	26.3	0.34	0.31
	4	20	29.2	29.2	0.38	0.35
	5	25	33.6	33.6	0.42	0.40
	6	30	36.2	36.2	0.46	0.43
	7	35	40.1	40.1	0.51	0.48
	8	40	43.3	43.3	0.55	0.51
	9	45	47.2	47.2	0.58	0.56
	10	50	50.1	50.1	0.62	0.60
	11	55	53.2	53.2	0.65	0.63
	12	60	55.6	55.6	0.68	0.66
Cross	1	5	11.2	11.2	0.06	0.04
	2	10	16.4	16.4	0.11	0.09
	3	15	24.8	24.8	0.15	0.13
	4	20	30.3	30.3	0.19	0.17
	5	25	33.9	33.9	0.25	0.22
	6	30	36.7	36.7	0.3	0.26
	7	35	40.4	40.4	0.35	0.31
	8	40	45.5	45.5	0.39	0.35
	9	45	49.3	49.3	0.44	0.39
	10	50	54	54	0.51	0.44
	11	55	57.3	57.3	0.55	0.48
	12	60	60.4	60.4	0.6	0.52
Spherical button	1	5	10.2	10.2	0.25	0.21
	2	10	22	22	0.48	0.44
	3	15	28.4	28.4	0.61	0.57
	4	20	32.9	32.9	0.68	0.66
	5	25	36.8	36.8	0.76	0.74
	6	30	40.2	40.2	0.84	0.81
	7	35	43.4	43.4	0.89	0.87
	8	40	47.6	47.6	0.99	0.96
	9	45	46.1	46.1	0.95	0.93
	10	50	45.9	45.9	0.93	0.92
	11	55	48.9	48.9	0.96	0.98
	12	60	47.8	47.8	0.98	0.96

Table 4.32 Comparison of results of FEM analysis (ANSYS) with static indentation tests for twelve load steps for moon white granite rock.

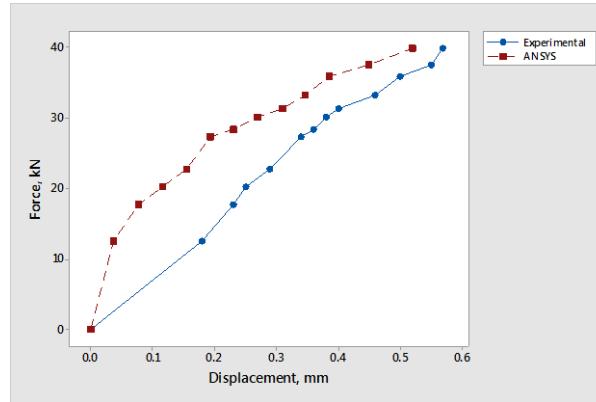
Bit type	Load step	Time (sec)	Force (kN)		Displacement (mm)	
			Experimental	ANSYS	Experimental	ANSYS
Rock Type: Moon white granite						
Chisel	1	5	12.8	12.8	0.2	0.17
	2	10	22.4	22.4	0.34	0.30
	3	15	29.8	29.8	0.45	0.41
	4	20	35.3	35.3	0.51	0.48
	5	25	40.8	40.8	0.59	0.56
	6	30	43.8	43.8	0.62	0.60
	7	35	47.2	47.2	0.66	0.64
	8	40	52.8	52.8	0.75	0.72
	9	45	57	57	0.81	0.78
	10	50	59.1	59.1	0.84	0.80
	11	55	62.4	62.4	0.87	0.85
	12	60	64.1	64.1	0.89	0.87
Cross	1	5	13.6	13.6	0.08	0.04
	2	10	18.5	18.5	0.13	0.09
	3	15	26.8	26.8	0.18	0.14
	4	20	30.8	30.8	0.25	0.19
	5	25	36.4	36.4	0.29	0.25
	6	30	39.2	39.2	0.33	0.30
	7	35	43.6	43.6	0.39	0.35
	8	40	48.2	48.2	0.46	0.40
	9	45	52.6	52.6	0.51	0.45
	10	50	55.4	55.4	0.59	0.50
	11	55	58.7	58.7	0.64	0.55
	12	60	60.1	60.1	0.69	0.60
Spherical button	1	5	12.4	12.4	0.27	0.24
	2	10	20.8	20.8	0.45	0.40
	3	15	26.3	26.3	0.57	0.51
	4	20	29.8	29.8	0.61	0.58
	5	25	33.4	33.4	0.69	0.64
	6	30	36.2	36.2	0.75	0.70
	7	35	40.4	40.4	0.81	0.78
	8	40	44.3	44.3	0.89	0.86
	9	45	46.6	46.6	0.92	0.90
	10	50	47.2	47.2	0.94	0.91
	11	55	49.3	49.3	0.99	0.95
	12	60	50.7	50.7	1.01	0.98

Table 4.33 Comparison of results of FEM analysis (ANSYS) with static indentation tests for twelve load steps for black galaxy granite rock.

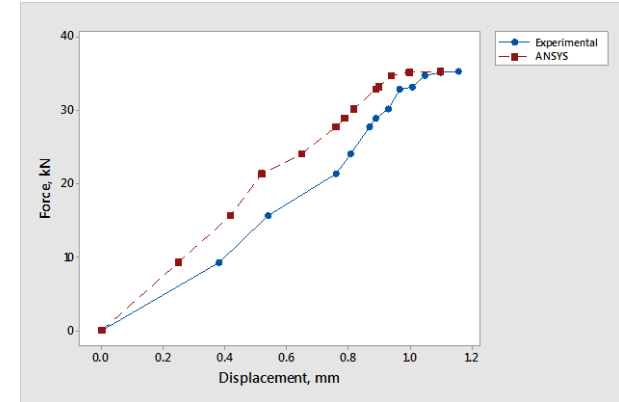
Bit type	Load step	Time (sec)	Force (kN)		Displacement (mm)	
			Experimental	ANSYS	Experimental	ANSYS
Rock Type: Black galaxy granite						
Chisel	1	5	16.5	16.5	0.28	0.18
	2	10	24.3	24.3	0.34	0.27
	3	15	29.4	29.4	0.38	0.32
	4	20	34.8	34.8	0.4	0.38
	5	25	38.9	38.9	0.43	0.42
	6	30	45.6	45.6	0.5	0.48
	7	35	48.6	48.6	0.53	0.52
	8	40	53.4	53.4	0.59	0.58
	9	45	54.9	54.9	0.62	0.59
	10	50	56.8	56.8	0.64	0.61
	11	55	57.9	57.9	0.72	0.63
	12	60	59.9	59.9	0.78	0.65
Cross	1	5	9.8	9.8	0.15	0.04
	2	10	11.8	11.8	0.24	0.09
	3	15	20.2	20.2	0.29	0.13
	4	20	27.1	27.1	0.32	0.18
	5	25	31.8	31.8	0.34	0.22
	6	30	34.6	34.6	0.37	0.27
	7	35	38.4	38.4	0.43	0.31
	8	40	41.9	41.9	0.48	0.36
	9	45	43.4	43.4	0.55	0.4
	10	50	45.8	45.8	0.59	0.44
	11	55	48.9	48.9	0.63	0.49
	12	60	51.1	51.1	0.66	0.53
Spherical button	1	5	11.2	11.2	0.3	0.2
	2	10	21.4	21.4	0.41	0.3
	3	15	27.6	27.6	0.54	0.51
	4	20	28.3	28.3	0.56	0.52
	5	25	31.9	31.9	0.64	0.58
	6	30	35.8	35.8	0.69	0.65
	7	35	39.2	39.2	0.74	0.72
	8	40	43.6	43.6	0.97	0.79
	9	45	46.9	46.9	1.02	0.86
	10	50	51.2	51.2	1.04	0.93
	11	55	52.6	52.6	1.06	0.96
	12	60	55.8	55.8	1.1	1.02



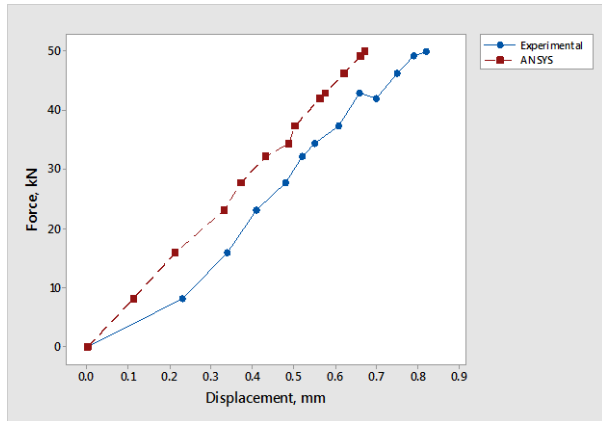
Rock type: Marble Bit geometry: chisel



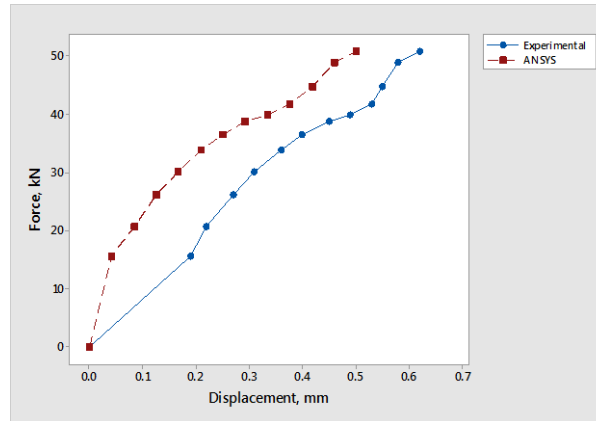
Bit geometry: cross



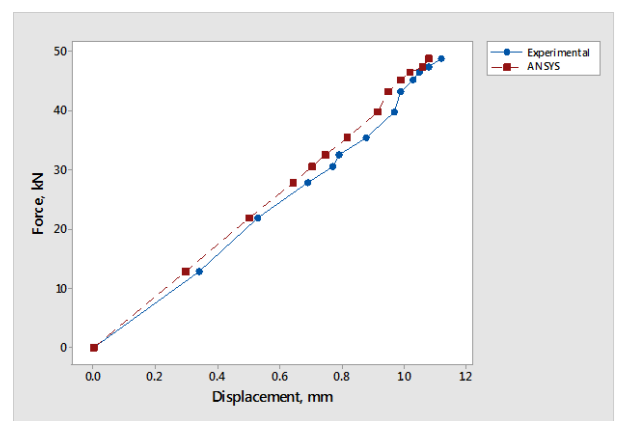
Bit geometry: Spherical button



Rock type: Limestone Bit geometry: chisel

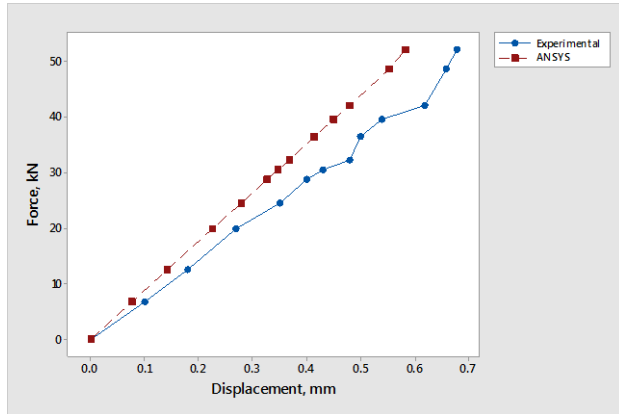


Bit geometry: cross

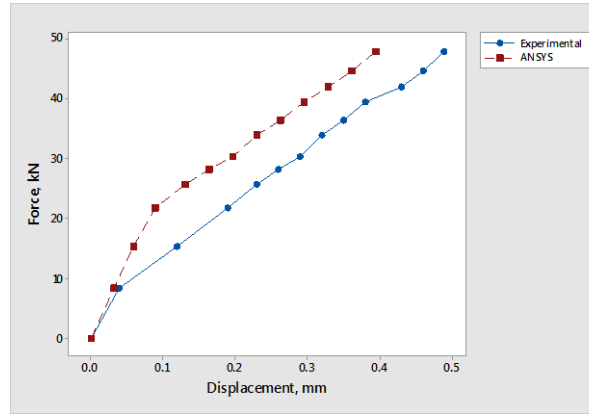


Bit geometry: Spherical button

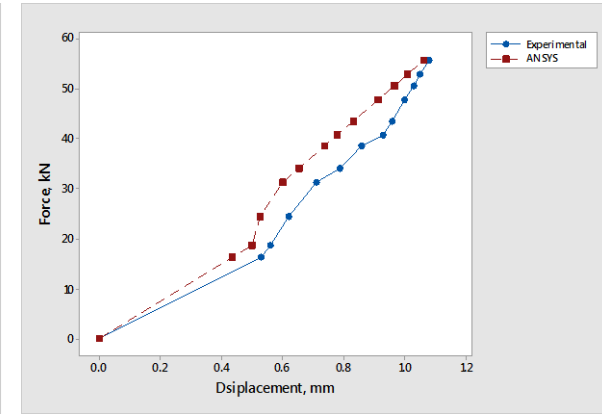
Figure 4.51(a) Relationship between Force-displacement of chisel, cross and spherical button bits of 48 mm diameter in two types of rocks



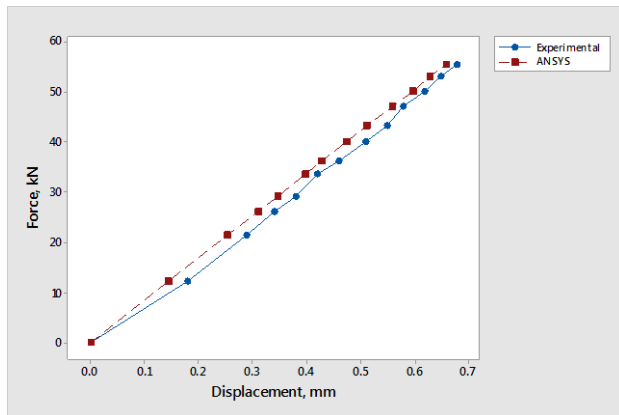
Rock type: Basalt Bit geometry: chisel



Bit geometry: cross

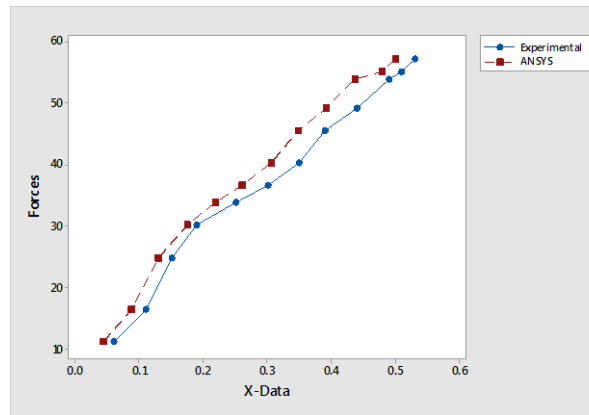


Bit geometry: Spherical button

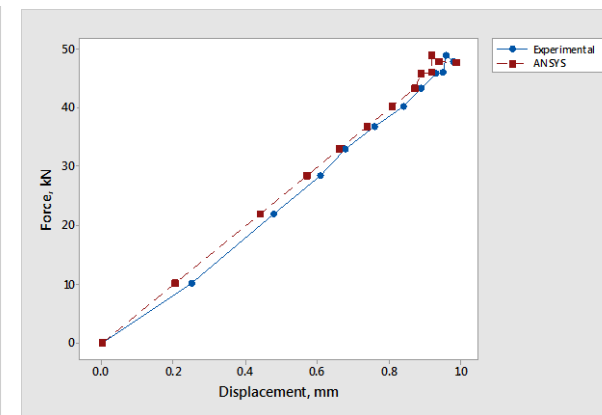


Rock type: Steel gray granite

Bit geometry: chisel

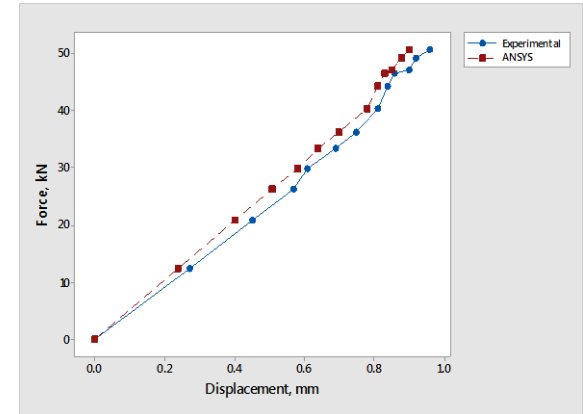
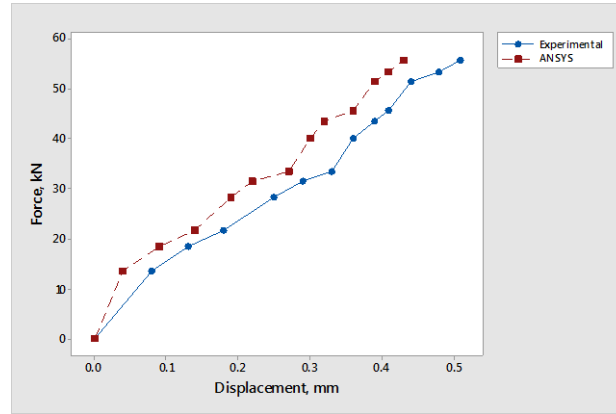
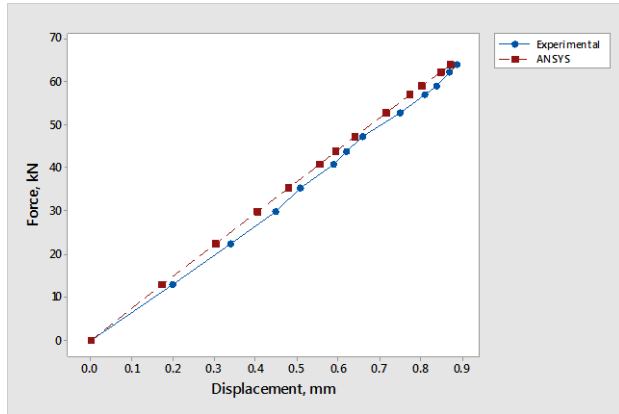


Bit geometry: cross

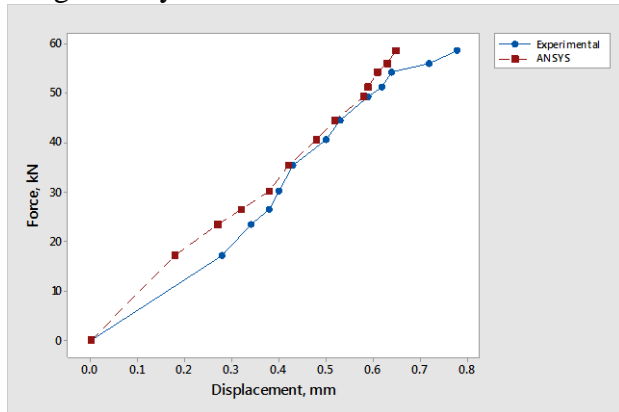


Bit geometry: Spherical button

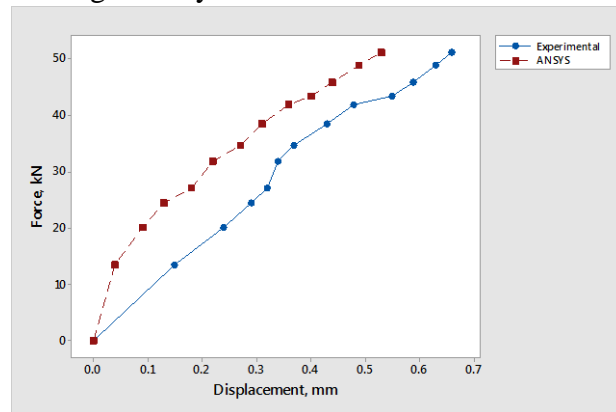
Figure 4.51(b) Relationship between Force-displacement of chisel, cross and spherical button bits of 48 mm diameter in two types of rocks



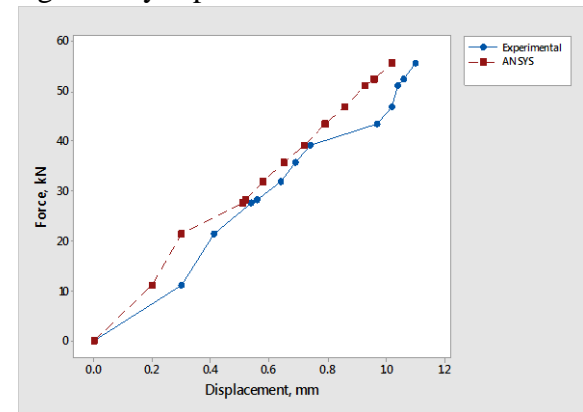
Rock type: Moon white granite
 Bit geometry: chisel



Bit geometry: cross



Bit geometry: Spherical button



Rock type: Black galaxy granite
 Bit geometry: chisel

Bit geometry: cross

Bit geometry: Spherical button

Figure 4.51(c) Relationship between Force-displacement of chisel, cross and spherical button bits of 48 mm diameter in two types of rocks

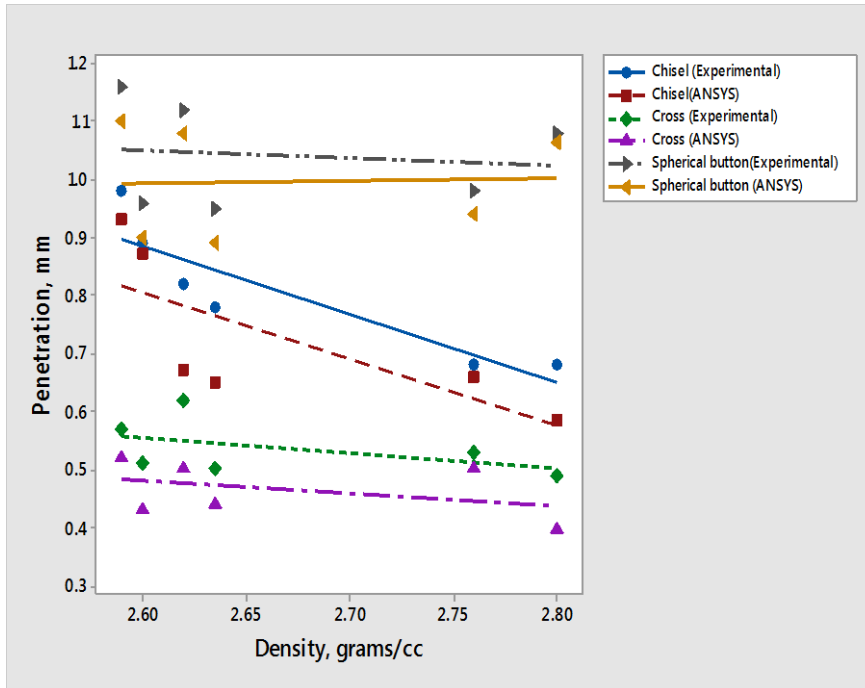


Figure 4.52(a) Relation between density of rocks and displacement obtained in static indentation tests and FEM analysis for three bit geometries

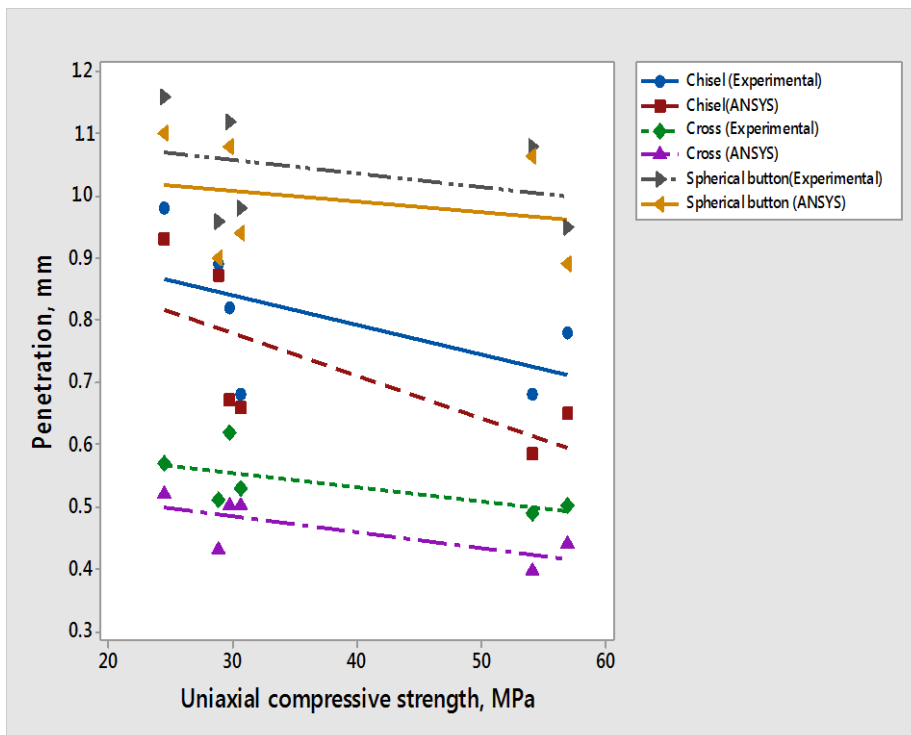


Figure 4.52(b) Relation between UCS of rocks and displacement obtained in static indentation tests and FEM analysis for three bit geometries

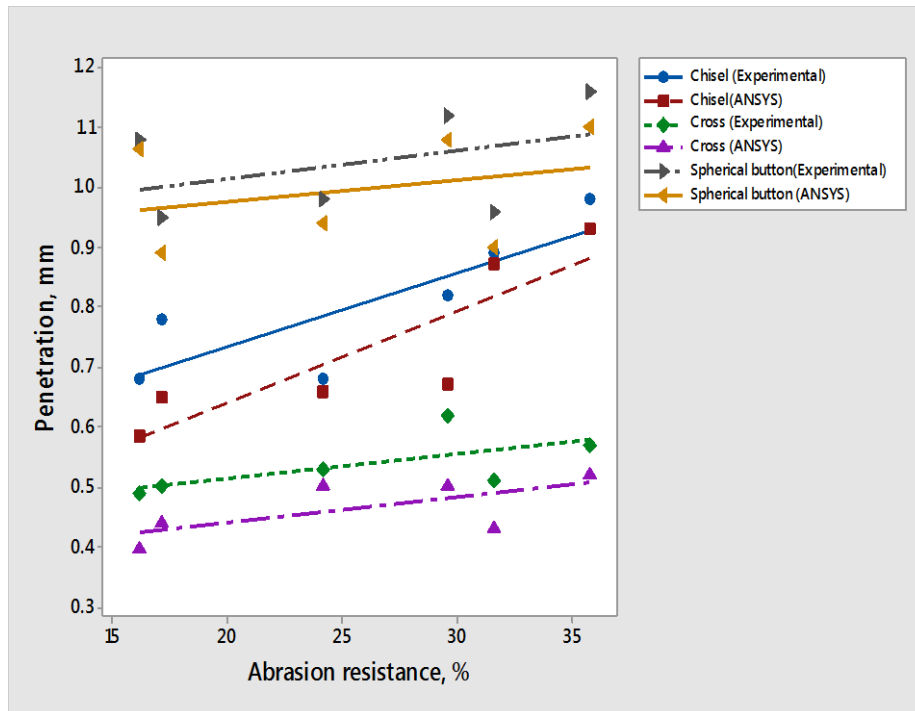


Figure 4.52(c) Relation between abrasion resistance of rocks and displacement obtained in static indentation tests and FEM analysis for three bit geometries

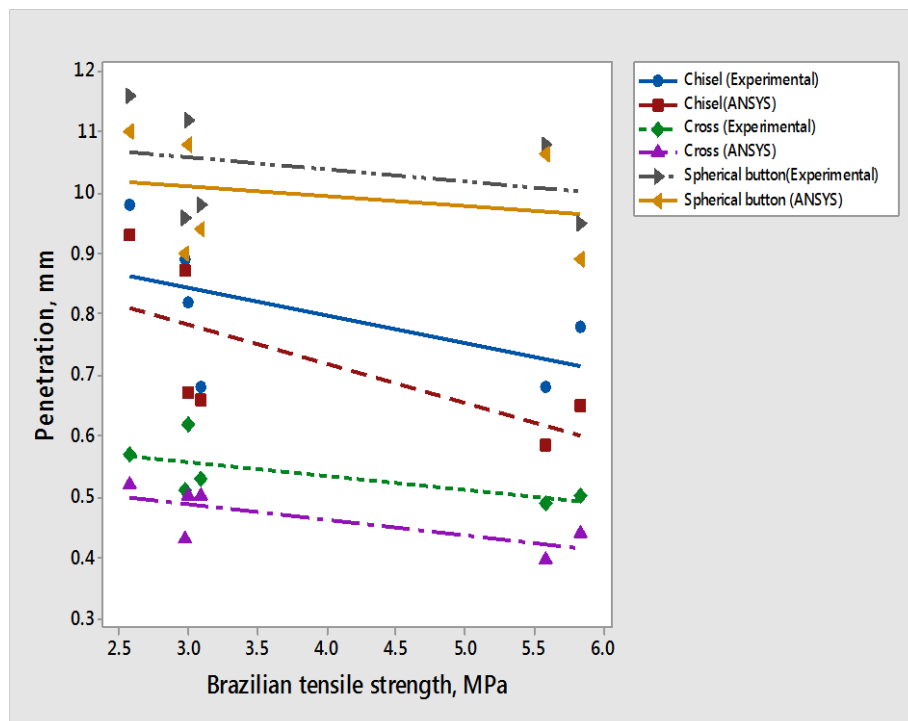


Figure 4.52(d) Relation between BTS of rocks and displacement obtained in static indentation tests and FEM analysis for three bit geometries

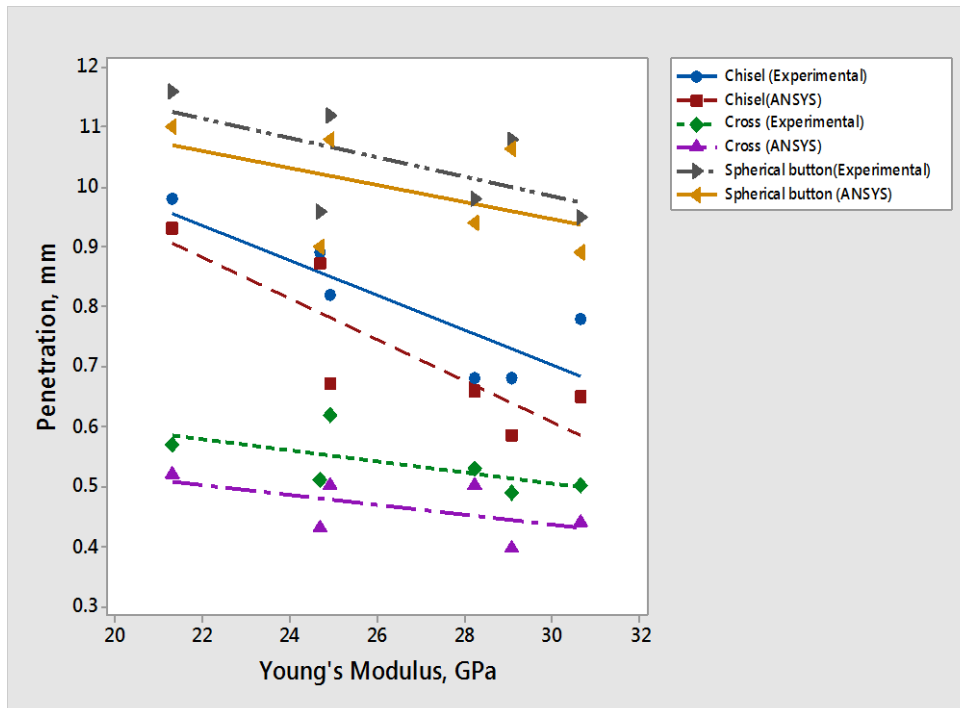


Figure 4.52(e) Relation between Young's Modulus of rocks and displacement obtained in static indentation tests and FEM analysis for three bit geometries

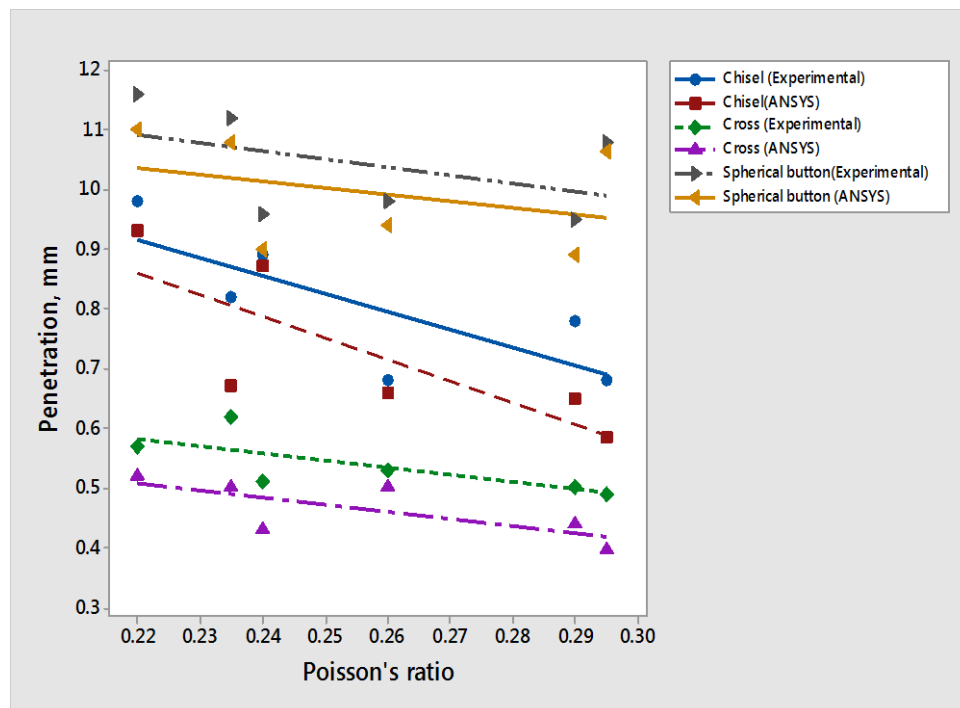


Figure 4.52(f) Relation between Poisson's ratio of rocks and displacement obtained in static indentation tests and FEM analysis for three bit geometries

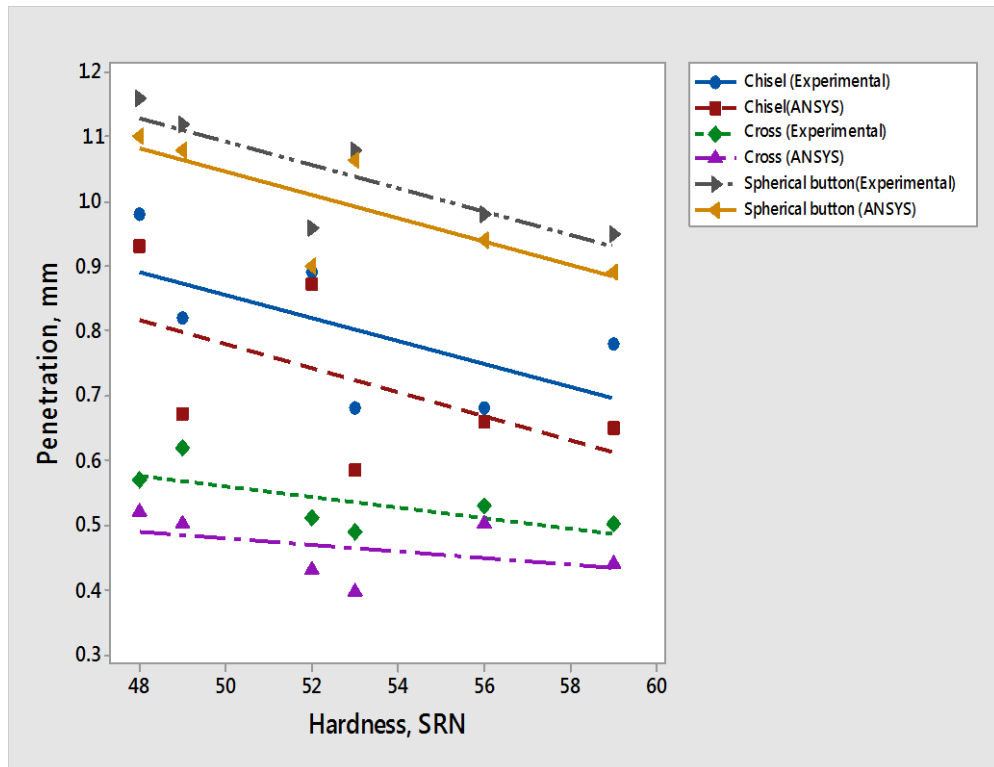


Figure 4.52(g) Relation between hardness (SRN) of rocks and displacement obtained in static indentation tests and FEM analysis for three bit geometries

Table 4.34: Magnitude of depth of indentation and the distance along X, Y and Z-axes as obtained in FEM analysis for marble rock

Distance along X-axis	Depth of indentation (mm)	Distance along Y-axis	Depth of indentation (mm)	Distance along Z-axis	Depth of indentation (mm)
Chisel bit					
0.000	0.000	0.000	-0.936	0.000	0.000
1.200	-0.086	3.175	-0.393	1.200	0.017
2.400	-0.074	6.350	-0.334	2.400	0.015
3.600	-0.073	9.525	-0.273	3.600	0.014
4.800	-0.071	12.700	-0.231	34.440	0.062
20.400	-0.041	15.875	-0.200	35.931	0.055
21.600	-0.040	19.050	-0.174	37.423	0.049
22.800	-0.038	22.225	-0.154	38.914	0.045
24.000	-0.037	25.400	-0.136	40.406	0.041
26.217	-0.034	28.575	-0.121	41.897	0.038
Cross bit					
0.000	0.000	0.000	-0.464	0.000	0.000
1.200	-0.017	3.175	-0.267	1.200	0.017
2.400	-0.023	6.350	-0.215	2.400	0.023
3.600	-0.025	9.525	-0.180	3.600	0.025
26.400	-0.042	12.700	-0.153	24.000	0.043
28.617	-0.039	15.875	-0.133	25.491	0.042
30.834	-0.031	19.050	-0.116	26.983	0.036
33.051	-0.027	22.225	-0.103	28.474	0.032
35.269	-0.024	25.400	-0.091	29.966	0.029
37.486	-0.022	28.575	-0.081	31.457	0.027
Spherical button bit					
0.000	-0.132	0.000	-0.959	0.000	0.132
0.346	-0.130	2.442	-0.698	0.346	0.131
0.692	-0.127	4.885	-0.494	0.692	0.127
1.039	-0.122	7.327	-0.362	1.039	0.122
1.385	-0.117	9.769	-0.282	1.385	0.117
1.731	-0.112	12.212	-0.228	1.731	0.112
2.077	-0.107	14.654	-0.189	2.077	0.107
2.423	-0.102	17.096	-0.160	2.423	0.102
2.769	-0.097	19.538	-0.138	2.769	0.098
3.115	-0.093	21.981	-0.121	3.115	0.093

Table 4.35: Magnitude of depth of indentation and the distance along X and Z-axes as obtained in FEM analysis for limestone rock

Distance along X-axis	Depth of indentation (mm)	Distance along Y-axis	Depth of indentation (mm)	Distance along Z-axis	Depth of indentation (mm)
Chisel bit					
0.000	-0.055	0.000	-0.672	0.000	0.012
1.200	-0.053	3.175	-0.282	1.200	0.012
2.400	-0.051	6.350	-0.239	2.400	0.010
3.600	-0.050	12.700	-0.166	3.600	0.009
4.800	-0.049	12.700	-0.166	24.000	0.006
24.000	-0.025	15.875	-0.196	25.491	0.060
26.217	-0.024	19.050	-0.166	26.983	0.049
28.434	-0.022	22.225	-0.144	28.474	0.042
30.651	-0.021	25.400	-0.125	29.966	0.038
35.086	-0.018	28.575	-0.110	31.457	0.034
Cross bit					
0.000	0.000	0.000	-0.502	0.000	0.000
1.200	-0.027	3.175	-0.290	1.200	0.017
2.400	-0.024	6.350	-0.234	2.400	0.024
3.600	-0.023	9.525	-0.195	3.600	0.026
4.800	-0.020	12.700	-0.166	4.800	0.027
31.017	-0.040	15.875	-0.144	25.491	0.044
33.234	-0.033	19.050	-0.126	26.983	0.037
35.451	-0.028	22.225	-0.111	28.474	0.033
37.669	-0.025	25.400	-0.099	29.966	0.030
39.886	-0.023	28.575	-0.088	31.457	0.028
Spherical button bit					
0.000	-0.149	0.000	-1.126	0.000	0.089
0.346	-0.147	2.442	-0.823	2.036	0.073
0.692	-0.143	4.885	-0.583	4.073	0.062
1.039	-0.138	7.327	-0.428	6.109	0.053
1.385	-0.132	9.769	-0.333	8.146	0.047
1.731	-0.126	12.212	-0.269	10.182	0.042
2.077	-0.121	14.654	-0.223	12.218	0.037
2.423	-0.115	17.096	-0.190	14.255	0.034
2.769	-0.110	19.538	-0.164	16.291	0.031
3.115	-0.105	21.981	-0.143	18.327	0.028

Table 4.36: Magnitude of depth of indentation and the distance along X, Y and Z-axes as obtained in FEM analysis for basalt rock

Distance along X-axis	Depth of indentation (mm)	Distance along Y-axis	Depth of indentation (mm)	Distance along Z-axis	Depth of indentation (mm)
Chisel bit					
0.000	0.000	0.000	-0.584	0.000	0.008
1.200	-0.027	3.175	-0.244	1.200	0.008
2.400	-0.034	6.350	-0.206	2.400	0.007
3.600	-0.035	9.525	-0.170	3.600	0.007
4.800	-0.034	12.700	-0.144	4.800	0.006
6.000	-0.033	15.875	-0.125	27.891	0.042
7.200	-0.031	19.050	-0.109	29.383	0.035
8.400	-0.030	22.225	-0.096	30.874	0.030
9.600	-0.029	25.400	-0.085	32.366	0.026
10.800	-0.027	28.575	-0.076	33.857	0.024
Cross bit					
0.000	0.000	0.000	-0.396	0.000	0.000
1.200	0.016	3.175	-0.230	1.200	0.010
2.400	0.015	6.350	-0.184	2.400	0.015
3.600	0.014	9.525	-0.155	3.600	0.017
4.800	0.013	12.700	-0.132	25.491	0.028
33.234	-0.021	15.875	-0.115	26.983	0.024
35.451	-0.018	19.050	-0.101	28.474	0.021
37.669	-0.016	22.225	-0.089	29.966	0.020
39.886	-0.014	25.400	-0.079	31.457	0.018
42.103	-0.013	28.575	-0.070	32.949	0.017
Spherical button bit					
0.000	-0.115	0.000	-1.066	0.000	0.069
0.346	-0.113	2.442	-0.798	2.036	0.057
0.692	-0.111	4.885	-0.569	4.073	0.048
1.039	-0.107	7.327	-0.418	6.109	0.042
1.385	-0.103	9.769	-0.325	8.146	0.036
24.142	-0.020	12.212	-0.263	12.218	0.029
26.948	-0.018	14.654	-0.218	12.218	0.029
29.755	-0.016	17.096	-0.185	14.255	0.032
32.561	-0.015	19.538	-0.160	16.291	0.029
38.173	-0.013	21.981	-0.139	18.327	0.027

Table 4.37: Magnitude of depth of indentation and the distance along X, Y and Z-axes as obtained in FEM analysis for steel grey granite rock

Distance along X-axis	Depth of indentation (mm)	Distance along Y-axis	Depth of indentation (mm)	Distance along Z-axis	Depth of indentation (mm)
Chisel bit					
0.000	0.000	0.000	-0.659	0.000	0.000
1.200	-0.047	3.175	-0.276	1.200	0.010
2.400	-0.044	6.350	-0.234	2.400	0.009
3.600	-0.044	9.525	-0.192	3.600	0.009
4.800	-0.045	12.700	-0.162	4.800	0.009
24.000	-0.025	15.875	-0.141	26.400	0.056
26.217	-0.024	19.050	-0.123	27.891	0.055
28.434	-0.023	22.225	-0.108	29.383	0.045
30.651	-0.021	25.400	-0.096	30.874	0.039
32.869	-0.020	28.575	-0.085	32.366	0.034
Cross bit					
0.000	0.000	0.000	-0.523	0.000	0.000
1.200	-0.016	3.175	-0.303	1.491	0.001
2.400	-0.023	6.350	-0.244	2.983	0.002
3.600	-0.025	9.525	-0.204	4.474	0.003
4.800	-0.026	12.700	-0.174	5.966	0.004
24.000	-0.042	15.875	-0.151	58.200	0.034
26.217	-0.039	19.050	-0.132	59.400	0.032
28.434	-0.032	22.225	-0.117	60.600	0.031
30.651	-0.027	25.400	-0.104	61.800	0.030
32.869	-0.024	28.575	-0.092	63.000	0.029
Spherical button bit					
0.000	0.000	0.000	-0.962	0.000	0.119
0.346	-0.117	2.442	-0.710	0.346	0.118
0.692	-0.114	4.885	-0.504	0.692	0.114
1.039	-0.110	7.327	-0.370	1.039	0.110
1.385	-0.106	9.769	-0.288	1.731	0.101
24.835	-0.021	12.212	-0.233	1.731	0.101
27.641	-0.019	14.654	-0.193	2.077	0.106
30.447	-0.017	17.096	-0.164	2.423	0.101
33.253	-0.015	19.538	-0.141	2.769	0.097
36.059	-0.014	21.981	-0.124	3.115	0.092

Table 4.38: Magnitude of depth of indentation and the distance along X, Y and Z-axes as obtained in FEM analysis for moon white granite rock

Distance along X-axis	Depth of indentation (mm)	Distance along Y-axis	Depth of indentation (mm)	Distance along Z-axis	Depth of indentation (mm)
Chisel bit					
0.000	0.000	0.000	-0.872	0.000	0.000
1.200	-0.053	3.175	-0.366	1.200	0.015
2.400	-0.063	6.350	-0.311	2.400	0.012
3.600	-0.064	9.525	-0.254	3.600	0.013
4.800	-0.062	12.700	-0.215	24.000	0.078
32.869	-0.028	15.875	-0.186	25.491	0.077
35.086	-0.026	19.050	-0.162	26.983	0.063
37.303	-0.025	22.225	-0.143	28.474	0.054
39.520	-0.023	25.400	-0.123	29.966	0.048
41.737	-0.022	28.575	-0.117	31.457	0.043
Cross bit					
0.000	0.035	0.000	-0.600	0.000	0.000
1.200	-0.030	3.175	-0.346	1.200	0.030
2.400	-0.028	6.350	-0.279	2.400	0.028
3.600	-0.027	9.525	-0.233	3.600	0.031
4.800	-0.025	12.700	-0.199	4.800	0.028
24.000	-0.051	15.875	-0.173	32.366	0.051
26.217	-0.047	19.050	-0.151	33.857	0.044
28.434	-0.038	22.225	-0.133	35.349	0.039
30.651	-0.033	25.400	-0.118	36.840	0.036
32.869	-0.030	28.575	-0.105	38.331	0.033
Spherical button bit					
0.000	-0.126	0.000	-0.979	0.000	0.075
0.375	-0.124	2.646	-0.697	0.375	0.068
0.750	-0.121	5.292	-0.481	0.750	0.061
1.125	-0.116	7.938	-0.348	1.125	0.053
1.500	-0.111	10.583	-0.269	1.500	0.046
29.193	-0.019	13.229	-0.216	1.688	0.038
32.280	-0.017	15.875	-0.179	1.875	0.031
35.367	-0.015	18.521	-0.151	2.063	0.023
38.453	-0.014	21.167	-0.130	2.250	0.016
41.540	-0.012	23.812	-0.113	2.438	0.008

Table 4.39: Magnitude of depth of indentation and the distance along X, Y and Z-axes as obtained in FEM analysis for black galaxy granite rock

Distance along X-axis	Depth of indentation (mm)	Distance along Y-axis	Depth of indentation (mm)	Distance along Z-axis	Depth of indentation (mm)
Chisel bit					
0.000	0.000	0.000	-0.651	0.000	0.010
1.200	-0.032	3.175	-0.272	1.200	0.009
2.400	-0.039	6.350	-0.230	2.400	0.008
3.600	-0.040	9.525	-0.189	3.600	0.008
4.800	-0.039	12.700	-0.160	4.800	0.007
25.200	-0.023	15.875	-0.139	25.491	0.049
26.400	-0.022	19.050	-0.121	26.983	0.040
27.600	-0.021	22.225	-0.107	28.474	0.035
28.800	-0.020	25.400	-0.095	29.966	0.031
31.017	-0.019	28.575	-0.084	31.457	0.028
Cross bit					
0.000	0.000	0.000	-0.532	0.000	0.000
0.875	-0.024	3.175	-0.295	0.875	0.012
1.750	-0.023	6.350	-0.233	1.750	0.019
2.625	-0.020	9.525	-0.191	2.625	0.022
25.150	-0.023	12.700	-0.159	3.500	0.024
27.556	-0.021	15.875	-0.136	27.563	0.025
29.959	-0.018	19.050	-0.117	29.240	0.023
32.361	-0.017	22.225	-0.102	30.917	0.021
34.764	-0.015	25.400	-0.089	32.594	0.019
37.167	-0.014	28.575	-0.078	34.271	0.018
Spherical button bit					
0.000	-0.114	0.000	-1.018	0.000	0.010
0.346	-0.110	2.442	-0.760	2.036	0.009
0.692	-0.113	4.885	-0.541	4.073	0.008
1.039	-0.110	7.327	-0.397	6.109	0.007
1.385	-0.106	9.769	-0.309	8.146	0.006
24.142	-0.023	12.212	-0.250	10.182	0.005
26.948	-0.020	14.654	-0.207	12.218	0.005
29.755	-0.018	17.096	-0.176	14.255	0.004
32.561	-0.016	19.538	-0.152	16.291	0.003
35.367	-0.015	21.981	-0.133	18.327	0.002

Table 4.40: Magnitude of compressive stresses and the distance along X, Y and Z-axes as obtained in FEM analysis for marble rock

Distance along X-axis	Magnitude of compressive stress (MPa)	Distance along Y-axis	Magnitude of compressive stress (MPa)	Distance along Z-axis	Magnitude of compressive stress (MPa)
Chisel bit					
0.0	-893.0	0.0	-2683.8	0.0	-257.3
1.2	-584.1	3.2	-1982.7	1.2	-231.4
2.4	-893.0	6.4	-388.8	2.4	-55.7
3.6	-584.1	9.5	-374.6	3.6	-49.5
4.8	-493.0	12.7	-237.1	34.4	47.2
20.4	21.3	15.9	-194.0	35.9	39.5
21.6	21.0	19.1	-153.7	37.4	33.9
22.8	20.5	22.2	-127.7	38.9	29.8
24.0	20.0	25.4	-106.9	40.4	26.5
26.2	19.6	28.6	-90.9	41.9	24.0
Cross bit					
0.0	-263.7	0.0	-1092.3	0.0	-277.2
1.2	-256.6	3.2	-882.5	1.2	-264.2
2.4	-253.7	6.4	-276.7	2.4	-107.9
3.6	-107.4	9.5	-222.3	3.6	-55.2
26.4	43.4	12.7	-156.5	24.0	43.4
28.6	20.5	15.9	-125.4	25.5	29.4
30.8	18.8	19.1	-101.3	27.0	25.2
33.1	14.9	22.2	-84.2	28.5	21.0
35.3	13.0	25.4	-70.9	30.0	18.2
37.5	11.3	28.6	-60.4	31.5	16.2
Spherical button bit					
0.0	-185.8	0.0	-2415.2	0.0	-1320.8
0.3	-78.7	2.4	-2469.9	0.3	-1302.9
0.7	97.4	4.9	-1496.9	0.7	-1278.4
1.0	131.8	7.3	-904.8	1.2	-1250.9
1.4	149.1	9.8	-563.0	1.4	-1260.9
1.7	157.2	12.2	-390.9	1.9	-1221.1
2.1	154.9	14.7	-280.8	2.3	-1168.5
2.4	145.9	17.1	-212.4	2.6	-1085.4
2.8	135.9	19.5	-165.3	2.8	-1033.6
3.1	113.6	22.0	-132.3	3.3	-856.9

Table 4.41: Magnitude of compressive stresses and the distance along X, Y and Z-axes as obtained in FEM analysis for limestone rock

Distance along X-axis	Magnitude of compressive stress (MPa)	Distance along Y-axis	Magnitude of compressive stress (MPa)	Distance along Z-axis	Magnitude of compressive stress (MPa)
Chisel bit					
0.0	-793.1	0.0	-2273.5	0.0	12.4
1.2	-754.2	3.2	-1669.1	1.2	-54.5
2.4	-200.3	6.4	-300.6	2.4	-229.5
3.6	-82.4	9.5	-315.8	3.6	-54.5
4.8	-30.5	12.7	-199.3	24.0	-65.0
24.0	14.4	15.9	-163.3	25.5	-80.8
26.2	13.4	19.1	-129.3	27.0	86.2
28.4	12.7	22.2	-107.4	28.5	54.7
30.7	11.9	25.4	-89.9	30.0	46.0
35.1	11.1	28.6	-76.5	31.5	37.1
Cross bit					
0.0	-340.5	0.0	-1399.5	0.0	-341.2
1.2	-350.6	3.2	-1123.9	1.2	-351.3
2.4	-153.1	6.4	-351.7	2.4	-153.8
3.6	-86.5	9.5	-283.2	3.6	-87.2
4.8	-59.5	12.7	-199.2	4.8	-60.2
31.0	15.6	15.9	-159.7	25.5	-35.6
33.2	13.6	19.1	-128.9	27.0	51.3
35.5	12.2	22.2	-107.2	28.5	34.6
37.7	11.0	25.4	-90.2	30.0	29.9
39.9	10.0	28.6	-76.9	31.5	25.1
Spherical button bit					
0.0	-294.3	0.0	-3356.4	0.0	18.5
0.3	-144.3	2.4	-3414.5	2.0	17.3
0.7	103.9	4.9	-2069.4	4.1	14.0
1.0	154.1	7.3	-1251.4	6.1	12.8
1.4	180.5	9.8	-778.0	8.1	11.9
1.7	196.0	12.2	-540.5	10.2	11.3
2.1	194.7	14.7	-388.2	12.2	10.9
2.4	185.4	17.1	-293.7	14.3	10.6
2.8	179.7	19.5	-228.5	16.3	10.3
3.1	173.9	22.0	-182.9	18.3	10.2

Table 4.42: Magnitude of compressive stresses and the distance along X, Y and Z-axes as obtained in FEM analysis for basalt rock

Distance along X-axis	Magnitude of compressive stress (MPa)	Distance along Y-axis	Magnitude of compressive stress (MPa)	Distance along Z-axis	Magnitude of compressive stress (MPa)
Chisel bit					
0.0	-513.8	0.0	-2405.0	0.0	-397.0
1.2	-233.9	3.2	-1714.1	1.2	-208.3
2.4	-38.4	6.4	-381.0	2.4	-213.5
3.6	28.0	9.5	-327.3	3.6	-211.6
4.8	18.9	12.7	-202.8	4.8	-212.9
6.0	12.1	15.9	-168.2	27.9	-206.9
7.2	9.0	19.1	-132.4	29.4	-54.7
8.4	8.2	22.2	-110.4	30.9	-135.8
9.6	6.9	25.4	-92.3	32.4	58.1
10.8	6.0	28.6	-78.6	33.9	35.3
Cross bit					
0.0	-378.6	0.0	-1354.8	0.0	-379.3
1.2	-213.8	3.2	-1058.1	1.2	-393.8
2.4	-152.9	6.4	-327.6	2.4	-214.5
3.6	-213.8	12.7	-286.8	3.6	-153.6
4.8	-393.1	12.7	-286.8	25.5	-60.5
33.2	-63.3	15.9	-267.7	27.0	32.1
35.5	39.2	19.1	-186.8	28.5	21.1
37.7	14.6	22.2	-150.5	30.0	19.4
39.9	15.6	25.4	-121.2	31.5	16.6
42.1	12.2	28.6	-101.0	32.9	14.7
Spherical button bit					
0.0	-524.2	0.0	-3927.9	0.0	17.8
0.3	-343.6	2.4	-3903.9	2.0	16.7
0.7	-150.0	4.9	-2366.1	4.1	13.2
1.0	-34.5	7.3	-1433.8	6.1	12.1
1.4	36.5	9.8	-887.3	8.1	11.3
24.1	17.6	12.2	-618.9	10.2	10.7
26.9	15.1	14.7	-443.3	12.2	10.3
29.8	13.1	17.1	-336.0	14.3	9.9
32.6	11.6	19.5	-261.1	16.3	9.7
38.2	9.2	22.0	-209.1	18.3	9.5

Table 4.43: Magnitude of compressive stresses and the distance along X, Y and Z-axes as obtained in FEM analysis for steel grey granite rock

Distance along X-axis	Magnitude of compressive stress (MPa)	Distance along Y-axis	Magnitude of compressive stress (MPa)	Distance along Z-axis	Magnitude of compressive stress (MPa)
Chisel bit					
0.0	-852.5	0.0	-2562.3	0.0	-134.3
1.2	-845.6	3.2	-1860.7	1.2	-128.1
2.4	-230.3	6.4	-382.1	2.4	-123.1
3.6	-98.5	9.5	-353.1	3.6	-321.7
4.8	-39.8	12.7	-221.4	4.8	-123.1
24.0	14.3	15.9	-182.2	26.4	-1.6
26.2	13.4	19.1	-144.0	27.9	71.9
28.4	12.7	22.2	-119.8	29.4	83.4
30.7	11.9	25.4	-100.2	30.9	52.2
32.9	11.2	28.6	-73.2	32.4	44.9
Cross bit					
0.0	-432.6	0.0	-1681.9	0.0	-77.7
1.2	-446.9	3.2	-1336.7	1.5	21.4
2.4	-336.9	6.4	-416.7	3.0	-55.3
3.6	-215.2	9.5	-337.3	4.5	21.4
4.8	-136.9	12.7	-236.5	6.0	20.6
24.0	24.0	15.9	-190.0	58.2	18.7
26.2	19.0	19.1	-153.2	59.4	17.2
28.4	16.7	22.2	-127.5	60.6	16.0
30.7	14.6	25.4	-107.3	61.8	15.0
32.9	13.1	28.6	-91.5	63.0	14.2
Spherical button bit					
0.0	-349.7	0.0	-3316.7	0.0	17.1
0.3	-199.8	2.4	-3344.5	0.3	16.1
0.7	-40.1	4.9	-2027.1	0.7	12.8
1.0	105.1	7.3	-1226.7	1.0	11.7
1.4	51.5	9.8	-761.4	1.7	10.9
24.8	18.3	12.2	-529.7	1.7	10.4
27.6	15.6	14.7	-380.1	2.1	10.0
30.4	13.5	17.1	-223.8	2.4	9.7
33.3	11.8	19.5	-203.8	2.8	9.4
36.1	10.5	22.0	-179.2	3.1	9.3

Table 4.44: Magnitude of compressive stresses and the distance along X, Y and Z-axes as obtained in FEM analysis for moon white granite rock

Distance along X-axis	Magnitude of compressive stress (MPa)	Distance along Y-axis	Magnitude of compressive stress (MPa)	Distance along Z-axis	Magnitude of compressive stress (MPa)
Chisel bit					
0.0	-634.1	0.0	-2927.1	0.0	-0.4
1.2	-970.0	3.2	-2144.3	1.2	309.9
2.4	-258.9	6.4	-385.5	2.4	84.3
3.6	-107.4	9.5	-405.9	3.6	97.2
4.8	-40.5	12.7	-255.8	24.0	30.3
32.9	15.9	15.9	-209.9	25.5	108.8
35.1	15.0	19.1	-166.1	27.0	107.9
37.3	14.0	22.2	-138.0	28.5	68.2
39.5	13.1	25.4	-115.5	30.0	57.6
41.7	12.3	28.6	-98.3	31.5	46.5
Cross bit					
0.0	-408.3	0.0	-1659.2	0.0	-439.1
1.2	-420.7	3.2	-1329.7	1.2	-421.5
2.4	-187.7	6.4	-415.8	2.4	-188.5
3.6	-109.1	9.5	-335.2	3.6	-109.9
4.8	-77.2	12.7	-235.6	4.8	-78.0
24.0	-74.5	15.9	-189.0	32.4	34.5
26.2	-72.7	19.1	-152.5	33.9	29.0
28.4	65.3	22.2	-126.9	35.3	25.2
30.7	61.3	25.4	-106.8	36.8	22.4
32.9	58.2	28.6	-78.3	38.3	20.3
Spherical button bit					
0.0	-317.6	0.0	-3422.5	0.0	18.6
0.4	-162.8	2.6	-3460.4	0.4	17.4
0.8	0.5	5.3	-1980.8	0.8	14.0
1.1	91.3	7.9	-1152.5	1.1	12.8
1.5	142.5	10.6	-705.6	1.5	12.0
29.2	35.0	13.2	-487.4	1.7	11.4
32.3	27.6	15.9	-347.8	1.9	10.9
35.4	22.4	18.5	-262.6	2.1	10.6
38.5	18.7	21.2	-203.7	2.3	10.4
41.5	15.9	23.8	-162.9	2.4	10.3

Table 4.45: Magnitude of compressive stresses and the distance along X, Y and Z-axes as obtained in FEM analysis for black galaxy granite rock

Distance along X-axis	Magnitude of compressive stress (MPa)	Distance along Y-axis	Magnitude of compressive stress (MPa)	Distance along Z-axis	Magnitude of compressive stress (MPa)
Chisel bit					
0.0	-999.5	0.0	-2800.0	0.0	-149.2
1.2	-918.2	3.2	-2005.2	1.2	-434.5
2.4	-257.8	6.4	-353.6	2.4	-215.5
3.6	-114.8	9.5	-382.2	3.6	-222.6
4.8	-50.6	12.7	-237.6	4.8	-220.8
25.2	14.2	15.9	-196.7	25.5	-149.2
26.4	14.0	19.1	-155.0	27.0	73.4
27.6	13.8	22.2	-129.1	28.5	45.0
28.8	13.2	25.4	-108.0	30.0	40.2
31.0	12.4	28.6	-91.9	31.5	32.9
Cross bit					
0.0	-661.3	0.0	-2100.2	0.0	-658.1
0.9	-657.3	3.2	-1643.2	0.9	-652.0
1.8	-418.4	6.4	-450.1	1.8	-419.2
2.6	-306.2	9.5	-399.2	2.6	-306.9
25.2	-90.2	12.7	-262.3	3.5	-250.8
27.6	59.5	15.9	-210.9	27.6	19.5
30.0	29.0	19.1	-163.8	29.2	17.3
32.4	22.3	22.2	-133.6	30.9	15.6
34.8	16.5	25.4	-109.4	32.6	14.2
37.2	14.8	28.6	-91.4	34.3	13.1
Spherical button bit					
0.0	-495.1	0.0	-3913.6	0.0	18.4
0.3	-315.8	2.4	-3904.0	2.0	17.3
0.7	-124.1	4.9	-2366.2	4.1	13.7
1.0	-10.8	7.3	-1433.3	6.1	12.5
1.4	58.1	9.8	-887.7	8.1	11.7
24.1	18.6	12.2	-618.8	10.2	11.1
26.9	15.9	14.7	-443.4	12.2	10.3
29.8	13.8	17.1	-336.0	14.3	10.6
32.6	12.1	19.5	-261.2	16.3	10.3
35.4	10.8	22.0	-209.1	18.3	10.0

List of Publications based on PhD Research Work

Sl. No.	Title of the Paper	Authors (In the same order as in the paper, underline the Research Scholar's name)	Name of the Journal / Conference /Symposium, Vol., No., Pages	Month & Year of Publication	Category*
1	Indentation indices as criteria in Rock Excavation Technology- A Critical Review	Balla Kalyan, Murthy, Ch.S.N., Choudhary R.P.	Global Challenges, Policy Framework & Sustainable for Mining of Mineral and Fossil Energy Resources, Procedia, Earth and Planetary Science (Elsevier Publications), Volume 11C, 149 – 158	April, 2015	3
2	Influence of Index angle on Specific Energy in Rock Indentation Test	Balla Kalyan, Murthy, Ch.S.N., Choudhary R.P.	International Journal of Earth Sciences and Engineering, 8(4), 1856-1864	August, 2015	1
3	Estimation of Specific Energy in Rock Indentation Test	Balla Kalyan, Murthy, Ch.S.N., Choudhary R.P.	International Journal of Research in Engineering and Applied Sciences, 5(8), 33-47.	August, 2015	1
4	Development of Predictive models for the Specific Energy in Indentation of Rocks.	Balla Kalyan, Murthy, Ch.S.N., Choudhary R.P.	International Conference (RARE-2016), Atlantis Press, 530-535	November 2016	3
5	Numerical Modeling of Rock Indentation	Balla Kalyan, Murthy, Ch.S.N., Choudhary R.P.	Intrantion conference on Deep Excavation, Energy Resources and Production, Abstract, 23	February 2017	3

*Category: 1 : Journal paper, full paper reviewed

2 : Journal paper, Abstract reviewed

3 : Conference/Symposium paper, full paper reviewed

4 : Conference/Symposium paper, abstract reviewed

5 : Others(including papers in Workshops, NITK Research Bulletins, Short notes etc.)

BIODATA

1. **Name** : Balla Kalyan
2. **Father's Name** : Balla Veerabhadra Rao
3. **Date of Birth** : 06-01-1970
4. **Nationality** : Indian
5. **Marital Status** : Married
6. **Present Position** : Head of the Department
7. **Address for Communication:** Department of Mining Engineering
Government Polytechnic, Gudur
Nellore district, Andhra Pradesh
India.
8. **Mobile** : +91-9949273003
9. **E-mail** : balla_kalyan@rediffmail.com

10. Academic Qualifications:

Degree	University/ Board	Year of awarding degree
Ph.D in Mining Engineering	N.I.T.K, Surathkal	2017
M.Tech (Computer Science)	J.N.T.U, Kakinada, Andhra Pradesh	2005
A.M.I.E (Mining Engineering)	Institution of Engineers (India)	1993
Diploma in Mining Engineering	State Board of Technical Education and Training	1990

11. Work Experience:

- Worked as Part-time Lecturer from 12-06-1990 to 02-02-1995 in Mining Engg department at Government Polytechnic, Narsipatnam, Andhra Pradesh
- Worked as Lecturer from 10-03-1995 to 13-01-2001 in Mining Engg department at Government Polytechnic, Narsipatnam, Andhra Pradesh

- Worked as Senior Lecturer from 14-01-2001 to 29-09-2007 in Mining Engg department at Government Polytechnic, Narsipatnam, Andhra Pradesh
- Worked as Head of Mining Engineeringg at Government Polytechnic, Narsipatnam, Andhra Pradesh from 30-09-2007 to 10-09-2016.
- Presently working as Head of Mining Engg at Government Polytechnic, Gudur, Nellore district, Andhra Pradesh.

12. Membership of professional Bodies

- Member of The Institution of Engineers (India).

Awards/ Medals:

Secured All India Rank 22 (Percentile 94.6) in Graduate Aptitude Test for Engineers (GATE) -1994.

13. Publications	:	Total No.
National Journals	:	4
National Seminars	:	3
International Conferences	:	4
International Journals	:	2